ELECTRICAL ACTIVATION STUDIES OF SILICON IMPLANTED ALUMINUM GALLIUM NITRIDE WITH HIGH ALUMINUM MOLE FRACTION

DISSERTATION

Elizabeth A. Moore

AFIT/DS/ENP/08-D01

DEPARTMENT OF THE AIR FORCE
AIR UNIVERSITY

AIR FORCE INSTITUTE OF TECHNOLOGY

Wright-Patterson Air Force Base, Ohio

The views expressed in this dissertation are those of the author and do not reflect the official policy or position of the United States Air Force, Department of Defense, or the United States Government.

AFIT/DS/ENP/08-D01

ELECTRICAL ACTIVATION STUDIES OF SILICON IMPLANTED ALUMINUM GALLIUM NITRIDE WITH HIGH ALUMINUM MOLE FRACTION

DISSERTATION

Presented to the Faculty

Graduate School of Engineering and Management

Air Force Institute of Technology

Air University

Air Education and Training Command

In Partial Fulfillment of the Requirements for the

Degree of Doctor of Philosophy

Elizabeth A. Moore, BS, MS

December 2007

AFIT/DS/ENP/08-D01

ELECTRICAL ACTIVATION STUDIES OF SILICON IMPLANTED ALUMINUM GALLIUM NITRIDE WITH HIGH ALUMINUM MOLE FRACTION

Elizabeth A. Moore, BS, MS

Approved By:

Yung Kee Yeo, PhD (Chairman)	10 Dec. 2007 Date
Lt Col Nathan Titus (Dean's Representative)	11 Dec 07 Date
Robert L. Hengehold, PhD (Member)	10 Dec 2007 Date
James A. Fellows, PhD (Member)	11 DEC 07 Date
William C. Mitchel, PhD (Member)	11 Dec 07 Date

Accepted:

M. U. Thomas, PhD Dean, Graduate School of Engineering and Management	17 Dec 07 Date

AFIT/DS/ENP/08-D01

Abstract

This research demonstrates a method for producing highly conductive Si-implanted n-type aluminum gallium nitride ($Al_xGa_{1-x}N$) alloys, and represents a comprehensive analysis of the resulting material's electrical and optical properties as a function of Al mole fraction, anneal temperature, anneal time, and implantation dose. Highly conductive alloys are critical to the fabrication of devices operating in deep UV, high-temperature, high-power, and high-frequency environments, and thus this research is significant in regard to the application of such devices. The $Al_xGa_{1-x}N$ wafers of this study, with Al concentrations of 10 to 50%, were implanted at room temperature with silicon ions at energies of 200 keV with doses of $1x10^{14}$, $5x10^{14}$, and $1x10^{15}$ cm^{-2} and annealed from 1100 to 1350 ºC for 20 to 40 minutes in flowing nitrogen. Excellent activation was achieved for each of the implanted silicon doses for all of the five Al mole fractions studied, with most activation efficiencies above 90%. These activation efficiencies are the highest reported activations, to the best of my knowledge. The $Al_{0.1}Ga_{0.9}N$ annealed for 40 minutes at 1200 ºC had electrical activations of 73, 94, and 100% for implanted silicon doses of $1x10^{14}$, $5x10^{14}$, and $1x10^{15}$ cm^{-2}, respectively. Higher activations of 83, 100, and 100% were achieved for the $Al_{0.2}Ga_{0.8}N$ implanted with the same doses and annealed at 1300 ºC for 20 minutes. These same annealing conditions, of 1300 ºC for 20 minutes, produced slightly lower activations of 74, 88, and

100% for the Si-implanted $Al_{0.3}Ga_{0.7}N$. Exceptional activation efficiencies were obtained for each of the implanted silicon doses in the $Al_{0.4}Ga_{0.6}N$. The $Al_{0.4}Ga_{0.6}N$ implanted with a dose of $1x10^{14}$ cm^{-2} silicon ions had an activation of 99% following a 20 minute anneal at 1350 ºC, while the samples implanted with the higher silicon doses of $5x10^{14}$ and $1x10^{15}$ cm^{-2} had activations of 100 and 96%, respectively, after being annealed at 1200 ºC for 40 minutes. The $Al_{0.5}Ga_{0.5}N$ exhibited activation efficiencies of 100, 96, and 66% for the three implanted silicon doses after being annealed at 1300 ºC for 20 minutes. The mobilities were found to decrease as the Al concentration of the $Al_xGa_{1-x}N$ was increased from 10 to 50% and also as the implanted silicon dose was increased. Typical mobilities ranged from 101 $cm^2/V{\cdot}s$ for the $Al_{0.1}Ga_{0.9}N$ implanted with $1x10^{14}$ cm^{-2} silicon ions to 35 $cm^2/V{\cdot}s$ obtained for the $Al_{0.5}Ga_{0.5}N$ implanted with $1x10^{15}$ cm^{-2} silicon ions. The cathodoluminescence results support the electrical results in determining the optimal annealing conditions.

Acknowledgements

Writing this dissertation has been one of the most significant academic challenges I have ever had to face. Without the support, guidance and patience of my colleagues, family and friends I would never have been able to complete this document. To all these people I owe my deepest gratitude. I must first thank my husband for his unwavering support and encouragement through all the years of graduate school, for without him this effort would be worth nothing. His love, patience, and support gave me the foundation I needed to complete this study. I am eternally grateful to my family for raising me in an environment that encouraged and cultivated my inquisitive mind. Their support was also instrumental in the development and completion of this project. I would like to thank my advisor, Dr. Yeo, for his guidance, support and sense of humor throughout this endeavor. He has been wonderful to work with and has taught me a lot, not only about physics, but also about developing from a student to a professional. I would like to acknowledge my committee members for their time and expertise. I would like to thank the AFIT lab technicians, especially Mike Ranft and Greg Smith, for all of their efforts in keeping my lab equipment functioning and me safe. They have been an invaluable resource for experimental design questions and maintenance. I would also like to thank the AFIT/ENP staff, in particular Jo Pollard, Kevin Pope and Jennifer Meier, for all their efforts and directions. Finally, I would like to thank the many friends I have made along the way, Matt Lange, Catherine Taylor, Glen Kading, and Greg Pitz for helping me to remember that life is a journey not a destination, and for reminding me to laugh and have fun along the way.

Table of Contents

Page

List of figures

Page

Page

Page

Page

Page

Page

Page

Page

Page

Page

List of Tables

ELECTRICAL ACTIVATION STUDIES OF SILICON IMPLANTED ALUMINUM GALLIUM NITRIDE WITH HIGHER ALUMINUM MOLE FRACTION

I. Introduction

Wide bandgap semiconductors, especially group-III nitrides, have become essential for the fabrication of optoelectronic devices that operate in the blue and ultraviolet (UV) spectral regions and for electronic devices capable of operating under high temperature, high frequency, and high power conditions. Research of group-III nitrides has made major strides in the last ten years. This research will further these advances by determining improved ion implantation and annealing conditions for silicon implanted aluminum gallium nitride, $Al_xGa_{1-x}N$, in order to create materials for more optimal device production.

Electronic devices have been reshaping the landscape of the modern world for almost 50 years. The evolution of electronics has had a major impact on the world with each new discovery.

The Electronic Revolution

Since the advent of the transistor in 1947, electronic devices have come to play an ever increasing roll in warfare, communications, information methods, medicine, and almost every aspect our daily lives. The advancements in research produced radio, television, radar, compact disks (CDs), lasers, and computers. Today, cell phones, high definition televisions, digital versatile disks (DVDs), digital video recorders (DVRs), portable media players (MP3, I-PODs), car dashboard displays, computers, and the internet are all made possible by the continuing development of optical and electronic devices, structures, and material characterization. Researchers continue to push the frontiers of science by manipulating the fundamental material characteristics of materials to realize more powerful and efficient optical and electronic devices.

The origin of solid state electronics dates back to 1874 when Karl Braun, a German scientist, discovered that the electrical resistance in metal sulfides varies with the magnitude and polarity of the applied voltage through the point-contact. This breakthrough had no particular application at the time, but would become instrumental thirty years later in the fabrication of the point contact transistor. Initially the advancement in semiconductor fundamental properties was under appreciated and therefore progress was slow. This began to change in 1904 when an Indian scientist, Jagadish Chandra Bose, invented a solid state diode detector using a galena crystal that greatly increased the sensitivity of radio receivers. By the 1930s, selenium (Se) rectifiers and silicon (Si) point contact diodes were being used commercially in devices such as radio receivers, photocells, thermistors and variable resistors. The development of radar in the late 1930s and the onset of World War II created a need for better understanding of

the fundamental properties of solid state devices as well as improved detector diodes and electronic mixers (1).

In December of 1947 the first point-contact transistor was created at Bell Telephone Labs by William Shockley. The transistor changed the world with its widespread implementation in a vast number of electronic applications. The initial transistor was a point contact device that used polycrystalline germanium (Ge), soon thereafter a transistor made of silicon was developed. Within two years single crystal silicon became available which greatly improved the performance of the transistor. Diffusion doping was used to form junctions so that the characteristics of devices could be better controlled and operated at higher frequencies.

Theoretical advancement to explain the conduction of electrons in semiconductors began to take place in the 1930s when A. H. Wilson published his theory of semiconductors (2). He put forth that valance electrons can not be associated with a single atom in a crystal structure. He also developed the concept of filled, partially filled, and empty bands. Felix Bloch, a Swiss physicist, showed quantum mechanically that particles in a quantum well have an increasing probability to occupy energy levels in adjacent wells as the separation distance becomes increasingly smaller, such as in crystal lattices. The two scientists had thus laid the foundation of semiconductor theory which satisfactorily explained electronic motion in a crystal lattice and also the inherent differences in metals, semiconductors, and insulators.

Their theory applies quantum mechanics to the Sommerfeld model of an atom and assumes that the atom cores in the crystal lattice create the effect of a periodic potential on the valence electrons of the atoms. The valance electrons are treated as free particles and when solving Schrödinger's equation the results are plane waves that are confined to

allowed energy bands. These allowed energy bands are separated by forbidden bands or an energy gap, E_g. The number of valance electrons and the spacing between the atom cores determine the structure of the energy bands which ultimately determine the optical and electronic properties of the material. For example, if the allowed bands overlap and there is no forbidden region, as is the case with metals, the electrons are available to participate in conduction. Whereas, if the energy gap between the allowed band and the forbidden band is large, electrons are not likely to obtain the energy required to bridge the gap and are therefore unable to contribute to the conduction of the material, i.e. insulators. For the case of semiconductors, the situation is not as defined. The forbidden band is small and the electrons can gain enough thermal energy to be excited into the higher energy band and thus partake in the conduction. A small energy gap is defined as less than 2 electron volts (eV). Introducing a small amount of a dopant species into a material can change the band properties and introduce energy levels in the forbidden energy band. This technique gives the researcher added control over the conductivity and has become the backbone of all modern optical and electronic devices. This technique enables conduction in materials even with energy gaps from 2 to 6 eV, a group of materials known as wide band gap semiconductors. These materials have recently came to light as promising materials for devices operating in high frequency, high temperature and high power regimes, where traditional devices made of Si breakdown.

Silicon, an elemental semiconductor from group IV of the periodic table, is accountable for an estimated 99% of the semiconductors used in commercial applications. In the beginning of semiconductor development, Si surpassed Ge for use in electronic materials production for three primary reasons. First, silicon is extremely prevalent in nature, as it is found in most rocks and can be easily extracted from sand

using chemical reduction. Secondly, silicon can be easily doped as both n and p-type, a modification required to make electron transport devices, such as diodes and transistors. Finally, Si forms a stable non–conducting oxide that can be used to define masks for microlithography (3).

Silicon's development was followed by gallium arsenide (GaAs) and other compound semiconductors (4). Devices made with silicon have high yields, excellent reliability and are low cost. With that being said, there is little reason to develop other semiconductor materials to replace Si applications. However, niche markets where the properties of silicon made it unable to function encouraged the advancement of other semiconductor materials. For instance, a light emitting diode (LED) has never been realized with silicon due to its indirect band gap that results in poor quantum efficiency. The first LEDs and laser diodes were developed with compound semiconductors such as GaAs and GaP and well as ternary compounds of them with Al (5). Another disadvantage to Si devices is that they do not operate well above 100 ^{o}C because with its narrow band gap the electrons thermally excite across the bandgap and swamp those introduced by dopants. This causes the electronic noise in the circuit to increase and has adverse effects on the efficiency of the device. However, the drawbacks associated with Si and other semiconductors with small band gaps did not halt the development in devices that utilize these materials.

The first light emitting diode was invented in 1957 by a group of British scientists using GaAs. The following year, Jack Kelley of Texas Instruments demonstrated the first integrated circuit (IC) with Ge. The integrated circuit was the primary electronic creation that spawned a multitude of other inventions that have defined modern living. They have made possible most devices that shape our daily lives such as the computer, internet, and

cell phones. Shortly after Kelley's IC, an integrated circuit of Si was introduced by Fairchild Semiconductors' researcher Robert Noyce using planar technology (bi-polar transistors). Another highly utilized invention from this decade was the metal oxide semiconductor (MOS) transistors, and today they are the most common field effect transistors (FET) used for digital circuits (1).

In 1960, an American scientist Theodore H. Maiman developed the first laser while working at Hughes Research Laboratories. He used a solid-state flash lamp-pumped synthetic ruby crystal to create a pulsed laser at 694 nm. Later the same year, an Iranian physicist, Ali Javan, fabricated the first gas laser using helium and neon. The first semiconductor laser was demonstrated two years later by Nick Holonyak Jr., an American physicist. These early laser diodes exhibited pulsed operation and had to be cooled to liquid nitrogen temperatures. In the 1970's, Bell Telephone Laboratories introduced the first continuous operation laser diodes (LD) that functioned at room temperature. Numerous other electronic inventions followed, such as the microprocessor in 1971, the charged couple device (CCD) camera for home videos and the GaAs compact disc (CD) in 1979.

Silicon and GaAs have become the most developed semiconductors for electronic and opto-electronic device applications. However, there are several disadvantages due to their fundamental material properties that make them not suitable for all environments. To overcome these shortcomings, researchers began looking at group-III nitrides because they have a wide direct bandgap that allows them to be used in optical devices, in high temperature regimes, in higher frequency, and in higher power applications.

Every material has unique fundamental properties that determine which type of devices they would be best suited. Table 1.1 shows the values of these properties for

various semiconductors that are considered for high temperature applications in addition to those for smaller band gap materials. The thermal conductivity is a good parameter to monitor. The higher the value the better the material conducts heat to its surrounding, which would mean that the device temperature would increase more slowly. Other properties that are good to note are the saturation velocity and breakdown field. A high value for the breakdown voltage is an indication that the material will be able to handle greater power levels. A higher frequency can be obtained from materials with a high saturation velocity.

The capability of semiconductor materials for a specific device function can be evaluated with figures of merit, which are based on the fundamental properties of the material. Figures of merit (FOM) are numerical expressions derived that take into account specific device qualities and the material properties that have an impact on the particular device characteristic. The FOMs are determined from physical properties of the material such as the critical field, saturation velocity, mobility, energy bandgap, thermal conductivity, and dielectric constant.

There are four commonly used figures of merit that indicate device performance in different areas. A high value of the figure of merit suggests a more suitable material for that application. The limitation of high frequency and power capabilities as impacted by material parameters on device performance was considered by Johnson in 1965 which led him to define the Johnson figure of merit (JFOM) as the power-frequency product for a low voltage transistor (6). The JFOM ($J_{FOM} = E_B \nu_s / 2\pi$) figure of merit is considered when determining which materials are best suited for power amplification or high frequency devices, where E_b is the breakdown voltage and ν_s is the saturation velocity.

Table 1.1. Summery of key intrinsic material parameters for various semiconductors. * An indirect bandgap is indicated with an I, and a direct bandgap by D (22).

	Si	GaAs	InP	GaP	4H-SiC	GaN	AlN	Diamond
Energy Band Gap at 300K (eV)*	1.12 I	1.42 D	1.34 D	2.89 D	3.26 I	3.44 D	6.13 D	5.47 I
Dielectric Constant	11.7 (dc)	13.2 (dc) 10.9 (∞)	12.4 (dc) 9.66 (∞)	11.1 (dc)	9.6 (dc) 6.7 (∞)	8.9 (dc) 5.35 (∞)	9.14 (dc)	5.57 (dc)
Thermal Expansion (10^{-6} K^{-1})	2.92	5.75	4.75	4.65	2.77	5.59	3.48	1.0
Lattice Constant (Å)	5.431	5.653	5.869	5.451	3.073 a 10.05 c	3.189 a 5.185 c	3.111 a 4.978 c	3.567
m_c^*/m_o	1.18	0.063	0.077	0.21	-	0.22	0.40	0.2
m_v^*/m_o	0.81	0.53	0.64	0.67	-	0.8	3.53	0.25
Electron Mobility ($cm^2/V{\cdot}s$)	1450	8500	4600	160	1140	900	300	2200
Hole Mobility ($cm^2/V{\cdot}s$)	500	400	190	135	50	150	14	1600
Saturation Velocity (10^7 cm/s)	1.0	1.0	-	-	2.0	2.5	-	2.7
Breakdown Field (MV/cm)	0.3	0.4	-	-	3	5	-	10
Thermal Conductivity (W/cm·K)	1.5	0.46	0.68	0.77	4.9	1.3	3.19	22
Melting Point (ºC)	1412	1238	1070	1749	Sublimes T>1827	Sublimes T > 1300	3025	3826

In 1972, Keyes derived a figure of merit which provides a thermal limitation to the switching behavior of transistors used in integrated circuits. A high value of the Keyes figure of merit ($K_{FOM} = \sigma_T (v_s / \kappa)^{1/2}$) indicates materials that are best appropriate for high speed digital ICs, where κ is $1/4\pi\varepsilon_0$. The KFOM is also a function of the thermal

conductivity, σ_T, which is responsible for setting the lower limit on the dimensions of a device. In 1983, Baliga defined a figure of merit ($B_{FOM} = \kappa\mu E_B^3$) which defines material parameters to minimize the conduction losses in power FETs, where μ is the mobility. High frequency systems have a non negligible amount of switching losses which are not accounted for in the above figure of merit, making it only valid for low frequency systems. In 1989, Baliga introduced the BHFFOM, a figure of merit for high frequency devices. To improve efficiency of high frequency power systems, you want a high value for BHFFOM. It is useful to consider all the FOMs when analyzing the impact of other semiconductor materials on device performance. Semiconductor materials suited for high frequency power switching applications should have a large critical breakdown fields and should have high carrier mobilities. These properties result in minimizing power loss in die area. Table 1.2 shows the values of the four figures of merit for several common semiconductor materials with the values normalized to silicon for ease of comparison.

There are other commonly used FOMs for semiconductor materials, such as the FSFOM used to compare materials suitability for FET switching speed or the BSFOM which is the equivalent FOM for bipolar transistors. There is also the FPFOM and BPFOM for power handling of FET and bipolar transistors, respectively. The power switching product of FET and bipolar transistors can be evaluated with the FTFOM and BTFOM figures of merit. In all of the above mentioned FOMs, GaN and AlN have numbers that far outreach the other conventional semiconductors, except diamond that has higher values. However, diamond can not be controllably doped and is therefore not useful as a device material at this time (7).

Table 1.2. Figures of merit for several semiconductor materials with the values normalized to silicon.

	Si	GaAs	InP	GaP	4H-SiC	GaN	AlN	Diamond
JFOM	1	11	13	37	410	790	5120	5330
KFOM	1	0.45	0.72	0.73	5.1	1.8	2.6	31
BFOM	1	28	10	16	290	910	31,670	14,860
BHFFOM	1	16	6.6	3.8	34	100	1100	1080

All of the solid state advancements mentioned in this section paved the way for the miniaturization of electronic and optical devices that are so prevalent today, and have transformed the way consumers, industry, and the military rely on electrical device components. Our modern military, with its heavy emphasis on technologically based platforms and operations, increasingly depends on these materials each year.

Electronic and optoelectronic device manufacturers search for new materials that can operate in harsher environments and in smaller devices. Advancements in understanding the fundamental properties of a material will lead to the production of more efficient devices with the characteristics required to meet the technical challenges of current and future applications. Development of wide band gap (WBG) semiconductor material characteristics and fabrication techniques can presumably thwart many of the device failure mechanisms that result from inefficient material properties.

The advantages of WBG materials for high temperature, high power, and high frequency devices are illustrated in the previous tables. They have much better FOM values than that of Si. SiC has a better thermal conductivity than GaN, but not that of AlN. $Al_xGa_{1-x}N$ is a new material and all of its fundamental properties have not been

cataloged to date. However, it is presumable that the properties of $Al_xGa_{1-x}N$ will start at those of GaN for x equal to zero and migrate towards those of AlN as the Al mole fraction is increased. What is still to be discovered is the relationship between how the properties of GaN and AlN will change with increasing Al concentration. For example, the energy band gap will increase in an almost linear fashion from 3.4 to 6.2 eV as the Al mole fraction is increased from 0 to 1.

The Era Beyond Silicon

The push for electronics to perform in more caustic environments and in optical devices that operate in the blue and ultraviolet regimes has increased research activity of materials with a wide band gap due to their predicted performance in devices based on the material properties illustrated in Table 1.1.

WBG semiconductors have many material properties, most of which are directly related the wide band gap, that make them desirable for high temperature, high power, and high frequency applications. For instance, the critical breakdown voltage is proportional to the energy gap, E_g, of the material, $V_{BR} \propto E_g^{2/3}$. Thus, the wider the energy gap, the higher the breakdown voltage and the better capable the material is in high power circumstances. WBG semiconductors have a high thermal conductivity and therefore can conduct heat quickly away from themselves making them more reliable at high temperatures and in high power situations. The internal electric field of a device increases linearly as the device dimensions become smaller, thus the size of the device is linked to the size of the energy gap. The wide band gap semiconductor by its nature requires a large amount of thermal energy for the electrons in the valance band to be excited in to the conduction band. This results in the material being able to function at

much higher temperatures before having a pronounced amount of thermal leakage current that degrades device functionality. Other useful properties of WBG semiconductors are large saturation velocities for high frequency operation and large cohesion energies which make them chemically inert and resistant to radiation damage.

Silicon carbide has received a lot of consideration because of its high thermal conductivity; however, it is not as good as group-III nitrides for optical devices due to its indirect bandgap. Nitrides initially attracted attention after the commercialization of bright blue light emitting diodes which were followed by the injection laser. They have several advantages over other WBG semiconductors such as silicon carbide and diamond. Nitrides have a direct bandgap, ability for both n- and p-type doping, for heterojunctions conducive for device applications, and they can be grown epitaxially over a number of substrates – which means that monocrystalline layers can be obtained over large surfaces. In the beginning, the brightness of nitride based LEDs was too weak to surpass SiC blue LEDs. In the late 1990s the brightness levels increased and bright violet, blue, and green LEDs were fabricated with InGaN and GaN quantum wells.

In the early nineties, group-III nitrides were barely studied, but by the end of the century GaN blue LEDs were taking over the market. The prospect of large payoffs led the market and nitride based devices (LEDs, lasers, ultraviolet detectors, high temperature, and microwave base electronics) were manufactured while their underlying physics still remained a mystery (8). Group-III nitrides such as GaN, $Al_xGa_{1-x}N$, AlN, and their alloys with indium are wide bandgap semiconductors that have direct band gaps. They have many intrinsic material properties like high ionicity, very short bond lengths, large energy gaps, low compressibility, high thermal conductivity, and high melting temperatures that make them ideal for certain device applications (8).

Group-III nitrides are different from other III-V compounds such as GaAs and GaP in many aspects. They have larger bandgap energies and therefore much larger effective masses. Nitrides crystallize in the wurtzite structure in nature rather than zinc-blende. They are found to be highly polar materials which can lead to strong piezoelectric fields and even spontaneous polarization due to the low-symmetry wurtzite structure (9).

Their wide band gaps lend to group-III-nitrides having low attenuation in the near-infrared wavelength region and as semiconductors their refractive index can be modified through carrier injection, making them prime candidates for use in fiber optic communications (10). The fact that they work well in harsh environments, at high temperatures, and with high power makes them good as tunable optical phased-array (PHASAR) devices for optical communication. Research thus far has focused mainly on the blue-UV wavelength applications. Their optical characteristics in the near infrared region remain largely unknown and their potential application in fiber-optic communication has just begun to be investigated. Rongqing Hui *et al*. developed an optical waveguide device using GaN and $Al_xGa_{1-x}N$ semiconductor materials (11). They found that the refractive index of GaN decreases with wavelengths reaching 2.31 in the 1551 nm region. This is a much improved refractive index match with optical fibers than InP, which is typically used. The refractive index of $Al_xGa_{1-x}N$ was found to monotonically decrease with increasing Al concentration, which will allow for precise index adjustments critical in integrated optical circuit design. Group III-nitride semiconductor materials are capable of making passive devices such as fixed wavelength filters and splitters, but they may also enable active functionalities such as tunable filtering and photonic switches (10).

Research advances into wide bandgap semiconductors composed of group-III nitrides are of particular interest in applications which operate in high temperature, high power, and high frequency environments, such as those associated with new hybrid cars and the more electronic aircraft, warships, and modern ordnance systems (12). These applications often require devices to operate under harsher conditions than those at which smaller bandgap semiconductors can effectively function. Group-III nitride semiconductor technology allows for the fabrication of UV light emitting diodes, laser diodes, and solar blind cells. The technology allows for a multitude of other promising devices such as the all white light emitting diode, which shows possibility of replacing current lighting devices with solid state lighting applications offering superior energy, endurance, and luminescence characteristics.

A New Material, $Al_xGa_{1-x}N$

GaN, $Al_xGa_{1-x}N$ and AlN, have a direct bandgap that span the energy range from 3.4 eV to 6.2 eV and give rise to properties which show tremendous potential for current and future electronic applications operating in high temperature, high power, and high frequency environments. They can produce light from 200-360 nm and have been used in lighting displays, green traffic signals, photo-catalytic processes, high resolution optics, and UV solar blind photodetectors. Potential applications of these semiconductors in opto-electronic devices include early missile plume detection, flame sensors, space-to-space communications, solar-UV monitoring, biological and chemical detection systems, water and air sterilization, and as a primary light source for phosphor-based white LEDs (11). These new devices are more compact, energy efficient, rugged, and reliable than

devices made from conventional semiconductor materials, and can be relatively easy to integrate with other electronics.

$Al_xGa_{1-x}N$ is recognized as a promising material for optoelectronic devices in the deep UV range. Highly conductive n and p-type alloys are necessary for device applications. A major problem in obtaining highly conductive n-type Al rich material (x >0.3) is the effect of compensation of electrons by cation vacancies and their complexes. Suppressing such defects could greatly improve the conductivity of Al rich material (13).

The conductivity of undoped $Al_xGa_{1-x}N$ decreases with increasing Al concentrations and Al rich $Al_xGa_{1-x}N$ alloys are normally found to be insulating. It has been suggested that the decrease in conductivity is due to a transition of oxygen from a shallow donor to a DX center. This same decrease in conductivity with increasing Al mole fraction is found in Si-doped $Al_xGa_{1-x}N$. In this case, it is attributed to the deepening of the Si donor level, compensation from acceptor-like defects, and an increase in dislocation density. Highly conductive $Al_xGa_{1-x}N$ materials are hard to come by due to the incorporation of compensating acceptor-like defects such as Al vacancies or V_{Al}-O_N complexes (14). Nakarmi *et al*. developed a growth technique that suppresses Al vacancies and complexes and were able to grow a highly conductive Si-doped $Al_{0.7}Ga_{0.3}N$ epilayer (15). The sample had a reported resistivity of 0.0075 Ω·cm, carrier concentration of $3.3x10^{19}$ cm^{-3}, and mobility of 25 $cm^2/V·s$. Although many devices have already been reported using $Al_xGa_{1-x}N$, improvements in material quality and conductivity are still needed.

Commercially available LEDs in the deep UV ($\lambda < 340$ nm) still face many challenges and have low internal quantum efficiency. Jong Kyu Kim *et al*. have developed a light emitting triode (LET) to try to overcome some of the challenges and

have produced a lighting device with increased quantum efficiency (16). $Al_xGa_{1-x}N$ has been used to make deep-ultraviolet light emitting diodes, and M. Khizar *et al*. found that using a mircolens array increased the output power by 55% over conventional methods (17). Their LED had a silicon doped $Al_{0.6}Ga_{0.4}N$ active layer and produced light through the sapphire substrate at a wavelength of 280 nm. Shakya *et al*. fabricated blue and UV LEDs, and found that the degree of polarization of the band edge emission changes with Al concentration (18). They suggest that the low efficiency of nitride UV LEDs is partially related to this polarization property.

GaN based high electron mobility transistors (HEMTs) are the leading candidates for high temperature and high power microwave applications due to GaN's unique material properties. The wide bandgap of GaN and its alloys leads to a high breakdown voltage for GaN based HEMTs. A high breakdown voltage is crucial for power performances of microwave power devices and circuits. There is still much work to be done to increase device uniformity and minimize trapping centers in the material surface. Researchers have tried a multitude of techniques to improve device performance.

An $Al_xGa_{1-x}N$/GaN (HEMT) fabricated with implanted Si ions was studied by Haijiang Yu *et al.* (19). They activated the Si dopants in the source and drain region with an ultra high temperature rapid thermal annealing technique that allowed them to anneal at 1500 ^oC with 100-bar N_2 overpressure for 1 minute without causing structural damage to the material. The implanted HEMT device exhibited comparable contact resistance, manifested DC, small signal and RF power performance comparable to HEMTs processed by conventional fabrication. $Al_xGa_{1-x}N$/GaN HEMTs were fabricated by Miyoshi *et al*. with Al concentration from 0.26 to 0.70 (20). They grew the structures by metalorganic chemical vapor deposition on 100 mm sapphire substrate with uniformity of

±3% for all Al concentrations. They found that the sheet carrier concentration of the $Al_xGa_{1-x}N$/GaN heterostructures increased with increasing Al content in the $Al_xGa_{1-x}N$ layers. They concluded that to achieve higher power densities for $Al_xGa_{1-x}N$/GaN HEMTs, the materials should be grown with high Al mole fraction $Al_xGa_{1-x}N$. Jaesun Lee *et al*. experimented with post annealing treatments on $Al_xGa_{1-x}N$/GaN HFETs and found the heating treatment improved device breakdown voltage and device uniformity as well as reducing trapping centers on the $Al_xGa_{1-x}N$ surface (21).

$Al_xGa_{1-x}N$ material exhibits many properties that make it an ideal candidate for next generation electronic and optical devices. Although the research into this material is still in the early stages of development, a wide variety of devices made from $Al_xGa_{1-x}N$ materials have already been fabricated in a number of research laboratories utilizing many different Al mole fractions. A major drawback of an intrinsic material in device performance is that the carrier density is too low and the resistivity is too high. This problem can be solved by introducing dopants into the material that will act as donors and acceptors. There are three major methods to accomplish this: in-situ doping, diffusion doping, and ion implantation doping. For wide bandgap semiconductors, diffusion doping is impractical due to the extended temperatures required for material production. In-situ doping is widely used and has shown some major progress in creating both n- and p-type materials. The ion implantation method is an alternative doping technique and offers some advantages over in-situ doping. This method allows for a selected area doping of the sample. It also offers advantages with respect to precise depth and doping profiles, and device isolation.

Methodology

The goal of this research is to improve the functionality of everyday electronics and optoelectronics by doing research at the material science level. $Al_xGa_{1-x}N$ material with Al concentrations from 0.1 to 0.5 are implanted with silicon ions and investigated as a function of ion dose, anneal temperature, anneal time and Al concentration. The objective was to find the conditions that most improved the carrier concentration as well as the crystal quality of the material. Ion-implanted $Al_xGa_{1-x}N$ has not been the subject of intense investigation up to this point, as most of the research to date focuses on in-situ doping.

In order to increase the conduction of $Al_xGa_{1-x}N$, silicon ions were implanted at an energy of 200 keV at a 7º tilt to the material surface to reduce channeling effects. The Si ions are amphoteric in the $Al_xGa_{1-x}N$ crystal lattice but they exhibit a high tendency to occupy donor positions. Three Si-implanted doses, $1x10^{14}$, $5x10^{14}$ and $1x10^{15}$ cm^{-2}, were investigated. A major draw back to the ion implantation technique is that the high energy ions damage the crystal structure of the base material. The substrates must then undergo a high temperature annealing treatment to restore the crystal structure and settle the implanted ions into electrically active positions.

The Si-implanted $Al_xGa_{1-x}N$ was annealed from 1100 to 1350 ºC for 20 to 40 minutes to determine the best possible conditions to achieve the highest activation efficiency, mobility and a strong exciton peak. The annealing took place in nitrogen ambient with all samples in a face-to-face configuration. These precautions were taken in order to prevent out diffusion of nitrogen during the anneal process and also to protect the sample surface.

Electrical material parameters were determined through temperature-dependent Hall Effect and resistivity measurements, while low-temperature cathodoluminescence measurements were used to investigate the optical properties. Together these measurements can provide insight in the process of implantation activation and the defect structures that result from it. This research effort aims to complete a comprehensive investigation into the material properties of Si-implanted $Al_xGa_{1-x}N$ as a function of Al concentration, ion implantation dose, anneal temperature, and anneal time, with the goal of enhancing the functionality of $Al_xGa_{1-x}N$ optical and electrical devices.

II. Theory

In order to manipulate the fundamental properties of a given semiconductor material, it is necessary to understand how these characteristics originate from the basic structure of the material. Many of the properties discussed in Table 1.1 such as dielectric constant, mobility, and electric breakdown field are a direct result of the material's structure. The arrangement and bonding of the atoms in a material determine how the electrons will interact with one another. This chapter describes the connection between the microscopic activities of electrons in a solid and the macroscopic properties they manifest. The discussion in this chapter follows the development and presentation found in Fellows' dissertation (22).

Semiconductors are single crystal materials, which means that they have a high degree of long range order (4). They have regular geometric periodicity throughout the entire volume. The electrical and optical properties of the material are determined from both the chemical composition and the arrangement of atoms. The two types of semiconductors, elemental and compound, are made up primarily of elements from the second through sixth columns of the periodic table. Elemental semiconductors consist, as the name suggest, of only one type of atom from the fourth column of the periodic table, such as Si and Ge. A compound semiconductor has two or more elements derived from periodic table columns such as II, III, V, and VI. Compounds comprised of two elements are referred to as binary compounds; those consisting of three elements are ternary alloys and denoted as $III_xIII_{1-x}V$ or $II_xII_{1-x}VI$.

Crystal Structure of Solids

The atomic arrangement of atoms in solids was first investigated in 1913 by W.H. and W. L. Bragg using their newly developed method of x-ray crystallography. They discovered that the atoms in a solid have highly organized spatial qualities through the study of the diffraction patterns produced by x-ray bombardment. The ordered structure of the atoms is a result of a delicate balance of Coulomb forces that the atoms experience due to their close proximity within the solid. As a result of these forces, the atoms maintain a fixed distance from each other creating an ordered lattice formation (5). The periodic nature of the single crystal allows for the entire lattice to be represented by a fundamental unit cell which repeats to recreate the entire crystal structure. A lattice is thus defined as the three-dimensional alignment of the crystal atoms. The arrangements of atoms are described by Bravais lattices, which in mathematical terms is an infinite array of discrete points with an arrangement and orientation that is exactly the same from each point in the array (3). A Bravais lattice is one of fourteen unique unit cells that represent the geometrical arrangement of the atoms in the solid. The 14 unique arrangements include 1 triclinic, 2 monoclinic, 4 orthorhombic, 2 tetragonal, 1 hexagonal, 1 rhombohedral and 3 cubic lattice structures. Most semiconductor materials crystallize in cubic or hexagonal crystal structure groups. Silicon and most III-V compounds crystallize into the cubic form. Cubic lattices are highly symmetric and have three classifications: simple (primitive), face-centered cubic (FCC), and the body-centered cubic (BCC). The simple cubic has an atom at each of its eight corners, as does the BCC, which also has an additional atom at its center. The FCC has atoms at each corner as well as an atom at the center of each plane.

A crystalline solid is distinguished from other solids in two ways, first, by a periodic arrangement of atoms, and second, by the binding forces that hold them together. The binding energy of a material is the amount of energy required to break up a solid into atoms and is interdependent on the type of bonds formed between the atoms. The binding force then is a result of the quantum mechanical interaction between the electrons. Electrons have a tendency to form filled outer electron shells and consequently they will share, gain, or lose electrons in order to obtain a full valance shell. The two types of bonding most prevalent in wide band gap semiconductors are ionic and covalent. When atoms lose or gain electrons in their valance shell, the atoms become positively or negatively charged ions which are then attracted to each other through Coulombic forces leading to ionic bonding of atoms. Covalent bonding, on the other hand, results when atoms share electrons with nearest neighbor atoms. They thus act as though they have full valance shells. Most semiconductor materials exhibit this type of bonding. A material determines which structure it will have based on the types of bonds that form among the atoms.

In compound semiconductors, the chemical bonding is predominately covalent and only slightly ionic, and therefore they have a tetrahedral bonding configuration which results in most III-V compounds forming zincblende structures as opposed to wurtzite structures. Both crystal arrangements are shown in Figure 2.1. A zincblende structure is one that is made up of two interpenetrating FCC sublattices with each sublattice containing only one kind of atom. Wurtzite materials have a primitive hexagonal Bravais lattice structure with each plane of tetrahedra having mirror images of each other. The physical arrangement of atoms in the lattice is the primary feature in determining the

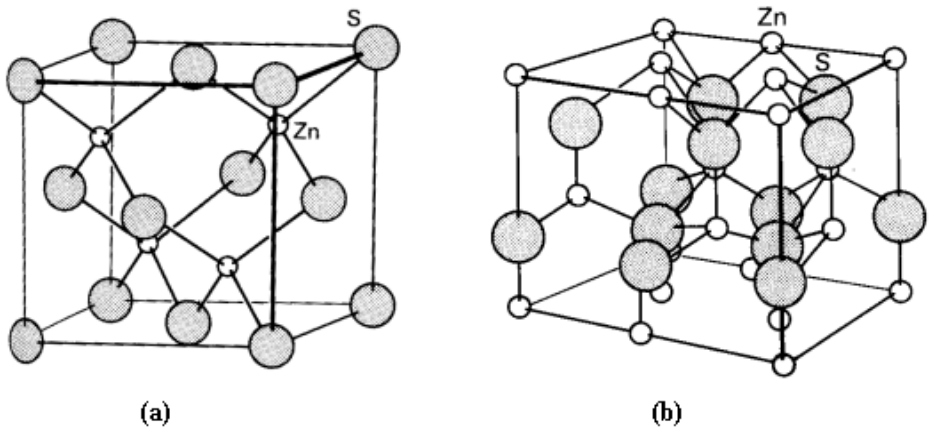

Figure 2.1 The crystal structure of ZnS is shown in both the (a) zincblende and (b) wurtzite structures. The zincblende structure has cubic symmetry and thus has only one lattice constant while the wurtzite formation has two lattice constants due to its hexagonal symmetry (3).

band structure and crystal potential of a material and are the governing factors in establishing the electrical and optical properties of a material.

Single crystal materials are further characterized by the inner atomic distances (or the length of one side of the unit cell) of the atoms in the solid, also called lattice constants. In cubic structures, as shown in Figure 2.1(a), the lengths of each side of the unit cells are the same, thus they are characterized by one lattice constant. Hexagonal structures, Figure 2.1(b), have two unique lattice constants to describe their structures. This parameter is of primary importance when choosing a growth substrate for epitaxial semiconductor growth. The lattice constants of the substrate and the semiconductor material would be close to aid in minimizing the formation of defects and imperfections during the growth process.

Crystal Growth

Advances in the area of crystal growth act as a catalyst for developing emerging materials that are not commonly found in nature. Growing good quality single crystal

material requires precise control over all aspects of the growth conditions, such as the temperature of the source materials and growth substrate, the distance between the two, the rotation speed of the substrate, and the cooling rate. Strict thermodynamic equilibrium conditions must be maintained throughout the entire growth process. This makes growth of compound semiconductors more difficult than elemental ones because the stoichiometry (the correct chemical ratio of the compounds' constituent elements) must be maintained, while at the same time the thermal parameters to grow the perfect crystal must be controlled. One component of the compound is generally more volatile than the other, and is therefore more readily evaporated at high temperatures. In group III-V semiconductors, this component is normally the group V element, leaving the material group III rich if the growth conditions are not correct.

There are two types of growth methods for semiconductors: bulk growth and epitaxial layer formation. In both growth types, it is important to minimize imperfections and defects as well as the amount of unwanted impurities. The most common bulk method is the Czochralski Method, in which a seed crystal is placed in contact with the same material in liquid form and then slowly rotated as it is retracted from the liquid solution. Bulk materials can be intentionally doped by adding a small amount of the desired impurity into the liquid solution. After the growth, the boule can be trimmed to the desired dimensions.

Epitaxy is a growth method of applying regularly oriented single crystals with controlled thickness over a similar single crystal (called a substrate) which is generally grown in bulk form. This growth method provides better control over purity, doping, and thickness profiles. Epitaxial growth is used extensively for device manufacturing. It

utilizes a single crystal substrate as the seed and can be performed at much lower temperatures than bulk growth. There are several methods of epitaxial growth including vapor-phase epitaxy (VPE), liquid phase epitaxy (LPE), and molecular beam epitaxy (MBE). For good quality epitaxial growth, it is essential that the substrate and the material have a close lattice match.

If the lattice constants are not close, it can cause strain and defects in the material, such as dislocations and vacancies (3, 20). A semiconductor material can be grown on a substrate if the lattice constants of the two materials are close; however the semiconductor will experience some type of strain as the lattice of the material tries to adopt the lattice constant of the substrate. Pseudomorphic materials assume the lattice constant of the substrate material. The chemical energy of the material, which defines its lattice constant, and the strain energy which results from the new lattice constant both contribute to the stability and quality of the crystalline formation. The strain energy increases linearly with the epitaxial layer thickness and defines the critical thickness as it approaches the value of the chemical energy. Below this thickness, the minimum energy state of the epitaxial structure is dominated by strain. Above this thickness, the energy is minimized by the formation of dislocation lines. The biaxial compression and tensile strain are proportional to the extent of the lattice mismatch. The strain energy is reduced through the formation of dislocations at the interface. Dislocations propagate upwards and multiply as they go, forming threading dislocations. Aberrations to the crystal lattice structure can affect the motion of the electrons within the crystal and have adverse effects on the electrical and optical properties of the material.

Crystal lattices are not perfect in the real world and often contain defects and imperfections which can have detrimental effects on the electrical properties of the material. Lattice vibrations represent one type of disturbance, wherein the atoms do not rest perfectly in the lattice position but actually vibrate around it. Point defects involve single atoms and are comprised of vacancies, with an atom missing from a lattice site, and interstitials, when atoms rest in between lattice sites. Point defects when grouped together form complexes. A vacancy-interstitial complex is known as a Frenkel defect and a line defect is one in which an entire line of atoms is missing. Dislocations are defects in which atoms are misplaced from the lattice site.

The optical and electrical properties observed in a semiconductor can not be completely explained by classical physics. To understand the movement of electrons in a solid, it is important to consider what happens to the discrete energy levels of the individual atoms as they are brought into close proximity to each other to form the crystal lattice. No two electrons can have the same energy, therefore, the energy levels spread into energy bands to accommodate all the electrons in the solid. The band theory of solids explains the spreading of the energy levels by examining the wave functions of the electrons. Significant outcomes to the theory are forbidden energy regions, the concept of a hole, effective mass of the carriers, and the conduction properties (3).

Band Structure

The band theory of solids can be used to better understand how the above crystal structure and residing defects can affect the fundamental properties of a semiconductor material. To explain the experimentally observed properties of semiconductors, the free electron model had to be expanded on. The free electron model of a solid is based on the

claim that conduction electrons are entirely free and do not interact with the other electrons or the positively charged ion cores. In semiconductors however, there is a periodic potential with the periodicity of the lattice that arises from the regular arrangement of the ion cores from the host atoms. It is the quantum mechanic interaction between the electrons and the periodic potential of the lattice that gives rise to the electronic band structure of solids.

To form the crystal lattice of a solid, atoms come in close contact with each other which enables the wave functions of the electrons to interact and cause the discrete energy levels of the individual atoms to split in order to accommodate the electrons from neighboring atoms. This splitting is a direct result of the fermionic nature of the electrons. The electrons interact with other electrons in the solid and also the ion cores that are positioned periodically at the lattice sites. The energy band structure for a solid is determined by the interactions of the electrons with the periodic potential of the lattice. The electrons in a solid can be considered as core electrons (those tightly bound to the atomic nuclei), and valance electrons (those less bound due to the effects of screening from the inner electrons). The microscopic nature of electrons in a solid is described in terms of this electronic band structure. The best way to visualize the electron in the lattice is to consider an infinite number of quantum wells with a periodic potential, V_0. When the energy of the electron, E, is less than the potential energy, $E < V_0$, the electron is bound to the atom. On the other hand, when the energy is greater than the potential, $E > V_0$, the electron is free to move around the crystal and to participate in conduction. Schrödinger's equation has to be solved in each region to determine the energy levels of the electron. However, since the valance electrons can be considered as nearly free

electrons, their approximate energy levels can be determined by considering the case of a free electron.

This is simplest case to solve because the free electron does not experience any outside potential forces from either the ion cores or other electrons. The energy levels of the free electron are determined by solving Schrödinger's equation, Equation 2.1, with the potential being equal to zero

$$H\psi(\vec{r}) = \left(-\frac{\hbar}{2m_0}\nabla^2 + U(\vec{r}) \right)\psi(\vec{r}) = E\psi(\vec{r}), \tag{2.1}$$

where H is the Hamiltonian operator, $\hbar$ is the reduced Plank's constant, m_0 is the mass of an electron, $U(\vec{r})$ is the potential, E is the energy, and $\psi(\vec{r})$ is the wave function describing the motion of the electrons. For a free electron in three dimensions, the solution to Schrödinger's equation are plane waves of the form

$$\psi_k(\vec{r}) = e^{i\vec{k}\cdot\vec{r}}, \tag{2.2}$$

where $\vec{k}$ is the electron's wave vector and $\vec{r}$ is the electron's position vector. The eigenvalues that satisfy the eigenstates for Equation 2.1 are then given by

$$E(\vec{k}) = \frac{\hbar^2 k^2}{2m_0}. \tag{2.3}$$

The variation of energy as a function of the wave number is known as the dispersion relation. Electrons are not completely free, thus the values of k are dependent on the periodicity of the lattice by

$$k = \frac{2\pi}{L}n, \tag{2.4}$$

where n is required to be an integer and L is the lattice constant. This relationship dictates that not all values of k will lead to acceptable electron wave functions. Not all energies

will be permitted due to the integral nature of the *k* values. The magnitude of this forbidden energy gap between allowed energy states has drastic effects on the conduction properties of solids and determines whether they will behave as conductors, insulators, or fall somewhere in between.

There are enormous quantities of atoms in a solid, each with their own number of electrons, making it a formidable task to solve the wave equations associated with each of these electrons. The symmetry of the crystal structure, both translation and rotational, simplifies this task tremendously. Also, assuming the mean field approximation (electrons experience the same forces in all directions regardless of lattice position) makes this task considerably easier. However, these considerations also show that the energy levels of the electrons are going to be highly degenerate. This is most easily illustrated by examining Equation 2.3. Since $\vec{k}$ is a three-dimensional vector ($k = k_x + k_y + k_z$), it is easy to see that there are multiple unique combinations of its component values that will sum to produce identical k^2 values. Though there is degeneracy in the energy levels, the quantum state themselves remain unique.
The actual values of the energy will be shifted from the calculated values by the periodic potential, $U(\vec{r})$. The shifting has the most drastic impact on the electronic energy band structure near the Bragg planes of symmetry. The general effect $U(\vec{r})$ has on the energy levels is to shift higher energies higher and cause lower energies to decrease. This shifting in opposite directions causes a gap in the allowed energy levels, known as the energy gap E_g. The width of the energy gap is determined by the strength of the periodic potential. Figure 2.2 shows the electronic band structure as a function of the wave vector for AlN. The symmetry points for a hexagonal structure that lie in the first Brillioun zone

are denoted on the k axis, the most important of which are the Γ point or center and the L and K points. These symmetry points as they relate to the crystal structure are illustrated in Figure 2.3 which shows the first Brillioun zone for the hexagonal AlN structure. These symmetry points are more relevant when considering optical transitions.

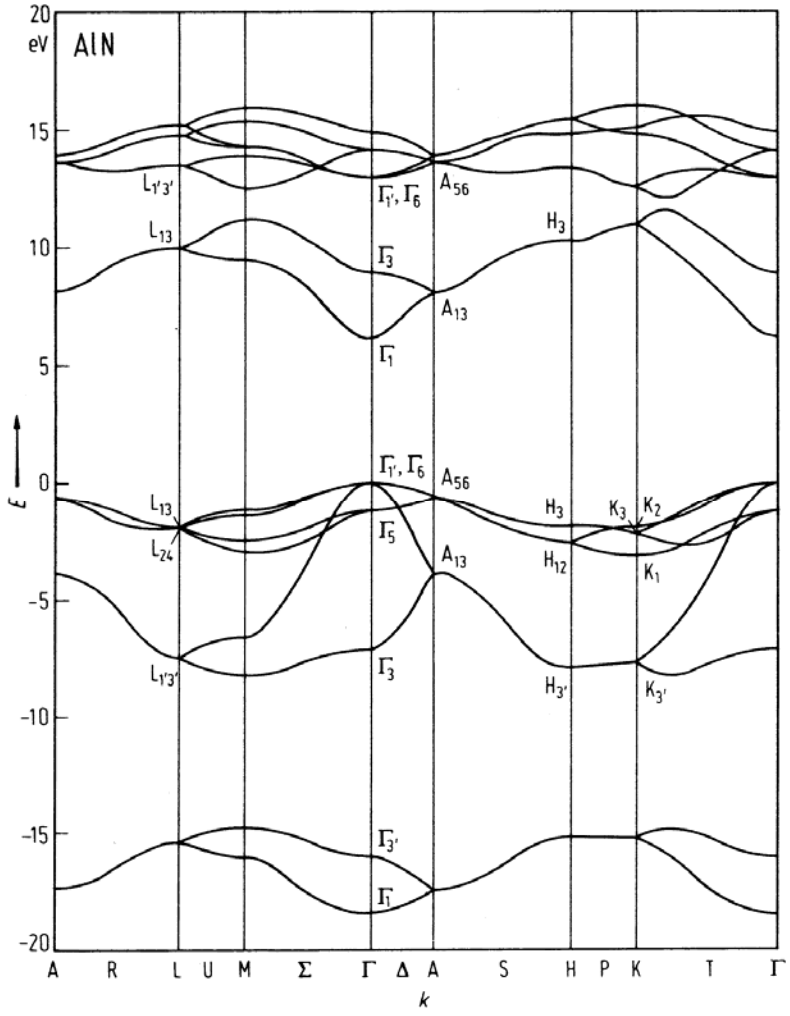

Figure 2.2. An energy band diagram for AlN which illustrates a variety of points of symmetry within the first Brillioun zone. The conduction band minimum and the valance band maximum both occur at the Γ point in k-space (77).

The motion of the electrons in the allowed bands is generally explained through the consideration of only two bands, the valance band (VB) and the conduction band (CB). At a temperature of absolute zero the electrons occupy their lowest energy configurations, the highest energy band that the electrons fill or partially fill is known as the valance band and the next highest band containing no electrons is the conduction band. The difference in energy between these two bands is the energy band gap for the material. The size of the band gap determines the material's fundamental electrical properties. A solid material then can be divided into three types: a conductor, an insulator, or a semiconductor depending on the magnitude of the energy gap. For metals the valance and conduction bands overlap so that there are always electrons available to partake in conduction. Insulators, on the other hand, have a large energy band gap ($E_g >$ 6 eV) requiring the electrons in the valance band to obtain a considerable amount of energy or extreme temperatures for the electrons to be able to move to the conduction band, thus insulators do not conduct electricity. Semiconductors are so named based on their ability to behave as both a conductor and an insulator. Semiconductors have an energy gap in the range of less then 1 eV to 6 eV, which allows them to act as both an insulator and a metal depending on the conditional settings. Semiconductors are distinguished from other solid materials by the behavior of their electrons and the gaps in their electronic spectra. Valance electrons, due to the effects of screening, experience only a weak periodic potential and can be considered free electrons (5). However, at absolute zero (0 K) semiconductors behave as insulators. As the temperature is increased ($T > 0$ K), the electrons will gain sufficient thermal energy to move to the conduction band, and contribute to the conduction.

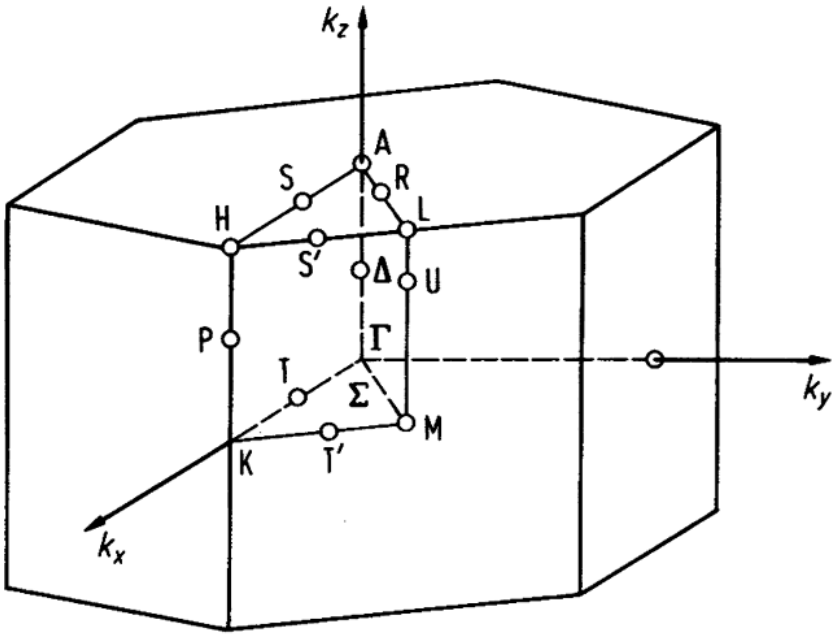

Figure 2.3. The first Brillioun zone of the hexagonal crystal structure of AlN showing various points of symmetry of the crystal structure (77).

Another important aspect to the energy diagrams is whether the band gap is direct or indirect. For a direct band gap, the valance band maximum and the conduction band minimum occur at the same point in *k*-space. For an indirect bandgap, the VB maximum and the CB minimum do not occur at the same point in *k*-space, i.e. the conduction band minimum is not at $k = 0$. This results in a phonon being required for optical transitions as a result of the conservation of crystal momentum. Materials with a direct band gap are more ideally suited for optical devices.

Semiconductor materials are not charged so that when an electron moves into the conduction band it must leave behind a positively charged state to maintain the charge

neutrality of the crystal. This positively charged state is actually the absence of the electron and is referred to as a hole. The hole is not an actual particle, but it behaves as one and has many similar properties of the electron.

The movement of the electron within the crystal is different from that in free space because of the positively charged ion cores that act as a periodic potential well. Their movement is restricted and as a result crystal momentum is not a constant of motion. This difference in motion makes the electron appear to have a generally smaller mass than m_0. The mass of the electron (or hole) in the lattice is called the effective mass. The effective mass of the electrons can be derived by knowing that the time rate of change of the momentum is equal to the force on an electron. The effective mass is mathematically represented as

$$m_{c,v}^{*} = h^2 \left[\frac{d^2 E_{c,v}}{dk^2} \right]^{-1} . \tag{2.5}$$

The effective mass for the electrons in the conduction band is generally not the same as the effective mass for holes in the valance band. This difference comes from the different curvatures of the energy bands. The effective mass takes into account the effects of the periodic potential on the electrons or holes, and thus they can be treated as free particles with mass m^*.

Semiconductor Physics

The electronic band structure discussed in the previous section is not composed of a continuous set of energy levels but rather they are discrete levels closely packed together. The density of levels and the extent to which they are filled determines the conduction properties of the material as well as the optical properties such as the rate of

absorption and emission. Current is due to a flow of charged particles in a material, so it is important to know the density of electrons or holes. The number of carriers is directly proportional to the number of available states. The density of states is defined as the number of states per unit volume and unit energy ($g(E) = (1/L^3)(\partial N/\partial E)$). This is easiest to do in *k*-space using the energy-momentum relation to give the density of states in terms of the energy.

From examining Equation 2.3, it can be seen that $E(\vec{k})$ forms spheres of constant energy in three dimensional *k*-space. The density of discrete energy levels per unit volume per unit energy is determined by first considering the smallest volume on the sphere that can contain one energy level. Since $k = 2\pi n/L$, the smallest possible volume in *k*-space is then $8\pi^3/L^3$. Accounting for spin degeneracy, the volume becomes $4\pi^3/L^3$. Dividing the density of states by this volume yields per volume measures. Consider the number of states in a generic volume in *k*-space with surface area $\Delta S_k(E)$ multiplied Δk_n measured outward from the surface. The change in the *k*-direction is equivalent to the reciprocal of the derivative of $E(\vec{k})$ with respect to *k*. The density of allowed states as a function of energy for both the valance band and the conduction band is defined as

$$g_{c,v}(E) = \frac{1}{4\pi^3}\int_{surface}\frac{ds}{\nabla_k E(k)} = \frac{\sqrt{2\,|E - E_{c,v}|}}{\pi^2\hbar^3}(m^*_{c,v})^{\frac{3}{2}} \tag{2.6}$$

with the integral over constant energy surfaces in *k*-space. Integrating over the entire constant energy surface, the number of states per energy per unit volume as a function of the effective mass is shown also in Equation 2.6. The density of states strictly describes

the number of available levels but not how the electrons are distributed in these levels. The Fermi-Dirac distribution function describes the allocation of electrons among the available energy levels. The Fermi-Dirac distribution is shown below

$$f_{FD}(E) = \frac{1}{\exp\left[\frac{E - E_F}{k_B T}\right] + 1}, \tag{2.7}$$

where E_F is the Fermi energy that is normally about $3k_B T$ lower than the conduction band, k_B is the Boltzman constant, and T is the temperature. The carrier concentration involves the integral of the product of the Fermi Dirac Function and the density of state function. The number of electrons occupying these states is given by

$$n(T) = \int_{E_c}^{\infty} g(E) f(E) dE \,. \tag{2.8}$$

Sometimes it is simpler to use the Maxwell-Boltzman distribution, which differs only slightly but significantly simplifies the math required to solve the integral in Equation 2.8. The Maxwell-Boltzman distribution can be used instead of the Fermi-Dirac distribution in the regime where $\Delta E >> k_B T$ holds true, where ΔE is difference in energy between the conduction band and the Fermi level. In this approximation the two distributions yield close to the same results. The Maxwell-Boltzman distribution is given by

$$f_{MB}(E) = \frac{1}{\exp\left[\frac{E_F - E}{k_B T}\right]}. \tag{2.9}$$

Solving Equation 2.8 using the $f_{MB}(E)$ yields the following for the number of electrons in the conduction band as a function of temperature.

$$n(T) = \frac{1}{\sqrt{2}}\left[\frac{m_c^* k_B T}{\pi\hbar^2}\right]^{\frac{3}{2}} \exp\left[\frac{E_F - E_c}{k_B T}\right] \tag{2.10}$$

For a non-degenerate semiconductor, the coefficient to the exponent represents the upper limit of the volume concentration of the conduction electrons and is referred to as the effective density of states. The concentration of holes in the valance band can be determined similarly and is shown in Equation 2.11. In intrinsic semiconductors, the concentrations of electrons and holes are equal and their product determines the intrinsic carrier concentration; a fundamental material constant for all temperatures.

$$p(T) = \frac{1}{\sqrt{2}}\left[\frac{m_v^* k_B T}{\pi\hbar^2}\right]^{\frac{3}{2}} \exp\left[\frac{E_v - E_F}{k_B T}\right] \tag{2.11}$$

The intrinsic carrier concentration is calculated as follows

$$n_i(T) = \sqrt{n(T)p(T)} = \frac{1}{\sqrt{2}}(m_c^* m_v^*)^{\frac{3}{4}}\left[\frac{k_B T}{\pi\hbar^2}\right]^{\frac{3}{2}} \exp\left[\frac{-E_g}{2k_B T}\right]. \tag{2.12}$$

The intrinsic carrier concentration is a fundamental material parameter that depends only on the effective mass and the energy gap. For a pure semiconductor, the intrinsic carrier concentration is equal to the electron concentration and also the hole concentration at any given temperature.

Effects of Impurities

A perfect crystal is something that only exists as an idea and can rarely be found in nature. Impurities in semiconductors have been found to enhance the conduction properties of the material. By introducing impurities in a controlled manner, the electrical properties can be manipulated in an accurate and reliable way. The main

properties that are of interest are conductivity, carrier concentration, and mobility. These three properties are related through Equation 2.13.

$$\sigma = e(n\mu_n + p\mu_p) . \tag{2.13}$$

Here e is the charge of the electron, n and p are the electron and hole carrier concentrations, and μ_n and μ_p represent the mobility for the electrons and holes, respectively.

Semiconductor materials are unique in that they exhibit conduction from both electrons and holes. In an intrinsic semiconductor, the concentration of electrons and holes are equal and their product defines the intrinsic carrier concentration, known as the law of mass action, as defined in Equation 2.12. The intrinsic carrier concentration is a fundamental constant of the crystal for all temperatures. In extrinsic semiconductors, the impurity atoms can donate electrons or holes to the crystal, and in this case the values of n and p are no longer equal. However, the law of mass action still holds, so that as the electron carrier concentration increases, the hole concentration must correspondingly decrease and vice versa. The type of conduction taking place in the material is determined by whether electrons or holes serve as the majority carriers. In n-type material, the majority carriers are electrons, while in p-type material the majority carriers are holes. A small amount of impurity atoms can have profound effects on the conduction of the material.

Semiconductors form closed valance shells through covalent bonding with their nearest neighbors. When impurity atoms from neighboring columns in the periodic table occupy a lattice site of the host crystal, they attempt to form all the bonds the crystal's atoms would have created. Sometimes the impurity atoms will complete all the bonds

but have one or more extra electrons, such as case when silicon ions (column IV) replace Ga (column III) atoms in a GaN crystal. These "extra" electrons are then free to join the conduction. In this case, the impurity ions are referred to as donors. On the other hand, the impurity ions may not have enough electrons to complete all the bonds (Si on an N site) and thus create holes that are readily available to participate in the conduction in the valance band. Impurity ions of this type are called acceptors. Impurities that can act as both acceptors and donors in a material, such as Si in GaN, are called amphoteric dopants. Silicon ions normally tend to occupy gallium sites, and act as donors when introduced into a GaN crystal.

The ionization energy of the impurity ions can be estimated by comparing the isolated impurity atom to the hydrogen model of an atom and seeing that they represent the same circumstance. The ionization energy can then be approximated by using the energy levels for the hydrogen model as shown in equation 2.14

$$E = -\frac{nm_0 e^4}{2\hbar^2 \kappa^2} = -13.06eV \quad \text{for n = 1} \tag{2.14}$$

Here $\kappa = 4\pi\varepsilon_0$, where ε_0 is the permittivity of a vacuum. In order for this equation to be valid for impurity atoms, m_0 must be replaced by the effective mass and ε_0 must be replaced with the relative dielectric constant of the semiconductor material.

The impurity ions create energy levels within the forbidden band gap region. Donor levels can be shallow, forming only a few meV below the conduction band for non-wide band gap semiconductors. Acceptor levels similarly form within a few meV above the valance band. It is possible, however, for energy levels to be deep within the band gap region. Shallow donors and acceptors are normally thermally ionized at room temperature, meaning the electrons (holes) have gained enough thermal energy to move

into the conduction (valance) band and participate in the conduction. Shallow and deep donor and acceptor energy levels in units of electron volts for GaAs are shown in Figure 2.4. The number of free carriers in a semiconductor crystal can be calculated by looking at the charge balance equation. The overall net charge of the crystal is zero, therefore the charge from the positive ions must be equal to the charge of the negative ions. This is expressed mathematically in Equation 2.15, where n and p are the concentrations of electrons and holes already taking part in the conduction. The concentration of unionized donors and acceptors is given by n_d and p_a, and $N_{d,a}$ represents the total concentration of the unionized electron and hole impurities, respectively (3).

$$n + (N_a - p_a) = p + (N_d - n_d). \tag{2.15}$$

Solving this equation for p_a and n_d yields an equation proportional to the ionization energy of the impurity.

$$p_a = \frac{N_a}{g_v e^{(E_F - E_a)/k_B T} + 1} \tag{2.16}$$

and

$$n_d = \frac{N_d}{g_c e^{(E_a - E_F)/k_B T} + 1} \tag{2.17}$$

where $g_{c,v}$ accounts for the degeneracy. These equations, along with experimental data of the carrier concentrations as a function of temperature, can be used to determine the ionization energy of the impurity atoms. This data curve can be fitted to extract the values of N_a, N_d, and E_a and is known as an Arrhenius plot. The extracted values for the activation energy can be lower than the actual values due to screening effects.

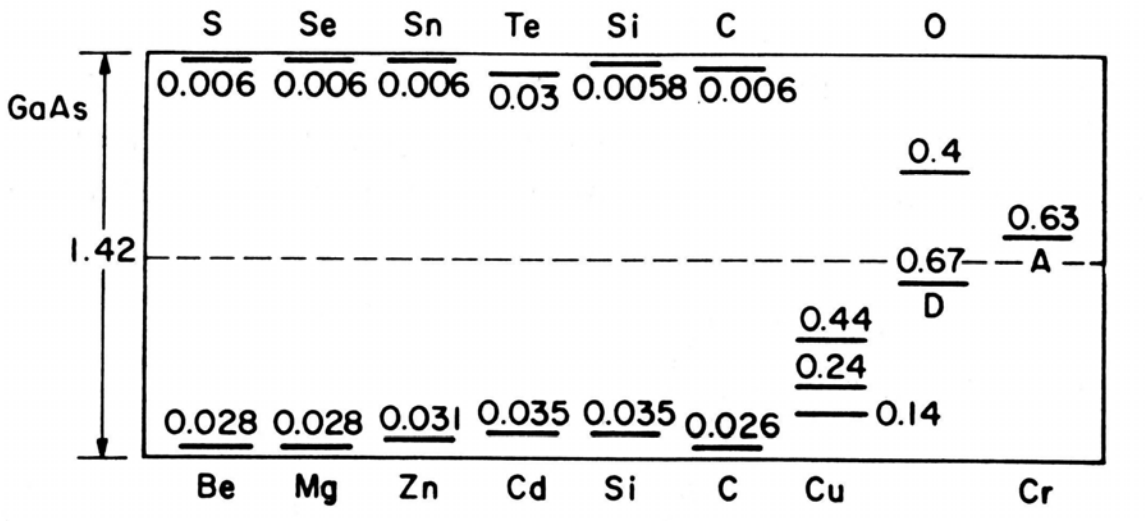

Figure 2.4. Impurity donor and acceptor levels in eV for various atoms in GaAs (71, 23).

When the impurity atom is embedded with the pure semiconductor, the binding energy is significantly reduced. The binding energy of an electron to an impurity atom is much smaller compared to the band gap. This makes it easier to thermally ionize the donor electrons to produce conduction. The conduction band can be approximated by a parabola. The conductivity of the material includes both the conduction due to electrons and holes as shown in Equation 2.13.

Intentional introduction of impurities can benefit the conduction up to the point at which the doping density becomes so large that the impurity atoms are separated by less than the Bohr radius. At this point the material undergoes a Mott transition and begins acting like a metal and control over the conductivity of the material is lost. The defining equation for the critical doping density is given in Equation 2.18, where $\kappa_r = 1/4\pi\varepsilon_r$. A

high level of doping can result in impurity band formation, band tailing, band filling and other effects that inhibit the control of the material's conduction properties.

$$N_{crit} = \left[\left(\frac{\kappa_r}{3} \frac{m_0}{m^*_{c,v}} \right) 5.29 \times 10^{-9} cm \right]^{-3} \tag{2.18}$$

When the doping concentration is much less than the critical concentration, the impurity atoms are isolated such that their wave functions do not overlap and form discrete energy levels. As the doping concentration approaches the critical limit, the wave functions of the donor electrons begin to overlap, forming an impurity energy band. If the critical doping density is exceeded, the impurity band merges with the conduction band or valance band depending on which type of impurity band was created.

The spatial distribution of impurity atoms is generally random, causing random fluctuations at the band edges, known as band tailing. As the impurity concentration grows, free carriers begin to occupy states above the bottom of the conduction band. This is known as band filling, and is common in highly doped, highly degenerate semiconductors (22).

There are several techniques to incorporate the dopants in the host material. These include diffusion doping, in-situ doping, and ion implantation doping. Diffusion doping takes place at high temperatures with the material placed in a gaseous atmosphere of the desired dopant. This is not feasible for nitrides due to the low evaporation temperature of nitrogen. In-situ doping (doping during growth) of group-III nitrides has shown much progress in the last few decades with both n and p-type GaN and low Al concentration $Al_xGa_{1-x}N$ alloys. However, there is still much progress to be made in this

area with regard to limiting the number of defects caused by the dopant incorporation. In-situ doping has become a viable method of doping a semiconductor material; however this method does not allow for selective area doping. Ion implantation has advantages over other methods because it is quick and cost effective and allows for doping of specific material areas as well as the aforementioned advantages with respect to device isolation and precise depth and doping profiles.

III. Characterization Techniques

There are many techniques available for determining the fundamental electrical, optical, and structural properties of semiconductor material. Each method stimulates the material in a way that forces a measurable response. The stimulus could be, for example, a magnetic field, an applied current, a laser, or a chemical etchant. The measured response is determined by the initial probe of the material. The majority of experiments are designed to test the electrical and optical properties of materials which are widely used in device manufacturing processes. The properties of primary interest are the carrier concentration, mobility, resistivity, and optical transitions that result from the implantation of the silicon ions.

Hall effect and cathodoluminescence measurements were conducted to determine the electrical and optical properties of $Al_xGa_{1-x}N$. Hall effect and magneto resistance measurements determine the Hall coefficient and resistivity of the material, which enable the calculation of the carrier concentration and mobility as well as the determination of the semiconductor type. Optical techniques such as cathodoluminescence (CL) measurements at low temperature are performed to measure the dominant transitions in the material and also to evaluate the level of crystal damage recovery.

Electrical Properties

A semiconductor material's electrical properties such as resistance, carrier concentration, and mobility determine how effective it will function in a given device. The Hall effect method is a relatively easy way to accurately determine these material properties, and in conjunction with resistivity measurements, comprise the most

commonly used characterization techniques utilized to determine a material's electrical properties in the semiconductor industry.

Hall Effect Theory

The Hall Effect theory was discovered in 1879 when Edwin H. Hall, an American physicist, discovered that a small transverse voltage was generated across a thin metal strip in the presence of an orthogonal magnetic field. The discovery of this transverse voltage, or Hall Voltage, enabled the independent calculation of the mobility and the carrier concentration of the material which was only accomplished up to that time through difficult measurements. Van der Pauw, in 1958, made the theory more experimentally testable when he showed that the shape of the measured sample was not a factor and only required that the sample be simply connected and exhibit highly ohmic point contacts on the periphery of the material (23).

According to the Hall Effect theory, electrons moving in a specimen find themselves subject to the Lorentz Force when in the presence of a perpendicular magnetic field. Hall Effect measurements are conducted by placing a sample in a magnetic field that is orthogonal to its surface as illustrated in Figure 3.1. A current is applied to the material so that the charged carriers move in the x direction. The moving charges induce an internal electric field in the material, which deflects the charges toward the edges of the material. Positively charged particles (holes) move to one edge, and the negatively charged particles (electrons) move to the opposite edge. This particle movement is the result of the charge carriers being subject to the Lorentz Force, which is normal to the magnetic field. The Lorentz Force is given by

$$\vec{F}_L = q(\vec{E} + \vec{v} \times \vec{B}), \tag{3.1}$$

where q is the charge of the particle, $\vec{E}$ is the electric field, $\vec{v}$ is the velocity of the electrons, and $\vec{B}$ is the magnetic field. If one type of carrier is dominant this shift causes a buildup of unequal surface charge which creates a potential difference across the sample surface, the Hall Voltage.

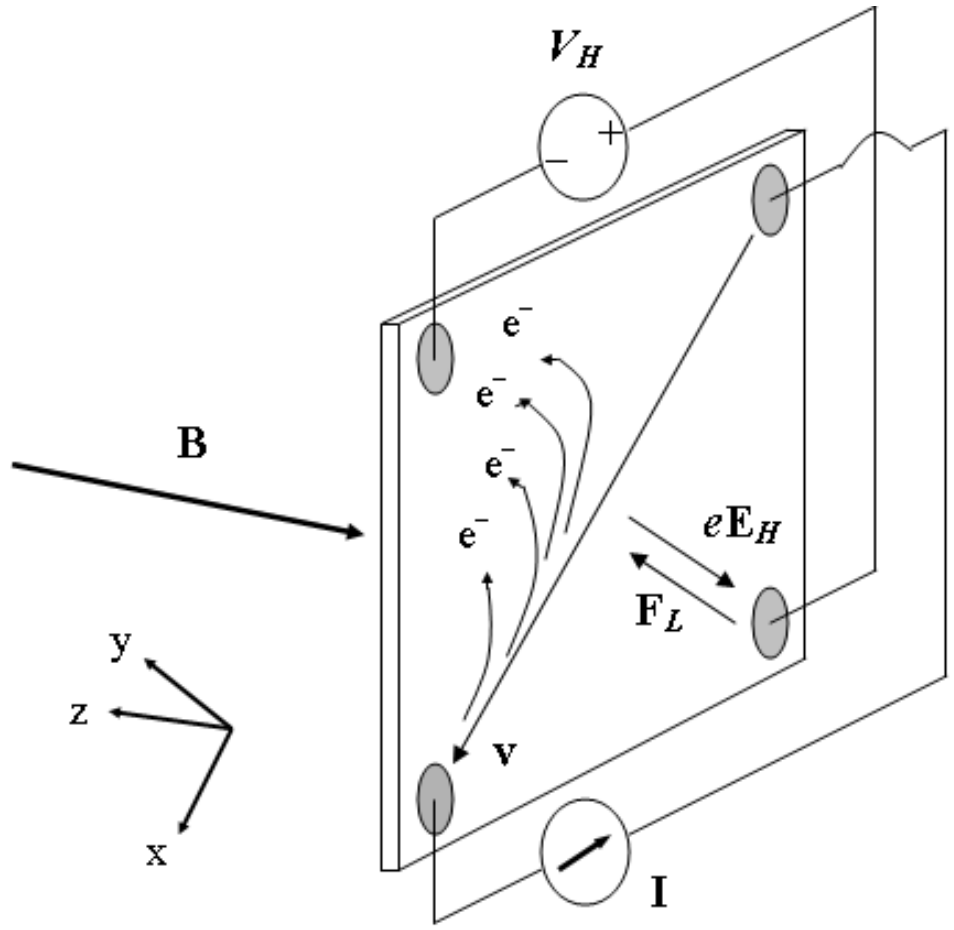

Figure 3.1. A schematic diagram illustrating the direction of the Lorentz Force, induced electric field, applied magnetic field and applied current to demonstrate the van der Pauw Hall Effect (22,47).

This generated transverse voltage will therefore have a different sign for n and p-type materials. Solving the cross product in Equation 3.1, it can be seen using Figure 3.1 that the Lorentz Force equation becomes

$$F_y = qE_y + qv_x B_z \tag{3.2}$$

The system will strive for equilibrium and therefore the Hall Voltage will grow until it becomes equal to the Lorentz Force. When this occurs, F_y is zero and equation 3.2 can be simplified to

$$E_y = -v_x B_z \tag{3.3}$$

The current density which is defined in equation (3.4) can be solved for the velocity and substituted into the electric field equation (3.3), rendering the equation to experimentally measurable quantities.

$$I_x = nqv_x r_H \quad \rightarrow \quad v_x = \frac{I_x}{nqr_H}. \tag{3.4}$$

The Hall factor is represented by r_H and denotes the Hall to drift mobility ratio which is usually approximated to be one, but can vary between one and two. This estimation causes the Hall Effect measurements to often underestimate the values of the carrier concentration. The substitution of v_x into equation (3.3) yields an equation for the electric field in terms of the Hall coefficient, applied current, and applied magnetic field that is given by

$$E_y = \frac{I_x B_z}{nqr_H} = R_H J_x B_z. \tag{3.5}$$

The above equation is then used to define the Hall voltage. The Hall voltage is the product of the generated electric field and the width of the sample, *w*.

$$V_H = E_y w = R_H J_x B_z w. \tag{3.6}$$

The Hall voltage, being a measurable quantity, is used to calculate the Hall coefficient. Rearranging equation (3.6) to solve for the Hall coefficient in all experimentally measurable values yields

$$R_H = \frac{V_H}{J_x B_z w}. \tag{3.7}$$

The magnitude of the Hall voltage is inversely proportional to the carrier concentration and the sign of this voltage indicates the dominant carrier type. For electron conductivity, the Hall coefficient is negative, and the coefficient is positive for hole conduction. This value, along with the resistivity of the material, is needed to determine the carrier concentration and mobility. These relationships are shown as equation (3.8).

$$N_s = \frac{r_H}{qR_H} \quad \text{and} \quad \mu_H = \frac{R_H}{\rho_s}. \tag{3.8}$$

Temperature-Dependent Hall (TDH) measurements provide carrier concentrations and mobility values as a function of temperature. At low temperatures the shallowest of impurities should freeze, leaving the material highly resistive. If the material is highly degenerate, TDH measurements will reveal this degenerate layer at low temperatures via the mobility and carrier concentration will be temperature independent. The impurity ionization energies are extracted by fitting the temperature-dependent carrier concentration data. The samples are placed in a vacuum during the TDH measurements to prevent condensation or oxidation, which would be damaging to the sample and adversely affect measurement accuracy (7).

Hall Effect Measurements

The Hall effect measurements are made with an automated Lake Shore 7505 system. A diagram of the system is provided in Figure 3.2. The samples are placed on Janis vacuum heads designed for low (10-320 K) and high temperature (300-700 K) measurements which are placed between two coil magnets that are capable of producing up to a 7 kG magnetic field. All measurements are done in a 5 kG field. Current is supplied to the sample with a Keithley 220 current source and the generated Hall Voltage is measured using a Keithley 2182 nanovoltmeter. Lake Shore Hall program version 3.3 automates the process and records the resisitivities and Hall data. Exact operating procedures can be found in appendix A.

There is a separate system for high and low temperature measurements. The systems are identical except for the Janis vacuum head. The high temperature system uses pressure contacts to make contact with the material while the low temperature system must use gold wires connected with indium solder.

Hall Measurements provide only average carrier concentration and mobility values over the entire conducting thickness. A total of 8 current-voltage pair measurements are averaged to calculate the sheet resistivity. Four current-voltage pair measurements taken under forward and reverse magnetic fields are averaged to calculate the Hall Coefficient. The Hall measurements are also used to determine the activation efficiencies of the implanted samples. The following relations are used:

$$A = \frac{n_s}{Dr_i} \qquad \text{and} \qquad r_i = \exp\left(-\frac{E_a}{k_B T}\right), \tag{3.9}$$

where A is the activation efficiency, n_s is the sheet carrier concentration, D is the

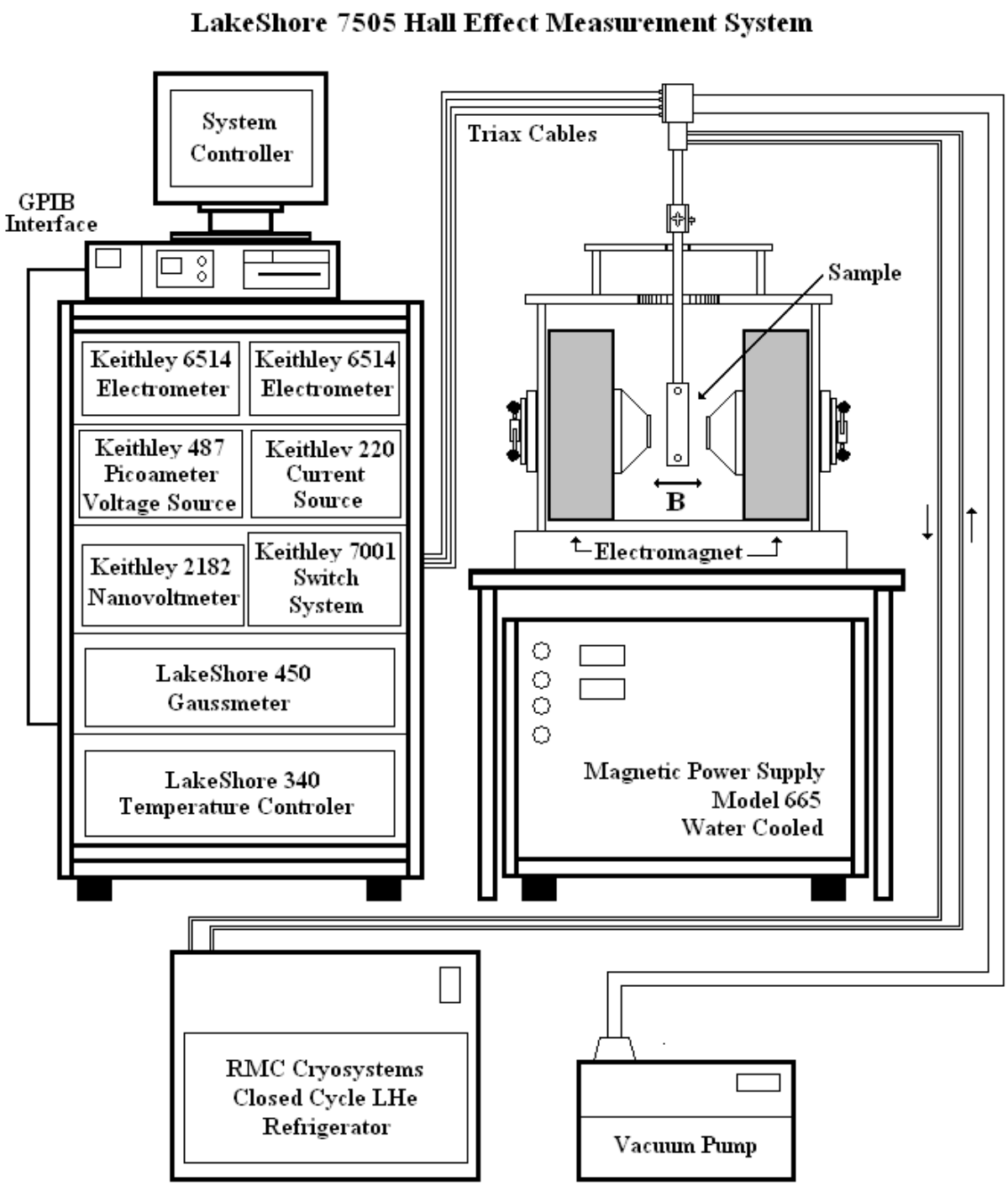

Figure 3.2. A schematic diagram of the LakeShore 7505 automated Hall measurement system for carrier concentration, resistivity, and temperature-dependent measurements. The board for room temperature measurements is illustrated and the system is also equipped with a low temperature and high temperature operating head.

implanted ion dose, r_i is the ionization rate, and E_a is the acceptor or donor ionization energy.

From these relations it can be seen that as the temperature rises more impurities become ionized causing the carrier concentration and mobility to change. For wide bandgap semiconductors the energy levels are deeper and thus require higher temperatures to activate these levels.

Optical Properties

The optical properties of the semiconductor material give insight into the dominant transitions, determination of the band gap, and the quality of the crystal structure. Materials with strong emission in a short wavelength band make for good optical device components in the UV and blue spectral regions. All the optical measurements in this study were performed using cathodoluminescence measurement techniques at low temperatures (T< 10 K).

Optical Theory

The discussion in this section follows the development and presentation found in Fellows' dissertation (22). When a solid is supplied with sufficient energy, it will emit photons as well as thermal radiation. The type of luminescence depends on the excitation source and the variance of the material's bandgap. Some examples of optical excitation are photoluminescence (PL, excitation by photons), cathodoluminescence (CL, excitation by energized electrons) and electroluminescence (EL, excitation by an electric field). There are two types of luminescence that semiconductors exhibit: fluorescence and phosphorescence. Fluorescence is the emission of photons due to a direct transition from

excited state to ground state, while phosphorescence utilizes intermediate transitions so that the luminescence persists after the excitation source is terminated. Materials that have this type of luminescence are generally referred to as phosphors (24). Semiconductors normally exhibit fluorescence.

Luminescence in semiconductors can be described in terms of the radiative recombination of electron-hole pairs. The wavelength of the luminescence is given by $h\nu = hc/\lambda = \Delta E$, where h is Plank's constant, ν is the frequency, c is the speed of light, λ is the wavelength, and ΔE is the initial energy, E_i minus the final energy, E_f, in the transition.

The electron-hole pairs relax to equilibrium through a succession of interactions with defect and impurity levels within the bandgap that eventually leads to recombination. This may include transitions from the valence to conduction band, or those levels within the band gap, such as donor and acceptor levels. The most common radiative transitions are illustrated in Figure 3.3.

Luminescence spectra can be collected for all radiative transitions that occur between two energy levels. The transition labeled as (a) in Figure 3.3 is a band-to-band transition and is generally dominant at room temperature. The energy of this transition is given by

$$h\nu = E_c - E_v = E_g, \tag{3.10}$$

where E_g is the energy gap. The free exciton (FE) transition is shown as (b) in the above figure. In this case the electron is bound to the hole through coulombic forces. The energy of this transition is the bandgap energy minus the binding energy of the two particles, and its mathematical representation is given in Equation 3.11.

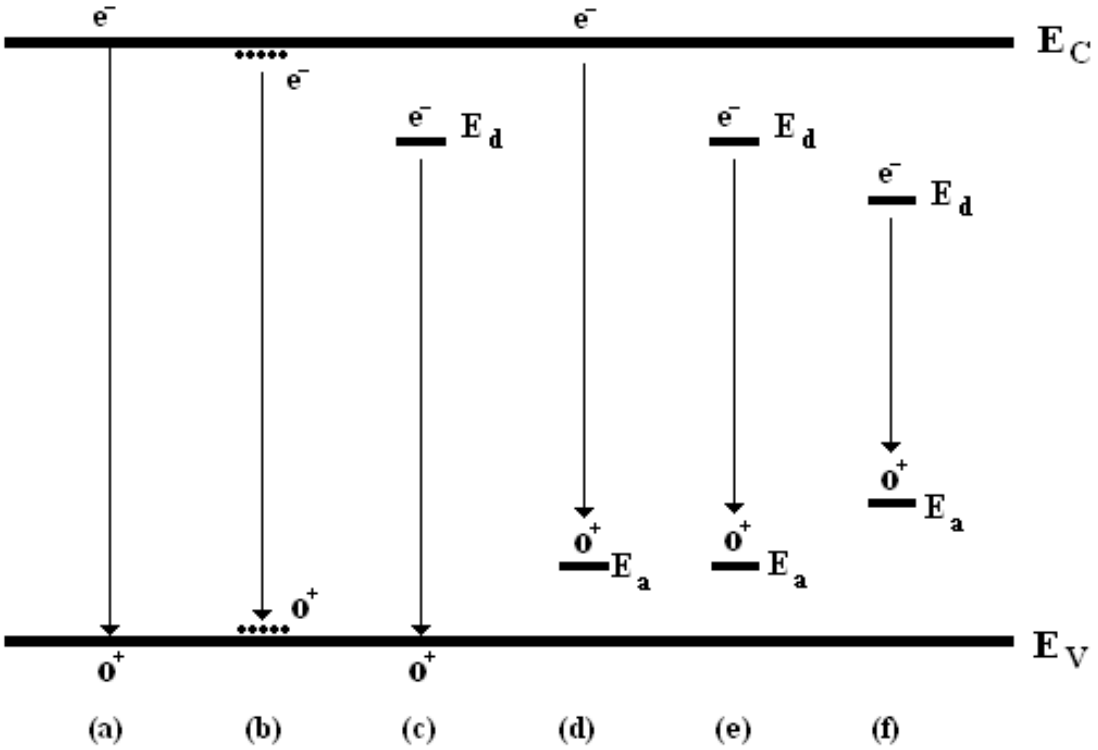

Figure 3.3. A two dimensional illustration of the most common radiative transitions that take place in semiconductors. The transitions shown are: the band-to-band transition (a), the free exciton transition (b), the neutral donor free hole recombination (c), a free electron transitioning to a neutral shallow acceptor (d), and the donor acceptor transitions for shallow and deep states (e) and (f) respectively (22).

$$h\nu = E_g - m_r^* \frac{q^4}{2\kappa\hbar^2} \tag{3.11}$$

where m_r^* is the reduced effective mass of the exciton, q is the charge, and κ is equal to $4\pi\varepsilon_r$, where ε_r is the reduce dielectric constant. Transitions (c) and (d) are the similar transitions in reverse. Transition (c) shows the transition from an electron on a neutral donor recombining with a free hole (D^0, h), while (d) illustrates the recombination of a

free electron in the conduction band and a hole on a shallow neutral acceptor (e, A^0). The energy for these transitions is given by

$$h\nu = E_g - E_{d,a}. \tag{3.12}$$

The last two transitions in the diagram are extremely important and are the same transition; only the depth of the acceptor and the donor levels change. They are the donor-acceptor pair (DAP) transitions, where an electron on a shallow donor recombines with a hole on a shallow neutral acceptor, or as seen in (f) where an electron in a deep donor recombines with a hole in the deep acceptor. The energy of this type of transition is given by

$$h\nu = E_g - E_d - E_a + \frac{q^2}{\kappa r}, \tag{3.13}$$

where r is the separation distance between the donor and the acceptor. The last term in the equation represents the electrostatic energy gained as the transition is complete and the neutral pair becomes a dipole.

The DAP transitions can have a broad spectrum due to the wide number of discrete values r can assume. This transition provides a good means of studying the interband transitions that occur in the semiconductor material. The FE transition dominates at low temperatures, with most semiconductor materials exhibiting strong excitation peaks. The DAP peak can serve as a measure of the compensation level of the material. A material which is highly compensated will exhibit strong DAP peaks and be highly resistive with a high level of shallow donor and acceptor levels.

The relative intensity of the transition feature can give insight into the electrical and structural properties of the semiconductor material. The intensity of unimplanted samples can be compared to those that have been implanted and annealed to monitor the

recovery of the lattice damage caused by the implantation. Deep defect levels in the bandgap region can trap electrons and prohibit luminescence.

Cathodoluminescence

Cathodoluminescence is achieved by exciting the semiconductor material with a stream of electrons. The incident electrons undergo a successive series of elastic and inelastic scattering events within the material. As a result of these collisions, the original trajectory of the electron is randomized. These incident electrons create thousands of electron hole pairs that eventually re-stabilize and emit photons in the process. The photons emitted are proportional to the bandgap of the material.

Electron beam penetration leads to emission by all the luminescence mechanisms of the material. This method can provide depth-resolved information by varying the electron beam energy. It can produce orders of magnitude greater carrier generation rates than typical optical excitation methods, which can be advantageous for wide bandgap semiconductors. Energies up to 100 keV can be used without inducing atomic displacement damage.

Cathodoluminescence Measurements

Cathodoluminescence (CL) measurements are taken at low temperature using a closed cycle helium refrigerator which has the ability to cool the sample stage to 5 K. The sample temperature for low temperature measurements is normally around 7.4 K due to the thermal heat generated from the samples due to the incident electrons. A Lakeshore 330 temperature controller is used to maintain the sample temperature during measurements from 5 to 300 K. The Kimball Physics EMG-12 Electron Gun and EGPS-

12 power supply with 2.4 amperes of source current provide the 10 keV electrons that are applied to the sample. The path between the beam source and the target, as well as the environment of the target, is held at a vacuum pressure of approximately $7x10^{-7}$ Torr. The electron bombardment causes the sample to emit radiation in the form of luminescence. This luminescence is collected into a lens to collimate the light and then through another lens to focus the light. The luminescence is focused into a Spex 0.5 m monochromator which then sends the signal into a GaAs photomultiplier tube (PMT) that is supplied with 1500 volts and interprets the signal as counts and sends it to the computer. The PMT is cooled using liquid nitrogen and is kept at a temperature of -30 ^{o}C during the experiment. A diagram of the experimental setup is shown in Figure 3.4 and complete operating instructions can be found in appendix A. The spectrum is taken as a function of wavelength from 1800 to 7000 Å with a step of 2 Å and an integration time of 0.1 second at each step. This data is later converted to units of eV using the conversion between energy and wavelength, $E(eV) = 1.2398/ \lambda (\mu m)$.

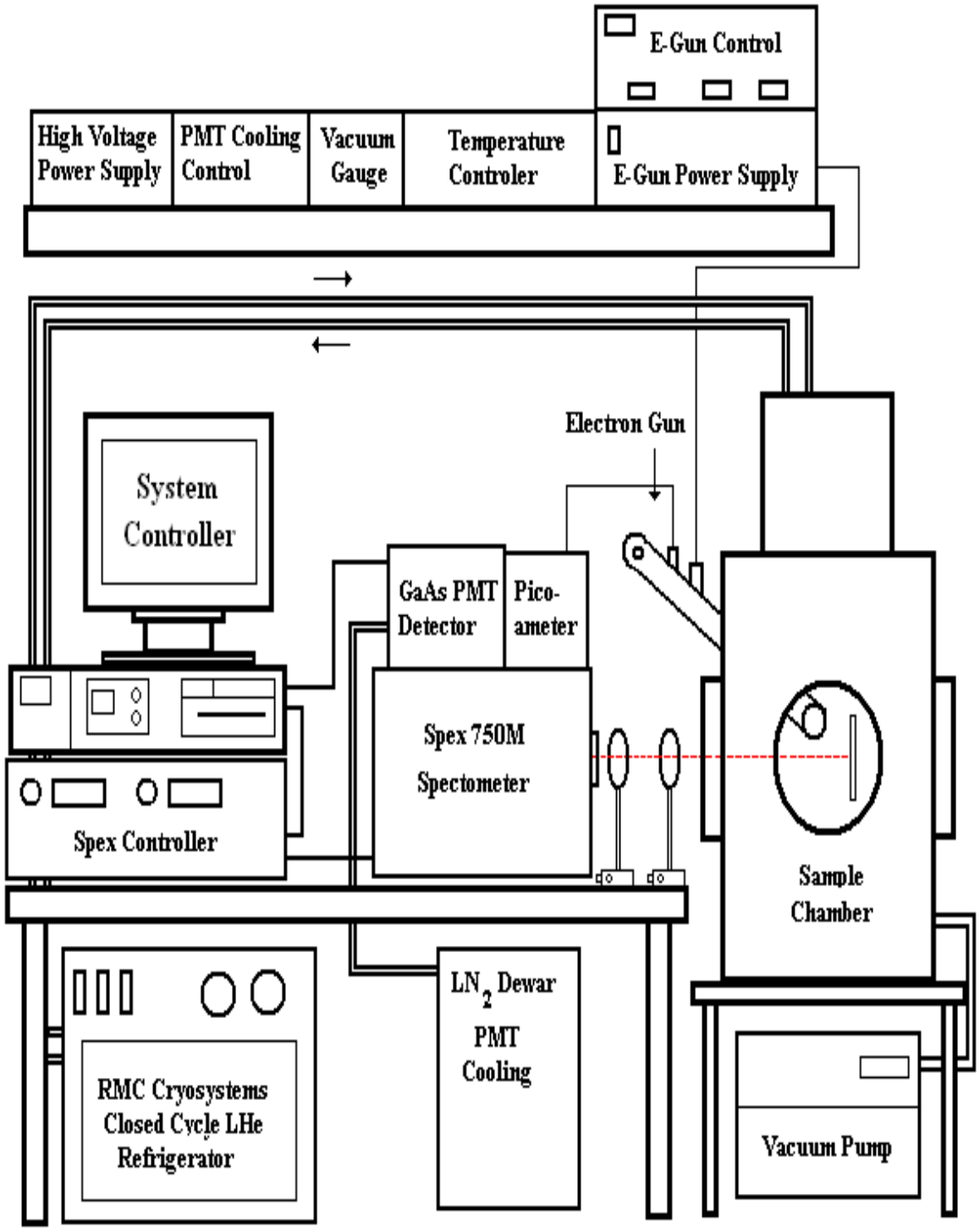

Figure 3.4. Schematic Diagram of the cathodoluminescence experimental setup designed to excite the samples through electron bombardment. It has both temperature and energy dependent capabilities.

IV. Experimental Method

In order to ensure the most accurate results, a strict sample regiment was performed so that all samples were treated identically. This process is detailed in this chapter, from arrival of the samples to completion of the measurements. Throughout the sample processing steps, precautions were taken to limit exposure to extreme moisture and temperature conditions and also to protect the samples' surfaces. Samples for this study were acquired from Sensor Electronic Technology, Inc. (SET). Detailed operating instructions for all equipment and preparation techniques can be found in appendix A.

Sample Specifications

Sample quality can be directly linked to the growth conditions of the material. Samples from SET were grown by a unique form of metal organic chemical vapor deposition (MOCVD), known as migration-enhanced MOCVD, or MEMOCVD. MEMOCVD has faster deposition rates and produces smaller screw dislocation densities than MOCVD (25). This growth method produces higher quality wafers, especially for $Al_xGa_{1-x}N$ with Al concentration above 20%. SET, Inc. developed the MEMOCVD growth method in 2003 and have reported excellent quality nitride material with this new growth technique. $Al_xGa_{1-x}N$ with Al content up to 50% from SET has always exhibited excellent optical quality upon arrival. The MEMOCVD technique ensures an improved material quality resulting in better device performance.

MOCVD and molecular beam epitaxy (MBE), both common growth techniques, have advantages and disadvantages in the growth of complex nitride materials, such as AlInGaN. MOCVD growth requires high temperatures, greater than 900 ^{o}C, which

impose limitations on the abruptness of the deposited heterointerfaces. This has a direct impact on the transport properties of the electrons. MBE growth takes place at lower temperatures; however, the GaN buffer layer grown at these temperatures is conducting, rendering it unsuitable for high frequency device performances (25). With MEMOVCD growth, the temperatures can be reduced further by at least 150 ^{o}C without compromising material quality. The growth was carried out using controlled precursor pulsed flows to achieve accurate thickness control over large area substrates. The Al content varies less than 3% over the entire wafer surface. The duration and waveforms of the precursor pulses might overlap, which allows for a continuum of growth techniques. For MEMOCVD, a better mobility of pre-cursor species on the surface is achieved, resulting in better atomic incorporation and improved surface coverage. Trimethyl aluminum, trimethyl gallium, and ammonia were used as the precursors for Al, Ga, and N, respectively. MEMOCVD combines a fairly high growth rate for buffer layers with reduced growth temperature and improved quality for active layers.

The samples were grown on c-plane sapphire substrates with a thin AlN buffer layer to help prevent crystal imperfections caused by the lattice mismatch between the sapphire and the $Al_xGa_{1-x}N$ lattice constants. AlN is a closer lattice match to $Al_xGa_{1-x}N$ and therefore reduces the number of material defects. This buffer layer is followed by the growth of 1 μm of $Al_xGa_{1-x}N$ and then a 500 Å AlN encapsulant to protect the surface of the sample during the annealing process. The AlN encapsulant was grown in-situ without breaking vacuum of the growth chamber. The thickness and growth conditions of the AlN cap were chosen based on research on encapsulants of GaN accomplished by Fellows (22).

Samples from SET, Inc. are grown on double-side polished sapphire substrates with only a small number scribed in the back surface, making it difficult to determine the front and back side once the samples have been cut. Extra precautions must be made to always mark the backside before cutting the wafer.

Cathodoluminescence Measurements

CL measurements were taken on the as-grown wafers to determine the Al concentration. The most dominant peak in the spectrum should correspond to a band-to-band transition which is equal in energy to the band gap of the material. The bandgap is proportional to the Al mole fraction and thus, the luminescence peak of the material can be used to determine the Al mole fraction of $Al_xGa_{1-x}N$. The mole fraction of the wafer is determined through use of the fact that the energy band gap of $Al_xGa_{1-x}N$ increases almost linearly from that of GaN (3.4 eV) to that of AlN (6.2 eV), as shown in Equation 4.1, where the bowing parameter, b, was taken to be one. The bowing parameter has been experimentally found to range from 0.78 to 1.14 depending on temperature (27).

$$E_g(x) = xE_g(AlN) + (1-x)E_g(GaN) - bx(1-x) \tag{4.1}$$

The measurements are taken at 7.4 K on three or more locations on the wafer to check for the uniformity of the Al distribution. The CL spectra of the wafers as they were received from SET, Inc are shown in Figure 4.1. The original CL spectra are taken as a function of wavelength. The relation, $E(eV) = 1.24/\lambda(\mu m)$, is used to convert the spectrum to photon energy. For all the samples, the spectra exhibited identical features regardless of whether the measurements were taken from the edge or middle of the wafer; however, the intensity decreased as the sampling moved from the middle to the edge. The spectra shown in the figure are the results from sampling the middle of the wafers.

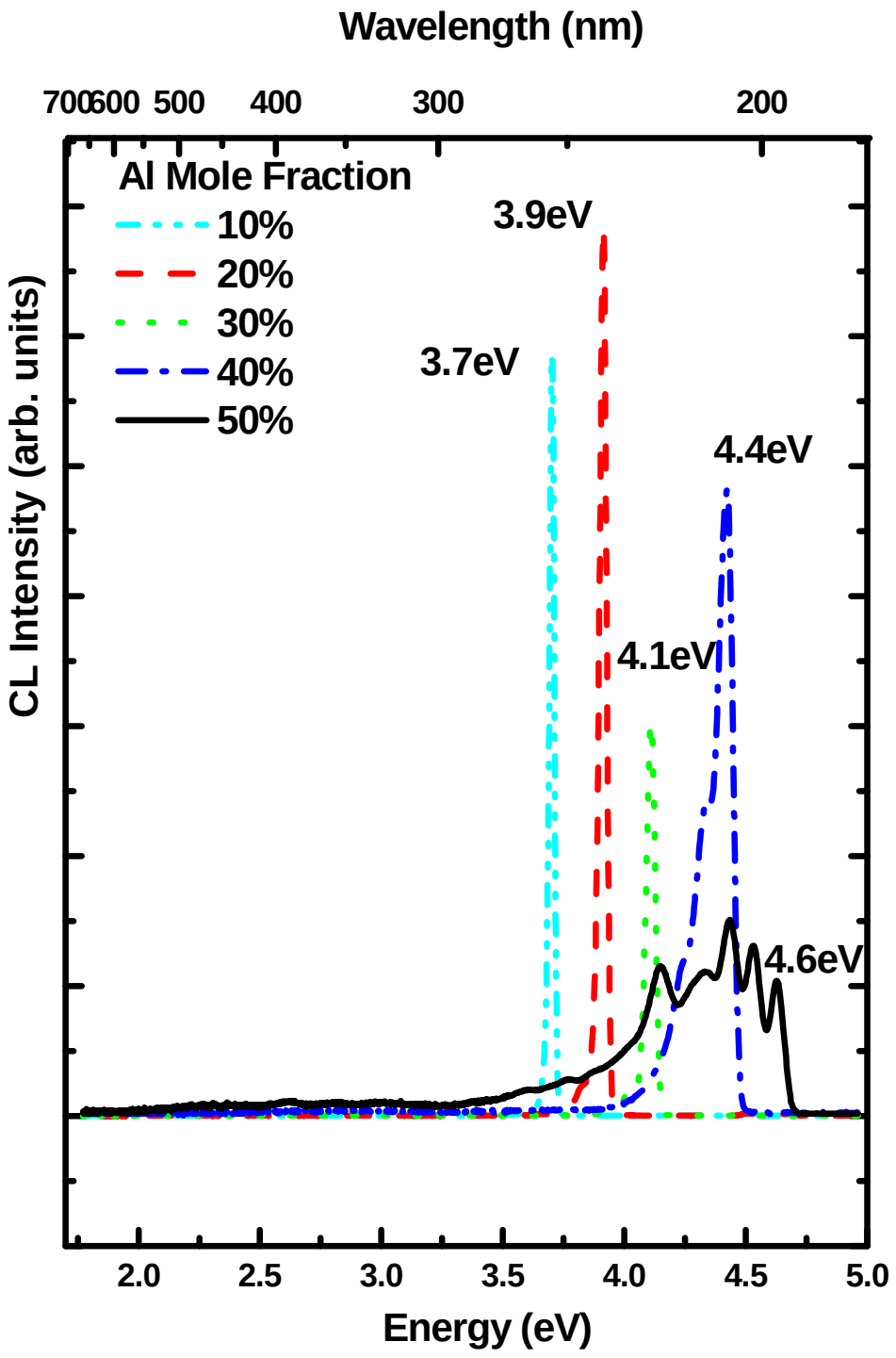

Figure 4.1. CL Spectra taken at 7.4 K on the original wafers sent from SET, Inc. in order to investigate the quality of the material, as well as determine the Al mole fraction of each wafer.

The CL spectrum for the $Al_xGa_{1-x}N$ wafers with 10, 20, and 30% Al concentration exhibit a sharp band-to-band peak at a 3.7, 3.9, and 4.1 eV, respectively. The spectrum of the $Al_{0.4}Ga_{0.6}N$ wafer shows a broadened band-to-band peak at 4.4 eV with two smaller peaks, seen as shoulders on the low energy side of the band-to-band peak. The spectrum of the $Al_{0.5}Ga_{0.5}N$ wafer has five peaks between 4.149 and 4.627 eV, with the peak at 4.425 eV exhibiting the highest intensity. The energies of these peaks are 4.149, 4.333, 4.425, 4.528, and 4.627 eV. From the CL spectra, it appears that the high Al concentration has degraded the crystal quality of the material. SET was contacted regarding the wafer quality of the $Al_{0.5}Ga_{0.5}N$ and responded by sending the transmission spectrum they had taken for the wafer, shown in Figure 4.2, which clearly shows that the band edge is about 271 nm, which would make the Al mole fraction of the wafer 51%. With this evidence, the sample could not be refused and further processing continued, assuming an Al mole fraction calculated from the transmission spectrum sent from SET, Inc. The energy of the band-to-band transition and equation 4.1 were used to calculate the Al mole fractions of the wafers and the results are summarized in Table 4.1.

Table 4.1. Values of interest for the determination of the Al concentration from CL spectra. The Al concentration of the $Al_{0.5}Ga_{0.5}N$ wafer was determined from transmission measurements sent from SET, Inc.

Mole Fraction (%) (Requested)	Peak Wavelength (nm) (Observed)	B-B Energy (eV) (Calculated)	Mole Fraction (%) (Calculated)
10	335.0	3.701	14.27
20	316.8	3.914	24.50
30	301.6	4.111	33.20
40	280.4	4.422	45.74
50	273.8	4.627	51

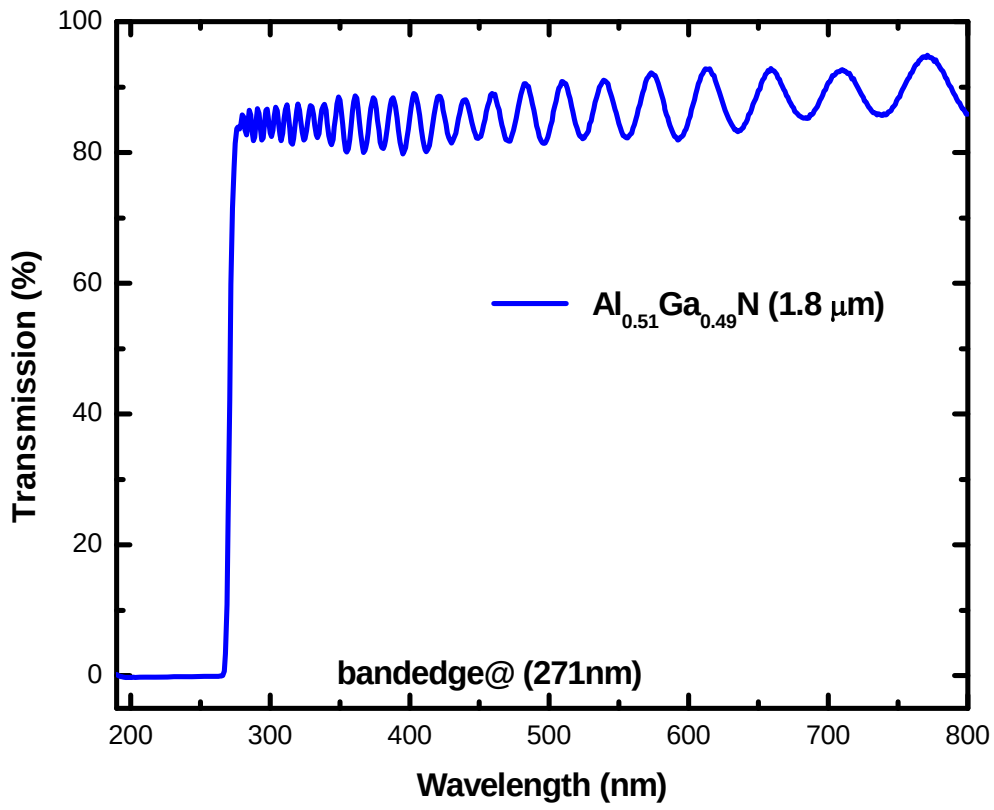

Figure 4.2. The transmission spectrum sent from SET, Inc., for the $Al_{0.5}Ga_{0.5}N$ wafer that shows a clear transition at 271nm indicating a good quality wafer that has 51% Al concentration.

Sample Cutting

The wafers are cut twice during the preparation process. First the wafers are carefully cut into four quadrants in preparation of silicon implantation, as illustrated in Figure 4.3(a). Each wafer quadrant is placed surface-side down on blue semiconductor dicing tape to secure and protect it during the cutting process. The quadrants are cut with a Loadpoint Limited Microace Series 3 saw, enabling precise adjustment of contact

pressure to ensure that the $Al_xGa_{1-x}N$ is not damaged in the process. This processing step was accomplished courtesy of Mr. Larry Callahan, of AFRL/SNDD.

The wafers from SET are polished on both the front and back sides and thus it is virtually impossible to determine which side is the front, except for a small etching at the bottom of the back of the sample. Prior to having these wafers cut, it is important to put a mark on the backside of each quadrant to ensure the front and the back side can be determined once the quadrants are removed from the tape.

The second cut, illustrated in Figure 4.3(b), comes after the ion implantation with each of the wafer quadrants cut into 5 by 5 millimeter pieces. During the cutting process, the small sample pieces can detach from the tape and become destroyed. Each quadrant yields approximately 15 samples and several scrap pieces. The small scrap pieces were used to determine the rate at which the AlN encapsulant is removed during a wet KOH etch of the various wafers.

The samples are returned from the cutting process still on the cutting tape. The samples should carefully be removed from the tape and scribed immediately before being placed in the glassine envelope to ensure that the front and back sides can be differentiated. A diamond tip pen is used to scribe the samples with a number corresponding to their placement in the wafer quadrant and also with a unique symbol that corresponds with their wafer quadrant. This ensures that each sample can be traced back to its original placement in the whole wafer and that each sample's markings are unique.

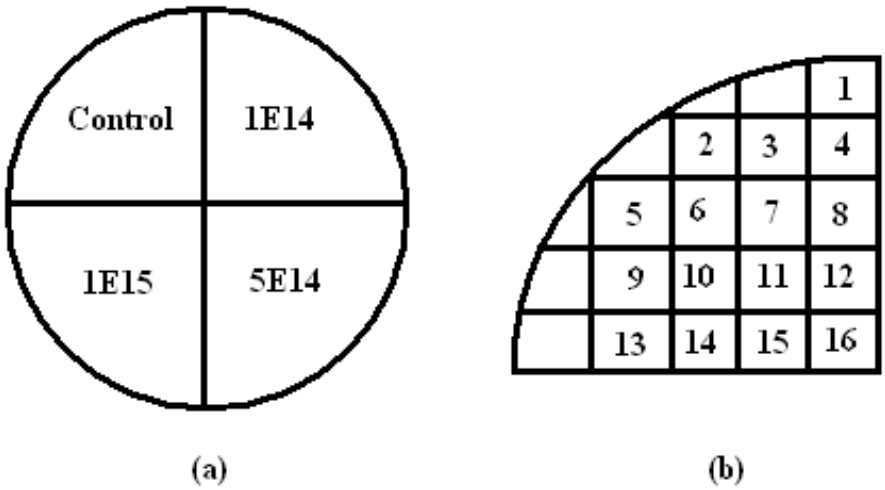

Figure 4.3. A diagram to illustrate how the wafers are divided in preparation (a) for ion implantation and (b) for the annealing processes. The wafer shown in (a) is marked with the Si implantation dose for each quadrant. The wafer quadrant in (b) illustrates the naming system to track the location of the samples.

Ion Implantation

The introduction of silicon as a dopant in the $Al_xGa_{1-x}N$ wafers was conducted with ion implantation rather than diffusion or in-situ doping, due to advantages it offers with regard to device manufacturing. Ion implantation enables doping profile predictability, strict control of doping concentrations, and the ability to dope selective areas of a material. These capabilities are critical for the design parameters of most integrated circuits. Most semiconductor manufacturers use ion implantation almost exclusively for doping in silicon ICs (1). There are also disadvantages associated with

this doping technique that must be a considered when ion implantation is chosen as the doping method.

Ion implantation is a surface modification process that consists of bombarding the sample surface with a high energy ion stream. The ions are produced in an accelerator and can have typical energy ranges of 10-500 keV. Directed into a beam, they are uniformly scanned across the wafer's surface until the desired dose is reached. A diagram of a typical ion implantation setup can be seen in Figure 4.4. Common implanted doses range from 10^{11} to 10^{16} ions per cm^2. The profile of the implanted ions can be realized by considering the stopping mechanisms of the implanted ions in the host material. The depth of the ions into the material depends on the mass and energy of the ions as well as the atomic mass and density of the host material.

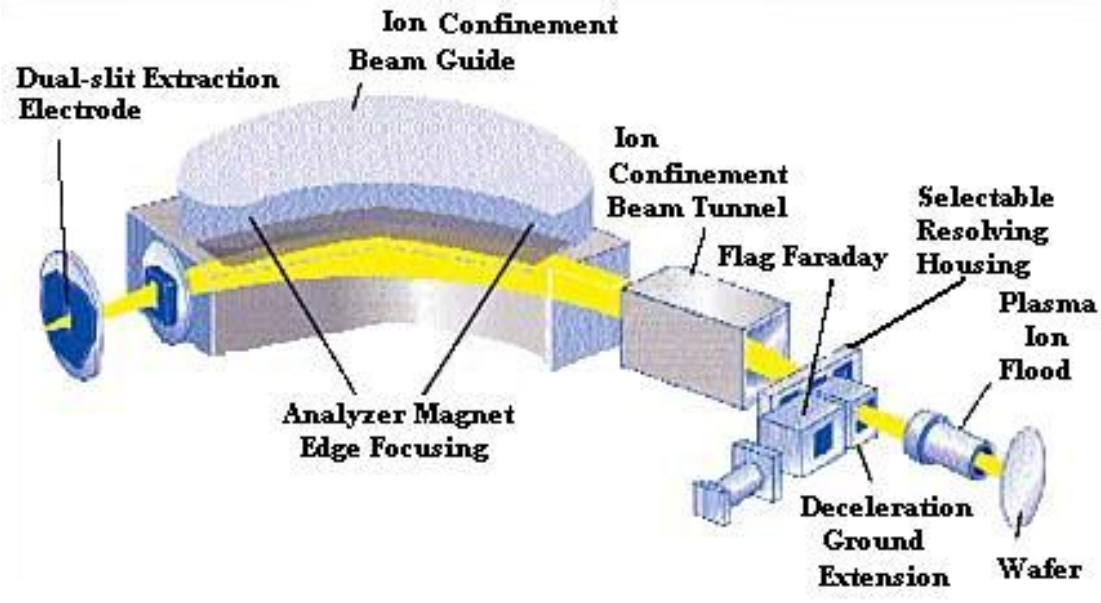

Figure 4.4. A schematic diagram of a typical ion implantation experimental design (78).

The implanted ions enter the material and dissipate their energy through interactions with the host atoms until they finally come to rest. Electronic and nuclear interactions are the two main stopping forces that affect the movement of the dopant ions (22). When the incoming ions collide in an inelastic manner with the host atoms' bound electrons, the energy is transferred into heat or excitation of the host atoms. This is the electronic stopping mechanism, and it is found to be proportional to the velocity of the ions. The nuclear stopping mechanism occurs when the incident ions collide with host atoms, causing equilibrium lattice position displacement of the host atoms. Displacing one host atom can have a domino effect, displacing atoms throughout the material. The electronic stopping dominates for ions with high energies, while the nuclear stopping is the main force in low energy ions. This is due to the high energy ions moving too fast to transfer enough energy to an incident atom during a collision to displace it. The projected stopping range is therefore found to be proportional to the incident energy of the implanted ions.

The first unified theory to determine the stopping and range of ions in matter came about in 1963 and is named the LSS-theory after the initiating scientists Lindhard, Scharff, and Schiott (78). The theory, in the beginning, made some broad approximations in the statistical model representing the atom to atom collisions as a Gaussian distribution centered around the average projected range, R_p, and having a standard deviation of ΔR_p. In the theory, the penetrating ion beam is considered to scan the target material uniformly to limit the variation to the projected direction only, i.e. to reduce the lateral straggle. The theory was valid for the entire atomic spectrum and found to be accurate to within a factor of two for single element amorphous targets (28).

The theory was improved in the next twenty years by replacing some of the initial approximations with new advances in theory, and the advent of computers introduced numerical techniques which also increased accuracy. As of 2003, the accuracy of determining the stopping ranges of ions in matter was within 5% margin of error overall, with a 6% margin of error for heavy ions, and a less than 2% margin of error for high velocity light ions (79).

The theory considers the mass and energy of the ions as well as the atomic weight and density of the host material to determine the parameters that are used to define the shape of the Gaussian profile, the projected range, and the projected straggle of the ions. The volume concentration of the ions is given in equation 4.2 with φ being the implanted ion dose (22).

$$N(x) = \frac{\varphi}{\sqrt{2\pi}\Delta R_p} \exp\left[-\left(\frac{x - R_p}{\sqrt{2}\Delta R_p} \right)^2 \right]. \tag{4.2}$$

The peak concentration will occur at a distance R_p beneath the surface. Considering equation 4.2, the peak concentration is easily determined and given by.

$$N(R_p) = \frac{\varphi}{\sqrt{2\pi}\Delta R_p}. \tag{4.3}$$

The Gaussian profile from the LSS theory is predicted for an amorphous target but has been found to be a good first order approximation for crystalline solids as well. When the ion implantation is performed, the target is tilted (normally 7º off axis) in relation to the incident ion beam, making the incoming beam's target appear more amorphous. Having the ion beam enter the material off-axis ensures that the ions do not travel in

between planes in the crystal and move unobstructed from collisions. The tilt, in effect, reduces the effects of channeling.

The calculations to determine the ion depth profile were accomplished using a prewritten commercial code called TRIM which is short for TRansport of Ions in Matter (28). TRIM is a comprehensive program that considers all of the kinetic mechanisms associated with the loss of energy of the ion such as sputtering, ionization, phonon production, and target damage. An example of the predicted depth profiles of silicon and gold ions into a GaN sample with a 500 Å AlN encapsulant can be seen in Figure 4.5 for an ion dose of $1x10^{15}$ cm^{-2} at various ion energies.

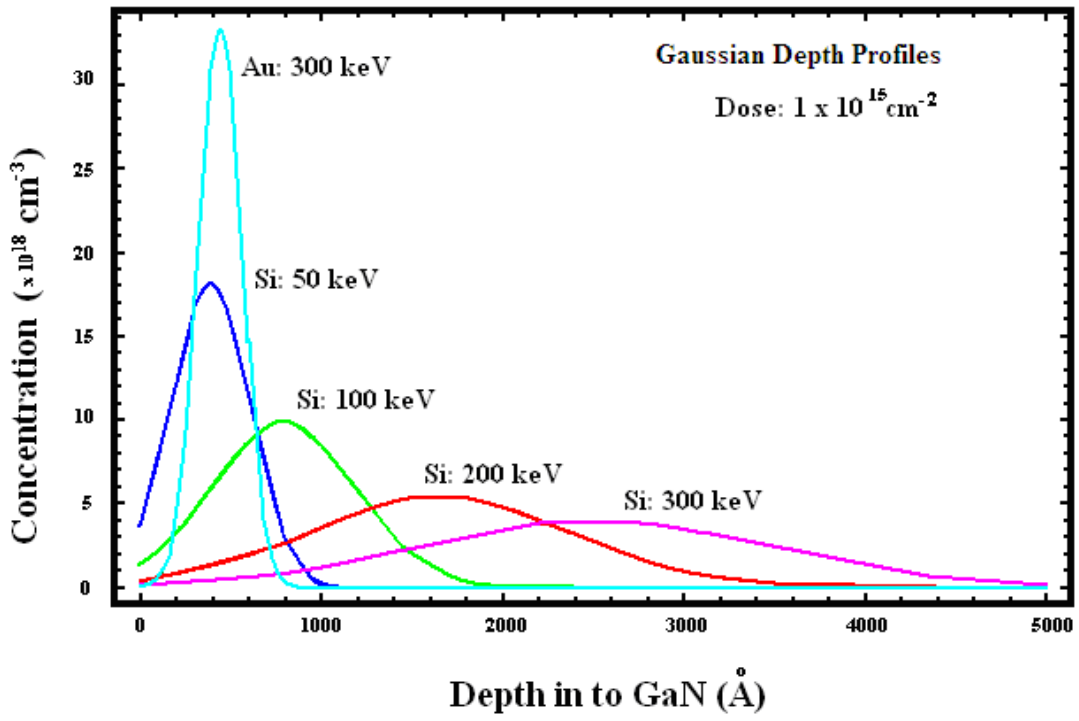

Figure 4.5. The predicted TRIM depth profiles for Si ions at various energies and Au at 300 keV in to GaN with a 500 Å AlN encapsulant to illustrate the effects that the ion's energy and mass have on the shape of the depth profile.

The program can be used for complex targets with up to eight unique layers and follows the atom trajectories in the target in-depth. Ideal implantation would result in the peak concentration lying directly beneath the surface of the $Al_xGa_{1-x}N$ material, requiring the Si ions to travel through the 500Å AlN encapsulant. The ion implantation conditions such as energy and dose were determined in advance using TRIM code. Ion implantation services are contracted out through CORE Systems (Sunnydale, CA). The implantation was accomplished with the $Al_xGa_{1-x}N$ wafers at room temperature, tilted at a 7º to minimize channeling. The implanted silicon ions had an energy of 200 keV and doses of $1x10^{14}$, $5x10^{14}$, and $1x10^{15}$ cm^{-3}.

Annealing

The discussion in this section follows the development and presentation found in Fellows' dissertation (22). The implanted ions enter the host lattice and slowly dissipate their energy through electronic and nuclear stopping mechanisms, leaving an assortment of defects in their wake. As mentioned previously, nuclear stopping involves an incident ion colliding with the host atom and displacing it from its equilibrium lattice position. The displaced host atom will then collide with other atoms/ions instituting a cascading effect that leaves the crystal lattice in a disordered state littered with simple and complex defects that will degrade the electrical and optical properties of the material. The implanted ions will most likely come to rest in an interstitial position within the crystal lattice. To repair the disordered state of the crystal and shift the implanted ions to electrically active lattice positions, the sample must endure a high temperature anneal. It is a general rule that the annealing temperature required to fully remove the defects is ⅔

of a semiconductor's melting point. Wide band gap semiconductors have high melting points and can require temperatures above 1300 ºC to repair all of the induced lattice disorder (80). Annealing is a thermodynamic process thus making the temperature and time theoretically interchangeable so that lower commercially viable temperatures can produce equivalent results as higher temperatures by extending the annealing time.

The extent of the damage to the lattice depends mostly on the mass, energy, and dose of the incident ion. Other factors such as the targets temperature, the atomic mass and density of the host, and the electronic structure of the target material also can affect the damage profile. The most relevant factors are the ion's mass and energy, because an increase in either produces magnitudes of greater damage to the crystal structure. Ions that have a light mass, as a proportion of the host atom's mass, tend to leave tracks within the crystal with relatively no damage. However, as these ions slow down, nuclear stopping begins to overshadow the electronic stopping, increasing the number of collisions with host atoms and thus increasing the damage concentration. Heavier ions leave a broad track of damage through the entire path they travel through the material. An illustration of the damage caused from light and heavy ions are shown in

Figure 4.6. The implanted ions will come to rest a short distance after their last collision, leaving a damage profile that has its heaviest concentration slightly closer to the surface than the implantation profile.

A single ion can cause hundreds or thousands of displacements depending on the experimental parameters of the incident ion and the target material. The damage profile

may be so large that the concentration of displacements is on the order of the atomic density of the crystal lattice; in this case the crystal structure is completely destroyed leaving an amorphous structure. Damage on this great of a level suppresses all electrical and optical properties of the material and may not be able to be repaired through high temperature annealing.

Ionic materials, which comprise the majority of semiconductors, are more resistant than most substances to becoming amorphous. These materials exhibit natural dynamic annealing in which they repair structural damage during the implantation process. Dynamic annealing is a beneficial property because it quenches the formation of stable lattice disorders that resist repair (29). Raising the substrate temperature during the implantation can enhance the effects of dynamic annealing. The added heat increases the lattice vibrations and aids in moving the atoms and ions into equilibrium lattice sites.

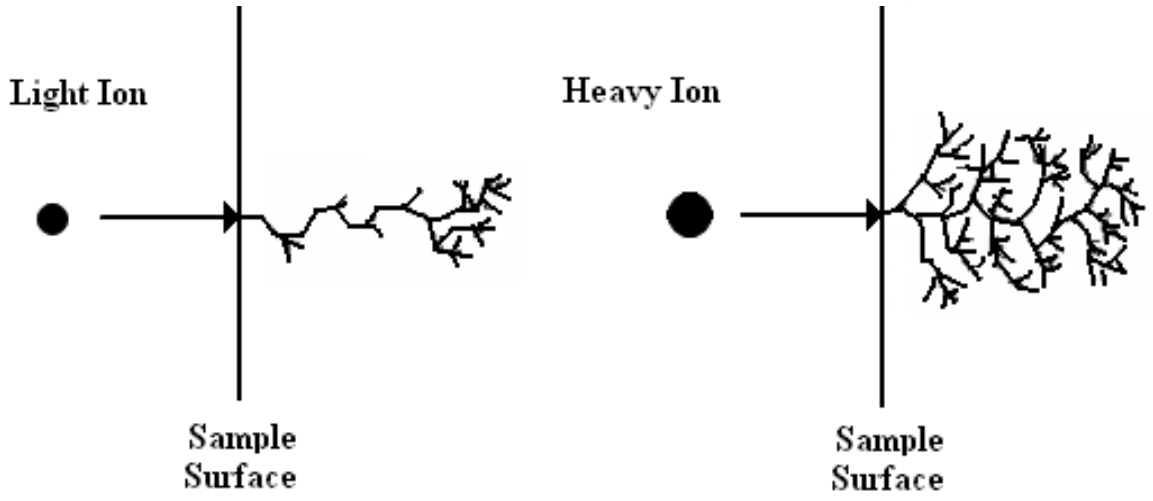

Figure 4.6. An illustration of the lattice disorder that results from the ion implantation of a light and heavy ion, respectively (22, 37).

The structural disorder of ion implanted $Al_xGa_{1-x}N$, with x from 0 to 0.6, was studied by Kucheyev and Williams, *et al*. (30). They observed that increasing Al content strongly enhanced the effects of dynamic annealing in $Al_xGa_{1-x}N$. They reported the amorphization behavior to be different from that of GaN, in that $Al_xGa_{1-x}N$ did not display any preferential surface disordering. Rather, the $Al_xGa_{1-x}N$ exhibited "a rapid transition from the saturation regime to the nucleation-limit amorphization in the crystal bulk" when implanted above the critical dose (Au, 300 keV, $3x10^{15}$ cm^{-2}) and that this effect is relatively independent of the Al concentration of the sample (30). The Au implantation resulted in lattice disorder mainly in the bulk region of the $Al_xGa_{1-x}N$ where the nuclear defect profile has a maximum with the given implant conditions and a dose up to $1x10^{15}$ cm^{-2}. The bulk region exhibits saturation while the damage level at the near surface region grows up to the saturation level. The surface of GaN shows a strong preferential site for amorphization resulting in the crystal becoming amorphous layer by

layer beginning at the surface. $Al_xGa_{1-x}N$, on the other hand, becomes amorphous spontaneously in the bulk region and then proceeds to the surface layers. XTEM (cross-sectional transmission electron microscopy) measurements show the existence of buried amorphous layers in the $Al_xGa_{1-x}N$ epilayers, which increase with Al content, when implanted above the critical dose. XTEM measurements also revealed similar extended defects and defect clusters as those found in GaN.

The incident ions collide with the host atoms resulting in a multitude of defect complexes involving vacancies, antisites, and interstitials. When any one of these defects occurs, they produce unpaired valance electrons that cause the defect to become ionized. An aluminum vacancy, V_{Al}, leaves four nitrogen atoms three electrons short of forming complete valance shells, making the defect a triple acceptor. On the other hand, a nitrogen vacancy, V_N, creates a center with four Al or Ga atoms, with each atom having three available valance electrons. Two of these atoms will bond, forming an electron-electron pair, thus leaving this defect a single donor. An antisite in group III-V compound semiconductors, when the anion host atom resides on the cation lattice site or vice versa, can act as a double donor or a double acceptor. For example, a gallium or aluminum antisite, Ga_N or Al_N, is two electrons short of completing all the necessary bonds of the N atom, thus producing a double acceptor. While a nitrogen antisite, N_{Ga} or N_{Al}, will have two extra electrons after completing all the bonds and is therefore a double donor.

The ionic nature of the defects will cause them to combine and form defect complexes with the defects mentioned above and those involving the Si-implanted ions. In III-V semiconductors, it is energetically favorable for a group IV dopant to occupy

either the cation or anion lattice position acting as a single donor or a single acceptor. A silicon ion occupying a gallium lattice site, Si_{Ga}, is a single donor. This defect will be attracted through Coulomb forces to a triple acceptor V_{Al}. These two defects combine to form a double acceptor complex. The host atoms and the implanted ions strive to achieve a lattice configuration with the most favorable energy configurations, which represents the primary determinate as to which types of defect complexes form.

These defects create deep energy levels within the band gap that act as non-radiative recombination centers for the free carriers, essentially trapping them and preventing their participation in the conduction. These traps compensate the shallow donors and acceptors that are intentionally introduced into the material to enhance the conduction properties. The random distribution of the atoms that results from the ion implantation increases the number of scattering centers which can reduce free carrier mobility. The material defects are not all a result of the ion implantation; some defects are inherent to the material growth techniques and result from the lack of a perfectly lattice-matched substrate on which to grow the $Al_xGa_{1-x}N$ epilayers. Evaluation of the as-grown material is essential for the determination of the as-grown defect level to provide a baseline for evaluating the degree of crystal damage recovery of the implanted samples. Defects, such as disassociated host atom, can also result from the high temperature anneal requirement.

The high temperature anneal is designed to give the host atoms and implanted ions enough thermal energy to form the ordered lattice structure that the material initially obtained. The goal is to repair the defects that were created and to shift the implanted ions to electrically active lattice positions. It is more difficult to recreate lattice order in

compound semiconductors compared to elemental semiconductors due to the difficulty involved in getting the atoms to occupy the correct anion or cation lattice sites. The stoichiometry of the crystal must be maintained, which is difficult due to the mass difference of the host atoms which allow lighter atoms to travel further once displaced from their equilibrium positions. At high temperatures, the nitrogen atoms become volatile and disassociation of these atoms becomes a setback.

There are three common techniques used to prevent disassociation of the material's host atoms: inert gas overpressure in the annealing chamber, face-to-face proximity annealing configuration, and a protective encapsulant deposited on the surface of the samples. With inert gas overpressure, an overpressure of the element with the lowest vapor temperature, normally the group V atoms, applies a slight pressure to the sample surface reducing the group V disassociation. In the face-to-face configuration, samples are placed on top of each other with the implanted surfaces in direct contact. This precautionary method forces the disassociated N atoms into the surface of the other sample. This configuration also protects the sample surface from pitting, cracking, and peeling from the high anneal temperatures. The most effective way to prevent group V evaporation is to cover the surface of the sample with an encapsulant that can be grown on epitaxially or deposited after growth. An in-situ grown encapsulant should be deposited uniformly, so that it does not affect the depth profile of the implanted ions. The encapsulant material should have a thermal expansion coeffient close to that of the sample material as to not induce strain related defects during the annealing process. Thin encapsulants have been shown to handle lattice mismatches better and also resist pealing and cracking better than thicker caps (22). Common encapsulants for nitride materials

are AlN and SiC due to their high thermal integrity and their ease of removal from the surface after the anneal.

A conventional furnace anneal, CFA, is the most common type of anneal used for post ion implantation treatments. They are characterized by their long rise times as well as long dwell times. CFA's are capable of reaching higher temperatures (≤ 1200 ºC) and maintaining them reliably for extended periods. Defect and defect complexes have different thermal activation energies and therefore restore themselves at different temperatures. The CFA anneal allows the sample to experience each temperature range for a short duration, thus allowing different types of defects to recover. Another type of annealing is a rapid thermal anneal, RTA, which is defined by its ability to quickly ramp the temperature to the desired set point using halogen lamps. Rapid thermal anneals have very short dwell times, typically less than a minute. Short dwell times limit the amount of dopant diffusion that takes place at high temperatures and prohibits the widening of the depth profile. RTA's are common on production lines due to their quickness and reliability. Annealing can also be accomplished using a high powered ion beam annealing to melt the surface layer of the material and allow it to rapidly solidify. High powered ion beam annealing is not often applied due to atom disassociation occurrences.

All samples for this study were annealed in an Oxy-Gon Industries furnace uniquely designed to shorten the rise and fall times of the sample. The furnace is equipped with separate chambers for sample access and heating, which allows samples to be inserted and removed via a preheated access chamber without altering the heating chamber's temperature. The quick temperature change from room temperature to temperatures higher than 1150 ºC allows the sample to spend more time at the actual

annealing set point temperature. The sample's temperature is rapidly decreased from the annealing temperature to room temperature once the annealing time has expired. The Oxy-Gon furnace has the capability to be heated to 2500 ^{o}C, however, most commercial furnaces do not exceed 1200 ºC. The $Al_xGa_{1-x}N$ samples in this study were annealed from 1150 to 1350 ^{o}C from 20 to 40 minutes. Specific operating instructions for the furnace can be found in appendix A.

In preparation for the anneal, this study's samples were placed face-to-face and held together by wrapping tantalum (Ta) wire around them at the center of the sample's width and depth planes, and intertwined and secured at top center, similar to the way packages are often wrapped with string. The sample "packets" are placed on the graphite hearth in the access chamber and then covered with a two inch sapphire wafer to ensure that the samples remain on the hearth during the transport into the heating chamber. The environment inside the sample access and heating chambers is placed under a vacuum of 10^{-6} Torr. In order to rid the chambers of oxygen and other contaminates the chambers were flushed several times before being filled with high purity nitrogen gas. The heating chamber is then warmed to the desired temperature. Once the anneal temperature has stabilized, the samples are moved into the heating chamber. The official start time for the anneal begins once the samples are in the heating chamber. Sample temperature profiles of set point and furnace stabilization rates are illustrated in Figure 4.7.

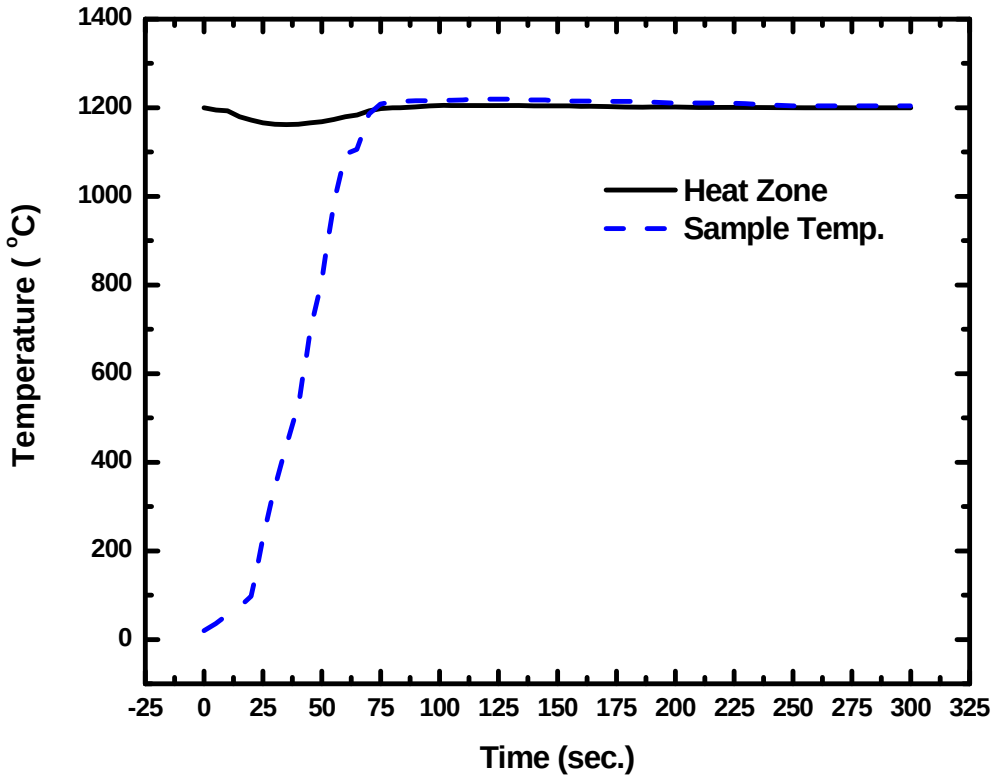

Figure 4.7. The temperature profile for the Oxy-Gon furnace used for the high temperature post implantation anneal. It takes about 75 seconds for the heat zones temperature to stabilize after the samples are introduced into the chamber and also to bring the samples up to temperature.

After the heating phase, the samples are quickly lowered from the heating chamber and cooled to room temperature in a flowing N_2 ambient to prevent surface oxidation. The Ta wrapping wire survives the anneal intact, but becomes brittle enough to easily break off. The samples are taken to the clean room before being separated and inspected for damage.

AlN Encapsulant Removal

After the high temperature anneal, the AlN encapsulant, which must be removed to expose the $Al_xGa_{1-x}N$ surface, was eliminated by soaking the samples in a 0.5 molar solution of potassium hydroxide (KOH) and de-ionized (DI) water. The etch rate of the AlN in the KOH solution varied as a function of the Al mole fraction of the sample material. The etch rate rapidly reduced as the Al mole fraction of the material increased from 10 to 50%. A systematic study of the AlN etch rate as a function of Al mole fraction in $Al_xGa_{1-x}N$ was carefully conducted to determine the time for each type of sample in the solution. The etch time varied from 5 minutes for GaN to 20 minutes for $Al_{0.5}Ga_{0.5}N$. Figure 4.8 illustrates the etch rate of the AlN as a function of Al concentration.

After the removal of the AlN cap, the samples were rinsed thoroughly with DI water before being placed in an acidic bath of 3:1 HNO_3 and HCl (known as aqua regia) for two minutes to clean the sample surface of oxidation. Following the acid bath, the samples were rinsed again with DI water and blown dry with N_2 in preparation for the deposition of metal ohmic contact stacks.

Ohmic Contacts

The electrical properties of the Si-implanted $Al_xGa_{1-x}N$ could not be obtained without the deposition of an ohmic contact. Once the samples were cleaned, they were placed in a van der Pauw shadow mask which only permits metal to be deposited in small points onto the four corners of the sample. The number of samples that could be processed at one time was restricted by the van der Pauw mask's ten sample limit and the evaporator's two mask capacity.

The metal stacks of Ti/Al/Ti/Au, with thicknesses of 120/40/80/55 nm, were deposited in the clean room using a Denton Evaporator (64). The evaporation was performed under vacuum of 10^{-7} torr, utilizing high purity metal sources. As-deposited contacts exhibit rectifying behavior, so they were heated for a short period to instill ohmic properties. The contacts were rapidly thermally annealed in a clean room furnace called an RTP (rapid thermal process), where they were heated to 900 ^{o}C for 30 seconds in flowing nitrogen ambient. The resulting samples with highly ohmic contacts then underwent electrical, and later, optical testing.

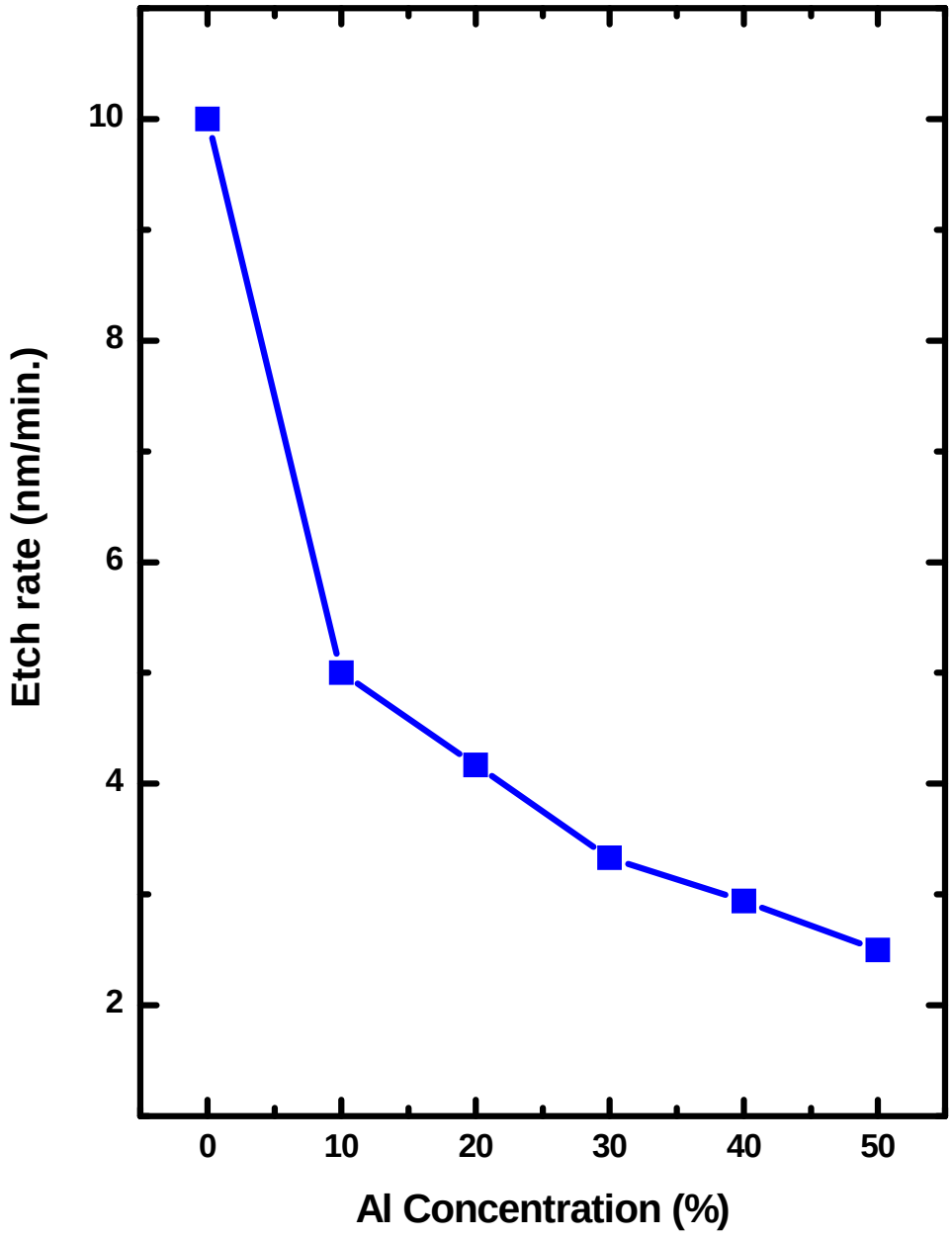

Figure 4.8. The etch rate of AlN on $Al_xGa_{1-x}N$ as a function of Al mole fraction when placed in a 5 M solution of KOH and DI water. The etch rate decreases rapidly as the Al concentration of the material increases.

V. Results

The results presented here provide a catalog of the electrical and optical properties of silicon implanted MEMOCVD grown $Al_xGa_{1-x}N$ as a function of aluminum concentration, implantation dose, anneal temperature and anneal time. This research will benefit device engineers by improving the performance of $Al_xGa_{1-x}N$ based devices that require ion implantation. The objective of this comprehensive study is to optimize the silicon ion implantation and anneal conditions for $Al_xGa_{1-x}N$ as a function of the Al mole fraction to create a more suitable material for optical and electronic device purposes.

Ion implantation is a commonly utilized technique for the fabrication of semiconductor devices that are based on Si and GaAs materials. It is a crucial processing step that lends for precise controlled doping of nitride-based devices. Ion implantation of various ions, doses, and energies is used for device isolation, creating highly conductive n-type regions for improving access resistance and the fabrication of the channel layer in transistors. The fabrication of many $Al_xGa_{1-x}N$ /GaN devices already involve ion implantation and more often the focus has begun to shift to activation of an implanted species into $Al_xGa_{1-x}N$ rather than GaN. The last decade has seen a drastic increase in the understanding of the defect structures caused by ion implantation into GaN and how their stability against annealing can affect the activation of the implanted species. At the present time, little research has been conducted into the properties of ion implanted $Al_xGa_{1-x}N$. The knowledge of GaN will undoubtedly aid in the investigation of $Al_xGa_{1-x}N$; however, how these properties change as a function of Al mole fraction has yet to be determined.

Successful application of ion implantation depends on understanding the production and annealing of radiation induced damage in the material. Ion implantation parameters that are responsible for the lattice damage are beam flux, implantation temperature, and the ion's mass and energy. Kucheyev *et al*. investigated damage profiles obtained from Rutherford backscattering spectrometry (RBS) and cross-sectional transmission electron microscopy (XTEM) measurements and found that the damage accumulation in GaN under bombardment occurs at the surface and in the bulk of the material (31). They found that the parameter that has the most profound effect on the amount of damage accumulation that will occur in GaN is the beam flux or implantation dose. Increasing the implantation dose above a critical dose will cause the surface damage and bulk damage to grow causing them to meet resulting in thick layer amorphization. The ion's mass also exhibited a great impact on the level of implantation produced lattice disorder. Heavy ion bombardment could cause amorphization of the material that would begin at the surface and proceed layer by layer into the bulk of the material. Kucheyev *et al*. observed that the ion implantation temperature was found to reduce damage accumulation as the temperature was raised from room temperature to 600 K, however lower and higher implantation temperatures had negative effects on the damage profile. According to Kucheyev's experiment, the ion's energy did not exhibit as great an influence on the damage profile when compared to the other parameters. Both Kucheyev and Zopler report that the effects of dynamic annealing, which are strong in GaN, help to suppress the formation of stable lattice defects during the ion implantation process and as a result the most common defects found in bombarded GaN are planar defects in the form of interstitials (31, 32). Most literature reports that an anneal temperature greater than 1300 ºC is required for optimal activation of an implanted

species in GaN and an even higher temperature is theorized for $Al_xGa_{1-x}N$ materials (29-32).

It is reported by Kucheyev *et al*. that $Al_xGa_{1-x}N$ experiences a stronger dynamic annealing effect than GaN, and that increasing the Al content acts to enhance this feature due to the larger energy of the Al-N bond as compared to the Ga-N bond (32). Kucheyev studied $Al_xGa_{1-x}N$ (x = 0.05-0.60) and observed that $Al_xGa_{1-x}N$, unlike GaN, did not exhibit disordering of the lattice at the surface (29, 31). Instead, the damage accumulation in $Al_xGa_{1-x}N$ occurred in the bulk of the material. Implantation above a critical dose ($>10^{20}$ cm^{-2}) resulted in rapid amorphization of the bulk material which spread layer by layer to the surface. Raising the concentration of Al in the material resulted in an elevated critical dose which could be due to the increased effects of dynamic annealing causing a decrease in implantation produced disorder.

For intentional n-type doping of $Al_xGa_{1-x}N$, silicon is the most widely used dopant due to its predicted shallow donor level over the complete spectrum of Al compositions. The silicon ionization energy is theorized to increase with increasing Al content from 20 meV for GaN to 90 meV for AlN (33). Experimentally, there have been few reports on n-type conductivity achieved through ion implantation in $Al_xGa_{1-x}N$ with high Al concentrations. The majority of the research thus far has focused on ion implanted $Al_xGa_{1-x}N$ with Al mole fractions less than 30% due to difficulty in growing good quality $Al_xGa_{1-x}N$ epilayers with higher Al mole fractions. Research of $Al_xGa_{1-x}N$ properties is minimal and at this time there exist no in-depth data on the fundamental properties of ion implanted $Al_xGa_{1-x}N$ for n-type conductivity. This study provides a systematic investigation into the electrical and optical properties of silicon implanted $Al_xGa_{1-x}N$ as a function of Al concentration, implant dose, anneal temperature, and anneal time to

determine the optimal conditions for creating highly conducting n-type material suitable for device applications.

The AlN protective encapsulant on the surface of the material was deposited during growth so that the Si implantation had to be accomplished through the 500 Å AlN cap. When this capping layer is removed, the Si ions that came to rest in it are also removed. Therefore, the implanted doses must be adjusted for loss of the implanted Si ions. Figure 5.1 shows the TRIM predicted depth profiles for silicon ions with an energy of 200 keV implanted into $Al_{0.1}Ga_{0.9}N$ and $Al_{0.5}Ga_{0.5}N$ with a dose of $1x10^{15}$ cm^{-2} to illustrate the amount of Si ions that will be removed with the 500Å AlN encapsulant.

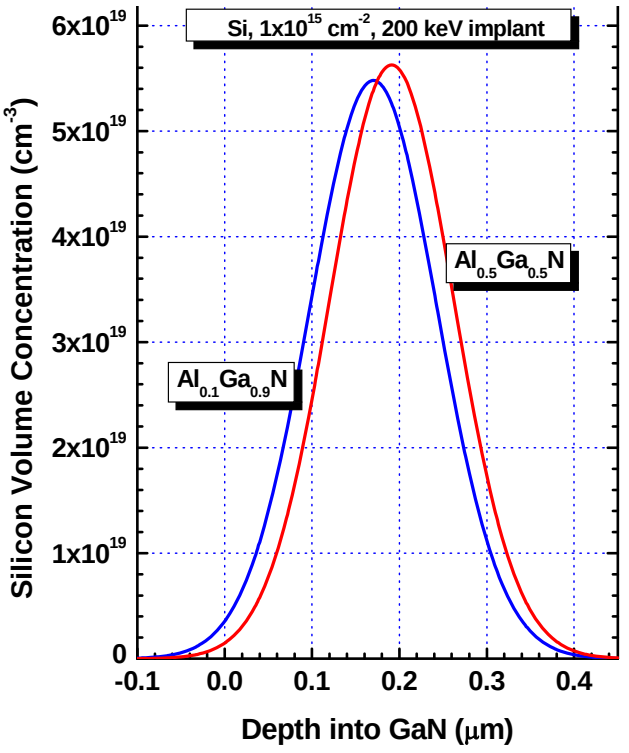

Figure 5.1. Silicon ion implantation profiles generated from TRIM code to illustrate the loss of ions from the removal of the 500 Å AlN encapsulant. The room temperature implantation conditions were silicon ions with an energy of 200 keV in a dose of $1x10^{15}$ cm^{-2} which produce peak concentrations of $5.62x10^{19}$ cm^{-3} and $5.78x10^{19}$ cm^{-3} for $Al_{0.1}Ga_{0.9}N$ and $Al_{0.5}Ga_{0.5}N$, respectively.

The $Al_xGa_{1-x}N$ sample surface begins at 0 μm on the graph. As can be seen from the figure, the quantity of removed Si ions decreases as the Al mole fraction in the sample is increased. This is due to the decreasing density of the material as the Al mole fraction is increased allowing for the implanted ions to come to rest further into the material with less residing near the surface. Simple integration of the curve shows that 1.9% of the implanted ions are removed for the $Al_{0.1}Ga_{0.9}N$ samples and 1.6%, 1.3%, 1%, and 0.7% of the ions are removed for the samples with Al with mole fractions of 0.2, 0.3, 0.4, and 0.5, respectively. The implanted dose will be corrected for this removal of ions and an *effective dose* will be used for calculation of the silicon activation efficiency and the silicon ionization energy.

As discussed by Fellows, the silicon electrical activation efficiency represents that the percentage of the implanted Si ions that contribute to the electrons in the conduction band (22). While the silicon ionization energy represents the energy required to ionize a silicon ion in a non-degenerately doped semiconductor and can be extracted from the relationship $exp(-E_d/k_BT)$. To calculate the activation efficiency the room temperature carrier concentration, n_s, is divided by the effective implanted silicon dose, φ_{eff}. The silicon electrical activation efficiency therefore only considers the percent of substitutional donors in the material. The *donor activation*, given in equation 5.1, incorporates the ionization energy and thus corresponds to the percent of ionized donors. In equation 5.1, E_d is the donor ionization energy, k_B is the Boltzman constant, and T is the temperature (22).

$$\eta = \frac{n_s}{\varphi_{eff} e^{-E_d / k_B T}} \tag{5.1}$$

Silicon Implanted $Al_{0.1}Ga_{0.9}N$

The studies of ion implanted $Al_xGa_{1-x}N$ are minimal with most of the work focusing on $Al_xGa_{1-x}N$ with lower Al concentrations. Y. Irokawa *et al*. investigated the electrical activation characteristics $Al_{0.13}Ga_{0.87}N$ implanted with silicon ions that had multiple energies to achieve a uniform concentration at 4 μm into the material (34). They achieved greater than 90% electrical activation for the samples implanted with a silicon dose of with $5.2x10^{14}$ and $1x10^{15}$ cm^{-2} after annealing at 1375 ºC for 5 minutes in a nitrogen environment. The sample implanted with $1x10^{14}$ cm^{-2} silicon ions had a considerably lower electrical activation of 55% under the same annealing conditions. Zopler *et al*. observed an electrical activation of only 34% after implanting $Al_{0.15}Ga_{0.85}N$ with silicon ions that had an energy of 100 keV and a high dose of $5x10^{15}$ cm^{-2} after annealing under high nitrogen pressures (32). Ryu *et al*. reported activation efficiencies of 45% and 76% for $Al_{0.14}Ga_{0.86}N$ implanted with silicon ions that had an energy of 200 keV at doses of $5x10^{13}$ and $1x10^{14}$ cm^{-2}, respectively, and subsequently annealed at 1250 ºC for 20 minutes in flowing nitrogen (35). Polyakov *et al*. achieved only 10% activation after annealing at 1140 ºC for $Al_{0.12}Ga_{0.88}N$ implanted with $5x10^{14}$ cm^{-2} silicon ions (36). Exhibiting such low activation energies at the lower temperature anneals reveals a shift in behavior from GaN which exhibited silicon activation efficiencies above 50% even in cases where structural damage recovery was incomplete (34). This trend indicates that higher anneal temperatures may be required for significant activation in $Al_xGa_{1-x}N$ to take place. This section details the findings of silicon implanted $Al_{0.1}Ga_{0.9}N$ as a function of anneal temperature and time through Hall Effect and cathodoluminescence measurements.

Room Temperature Hall Effect Measurements

The MEMOCVD grown $Al_{0.1}Ga_{0.9}N$ was capped with 500Å of AlN and then implanted at room temperature with silicon ions that had an energy of 200 keV to produce the desired dose. The Si doses were $1x10^{14}$, $5x10^{14}$, and $1x10^{15}$ cm^{-2} which after taking into account the 500Å AlN cap the effective doses are $9.8x10^{13}$, $4.9x10^{14}$, and $9.8x10^{14}$ cm^{-2}, respectively. The samples were annealed from 1100 to 1250 ºC for 20 to 40 minutes in a flowing nitrogen environment. All the samples had excellent surface morphology following the anneal at 1250 ºC, increasing the anneal temperature to 1300 ºC however, caused significant damage to the surface for these samples. Room temperature Hall Effect measurements were conducted to determine sheet carrier concentrations for the samples annealed for 20 minutes and the results are shown in Figure 5.Figure 5.2. The unimplanted samples both as-grown and annealed were highly resistive making it impossible to collect any meaningful data. However, there was one exception. The room temperature carrier concentration of the unimplanted sample that had been annealed at 1250 ºC for 20 minutes was $6.5x10^{12}$ cm^{-2}, and this value was subtracted from the implanted sample's measurements as the background carrier concentration. The fact that an annealed unimplanted sample had a measurable carrier concentration, while the as-grown material did not, could indicate that the as-grown defects were compensating residual shallow donors that were repaired during the annealing process, thus allowing the shallow donors to contribute to the conduction.

The sheet carrier concentrations for each implanted silicon dose respond differently to an increase in the anneal temperature. The carrier concentration for the $Al_{0.1}Ga_{0.9}N$ implanted with a silicon dose of $1x10^{14}$ cm^{-2}, shown as a solid square, increases almost linearly as the anneal temperature is increased from 1100 to 1200 ºC, but

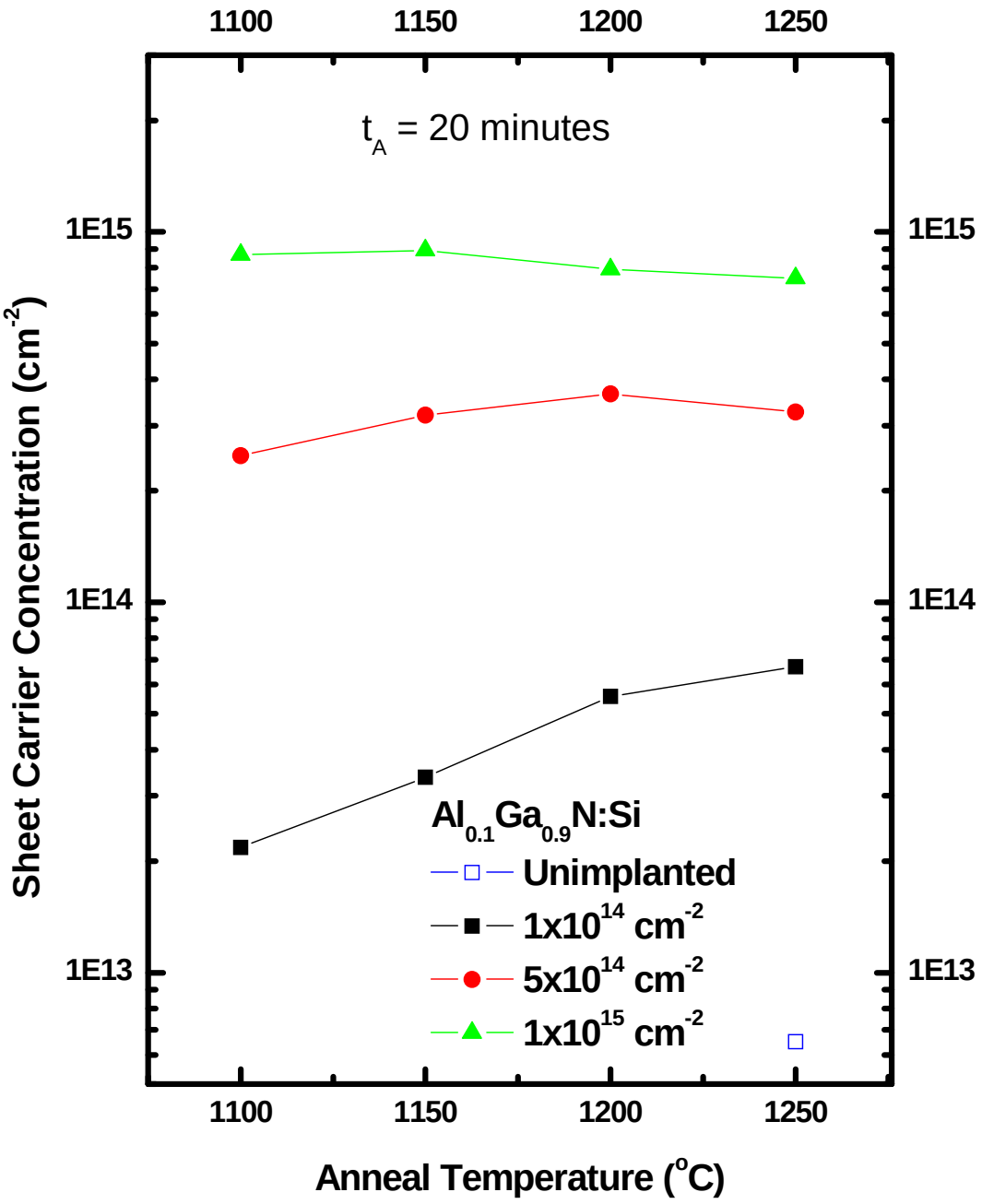

Figure 5.2. Room temperature sheet carrier concentrations for $Al_{0.1}Ga_{0.9}N$ implanted with Si at 200 keV at room temperature with doses of $1x10^{14}$, $5x10^{14}$, and $1x10^{15}$ cm^{-2} and subsequently annealed from 1100 to 1250 ºC for 20 minutes in flowing nitrogen.

the increase in carrier concentration is much less between the 1200 and 1250 ºC anneal. These samples experienced a maximum carrier concentration of 6.69×10^{13} cm^{-2}, after being annealed at 1250 ºC for 20 minutes in nitrogen ambient. The rapid increase in carrier concentration was only witnessed in the $Al_{0.1}Ga_{0.9}N$ implanted with the lowest silicon dose. The $Al_{0.1}Ga_{0.9}N$ samples implanted with a silicon dose of 5×10^{14} cm^{-2}, shown by the solid circle, exhibit their most noticeable increase in carrier concentration between the 1100 and 1150 ºC anneals although concentrations at that dose were relatively weak. The carrier concentration for these samples continues to increases through the 1200 ºC anneal, reaching a maximum of 3.66×10^{14} cm^{-2} at this anneal temperature. Further increasing the anneal temperature to 1250 ºC causes the carrier concentration to decrease back to the value obtained for the sample that was annealed at 1150 ºC. The $Al_{0.1}Ga_{0.9}N$ samples implanted with the highest Si dose of 1×10^{15} cm^{-2}, shown by the solid triangle, have very high carrier concentration even after being annealed at 1100 ºC and 1150 ºC of roughly the same value, with the sample annealed at 1150 ºC being only slightly higher at 8.92×10^{14} cm^{-2}. Increasing the anneal temperature for the samples implanted with this dose to 1200 ºC results in a decrease in the carrier concentration and even more so when the anneal temperature is raised to 1250 ºC. The samples implanted with the highest silicon dose show a decrease in the carrier concentration as the temperature is elevated above 1150 ºC while the samples implanted with the middle dose of 5×10^{14} cm^{-2} does not begin to decrease until after the anneal temperature is above 1200 ºC. The carrier concentration for the samples implanted with the lowest silicon dose increases throughout the given temperature range.

The silicon electrical activations, are shown in Figure 5.3, of these samples are closely related to the carrier concentrations and thus follow the same trends with the

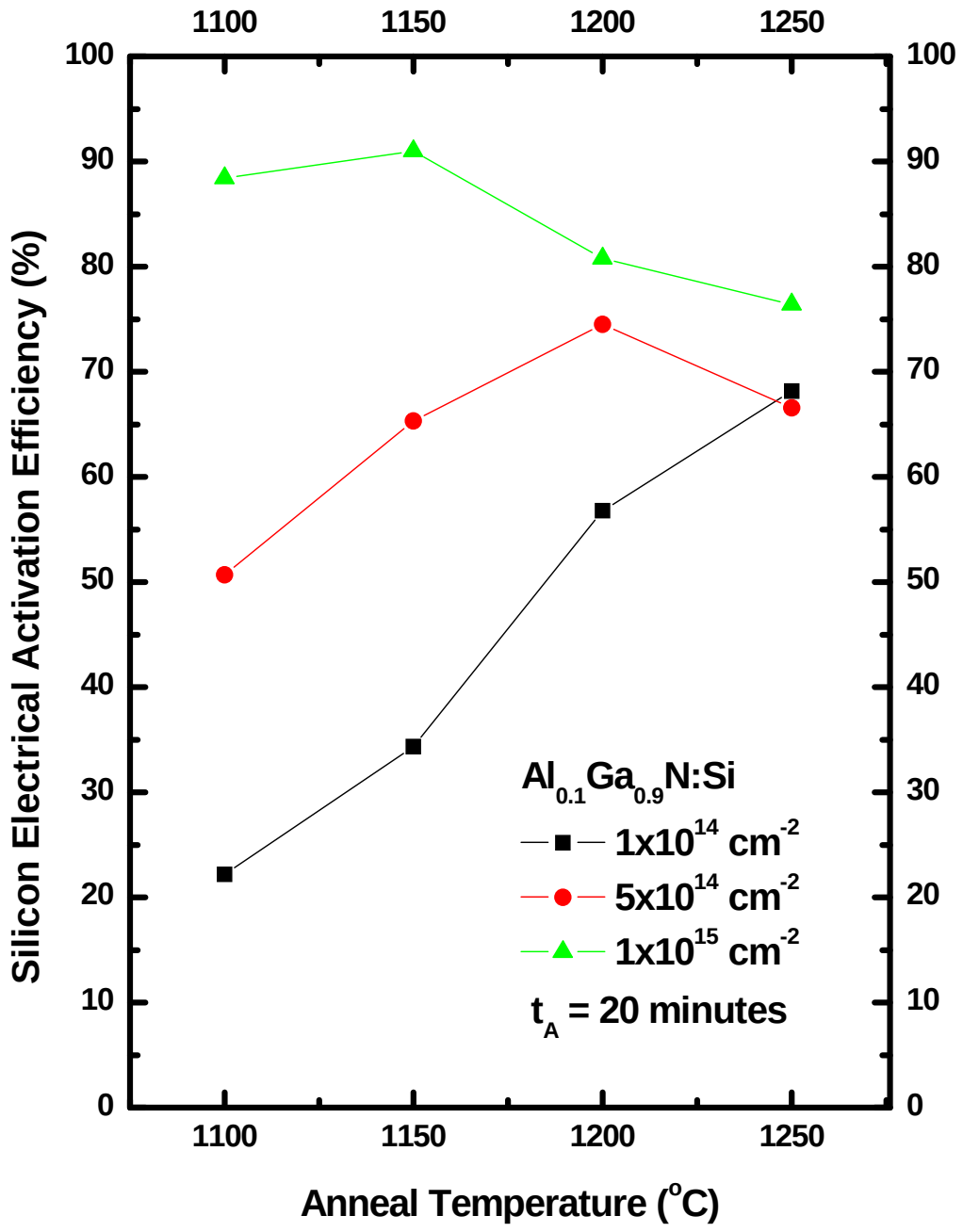

Figure 5.3. Electrical activation efficiency for silicon implanted $Al_{0.1}Ga_{0.9}N$ calculated from the room temperature Hall measurements doses of $1x10^{14}$, $5x10^{14}$, and $1x10^{15}$ cm^{-2} and annealed from 1100 to 1250 °C for 20 minutes.

anneal temperature as mentioned above. The electrical activation efficiency was calculated using the effective dose, and the room temperature carrier concentration. Higher implanted doses resulted in higher silicon activation efficiencies for anneal temperatures up to 1250 ºC, except in the case of the sample implanted with $1x10^{14}$ cm^{-2} and annealed at 1250 ºC which exhibits a slightly higher activation than the sample implanted with $5x10^{14}$ cm^{-2} and annealed at 1250 ºC. The silicon electrical activation for the samples implanted with $1x10^{14}$ cm^{-2} silicon ions exhibits the most improvement over the given temperature range, increasing from 22% to 68% after being annealed for 20 minutes at 1100 ºC and 1250 ºC, respectively. The samples implanted with a dose of $5x10^{14}$ cm^{-2} silicon ions have a significant activation efficiency of 51% after the 1100 ºC, 20 minute anneal, and steadily increases to a maximum of 75% following the 1200 ºC anneal before dropping off at the 1250 ºC anneal to the same activation as the 1150 ºC anneal. The decrease in activation efficiency could be due to out diffusion of silicon or compensating acceptor-like defects that were created during the higher temperature anneals. The samples implanted with the highest silicon dose, $1x10^{15}$ cm^{-2}, exhibit the highest activation efficiencies of all the implanted doses reaching 88% and 91% following the lower temperature anneals of 1100 ºC and 1150 ºC, respectively. The activation for the high dose implanted samples then declines to 80% and 76% for the higher temperature anneals of 1200 ºC and 1250 ºC, respectively. The samples implanted with the higher silicon dose experience more damage from the ion bombardment which would create more lattice damage. That, paired with the high temperature anneal which can also create defects in the material, may allow for the implanted silicon ions to be more inclined to occupy nitrogen lattice sites. If this were to occur, the silicon ions that occupy nitrogen sites would compensate the electrons donated to the conduction by the

silicon ions that occupy gallium or aluminum sites and the activation efficiency would decrease. All three doses display their peak electrical activation at different temperatures, with optimal anneal temperatures decreasing in inverse relation to increased implantation doses.

The higher implanted silicon doses were more readily activated than the lower implanted silicon doses into $Al_{0.1}Ga_{0.9}N$. To better illustrate the improvement in activation with dose, the sheet carrier concentration is plotted as a function of the implanted silicon dose in Figure 5.4. It is clear from the figure that the samples implanted with the highest silicon dose achieve higher electrical activation efficiencies at lower anneal temperatures than the samples implanted with the lower silicon doses. The $Al_{0.1}Ga_{0.9}N$ implanted with the lower silicon doses, even at the highest annealing temperatures, do not respond as well as the high dose implantation at its worst activation. Implanted silicon in GaN was found to behave similarly, though GaN did not exhibit a decrease in the activation efficiency as the anneal temperature was increased even for implanted silicon doses as high as $5x10^{15}$ cm^{-2} and anneal temperatures as high as 1350°C (22).

The electrical activations are comparable to other previous findings. The low silicon dose implantation, $1x10^{14}$ cm^{-2}, exhibits an electrical activation of 68% following a 1250 ºC anneal for 20 minutes in flowing nitrogen. Ryu *et al*. reported a slightly higher activation of 76% for Si implanted MBE grown $Al_xGa_{1-x}N$ under the same implantation and anneal conditions (35). The silicon implantation dose of $5x10^{14}$ cm^{-2} reached a maximum electrical activation of 75% after being annealed at 1200 ºC for 20 minutes. Irokawa *et al*. reported a higher activation of 90% for a sample implanted with a similar dose but the annealing temperature was considerably higher at 1375 ºC with an

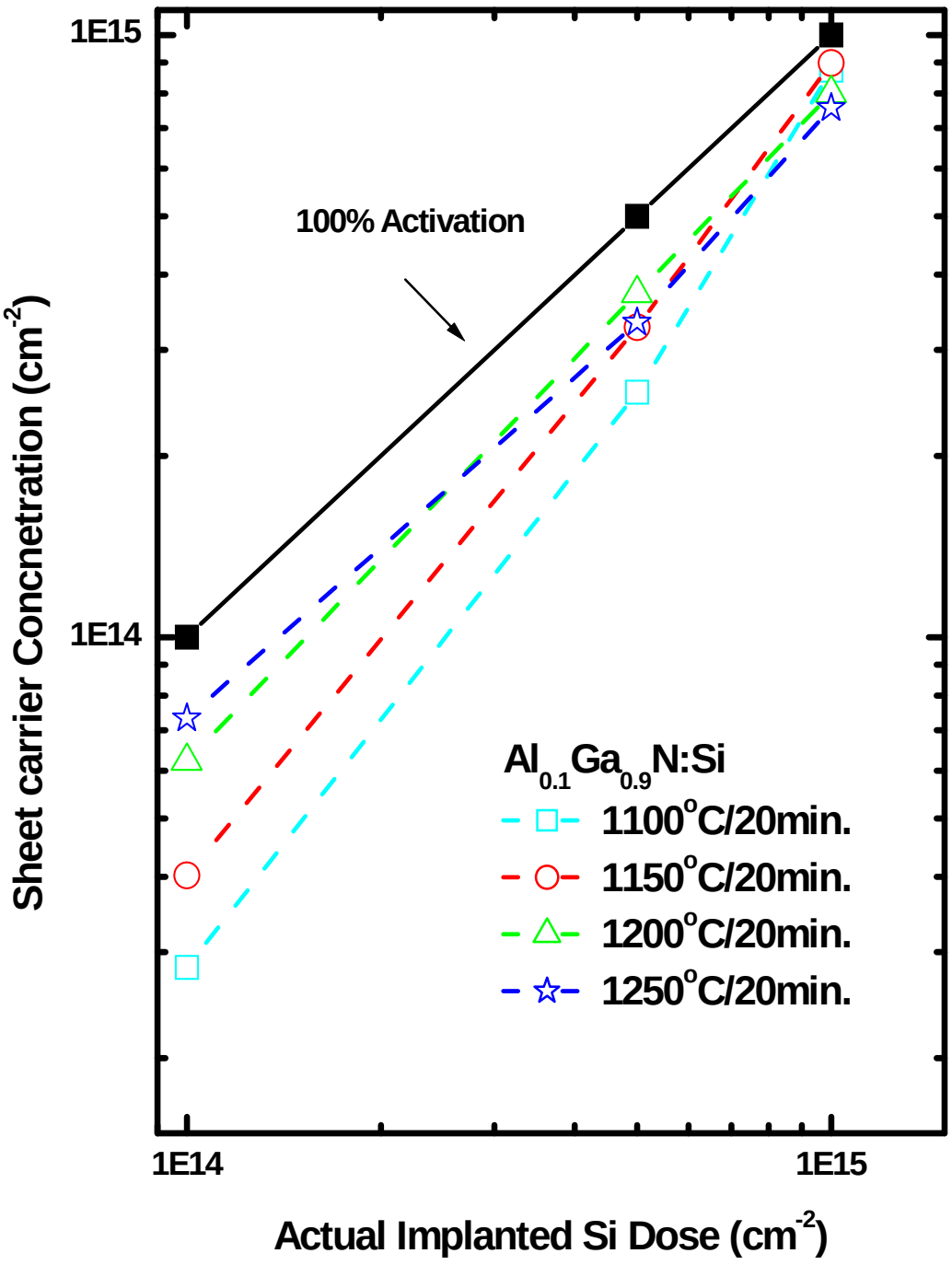

Figure 5.4. The room temperature sheet carrier concentrations versus the actual implantation dose for $Al_{0.1}Ga_{0.9}N$ implanted with 200 keV silicon at room temperature with doses of $1x10^{14}$, $5x10^{14}$, and $1x10^{15}$ cm^{-2} and annealed from 1100 ºC to 1250 ºC for 20 minutes in a nitrogen ambient.

anneal time of 5 minutes (34). Irokawa *et al.* also reported 90% activation for a sample implanted with a silicon dose of $1x10^{15}$ cm^{-2} under the same anneal conditions. In this study, however, 91% activation was achieved for this dose at a much lower annealing temperature of 1150 ºC, with an extended time, 20 minutes.

The data show that for the low dose Si-implantation into $Al_{0.1}Ga_{0.9}N$, the optimal anneal temperature may be higher than 1250 ºC while the optimal anneal temperature for the samples implanted with the higher doses of $5x10^{14}$ and $1x10^{15}$ cm^{-2} are 1200 ºC and 1150 ºC, respectively, when the anneal time is fixed for 20 minutes. The data illustrate that the optimal anneal temperature for Si-implanted $Al_{0.1}Ga_{0.9}N$ is dose dependent with lower implanted silicon doses requiring higher temperatures to achieve high electrical activation as is seen in the case of Si-implanted GaN (22).

The low activation for the low dose Si-implanted $Al_{0.1}Ga_{0.9}N$ could be related to the high resistivity of these samples. The resistivity values for the $Al_{0.1}Ga_{0.9}N$ implanted with all three silicon doses are shown in Figure 5.5. The samples implanted with the low silicon dose of $1x10^{14}$ cm^{-2} has resistivity values 8 and 24 times higher than those for the samples implanted with $5x10^{14}$ and $1x10^{15}$ cm^{-2} silicon ions when annealed at 1100 ºC for 20 minutes, respectively. However, the resistivity for these samples falls 3 kΩ/□ to 830 Ω/□ as the anneal temperature is increased to 1250 ºC. The largest measured resistivity of 3.83 kΩ/□ was obtained for the samples implanted with $1x10^{14}$ cm^{-2} silicon ions and annealed at 1100 ºC for 20 minutes. However, this is much smaller than that of the unimplanted sample annealed at 1250 ºC, which has a resistivity of 9.4 kΩ/□. In general, the resistivities of the samples decrease as the anneal temperature is increased, with the highest dose showing the least improvement and the lowest dose showing the most

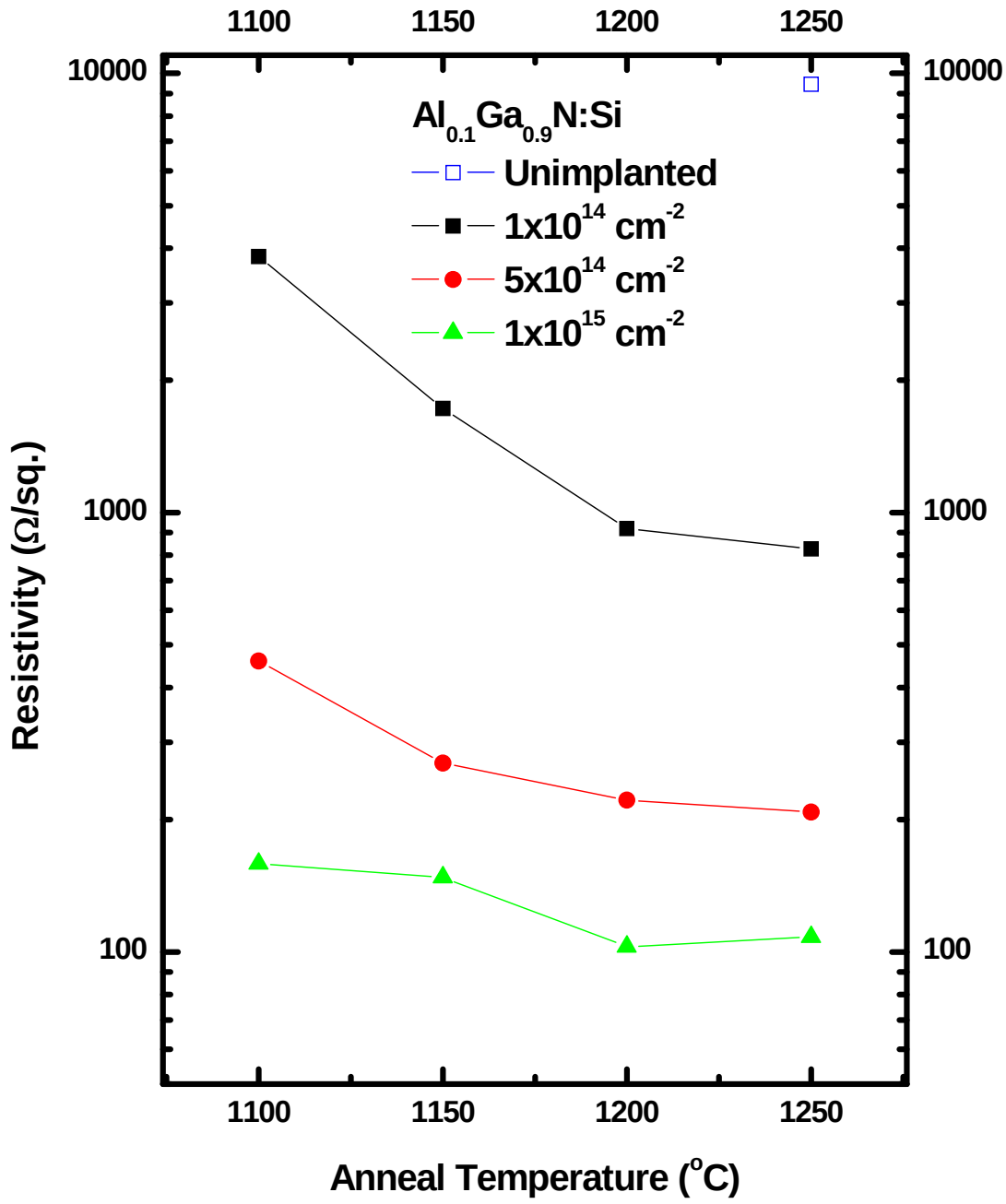

Figure 5.5. Room temperature resistivity measurements taken under zero magnetic field for $Al_{0.1}Ga_{0.9}N$ implanted with 200 keV silicon at room temperature with doses of $1x10^{14}$, $5x10^{14}$, and $1x10^{15}$ cm^{-2} and annealed from 1100 ºC to 1250 ºC for 20 minutes in a nitrogen ambient.

improvement. The measured resistivities of the higher-dose implanted samples are well below 1 k Ω/□. The samples implanted with $5x10^{14}$ cm^{-2} silicon ions show a dramatic decrease in resistivity between the 1100 and 1150 ºC anneal and then only show a small decrease for the rest of the anneal temperature span. The resistivities for these samples drop from 460 Ω/□ after being annealed at 1100 ºC to 208 Ω/□ after the 1250 ºC anneal. The $Al_{0.1}Ga_{0.9}N$ implanted with the high silicon dose exhibited an only a small decrease in resistivity from the 1100 ºC anneal to the 1150 ºC anneal before decreasing at a much larger rate for the 1200 ºC anneal. The samples implanted with $1x10^{15}$ cm^{-2} silicon ions had resistivities of 158 Ω/□ and 103 Ω/□ after being annealed at 1100 and 1200 ºC, respectively. The resistivity for the samples implanted with the highest silicon dose increases slightly to 108 Ω/□ after being annealed at 1250 ºC. This increase in resistivity could be caused by an increase in defects in the crystal lattice from the high temperature anneal. When the high and low dose silicon implanted $Al_{0.1}Ga_{0.9}N$ experience their lowest resistivity values, they also have their maximum carrier concentrations, and thus activations. This is not true for the samples implanted with $5x10^{14}$ cm^{-2} silicon ions; however, the difference in resistivity between the highest activation anneal temperature (1200 ºC) and anneal temperature that produces the lowest resistivity (1250 ºC) is only 14 Ω/□.

When choosing a material for device applications, the carrier concentration as well as the mobility is an important aspect of a material to consider. The mobilities for the Si-implanted $Al_{0.1}Ga_{0.9}N$ annealed for 20 minutes at various temperatures are shown in Figure 5.6. Room temperature mobility values for Si-implanted GaN have been reported to be as high as 250 $cm^2/V{\cdot}s$ for samples implanted with a dose of $1x10^{13}$ cm^{-2}

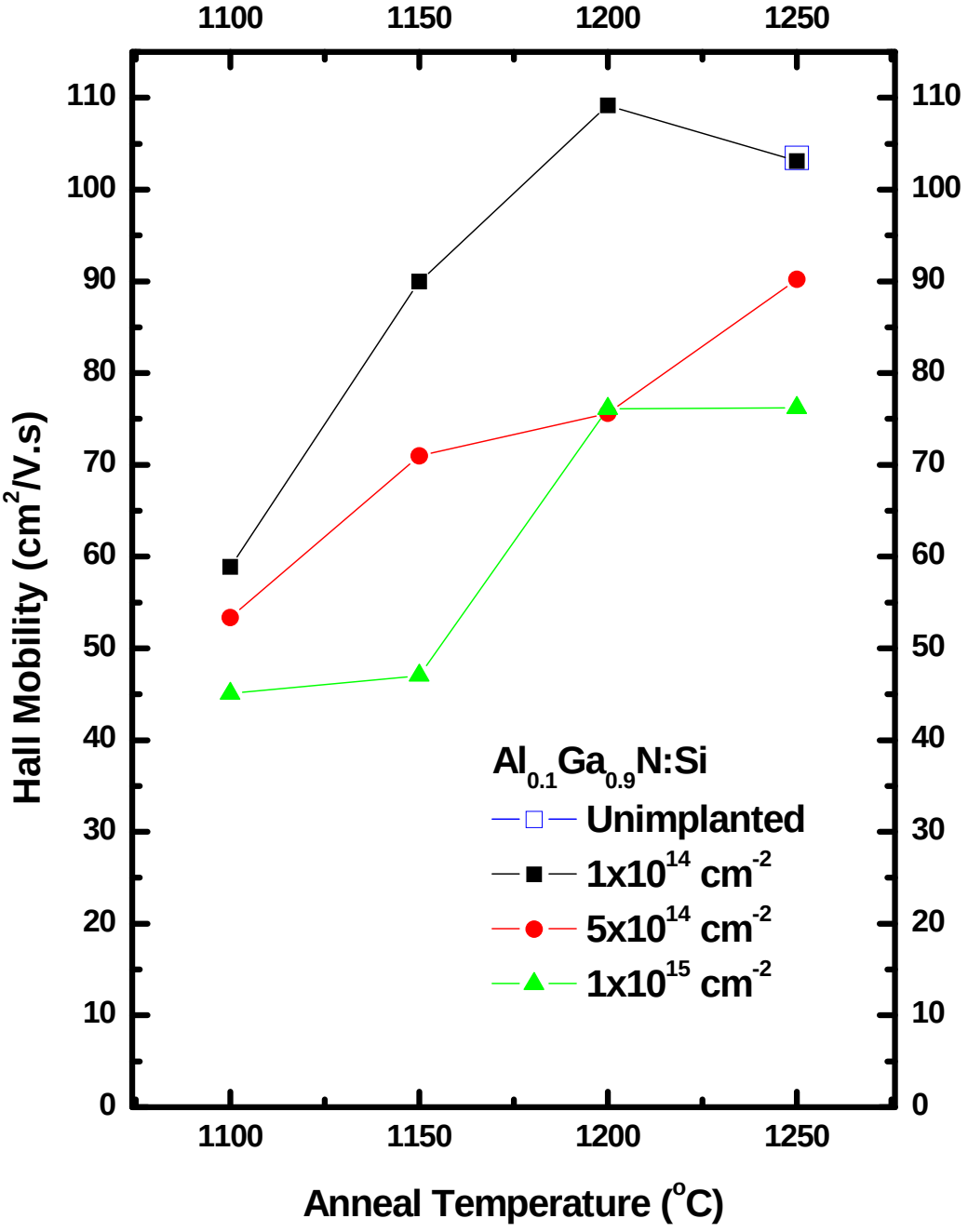

Figure 5.6. The room temperature mobility values obtained from the Hall measurements on $Al_{0.1}Ga_{0.9}N$ implanted with 200 keV silicon at room temperature with doses of $1x10^{14}$, $5x10^{14}$, and $1x10^{15}$ cm^{-2} and annealed from 1100 to 1250 °C for 20 minutes in a nitrogen ambient.

silicon ions and annealed at 1350 ºC for 17 seconds (22). The reported mobility values for $Al_{0.1}Ga_{0.9}N$ to date are not as high. Irokawa *et al*. observed mobility values of 48, 63, and 65 $cm^2/V{\cdot}s$ for $Al_{0.13}Ga_{0.87}N$ implanted with a dose of $1x10^{14}$, $5.2x10^{14}$, and $1x10^{15}$ cm^{-2} silicon ions, respectively, and annealed for 5 minutes at 1375 ºC (34). Ryu *et al*. had a mobility value of 89 $cm^2/V{\cdot}s$ for $Al_{0.14}Ga_{0.86}N$ implanted with a dose of $1x10^{14}$ cm^{-2} silicon ions after annealing at 1250 ºC for 20 minutes (35). The mobilities determined for $Al_{0.1}Ga_{0.9}N$ implanted with similar doses in this study are found to be higher than those reported.

The mobilities of each set of samples increase as the anneal temperature is increased, with the only exception being the $Al_{0.1}Ga_{0.9}N$ implanted with the lowest dose and annealed at 1250 ºC where the mobility declines by about 4% of the value following the 1200 ºC anneal. This decrease in mobility for the $Al_{0.1}Ga_{0.9}N$ implanted with $1x10^{14}$ cm^{-2} silicon ions and annealed at 1250 ºC can be attributed to an increase in ionized impurity scattering, which signifies that the lattice damage associated with the ion implantation has been repaired. The mobility increases in spite of an increase in the number of ionized impurities indicating that the recovery of the crystal lattice is more pertinent to the mobility value than ionized impurity scattering. The unimplanted sample annealed for 20 minutes at 1250 ºC had a mobility value of 103 $cm^2/V{\cdot}s$. The $Al_{0.1}Ga_{0.9}N$ implanted with the lowest implantation dose of $1x10^{14}$ cm^{-2} silicon ions has the highest observed mobilities of the three doses studied, as expected. The mobility values increase almost linearly from 59 to 109 $cm^2/V{\cdot}s$ as the temperature is increased from 1100 to 1200 ºC. The mobility for these samples then decreases slightly to 103 $cm^2/V{\cdot}s$, the same as the unimplanted sample, as the anneal temperature is increased to 1250ºC, at which the activation for this dose is a maximum and the resistivity is a minimum. The samples

implanted with a dose of $5x10^{14}$ cm^{-2} silicon ions show an increase in mobility of about the same magnitude between the 1100-1150 ºC range and the 1200-1250 ºC range, however, the change in mobility between 1150 and 1200 ºC is less than 4 $cm^2/V{\cdot}s$. The mobilities $Al_{0.1}Ga_{0.9}N$ implanted with this dose increases from 53 to 90 $cm^2/V{\cdot}s$ as the temperature increases from 1100 to 1250 ºC. Again, anneal temperature for the peak mobility does not correspond to that of the peak activation. In this case, the mobility increase can be attributed to a decrease in ionized impurity scattering caused by the decrease in activation efficiency or that more of the ion implantation induced damage has been repaired with the higher temperature anneal. The high dose Si-implanted samples, like the samples implanted with $5x10^{14}$ cm^{-2} silicon ions, show the same magnitude of mobility change for the 1100-1150 ºC range and the 1200-1250 ºC range, however, the change in mobility between 1150 and 1200 ºC is a much larger 30 $cm^2/V{\cdot}s$. The peak mobility for the $Al_{0.1}Ga_{0.9}N$ implanted with a silicon dose of $1x10^{15}$ cm^{-2} is 76 $cm^2/V{\cdot}s$ after being annealed at 1250 ºC for 20 minutes. These samples have low mobility values (~45$cm^2/V{\cdot}s$) for anneal temperatures (1100-1150 ºC) that produce the higher electrical activations, and high mobility values at 1200 and 1250 ºC when the activation is low. One could expect the opposite to be true since the inactive Si and residual damage serve as scattering centers which would degrade the mobility. However in this case, the ionized impurity scattering from higher carrier concentrations limits the mobility at lower anneal temperatures. As the anneal temperature is increased the carrier concentration declines significantly, reducing the effects of scattering from ionized impurities, which is reflected as an increase in the mobility. Overall, the mobilities obtained in this study are higher than most other values reported in the literature to date.

To improve the electrical activation efficiency of the Si-implanted $Al_{0.1}Ga_{0.9}N$ samples, the anneal time was extended from 20 to 40 minutes for a set anneal temperature of 1200 ºC. A comparison of the results obtained for both the 20 and 40 minute anneals at 1200 ºC are listed in Table 5.1. A temperature of 1200 ºC is more commercially viable and therefore more practical for incorporation into device manufacturing techniques. Achieving a higher activation efficiency at a lower anneal temperature is more readily incorporated into the production line due to the limitations of the furnaces currently in place. Extending the anneal time had positive effects on all of the physical aspects studied except for the mobility. The carrier concentrations of the samples for each dose of implanted silicon increased following the 40 minute anneal. The increase in the sheet carrier concentration is reflected in silicon electrical activation efficiency as an improvement of at least a 15% for all three Si-implanted doses. The electrical activation for the samples implanted with the lowest dose of $1x10^{14}$ cm^{-2} silicon ions increases from 57% to 73% by extending the anneal time. Thus a higher activation was reached by lengthening the anneal time than the anneal temperature. The activation for the samples implanted with this dose and annealed at 1250 ºC for 20 minutes was only 68%. The $Al_{0.1}Ga_{0.9}N$ that was implanted with a dose of $5x10^{14}$ cm^{-2} silicon ions increased in electrical activation going from 75% to 94% after the 20 and 40 minute anneals, respectively. The $Al_{0.1}Ga_{0.9}N$ implanted with the high silicon dose exhibit the largest increase in electrical activation increasing from 81% to 101% by extending the anneal time to 40 minutes. The 101% activation may be due to underestimating the amount of the silicon ions removed with the AlN encapsulant when calculating the effective dose or the background carrier concentration could become higher. At most this can be counted

Table 5.1. Room temperature Hall Effect results for $Al_{0.1}Ga_{0.9}N$ implanted with three doses of silicon ions that had an energy of 200 keV and annealed at 1200 ºC for 20 and 40 minutes in flowing nitrogen.

Dose (cm^{-2})	Time (min.)	Carrier Concentration (cm^{-2})	Activation (%)	Resistivity (Ω/□)	Mobility ($cm^2/V \cdot s$)
$1x10^{14}$	20	$5.57x10^{13}$	56.78	920.48	109.19
$1x10^{14}$	40	$7.13x10^{13}$	72.68	792.03	101.28
$5x10^{14}$	20	$3.66x10^{14}$	74.52	221.72	75.63
$5x10^{14}$	40	$4.61x10^{14}$	93.86	190.24	70.32
$1x10^{15}$	20	$7.93x10^{14}$	80.78	102.64	76.11
$1x10^{15}$	40	$9.95x10^{14}$	101.43	95.85	64.35

as 100% activation, which is a an improvement over the 91% activation achieved for the sample implanted with this dose after annealing at 1150 ºC for 20 minutes.

The resistivity of the Si-implanted $Al_{0.1}Ga_{0.9}N$ improved about 15% for the samples implanted with the lowest silicon dose and only about 7% for the samples implanted with the highest dose of silicon ions. The $Al_{0.1}Ga_{0.9}N$ implanted with $1x10^{14}$ cm^{-2} silicon ions exhibited a resistivity drop from 920 Ω/□ to 792 Ω/□ after extending the anneal time to 40 minutes. This resistivity is lower than the resistivity obtained from these samples after annealing at 1250 ºC for 20 minutes. The resistivity of the samples implanted with $5x10^{14}$ cm^{-2}silicon ions improved to 190 Ω/□from 222 Ω/□ after increasing the anneal time to 40 minutes and annealing at 1200 ºC. The $Al_{0.1}Ga_{0.9}N$ implanted with this silicon dose and annealed at 1250 ºC for 20 minutes produced a slightly lower resistivity of 208 Ω/□. The $Al_{0.1}Ga_{0.9}N$ implanted with $1x10^{15}$ cm^{-2} silicon

ions exhibit a small decrease in resistivity from 103 to 96 Ω/□ after increasing the anneal time to 40 minutes. This is a slight decrease from the samples implanted with this dose that were annealed for 20 minutes at 1250 ºC that had a resistivity of 108 Ω/□. Lengthening the anneal time to 40 minutes at a lower anneal temperature improved the resistivities for the $Al_{0.1}Ga_{0.9}N$ that were obtained after annealing at both 1200 and 1250 ºC for the 20 minutes.

The mobility values for the $Al_{0.1}Ga_{0.9}N$ show a slight decrease after lengthening the anneal time from 20 to 40 minutes, which can be attributed to an increase in the number of ionized impurities that serve as scattering centers and degrade the mobility. The samples implanted with the lower doses both show about a 7% drop in mobility between the two anneals. The samples implanted with $1x10^{14}$ cm^{-2} silicon ions show a drop from their peak mobility of 109 to 101 $cm^2/V{\cdot}s$ after being annealed at 1200 ºC for 20 and 40 minutes, respectively. The mobility obtained for the sample that were annealed for 40 minutes is lower than the mobility achieved for the sample implanted with this silicon dose and annealed at 1250 ºC anneal for 20 minutes, which was 103 $cm^2/V{\cdot}s$. The $Al_{0.1}Ga_{0.9}N$ implanted with the middle dose of $5x10^{14}$ cm^{-2} silicon ions, exhibited a mobility drop from 76 to 70 $cm^2/V{\cdot}s$ after extending the anneal time to 40 minutes, which is much lower than the peak mobility of 90 $cm^2/V{\cdot}s$ obtained for the samples implanted with this silicon dose after being annealed at 1250 ºC for 20 minutes. The most dramatic decline in mobility was 16% from the peak mobility of 76 $cm^2/V{\cdot}s$ for the $Al_{0.1}Ga_{0.9}N$ implanted with $1x10^{15}$ cm^{-2} silicon ions after lengthening the anneal time to 40 minutes.

Most Si-implanted $Al_{0.1}Ga_{0.9}N$ samples achieved high silicon electrical activation efficiencies above 70% for each implantation dose. The samples implanted with the low

silicon dose had the lowest overall activation, reaching 68% for the 20 minute 1250 ºC anneal and 73% activation after being annealed at 1200 ºC for 40 minutes. The samples implanted with $5x10^{14}$ cm^{-2} silicon ions reached an activation of 75% after being annealed for 20 minutes at 1200 ºC, which improved to 94% by extending the anneal time to 40 minutes. The $Al_{0.1}Ga_{0.9}N$ implanted with the highest dose had the best activation of 100% following the 1200 ºC anneal for 40 minutes. The samples implanted with this silicon dose also had considerable activation of 91% following the 1150 ºC anneal for 20 minutes. Lowering the anneal temperature and lengthening the anneal time benefited all the material parameters for the Si-implanted $Al_{0.1}Ga_{0.9}N$ except for the mobility which is due to the increased number of ionized donors, thus implying that the lattice damage has been fully recovered for all the implanted samples after annealing at 1200 ºC for 20 minutes.

Temperature-Dependent Hall Effect Measurements

Temperature-dependent Hall Effect measurements were taken on the $Al_{0.1}Ga_{0.9}N$ samples that were annealed at 1200 ºC for 20 minutes in flowing nitrogen to determine the nature of the carriers as a function of temperature as well as to determine the ionization energy of the implanted silicon ions. The sheet carrier concentration as a function of temperature from 10 to 700 K for the samples implanted with each of the three silicon doses and annealed at 1200 ºC for 20 minutes are shown in Figure 5.7. To display the temperature-dependent carrier concentration more conveniently, the x-axis is displayed as 1000/T and split at 20-30 K^{-1} (50-33 K) to expand the high temperature regime. The carrier concentrations for all the $Al_{0.1}Ga_{0.9}N$ implanted with each of the three silicon doses remain relatively constant as the temperature increased from 10 to 50

K. The carrier concentration for the samples implanted with the two lower doses of $1x10^{14}$ and $5x10^{14}$ cm^{-2} silicon ions begin to decrease around 50 K, reaching a minimum at 140 and 300 K, respectively, before increasing continuously to 700 K. The samples implanted with a dose of $1x10^{15}$ cm^{-2} silicon ions have a relatively constant carrier concentration at lower temperatures, and increasing gradually over the measured temperature range. The temperature-independent nature of the carrier concentration indicates that the implanted silicon ions have formed a degenerate impurity band in the band gap. A non-degenerate semiconductor would experience carrier freeze out at low temperatures and the carrier concentration would thus decrease, which is not observed in the temperature-dependent data for these samples. According to Look, the absence of a decline in the carrier concentration is due to conduction taking place in the donor level rather than in the conduction band (72, 113). The critical doping density of $Al_{0.1}Ga_{0.9}N$ is calculated from equation 2.18 to be $1.83x10^{18}$ cm^{-3}. This is the density at which the material undergoes a Mott transition and most of the donors become ionized independent of the temperature. The predicted peak carrier concentrations determined from TRIM calculations for the three implantation doses of $1x10^{14}$, $5x10^{14}$, and $1x10^{15}$ cm^{-2} silicon ions are $5.62x10^{18}$, $2.81x10^{19}$, and $5.62x10^{19}$ cm^{-3}, respectively. All three of the implanted doses create volume carrier concentrations that exceed the critical Mott concentration of $Al_{0.1}Ga_{0.9}N$ which explains the metallic-like behavior of the samples.

The $Al_{0.1}Ga_{0.9}N$ implanted with the highest silicon dose has the most temperature independent carrier concentration as would be expected since this silicon dose produces the most degenerate samples. The carrier concentration for the lower Si-implanted dose dips between 100 and 500 K signifying the presence of a multi-channel conduction band,

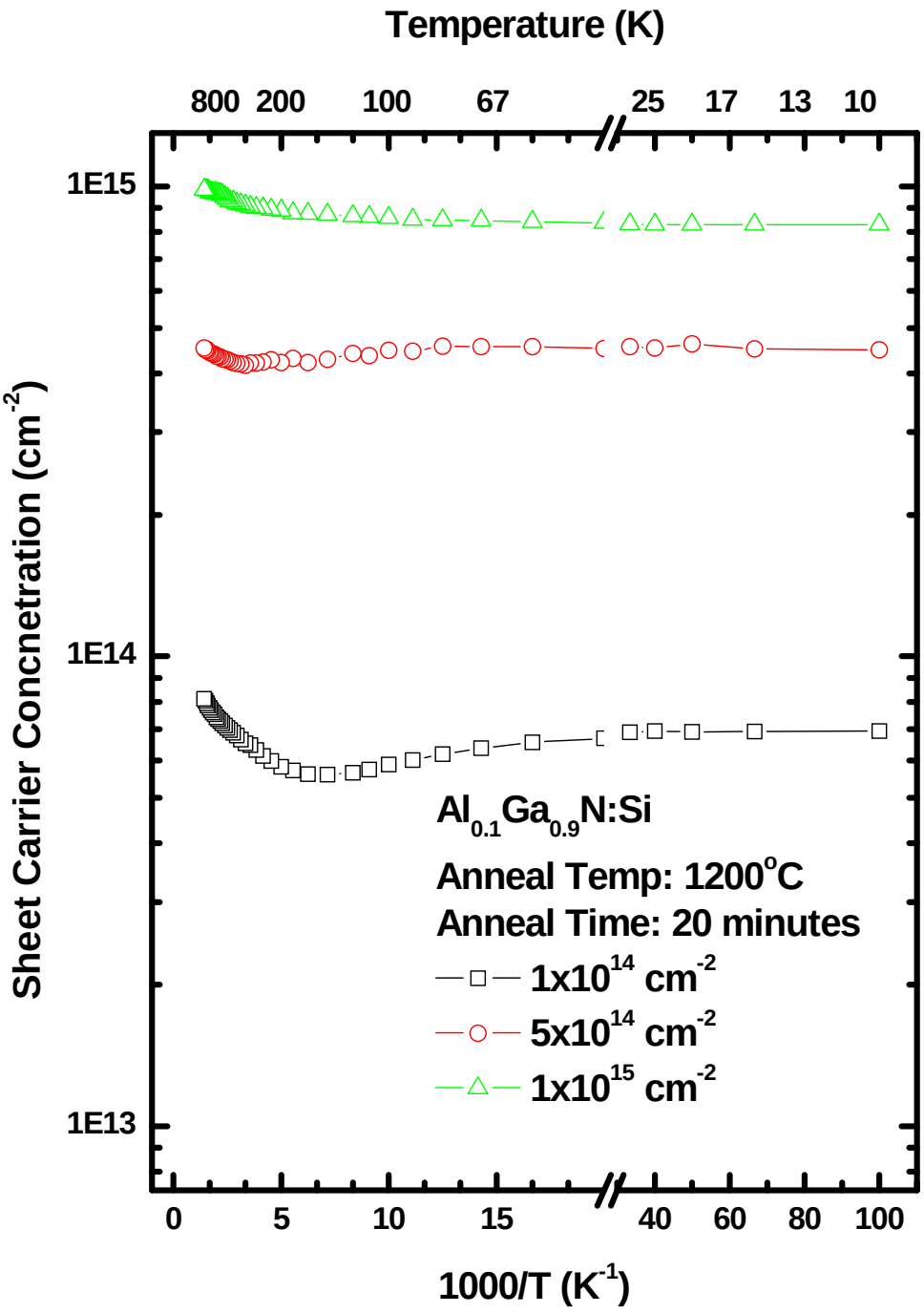

Figure 5.7. Temperature-dependent sheet carrier concentrations of $Al_{0.1}Ga_{0.9}N$ determined from Hall Effect measurements taken from 10 to 700 K. The $Al_{0.1}Ga_{0.9}N$ was implanted with three different doses of Si ions that had an energy of 200 keV and annealed at 1200 ºC for 20 minutes in a flowing nitrogen environment.

one being the degenerate impurity band and the other the non-degenerate n-type $Al_{0.1}Ga_{0.9}N$ layer that results from the Gaussian distribution of the implanted ions (37, 68). The samples implanted with $5x10^{14}$ cm^{-2} silicon ions also have a slight dip in the carrier concentration only at higher temperatures.

As the sample temperature is increased one would expect the carrier concentration to approach a constant as all the donor electrons become excited into the conduction band. However, the temperature-dependent carrier concentration for samples implanted with all three silicon doses begins to increase as the sample temperature approaches 800 K. This sudden increase, along with the dip in carrier concentration for the samples implanted with the lower silicon doses, indicates the presence of more than one conducting layer in the material. The dip in the carrier concentration around 140 and 300 K for the samples implanted with $1x10^{14}$ and $5x10^{14}$ cm^{-2} silicon ions is similar to the temperature-dependent carrier concentrations observed by Look *et el*. in highly degenerate GaN samples grown on sapphire substrates with a sputtered ZnO buffer layer (37). They modeled the dependency using a two-layer Hall effect model and attributed the conduction to the GaN layer as well as the interfacial region between the GaN and sapphire substrate.

The temperature-dependent nature of the carrier concentration indicates that the samples have transitioned from activated conduction to metallic like conduction. This signifies that the donor impurity level of the silicon has formed into a degenerate band and as the carrier concentration of the samples increases this impurity band merges with the conduction band. The effects of impurity screening are enhanced by an increase in the concentration of ionized donors and will act to reduce the donor ionization energy. Thus the ionization energy for silicon in $Al_{0.1}Ga_{0.9}N$ can not be accurately estimated from

the implanted samples in this study. For the sake of comparison with other literature, the extracted ionization energies for the three implanted silicon doses in $Al_{0.1}Ga_{0.9}N$ that were annealed at 1200 ºC are shown in Figure 5.8.

The reported values for the ionization energy of silicon in $Al_{0.1}Ga_{0.9}N$ are on the order of 1-30 meV. Irokawa *et al*. reported an ionization energy of 23 meV for $Al_{0.13}Ga_{0.87}N$ implanted with $1x10^{14}$ cm^{-2} silicon ions and annealed at 1300 ºC for 5 minutes in a nitrogen ambient (34). This energy is consistent with other reported values for Si ionization energy in $Al_xGa_{1-x}N$ with this Al concentration for in-situ doped material (38-40). Polyakov *et al*. reported ionization energies on the order of 10 to 16 meV for $Al_xGa_{1-x}N$ with Al concentrations of 10 to 20% (36). While Ryu *et al*. achieved ionization energies as low as 1.4 meV and 3.1 meV for $Al_{0.18}Ga_{0.82}N$ that had been implanted with $5x10^{14}$ cm^{-2} silicon ions and annealed at 1150 ºC and 1250 ºC, respectively, for 25 minutes in a nitrogen ambient (35). Hwang *et al*. show that from a simple hydrogen model, the donor ionization energy of silicon in $Al_xGa_{1-x}N$ increases from 34 to 90 meV as the Al mole fraction is increased from zero to one for a non-degenerate sample (51).

The ionization energy of the implanted Si ions is determined by assuming that the carrier concentration is proportional to $\exp(-\Delta E/k_BT)$ for high temperatures. In the low temperature regime, the ionization energy can then be extracted from the slope of a least squares fit of the data graphed as the ln(sheet carrier concentration) versus 1/T, which is referred to as an Arrhenius plot (72,113). The resistivity has a temperature dependence that is the reciprocal that of the carrier concentration so that resistivity data can also be

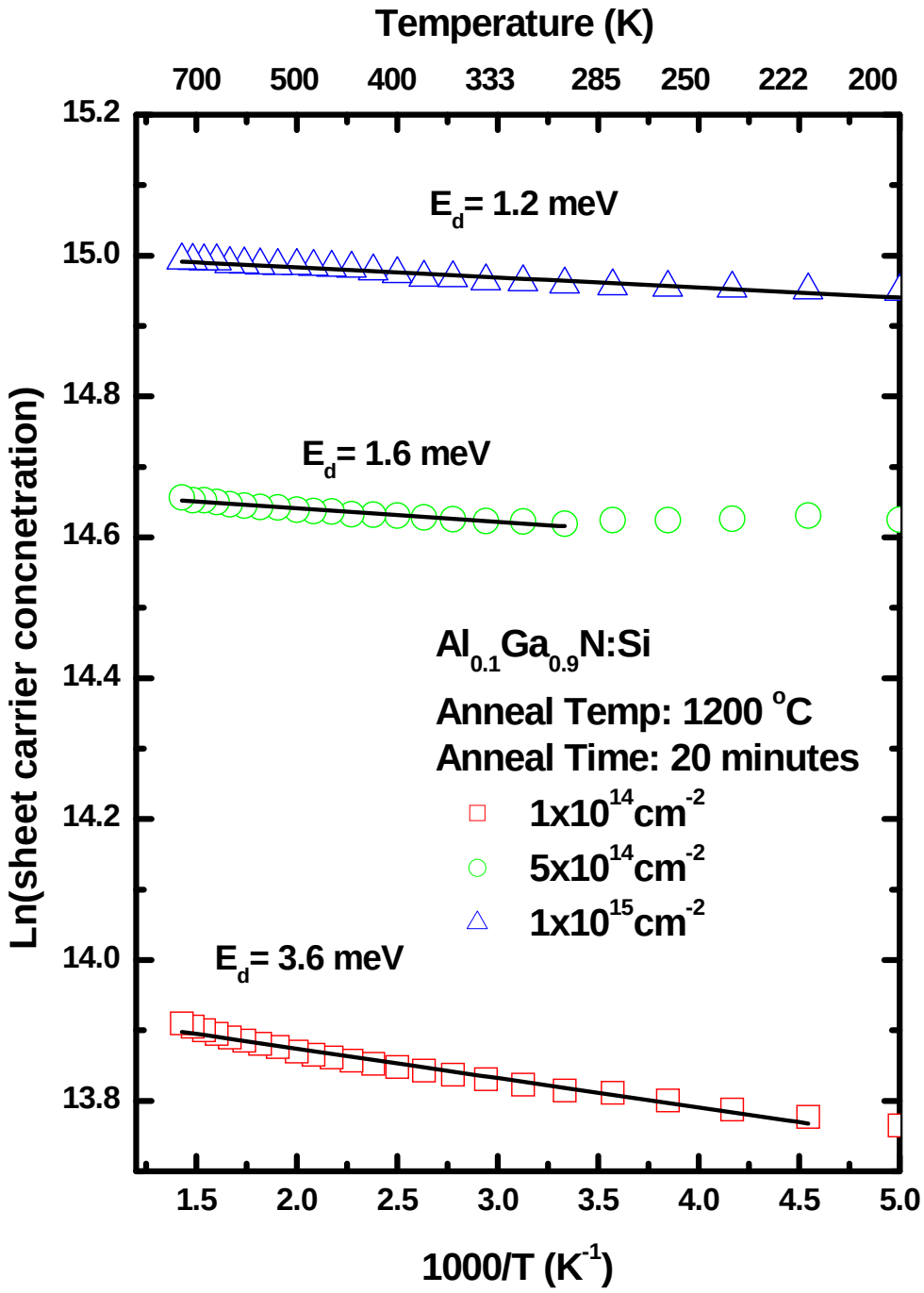

Figure 5.8: Arrhenius plot used to calculate the ionization energy of the implanted Si for all three doses in $Al_{0.1}Ga_{0.9}N$. The samples were annealed at 1200 ºC for 20 minutes in a nitrogen ambient. The ionization energies are calculated from the slope of the fit to the Hall data and are shown by the black line.

used for extracting the ionization energy. The carrier concentration data used for the fit spanned the temperature range from 200 to 700 K.

The $Al_{0.1}Ga_{0.9}N$ implanted with $1x10^{14}$ cm^{-2} silicon ions exhibits the highest ionization energy of 3.6 meV of all the implanted silicon doses studied however, this energy is lower than expected due to degeneracy. The samples implanted with doses of $5x10^{14}$ and $1x10^{15}$ cm^{-2} silicon ions have similar ionization energies of 1.6 and 1.2 meV, respectively. These empirically determined ionization energies are much lower than those predicted by Hwang *et al.* and those reported in the literature due to the degeneracy of the samples (51). However, they agree well with the results that were reported by Ryu *et al.* (35). The actual ionization energy can only be determined if the impurity band is non-degenerate. The low ionization energy can be attributed to the formation of a degenerate impurity band caused from exceeding the Mott concentration of $1.8x10^{18}$ cm^{-3} with the implanted silicon doses. The ionization energy levels become shallower as the implanted silicon doses are increased revealing the higher degeneracy of the samples, similar to that observed by Fellows in Si-implanted GaN (22).

The temperature-dependent Hall mobilities for the Si-implanted $Al_{0.1}Ga_{0.9}N$ are shown in Figure 5.9. The samples implanted with each of the three of the silicon doses exhibit a peak in their mobility curve around 300 K, with the lowest dose exhibiting the highest mobility of 109 $cm^2/V{\cdot}s$. The mobility curves for all the Si-implanted $Al_{0.1}Ga_{0.9}N$ increase as the temperature is raised from 10 to 300 K, at which point they reach their maximum. The samples implanted with $1x10^{14}$ cm^{-2} silicon ions exhibit the greatest change in mobility over the given temperature range initially increasing sharply and then experiencing a more subtle decline. The samples implanted with $5x10^{14}$ and $1x10^{15}$ cm^{-2}

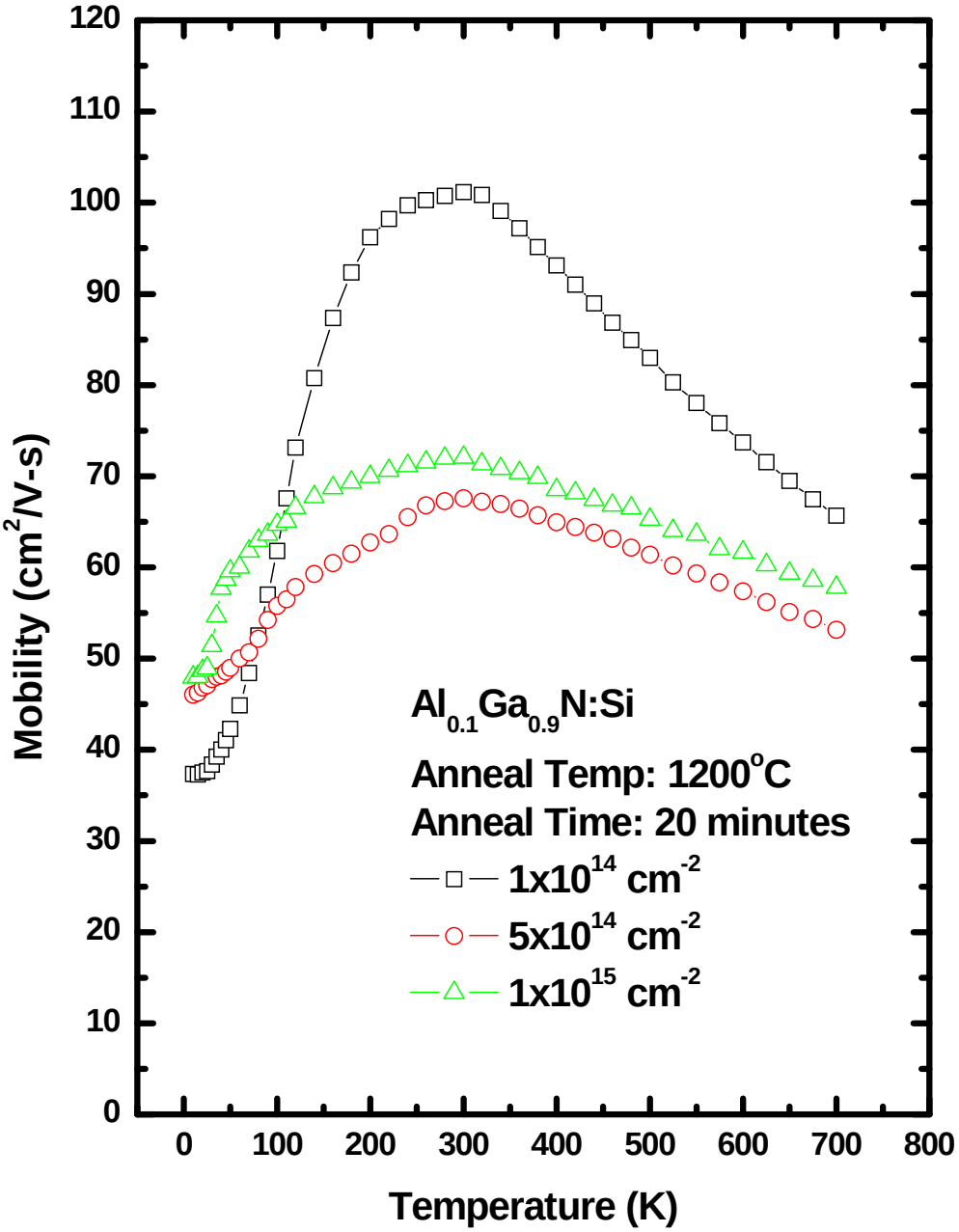

Figure 5.9. Temperature-dependent Hall mobilities taken from 10 to 700 K for $Al_{0.1}Ga_{0.9}N$ implanted at room temperature at different doses of silicon ions that had an energy of 200 keV and annealed at 1200 ºC for 20 minutes.

silicon ions have mobilities very close together, however the mobility is higher for the $Al_{0.1}Ga_{0.9}N$ implanted with $1x10^{15}$ cm^{-2} silicon ions, as it was for the room temperature mobility for these samples. The sudden increase in the mobility for the samples implanted with a dose of $1x10^{15}$ cm^{-2} silicon ions is attributed a decrease in ionized impurity scattering resulting from the decrease in activation efficiency for the samples annealed at 1200 °C. These samples a weaker temperature-dependence than the samples implanted with the lower silicon dose. In general, the mobility decreases as the dose is increased due to the stronger effects of ionized impurity and polar phonon lattice scattering. However, at low temperatures (< 100 K), the mobility behavior changes and begins to increase as the Si-implanted dose is increased. The mobility of non-degenerate semiconductors should approach zero as the sample temperature is brought down to absolute zero and then increase rapidly as the temperature is raised due to screening of ionized impurity scattering that is dominant. The $Al_{0.1}Ga_{0.9}N$ mobilities for the three implanted silicon doses of $1x10^{14}$, $5x10^{14}$, and $1x10^{15}$ cm^{-2} are 37.3, 46.1, and 47.9 $cm^2/V{\cdot}s$, respectively, at a temperature of 10 K. The degenerate impurity band causes the low temperature mobility to be temperature-independent and also to increase with the doping level. The temperature-dependent mobility curve for the $Al_{0.1}Ga_{0.9}N$ implanted with the lowest silicon dose most resembles that which is predicted by theory for a non-degenerate sample. The higher dose curves are more flat and temperature independent as would be expected by a degenerate sample.

Figure 5.10 shows the temperature-dependent resistivities of the $Al_{0.1}Ga_{0.9}N$ samples for all three silicon implantation doses. The resistivity decreases significantly as the implantation dose is increased and also becomes more temperature-independent. All

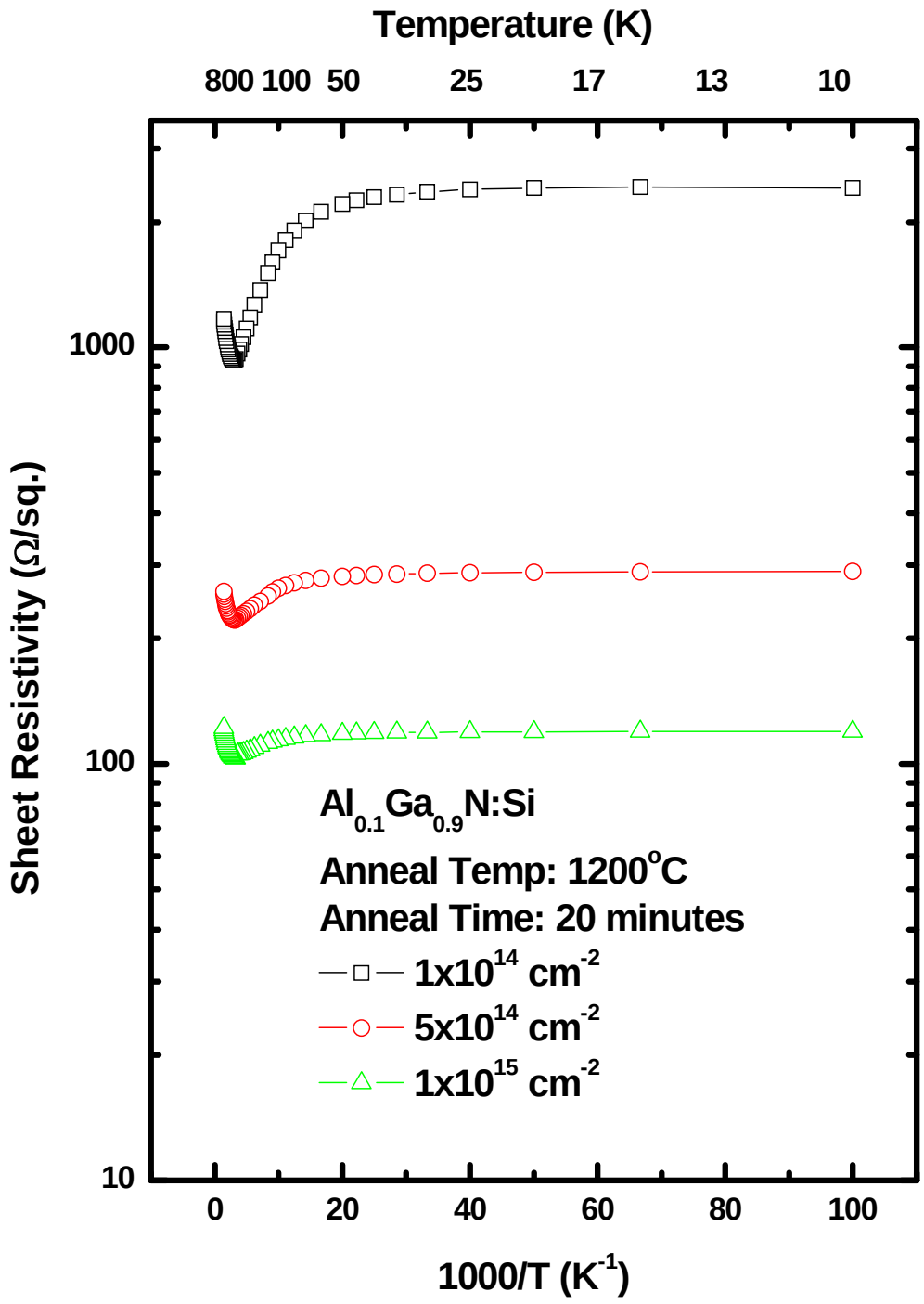

Figure 5.10. Temperature-dependent resistivity values calculated from Hall measurements taken from 10 to 700 K for $Al_{0.1}Ga_{0.9}N$ that had been implanted with $1x10^{14}$, $5x10^{14}$, and $1x10^{15}$ cm^{-2} silicon ions at 200 keV and annealed at 1200 °C for 20 minutes in flowing nitrogen.

three implantation doses show a relative temperature-independent resistivity from around 10 to 50 K before slowly dipping to a minimum at around 300 K followed by an increase up through sample temperatures of 700 K. The drop in the resistivity for the samples implanted with $1x10^{14}$ cm^{-2} silicon ions being the most pronounced and the drop in the samples implanted with $1x10^{15}$ cm^{-2} silicon ions being almost unnoticeable. The increase in the resistivity for high temperatures is a result of the dramatic decrease in the mobility at this temperature range which results from an increase in ionized impurity scattering. The bend in the resistivity around 300 K for each dose is a manifestation of the resistivity's dependence on the mobility, which is dependant on different scattering mechanisms at different temperatures and thus changes considerably with temperature.

Experiencing a minimum resistivity and a maximum mobility at room temperature can be beneficial for device performance considering this temperature is the most common temperature at which devices are required to function. The temperature independent nature of the carrier concentration, mobility and resistivity as well as the low ionization energies reveal that the samples increasingly become more degenerate as the Si-implanted dose is increased from $1x10^{14}$ to $1x10^{15}$ cm^{-2}.

Low Temperature Cathodoluminescence Measurements

Cathodoluminescence (CL) measurements were taken with an electron energy of 10 keV with 50 μA of source current. The temperature in the chamber was 7.4 K, and the slits on the spectrometer were 200 μm both at the entrance and the exit. The range scanned was 1800 to 7000 Å with a step size of 2 Å and an integration time of 0.1

second. The CL spectra give insight into the nature of the energy transitions taking place in the material, and therefore give the type of defect and impurity levels that may occur in the band gap.

The spectra of the unimplanted samples shown as a function of anneal temperature are given in Figure 5.11. To gauge the level of damage recovery in the Si-implanted samples, the behavior of the unimplanted samples must first be observed. The dominant feature in $Al_xGa_{1-x}N$ luminescence at low temperatures is found to involve the transition of a localized exciton (44, 60-61). Each of the CL spectra for the given anneal temperatures show a strong neutral-donor-bound exciton (D^o,X) peak at 3.69 eV. The spectrum for these samples also exhibits a small peak at 3.61 eV, whose source is unknown. The spectrums for the samples annealed at 1100 and 1150 ºC have been reduced by a factor of two. The sample annealed for 20 minutes at 1150 ºC has the strongest intensity followed by the sample annealed at 1100 ºC. The intensity of the (D^o,X) peak at first increases with temperature peaking after the 1150 ºC anneal. However, increasing the temperature further results in decreasing the (D^o,X) intensity. The sample annealed at 1250 ºC for 20 minutes exhibits the lowest intensity however; the peak is still very sharp. The reason for the decrease in the intensity of the (D^o,X) peak for this sample are unknown, probably due to the nature of the particular sample, but it is noticed that the unimplanted sample that was annealed at 1250 ºC was the only unimplanted sample that had a measurable carrier concentration. The CL spectra for the unimplanted samples indicate that 1150 ºC is the optimal annealing temperature for repairing defects that occurred during growth.

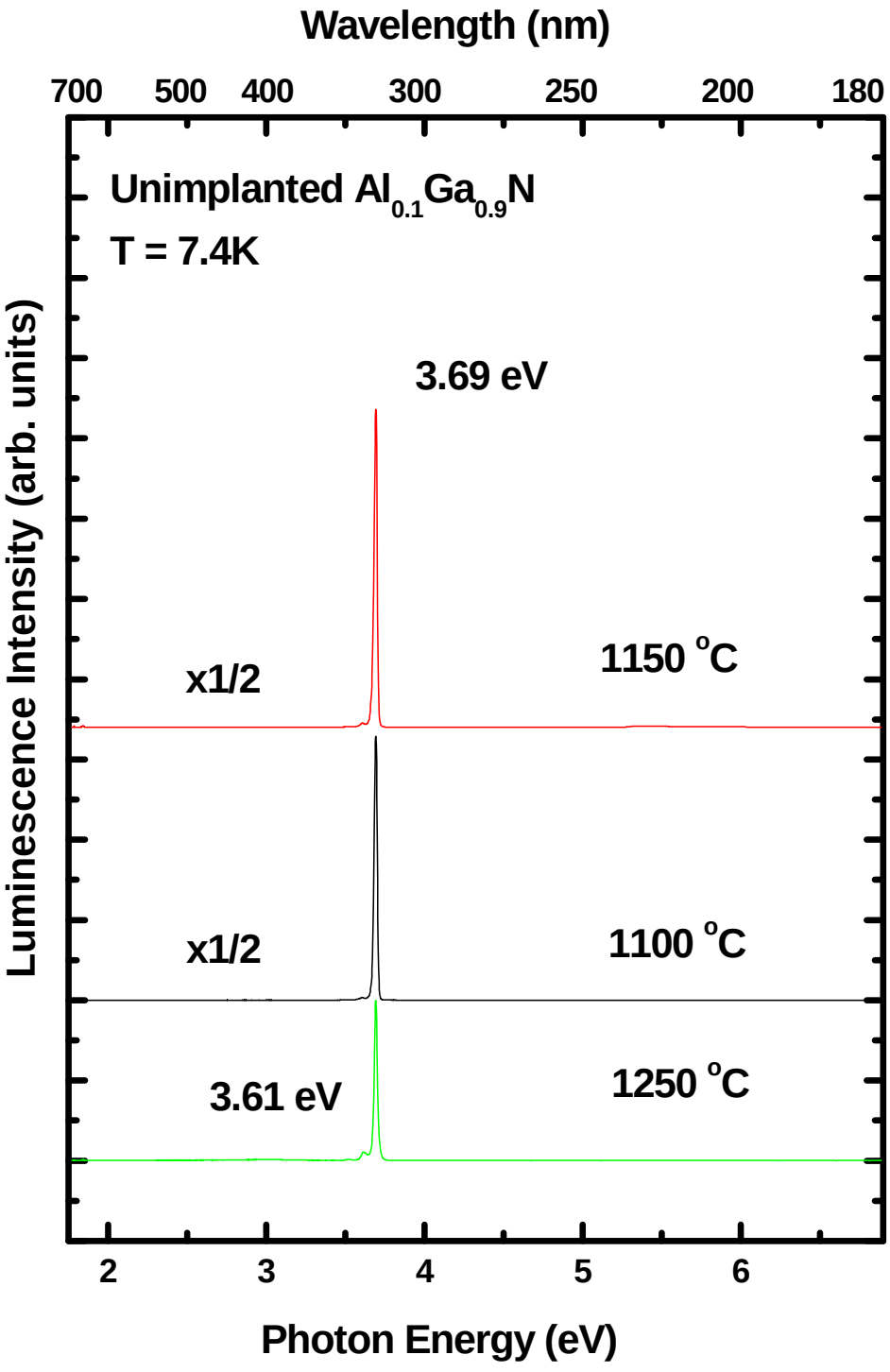

Figure 5.11. CL spectra taken at 7.4 K for unimplanted $Al_{0.1}Ga_{0.9}N$ that have been anneal at 1100, 1150 and 1250 °C for 20 minutes in flowing nitrogen.

The low temperature CL spectra, for the silicon implanted $Al_{0.1}Ga_{0.9}N$ annealed for 20 minutes at 1150 ºC, are shown in Figure 5.12. The spectrum for the unimplanted sample is $1/20^{th}$ of its original intensity and shows a sharp (D^o,X) peak at 3.69 eV. The intensities of the (D^o,X) peaks for the implanted $Al_{0.1}Ga_{0.9}N$ decrease as the silicon dose is increased, due to the increased number of donors in the degenerate level. The sample implanted with a dose of $1x10^{14}$ cm^{-2} silicon ions showed the strongest (D^o,X) peak at 3.69 eV, with a shoulder on the lower energy side at 3.61 eV. The spectrum also shows a broad yellow band (YL) with a peak around 2.4 eV that is not observed in the unimplanted samples, similar to that observed in GaN (22). Also, this YL band shows interference patterns. The samples implanted with $5x10^{14}$ cm^{-2} silicon ions exhibit a similar spectrum only the (D^o,X) peak and YL band have weaker intensity. The (D^o,X) peak in the spectrum of the sample implanted with $1x10^{15}$ cm^{-2} silicon ions is much broader than those for the other implanted doses. The (D^o,X) peak is blueshifted to 3.60 eV and has broadened both toward lower and higher energies. The luminescence of this sample covers a range from 3.5 to 4.0 eV. The near band edge broadening on the low energy side of the (D^o,X) peak or the sample implanted with $1x10^{15}$ cm^{-2} silicon ions is due to band tailing effects.

These effects are small but are noticeable for the $Al_{0.1}Ga_{0.9}N$ implanted with the lower silicon doses. The impurity band formation, which was confirmed by the temperature-dependent Hall effect measurements, can cause random band-edge effects such as band tailing and band filling. Only the samples implanted with the highest silicon dose of $1x10^{15}$ cm^{-2} had a volume carrier concentration high enough for band filling to occur. This effect is seen in the CL spectrum as broadening of the (D^o,X) peak towards higher energies, which is only present in the spectrum of this sample.

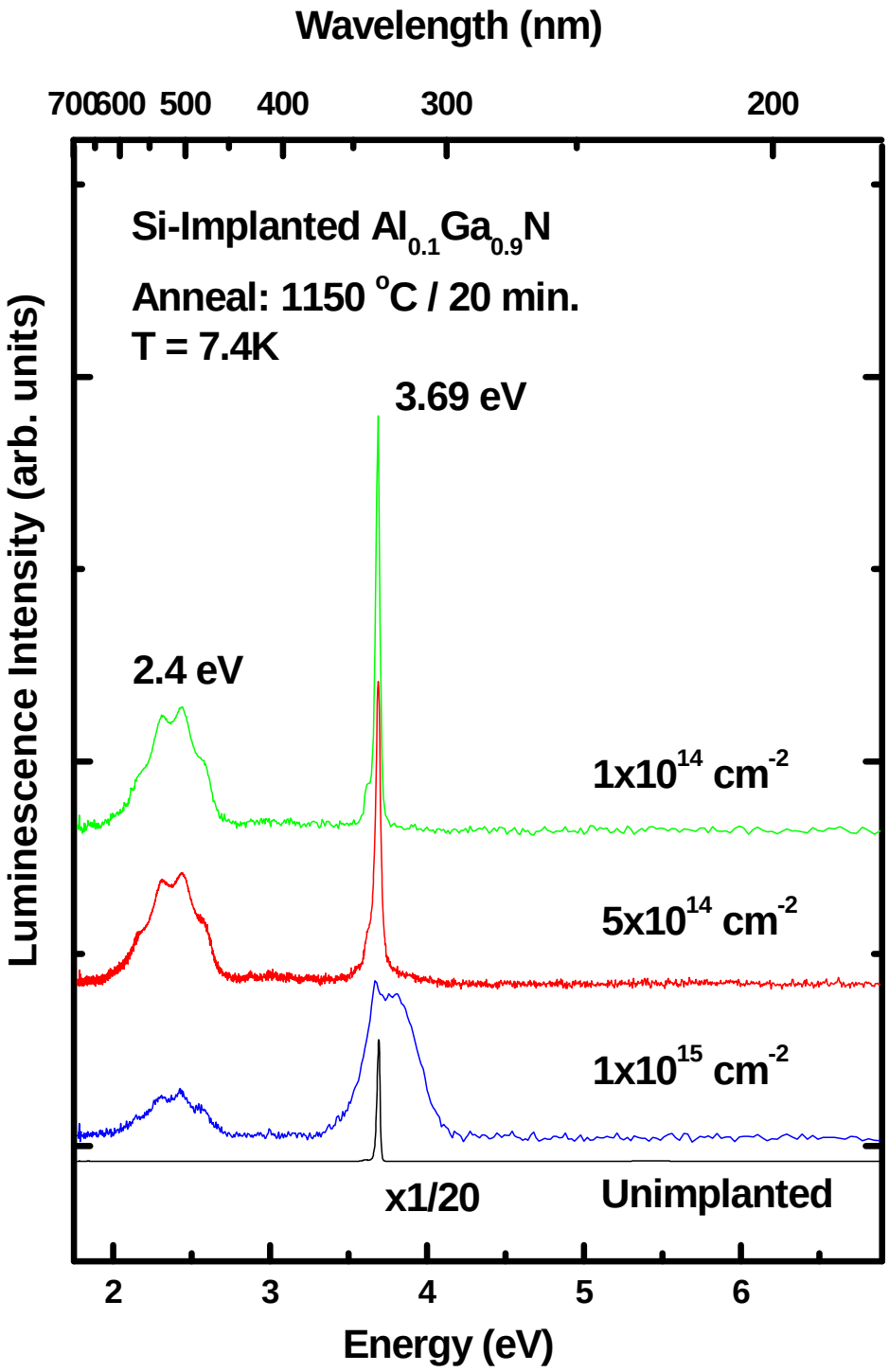

Figure 5.12. CL spectra taken at 7.4 K for $Al_{0.1}Ga_{0.9}N$ that have been anneal at 1150 ºC for 20 minutes in flowing nitrogen.

The YL band for the $Al_{0.1}Ga_{0.9}N$ implanted with a dose of $1x10^{15}$ cm^{-2} silicon ions is not as intense as it was in the spectra of the samples implanted with other doses. The observed YL band decreases as the Si-implanted dose of the $Al_{0.1}Ga_{0.9}N$ is increased (and therefore activation efficiency) and also as the anneal temperature is increased, which can be seen in Figure 5.13. There is still much debate over the origin of the yellow band in GaN and in $Al_xGa_{1-x}N$ materials in the literature. Glaser *et al*. claim the band is the result of radiative recombination between deep donors and shallow acceptors (41). While others like Ogino *et al*. attribute the band to transitions from native shallow donors and deep carbon related acceptors (42). Polyakov *et al*. noticed that the peak of the yellow band shifts to higher energy as the Al concentration of the material is increased. They claim that it is consistent with a recombination process between native donor defects and a defect in the middle of the band gap, possibly carbon related (43). Nam *et al*. also noticed this shift in the YL band to a violet band, VL, as the Al mole fraction was increased from 0 to 1 (44). They attribute the formation of this band to DAP transitions that involve shallow donors, either Si or oxygen, whose ionization energies increase with increasing Al content and a deep acceptor whose energy does not change with mole fraction, such as an Al or Ga vacancy or vacancy complex.

The low temperature CL spectra for the silicon implanted $Al_{0.1}Ga_{0.9}N$ annealed for 20 minutes at 1250 ºC are shown in Figure 5.13. The spectrum of the unimplanted sample has a strong (D^o,X) peak at 3.69 eV with intensity higher than the samples implanted with $1x10^{14}$ and $5x10^{14}$ cm^{-2} silicon ions. However, as seen in Figure 5.11, the intensity of the (D^o,X) peak for the unimplanted sample annealed at 1250 ºC is significantly reduced from that of the unimplanted samples annealed at lower temperatures. The sample implanted with the highest silicon dose exceeds the intensity

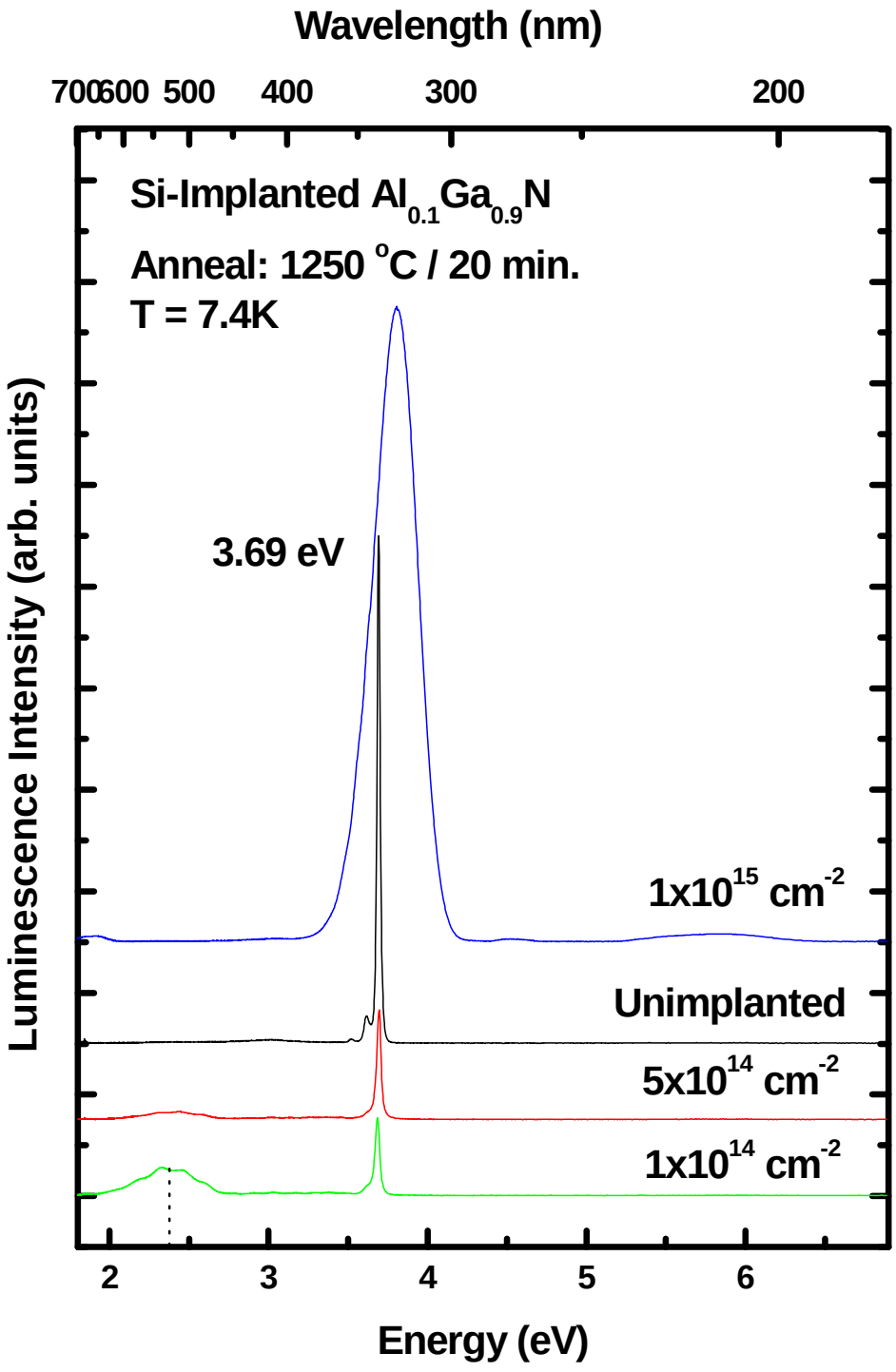

Figure 5.13. CL spectra taken at 7.4 K for Si-implanted $Al_{0.1}Ga_{0.9}N$ that have been annealed at 1250 °C for 20 minutes in flowing nitrogen.

of the unimplanted sample after the 1250 ºC anneal however, the peak has broadened considerably due to band tailing and band filling effects. At this anneal temperature, 1250 ºC, the intensity of the (D^o,X) peak increases slightly as the implantation dose in increased, which is a little different from what occurred for the 20 minute 1150 ºC anneal. The sample implanted with $1x10^{14}$ cm^{-2} silicon ions has a sharp (D^o,X) peak at 3.69 eV however, the intensity is weak and band tailing effects are barely noticeable as is for the samples implanted with a dose of $5x10^{14}$ cm^{-2} silicon ions. The YL band that was prominent in the spectrum for the 1150 ºC anneal has also lost most of its intensity after the higher temperature anneal. The YL band is barley distinguishable for the $Al_{0.1}Ga_{0.9}N$ implanted with $5x10^{14}$ cm^{-2} silicon ions and is no longer visible for the samples implanted with the highest silicon dose after the 1250 ºC anneal. The spectrum of the samples implanted with a dose of $5x10^{14}$ cm^{-2} silicon ions exhibits a sharp (D^o,X) peak at 3.69 eV with weaker intensity than the unimplanted sample. The sample implanted with $1x10^{15}$ cm^{-2} silicon ions has a broad peak centered on 3.80 eV that is as intense as the unimplanted sample. The peak is more intense and broader than the peak observed for the 1150 ºC anneal. The YL band luminescence has also been quenched after the high temperature anneal for the sample implanted with this silicon dose.

The samples annealed at 1250 ºC produce clear spectra that more closely resemble those of the unimplanted samples, signifying greater recovery of the crystal lattice structure.

The low temperature CL spectra for the $Al_{0.1}Ga_{0.9}N$ implanted with $1x10^{14}$ cm^{-2} silicon ions annealed for 20 minutes at various temperatures are shown in Figure 5.14. All of the samples result in spectra with sharp (D^o,X) peak centered at 3.69 eV. The (D^o,X) peak is very weak for the samples annealed at 1100 ºC but increases rapidly as the anneal temperature is increased. Apparently, an anneal temperature of 1100 ºC is too low

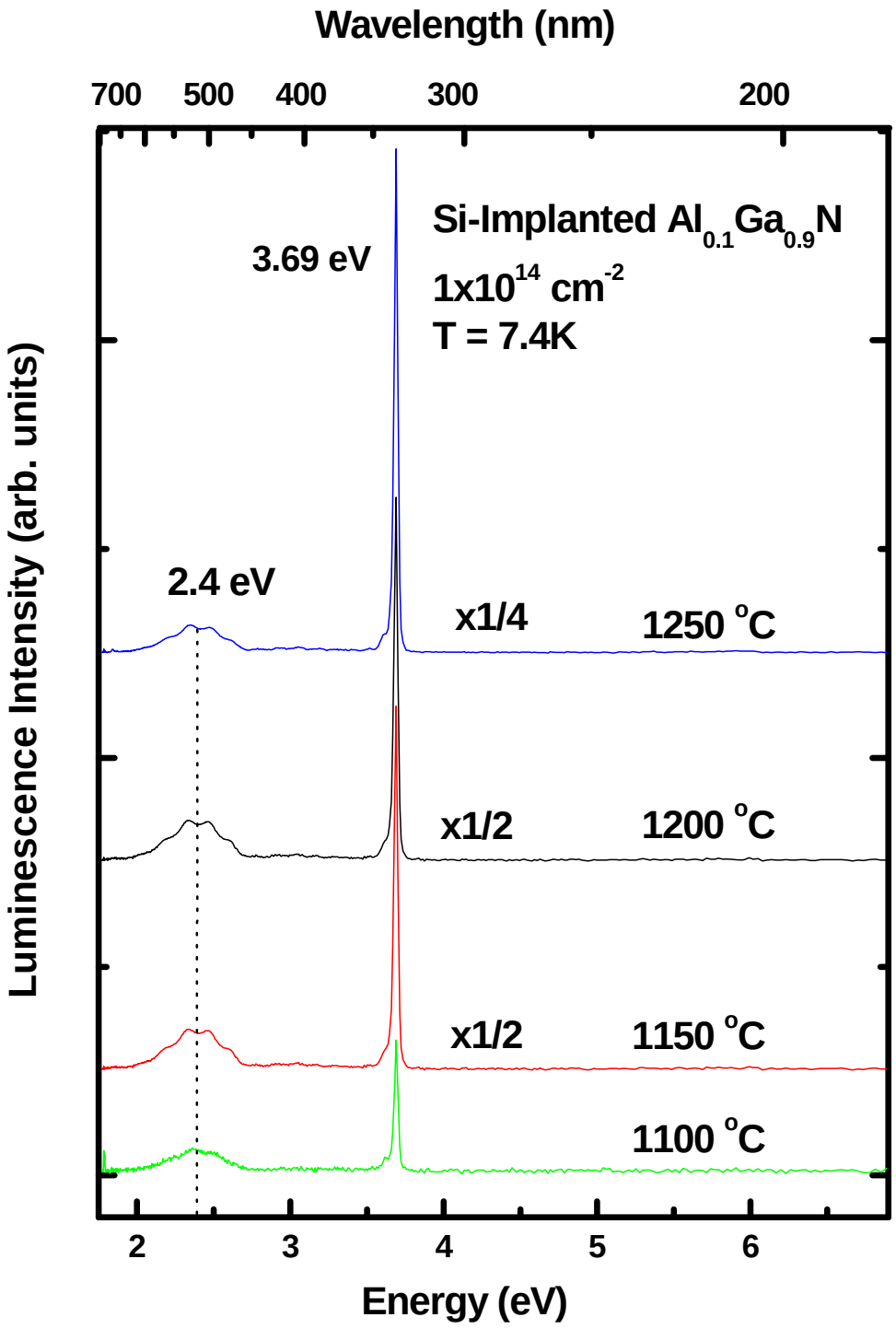

Figure 5.14. CL spectra taken at 7.4 K for $Al_{0.1}Ga_{0.9}N$ that has been implanted with $1x10^{14}$ cm^{-2} silicon ions and then annealed at various temperatures for 20 minutes in flowing nitrogen.

for significant recovery of the implantation induced damage to occur. The spectrum of the sample annealed at 1250 ºC has been reduced by a factor of 4, and the spectra for the samples annealed at 1150 and 1200 ºC have been reduced be a factor of 2. The increase in intensity of the (D^o,X) peaks observed for the other anneal temperatures of 1150, 1200, and 1250 ºC indicate that more of the implanted silicon ions have become electrically active, and successive improvement in the crystal recovery has taken place with each increase in the anneal temperature.

The YL band in the spectra for the sample annealed at 1100 ºC is barely observable but quickly becomes prevalent following the 1150 ºC anneal. The YL band declined in intensity as the anneal temperature was increased from 1150 to 1250 ºC. The YL band is believed to be caused from transition of a shallow donor and a deep acceptor. The shallow donor level has been theorized to be the result of silicon or oxygen impurities in the crystal. The YL band was not observed in any of the spectrum of the unimplanted samples, even after annealing at 1250 ºC, so that its origin it not believed to be caused from annealing related defects. The YL band for the samples implanted with $1x10^{14}$ cm^{-2} silicon ions is most prominent is samples that exhibited low activation efficiency and decreases as the activation of the samples increased. The YL band could then be attributed to the residual damage from the ion implantation or from the silicon ions.

These CL results agree very well with the electrical data obtained from Hall Effect measurements for this implanted silicon dose. The sharpness and strong intensity of the peak correlate well with the high mobility values obtained on this sample. The exciton peak and the high mobilities (page 94) observed on the samples implanted with the low silicon dose indicate excellent implantation damage recovery after annealing at

1200 ºC for 20 minutes in flowing nitrogen. This is supported by the decrease in mobility for the samples annealed at 1250 ºC, which results from an increase in ionized impurity scattering whose effects can be observed once the lattice damage has been recovered.

The CL spectra of the samples annealed at temperatures from 1100 to 1250 ºC and implanted with a silicon dose of $5x10^{14}$ cm^{-2} are shown in Figure 5.15. The strongest (D^o,X) peak is observed for the sample annealed at 1150 ºC for 20 minutes. The spectrum for this sample has been reduced by a factor of twelve. An anneal temperature of 1100 ºC was not sufficient enough to restore a significant amount of lattice damage caused by the ion implantation. The (D^o,X) peak at 3.69 eV in the CL spectrum of this sample is barely observable and matched in intensity to the YL band. However, increasing the anneal temperature 50 ºC enhances the exciton peak 200 times signifying a considerable amount of damage recovery has taken place. The unimplanted sample annealed at 1150 ºC also exhibited the most intense (D^o,X) peak. Increasing the temperature any further causes the (D^o,X) peak to diminish considerably. The YL band decreases slightly as the temperature is raised from 1150 to 1200 ºC however the YL band luminescence gets stronger following the 1250 ºC anneal. The peak for the sample annealed at 1250 ºC is weak and broad showing evidence of band tailing and band filling effects. The peak is redshifted from the (D^o,X) peak to 3.61 eV, which was evident in the spectrum of the unimplanted samples as a small peak, and is matched in intensity to the YL band.

The CL spectra would indicate that the optimum anneal temperature for the (D^o,X) signal in the samples that were implanted with this silicon dose is 1150 ºC whereas the room temperature electrical data indicates that complete lattice damage recovery takes place after annealing at 1200 ºC. The peak electrical activation efficiency

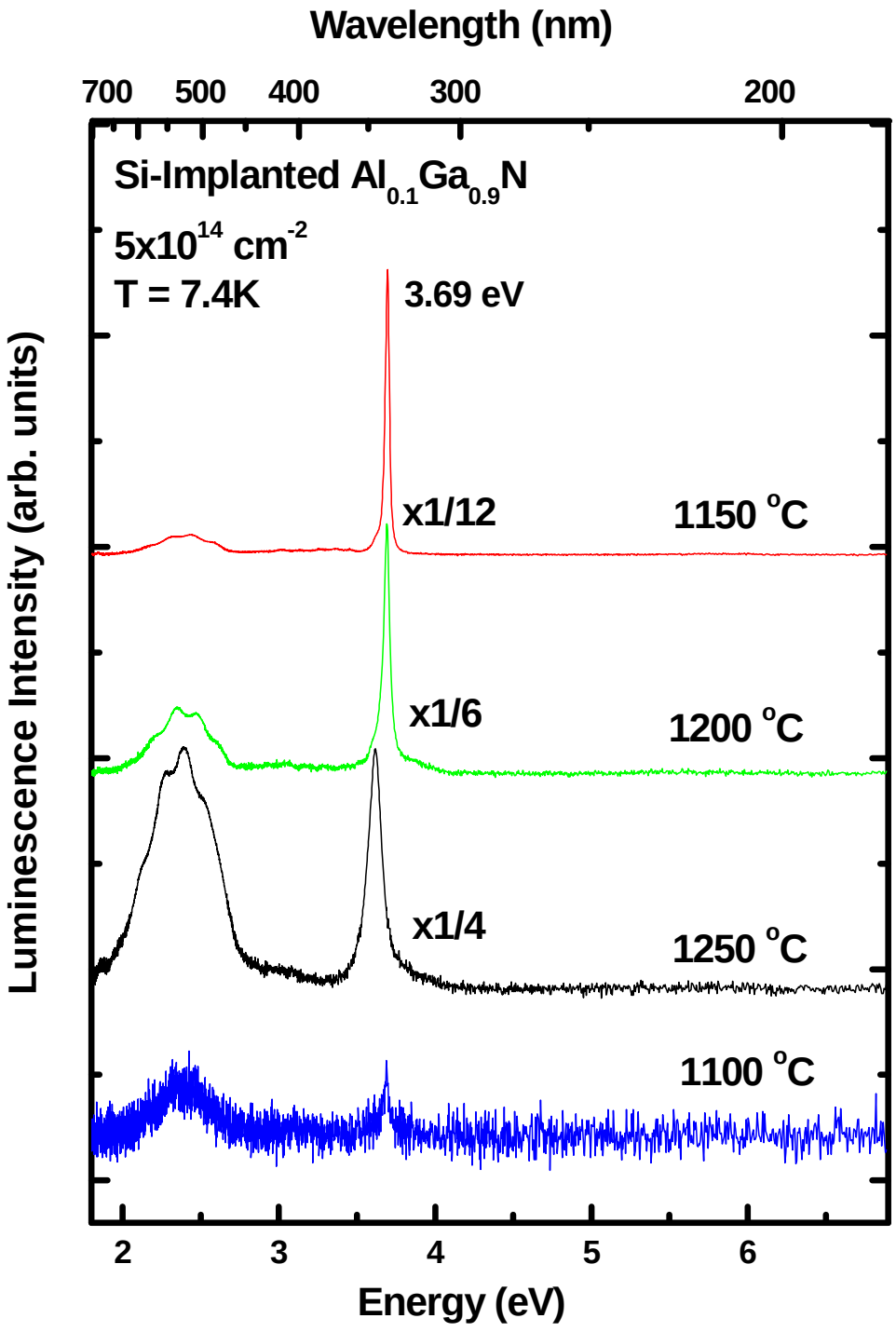

Figure 5.15. CL spectra taken at 7.4 K for $Al_{0.1}Ga_{0.9}N$ that has been implanted with $5x10^{14}$ cm^{-2} silicon ions and then annealed at various temperatures for 20 minutes in flowing nitrogen.

for samples implanted with this dose occurred after the samples were annealed at 1200 ºC. Increasing the anneal temperature to 1250 ºC causes the activation to decrease which in turn causes a decrease in ionized impurity scattering which allows the mobility to increase. This is also witnessed in the time-dependent annealing in which the activation efficiency increases after lengthening the anneal time, but the mobility decreases due to the increase in ionized impurity scattering. As mentioned previously, the effects of ionized impurity scattering are weaker then those of the lattice recovery and as a result are normally not witnessed until lattice recovery has taken place. Thus the electrical data indicates that the lattice damage has been restored after annealing at 1200 ºC. The YL band decreases slightly as the anneal temperature is raised which could possibly be attributed to an increase in activation. This line of thinking would also explain the increase in the YL band as the anneal temperature is increased to 1250 ºC. The decline in intensity of the (D^o,X) peak could be due to the silicon ions forming trapping centers that are charged but are non-radiative. The broadening and redshifting of the peak in the sample annealed at 1250 ºC could be due to a new transition that is compensating.

The CL spectra of the $Al_{0.1}Ga_{0.9}N$ implanted with the highest silicon dose of $1x10^{15}$ cm^{-2} are shown in Figure 5.16. As the anneal temperature is increased, the intensity of the (D^o,X) peak increases significantly. The samples annealed at lower temperatures, where the silicon electrical activation was at its maximum, show very weak (D^o,X) peak. The sample annealed at 1100 ºC has a weak (D^o,X) peak at 3.69 eV and a slightly observable YL band. The (D^o,X) peak is observable for the sample that had been annealed at 1150 ºC, but it is not sharp. The dominant luminescence from this sample has broadened considerably to cover the range 3.5 to 4.1 eV. The YL band is enhanced

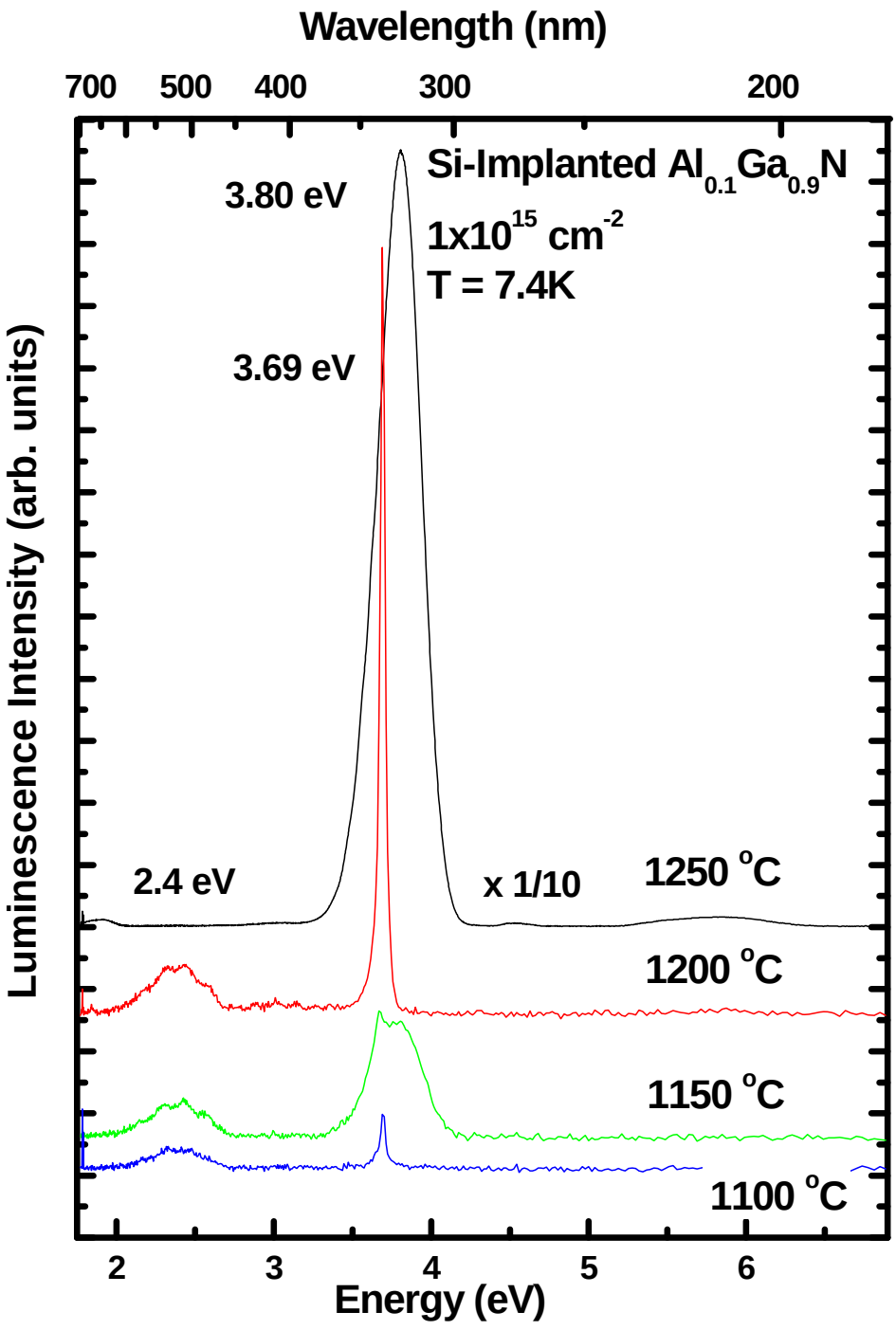

Figure 5.16. CL spectra taken at 7.4 K for $Al_{0.1}Ga_{0.9}N$ that has been implanted with $1x10^{15}$ cm^{-2} silicon ions and then annealed at various temperatures for 20 minutes in flowing nitrogen.

in the sample annealed at 1150 ºC from the sample annealed at 1100 ºC. The sample annealed at 1200 ºC show recovery of the (D^o,X) centered at 3.69 eV that is sharp but weak when compared to the intensity of the sample annealed at 1250 ºC whose spectrum has been reduced by a factor of 10. As the anneal temperature is increased to 1250 ºC, the band edge peak is broadened considerably due to band tailing and band filling and its peak occurs at a higher energy of 3.80 eV. However, the (D^o,X) peak appears clearly after annealing at 1200 ºC and also the full width half max of the peak is improved upon extending the anneal temperature to 1200 ºC. The decrease in the full width half max of the peak observed when increasing the anneal temperature to 1200 ºC is lost upon raising the anneal temperature to 1250 ºC. The intensity of the peak annealed at 1250 ºC supersedes that of all the other anneal temperatures. The YL band for these samples increases as the anneal temperature is increased from 1100 to 1200 ºC and then disappears for the sample that was annealed at 1250 ºC. Thus the YL band does not decrease as the activation increases as it has for the samples implanted with the lower silicon doses.

The optical data indicates the optimal annealing temperature for $Al_{0.1}Ga_{0.9}N$ implanted with $1x10^{15}$ cm^{-2} silicon ions would be 1200 ºC considering that this is the only sample that displays a sharp (D^o,X) peak, like the as-grown material. The weak intensity could be related to the decline in the activation efficiency that occurred for the sample annealed at this temperature. As the anneal temperature is increased the silicon ions begin to occupy nitrogen sites and thus begin to compensate the electrons donated to the conduction by the silicon ions that are on gallium or aluminum sub-lattice positions. The electrical data indicates that the lattice damage has been greatly restored after annealing at 1150 or 1200 ºC. The sample that obtained the highest activation efficiency

was annealed at 1150 ºC and based on the changes of the mobility for the other annealing temperatures (increasing from decrease in activation for the 1200 and 1250 ºC anneals and decreasing from an increase in activation from the extended time anneals at 1200 ºC) it would appear that the optimal annealing temperature was 1150 ºC. However, the mobility and the spectral response are weaker than expected if the majority of the lattice damage has been recovered. When considering all of the data, the optimal annealing temperature for $Al_{0.1}Ga_{0.9}N$ implanted with $1x10^{15}$ cm^{-2} silicon ions must be 1200 ºC.

In the latter two implantation doses the CL spectrum exhibiting the most lattice damage recovery does not correspond to the anneal temperature that produces the best silicon activation. The increased activation at lower anneal temperatures in the samples implanted with the higher silicon doses is attributed to an increase in the implantation damage which creates more vacancies and thus a place in the lattice for the implanted Si ions. The samples implanted with the lowest silicon doses experience the least amount of radiation damage and exhibits the best lattice recovery yet the lowest silicon electrical activation.

Silicon Implanted $Al_{0.2}Ga_{0.8}N$

$Al_xGa_{1-x}N$ with Al concentrations around 20% have been less investigated by other groups than $Al_{0.1}Ga_{0.9}N$. The most comprehensive studies have come from Ryu *et al*. who have shown great success implanting silicon at various doses into MBE-grown $Al_xGa_{1-x}N$ with Al concentrations of 18 and 24 % (35, 45-46). The $Al_{0.18}Ga_{0.82}N$ was implanted with Si ions at 200 keV with doses of $5x10^{14}$ and $1x10^{15}$ cm^{-2}. These samples were annealed at 1250 ºC for 25 minutes and exhibited 100% and 94% electrical

activations, respectively. They found the electrical activation efficiencies to be strongly dependent on anneal time as well as anneal temperature. In their study, they focused on annealing at lower temperatures and slowly increasing the anneal time to show that time variation can have a greater impact on the activation and produce more commercially viable results. The same group implanted $Al_{0.24}Ga_{0.76}N$ with silicon ions at 200 keV with doses of $5x10^{13}$ and $1x10^{14}$ cm^{-2}. The $Al_{0.24}Ga_{0.76}N$ exhibited nearly 100% activation for both doses following a 20 minute anneal at 1350 and 1300 ºC, respectively. Another study, conducted by Chitwood achieved 65% and 87% activation for MBE-grown $Al_{0.25}Ga_{0.75}N$ implanted with silicon ions at 200 keV for doses of $1x10^{14}$ and $1x10^{15}$ cm^{-2}, respectively, after annealing at 1350 ºC for 2 minutes (47). Researchers have found that even with an Al mole fraction of 20%, $Al_xGa_{1-x}N$ material's resistive properties can be hard to overcome. Nakano *et al*. implanted $Al_{0.2}Ga_{0.8}N$ with oxygen ions that had an energy of 83 keV in a dose of $5.8x10^{14}$ cm^{-2} and found the material too resistive to collect data even after annealing at 1300 ºC for 5 minutes in flowing nitrogen (48). However, this was not the case for the Si-implanted $Al_{0.2}Ga_{0.8}N$ grown by MEMOCVD used in this study.

Room Temperature Hall Effect Measurements

The MEMOCVD grown $Al_{0.2}Ga_{0.8}N$ was capped with 500Å of AlN and implanted at room temperature with Si ions that had an energy of 200 keV with three different doses. The Si doses were $1x10^{14}$, $5x10^{14}$, and $1x10^{15}$ cm^{-2} and the effective doses are $9.84x10^{13}$, $4.92x10^{14}$, and $9.84x10^{14}$ cm^{-2}, respectively when taking into account the AlN cap. The samples were annealed from 1150 to 1300 ºC for 20 minutes

in a flowing nitrogen environment. The $Al_{0.2}Ga_{0.8}N$ samples experienced minor damage to the surface morphology following the anneal at 1300 ºC, increasing the anneal temperature to 1350 ºC however, caused significant damage to the surface for these samples. Annealing at 1200 ºC for 40 minutes also produced highly damaged samples that had visible amounts of liquid gallium and aluminum on the surface, however during the anneal the sample lifting rod malfunctioned which extended the sample decent considerably. Room temperature Hall effect measurements were conducted to determine sheet carrier concentrations for the samples and the results are shown in Figure 5.17. The unimplanted samples both as-grown and annealed were highly resistive making it impossible to collect any meaningful data. Thus, the silicon electrical activation was calculated using the measured room temperature carrier concentration with no correction for background carriers.

The sheet carrier concentrations for the $Al_{0.2}Ga_{0.8}N$ implanted with each silicon dose respond uniformly to an increase in the anneal temperature. The carrier concentrations for these samples increase as the anneal temperature is increased from 1150 to 1300 ºC, with the samples implanted with the lowest silicon dose experiencing the most dramatic incline across the given temperature span. The $Al_{0.2}Ga_{0.8}N$ implanted with $1x10^{14}$ cm^{-2} silicon ions exhibit a large increase in carrier concentration between the 1150 and 1200 ºC anneal, after which it increases linearly as the temperature is increased from 1200 to 1300 ºC. The maximum carrier concentration obtained for the samples implanted with this silicon dose was $8.25x10^{13}$ cm^{-2} following an anneal at 1300 ºC for 20 minutes in a nitrogen ambient. The carrier concentrations for the $Al_{0.2}Ga_{0.8}N$ samples implanted with doses of $5x10^{14}$ and $1x10^{15}$ cm^{-2} silicon ions have the same dependence on the anneal

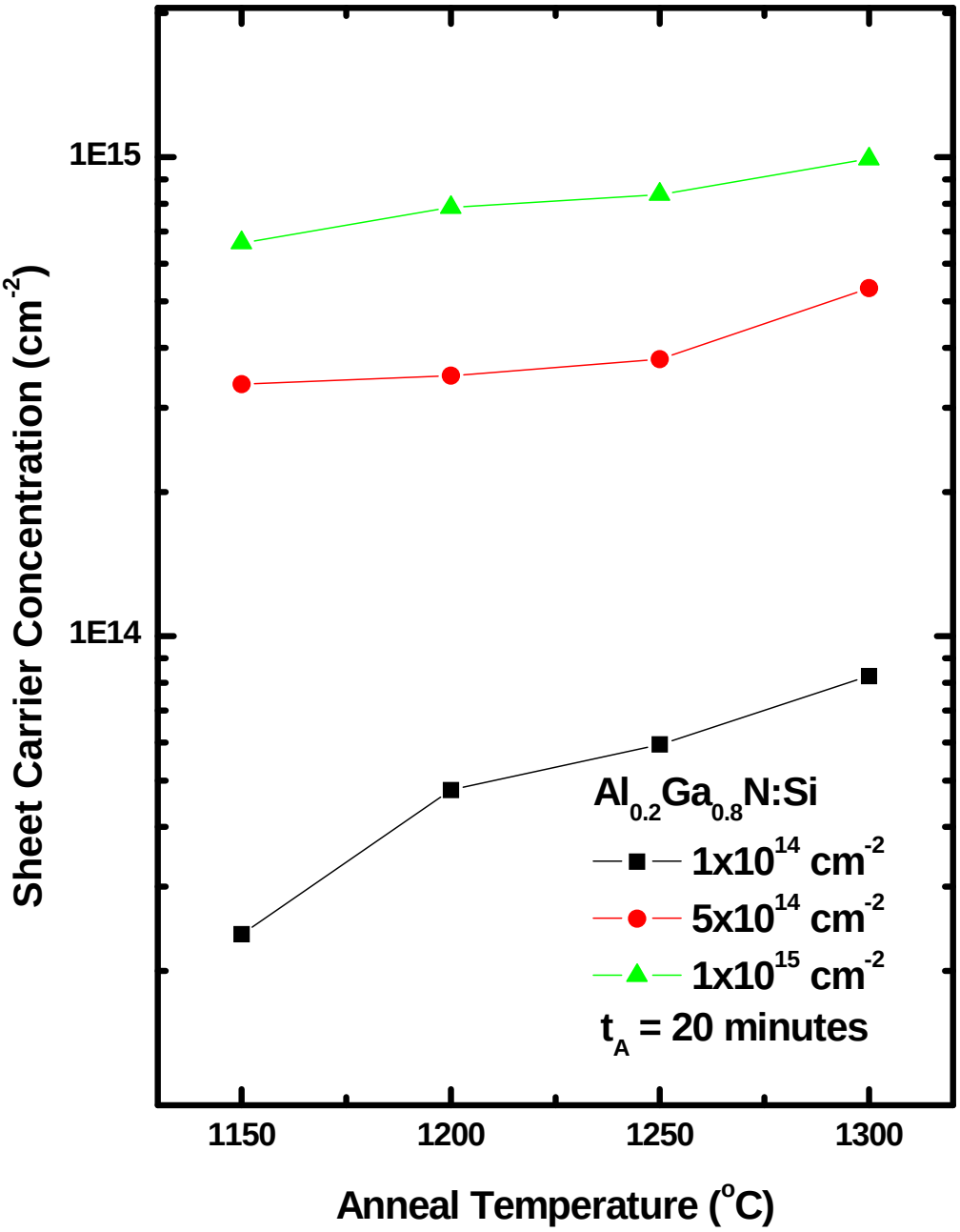

Figure 5.17. Room temperature sheet carrier concentrations for $Al_{0.2}Ga_{0.8}N$ implanted with silicon ions at 200 keV at room temperature with doses of $1x10^{14}$, $5x10^{14}$, and $1x10^{15}$ cm^{-2} and subsequently annealed from 1150 to 1300 °C for 20 minutes in flowing nitrogen.

temperature. The carrier concentrations for both samples increase linearly as the anneal temperature is raised from 1150 to 1250 ºC and then spikes for the samples annealed at 1300 ºC. The maximum carrier concentrations obtained for the $Al_{0.2}Ga_{0.8}N$ implanted with silicon doses of $5x10^{14}$ and $1x10^{15}$ cm^{-2} were $5.33x10^{14}$ and $9.92x10^{14}$ cm^{-2}, respectively, after being annealed for 20 minutes at 1300 ºC.

The $Al_xGa_{1-x}N$ with Al mole fractions of 10 and 20% implanted with a silicon dose of $1x10^{14}$ cm^{-2} have carrier concentrations that increase steadily as the anneal temperature is raised however, the $Al_{0.1}Ga_{0.9}N$ samples exhibit slightly higher carrier concentrations at any given temperature. The carrier concentrations for the $Al_xGa_{1-x}N$ implanted with a dose of $5x10^{14}$ cm^{-2} silicon ions also show similar dependencies on the anneal temperature between the two Al mole fractions. The $Al_{0.1}Ga_{0.9}N$, however, decreased in carrier concentration after being annealed at 1250 ºC; whereas the $Al_{0.2}Ga_{0.8}N$ samples continued to show increasing carrier concentrations for anneal temperatures up to 1300 ºC. The $Al_xGa_{1-x}N$ samples implanted $5x10^{14}$ cm^{-2} silicon ions, unlike the samples implanted with $1x10^{14}$ cm^{-2}, have higher carrier concentrations for the $Al_{0.2}Ga_{0.8}N$ than $Al_{0.1}Ga_{0.9}N$ at any given temperature. The samples implanted with $1x10^{15}$ cm^{-2} exhibit the most remarkable change in behavior between the two different Al concentrations. The $Al_{0.1}Ga_{0.9}N$ samples reached their peak carrier concentration after being annealed at 1150 ºC, and further increasing the anneal temperature caused the carrier concentration to decline. The carrier concentrations of the $Al_{0.2}Ga_{0.8}N$, however, are enhanced as the anneal temperature is increased from 1150 to 1300 ºC.

The silicon electrical activations, shown in Figure 5.18, of these samples are closely related to the carrier concentrations and follow the same trends with the anneal temperature as mentioned above. The electrical activation efficiency for $Al_{0.2}Ga_{0.8}N$ was

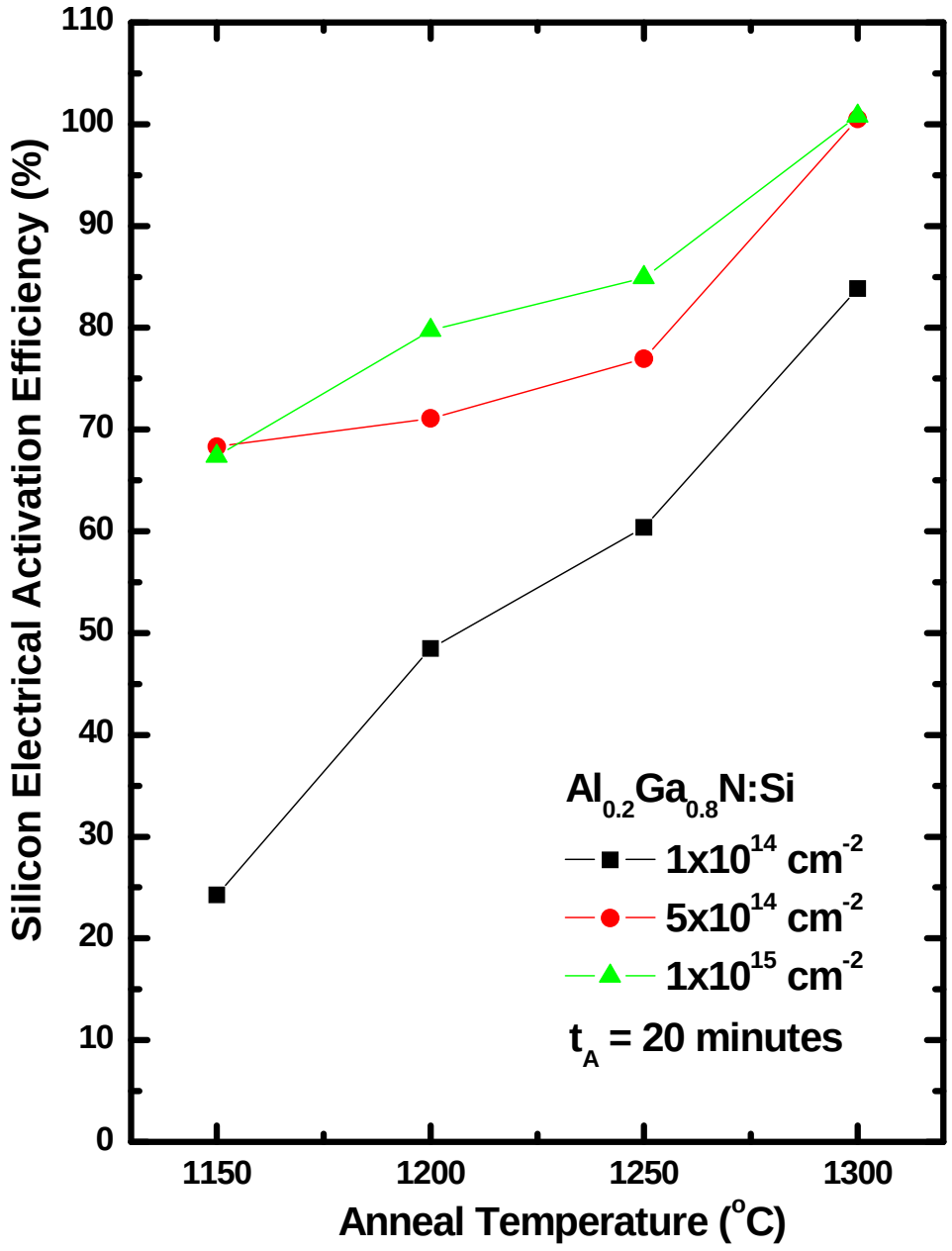

Figure 5.18. Electrical activation efficiency for Si-implanted $Al_{0.2}Ga_{0.8}N$ calculated from the room temperature Hall measurements for doses of $1x10^{14}$, $5x10^{14}$, and $1x10^{15}$ cm^{-2} and annealed from 1150 to 1300 °C for 20 minutes.

calculated using the effective dose and room temperature sheet carrier concentrations. Higher implantation doses resulted in higher silicon activation efficiencies for anneal temperatures up to 1300 ºC. The silicon electrical activation for the samples implanted with $1x10^{14}$ cm^{-2} silicon ions exhibits the most improvement over the given temperature range, increasing from 24% to 83% after being annealed for 20 minutes at 1150 ºC and 1300 ºC. The samples implanted with a dose of $5x10^{14}$ cm^{-2} silicon ions have a significant activation efficiency of 68% after the 1150 ºC twenty minute anneal and steadily increases to a maximum of 100% following the 1300 ºC anneal. The samples implanted with the highest silicon dose of $1x10^{15}$ cm^{-2} also reaches 100% activation after being annealed at 1300 ºC for 20 minutes in a nitrogen ambient.

The increased activation for the samples implanted with the higher doses is attributed to an increase in the implantation damage which creates more vacancies to better incorporate the implanted Si ions. The samples implanted with the lowest dose experience the least amount of radiation damage and exhibit the best lattice recovery however; they have the lowest silicon electrical activation.

The $Al_{0.1}Ga_{0.9}N$ implanted with all three silicon doses display their peak electrical activations at different anneal temperatures while the $Al_{0.2}Ga_{0.8}N$ exhibit their peak activation at 1300 ºC for all the implanted silicon doses. The samples implanted with the highest silicon dose generally exhibit the best activations for both Al mole fractions at any given anneal temperature. The $Al_xGa_{1-x}N$ implanted with the lowest silicon dose had the lowest activations but showed the best response to an increase in anneal temperature, indicating that a further increase in the anneal temperature may result in higher activation. Like the $Al_{0.1}Ga_{0.9}N$, the higher implanted silicon doses are more readily activated than lower silicon doses in $Al_{0.2}Ga_{0.8}N$, which is illustrated in Figure 5.19.

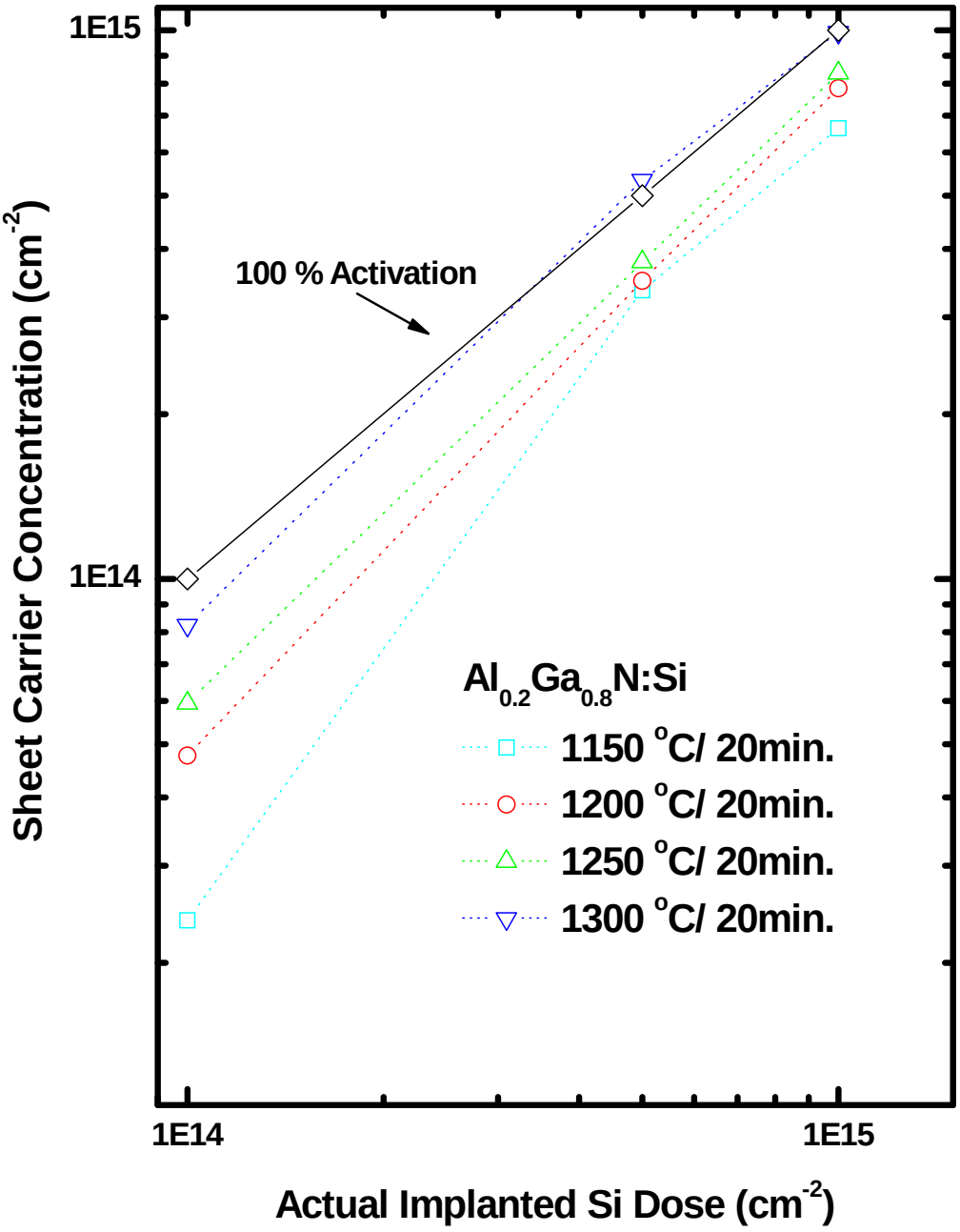

Figure 5.19. The room temperature sheet carrier concentrations versus the actual implantation dose for $Al_{0.2}Ga_{0.8}N$ implanted at room temperature with silicon at 200 keV with doses of $1x10^{14}$, $5x10^{14}$, and $1x10^{15}$ cm^{-2} and annealed from 1150 to 1300 °C for 20 minutes in a nitrogen ambient.

The $Al_{0.2}Ga_{0.8}N$ implanted with $1x10^{14}$ cm^{-2} silicon ions exhibits an electrical activation of 83% following a 1300 ºC anneal for 20 minutes in flowing nitrogen. Ryu *et al*. reported a slightly higher activation of ~100% for Si-implanted MBE-grown $Al_{0.24}Ga_{0.76}N$ under the same implantation and anneal conditions, while Chitwood achieved only 65% after annealing at 1350 ºC for 2 minutes (35, 47). The $Al_{0.2}Ga_{0.8}N$ implanted with a silicon dose of $5x10^{14}$ cm^{-2} reach a maximum electrical activation of 100% after being annealed at 1300 ºC for 20 minutes. Ryu reported the same activation for $Al_{0.24}Ga_{0.76}N$ implanted with the same silicon dose after annealing at 1250 ºC for 25 minutes. In this study, the electrical activation of the $Al_{0.2}Ga_{0.8}N$ implanted with $1x10^{15}$ cm^{-2} silicon ions was 100% following a 20 minute anneal at 1300 ºC. Ryu reported an activation of 94% for similar samples after annealing at 1250 for 25 minutes while, Chitwood only reported an 87% activation after annealing $Al_{0.25}Ga_{0.75}N$ at 1350 ºC for two minutes. The optimal anneal temperature for the $Al_{0.2}Ga_{0.8}N$ implanted with a dose of $1x10^{14}$ cm^{-2} silicon ions may be higher than 1300 ºC, while the optimal anneal temperature for the samples implanted with the higher silicon doses of $5x10^{14}$ and $1x10^{15}$ cm^{-2} is 1300 ºC for an anneal time of 20 minutes. The optimal anneal temperature is found to be dose dependent, requiring higher anneal temperatures as the ion dose is decreased to achieve high electrical activation.

The resistivity values for the $Al_{0.2}Ga_{0.8}N$ implanted with each silicon dose are shown in Figure 5.20. The resistivity of all the samples decreased as the anneal temperature was increased. The samples implanted with a dose of $1x10^{15}$ cm^{-2} silicon ions exhibit the least improvement in resistivity over the given temperature span and the samples implanted with a silicon dose $1x10^{14}$ cm^{-2} show the greatest. The samples implanted with a dose of $1x10^{14}$ cm^{-2} silicon ions have resistivity values 10 and 24 times

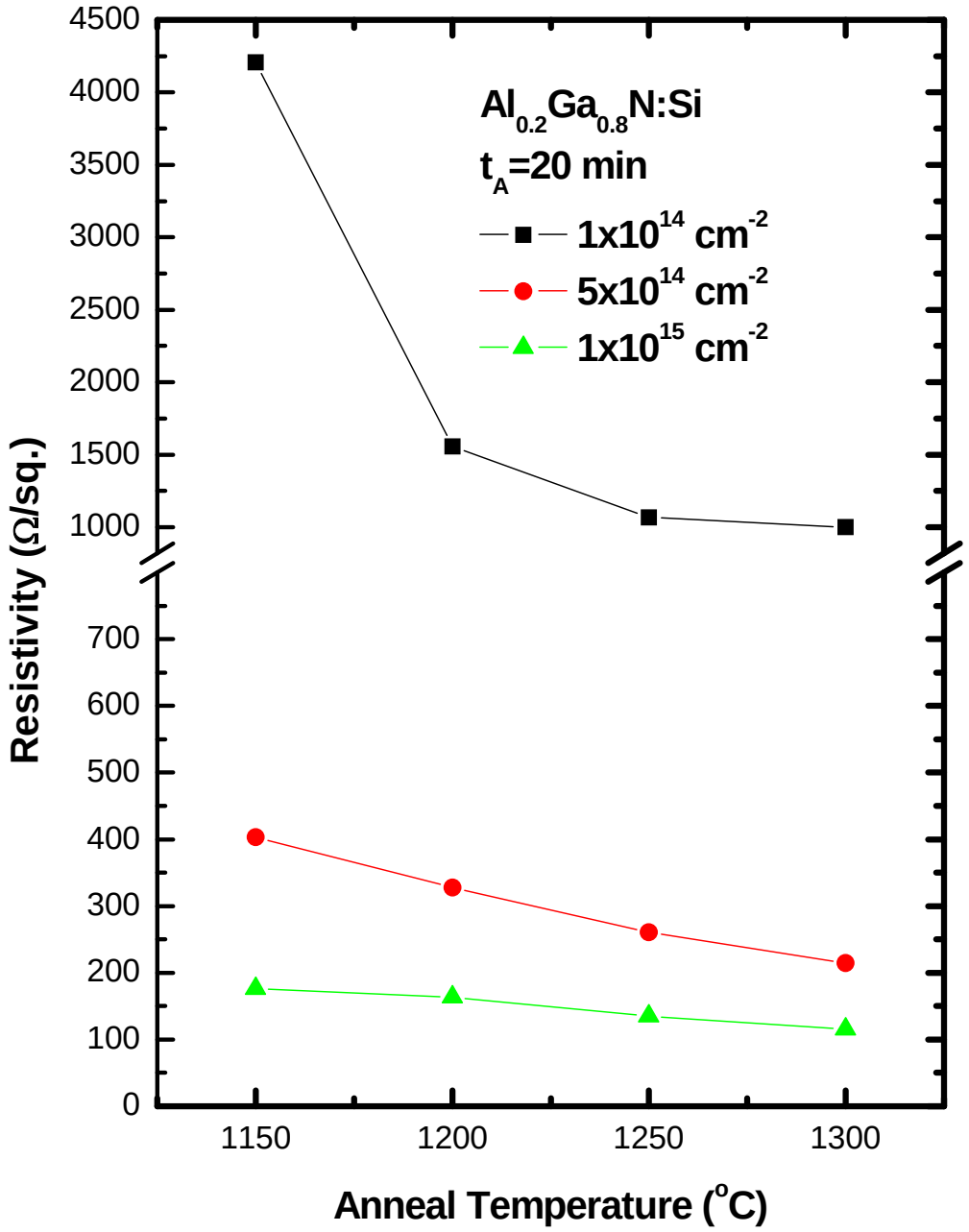

Figure 5.20. Room temperature resistivity measurements taken under zero magnetic field for $Al_{0.2}Ga_{0.8}N$ implanted at room temperature with silicon ions at 200 keV with doses of $1x10^{14}$, $5x10^{14}$, and $1x10^{15}$ cm^{-2} and annealed from 1150 ºC to 1300 ºC for 20 minutes in a nitrogen ambient.

higher than the samples implanted with $5x10^{14}$ and $1x10^{15}$ cm^{-2} silicon ions after being annealed at 1150 ºC for 20 minutes. However, the resistivity for the samples implanted with this silicon dose decreases 3.2 kΩ/□ as the anneal temperature is increased to 1300 ºC. The largest measured resistivity is 4.2 kΩ/□ for the samples implanted with $1x10^{14}$ cm^{-2} silicon ions after being annealed at 1150 ºC for 20 minutes. The measured resistivities of the samples implanted with $5x10^{14}$ and $1x10^{15}$ cm^{-2} silicon ions are all below 500 Ω/□. The $Al_{0.2}Ga_{0.8}N$ implanted with $5x10^{14}$ cm^{-2} silicon ions show a linear decrease in resistivity over the entire temperature span dropping from 403 Ω/□ to 214 Ω/□. The samples implanted with $1x10^{15}$ cm^{-2} silicon ions also show a linear decrease in resistivity as the anneal temperature is increased from 1150 to 1300 ºC dropping from 176 Ω/□ to 115 Ω/□, respectively. The anneal temperature that produces the lowest resistivity in $Al_{0.2}Ga_{0.8}N$ is also the anneal temperature that corresponds to the maximum in carrier concentration, and thus activation efficiency for all of the implanted $Al_{0.2}Ga_{0.8}N$. The resistivity, for both the 10 and 20% $Al_xGa_{1-x}N$, of the implanted samples was found to increase as the silicon dose was lowered from $1x10^{15}$ cm^{-2} to $1x10^{14}$ cm^{-2} silicon ions, which is consistent with that of the carrier concentration.

The room temperature mobilities for each dose of the Si-implanted $Al_{0.2}Ga_{0.8}N$ samples are shown in Figure 5.21. The mobility for all the samples increased as the anneal temperature was increased up to 1250 ºC, and then declines at an anneal temperature of 1300 ºC. The mobility of the samples implanted $1x10^{14}$ cm^{-2} silicon ions had much higher mobilities than the samples implanted with the two higher silicon doses due to an increase in ionized impurity scattering for the higher dose implanted samples. The samples implanted with $1x10^{14}$ cm^{-2} silicon ions show a dramatic rise in mobility from 62 $cm^2/V{\cdot}s$ to 98 $cm^2/V{\cdot}s$ as the anneal temperature is increased from 1150 to

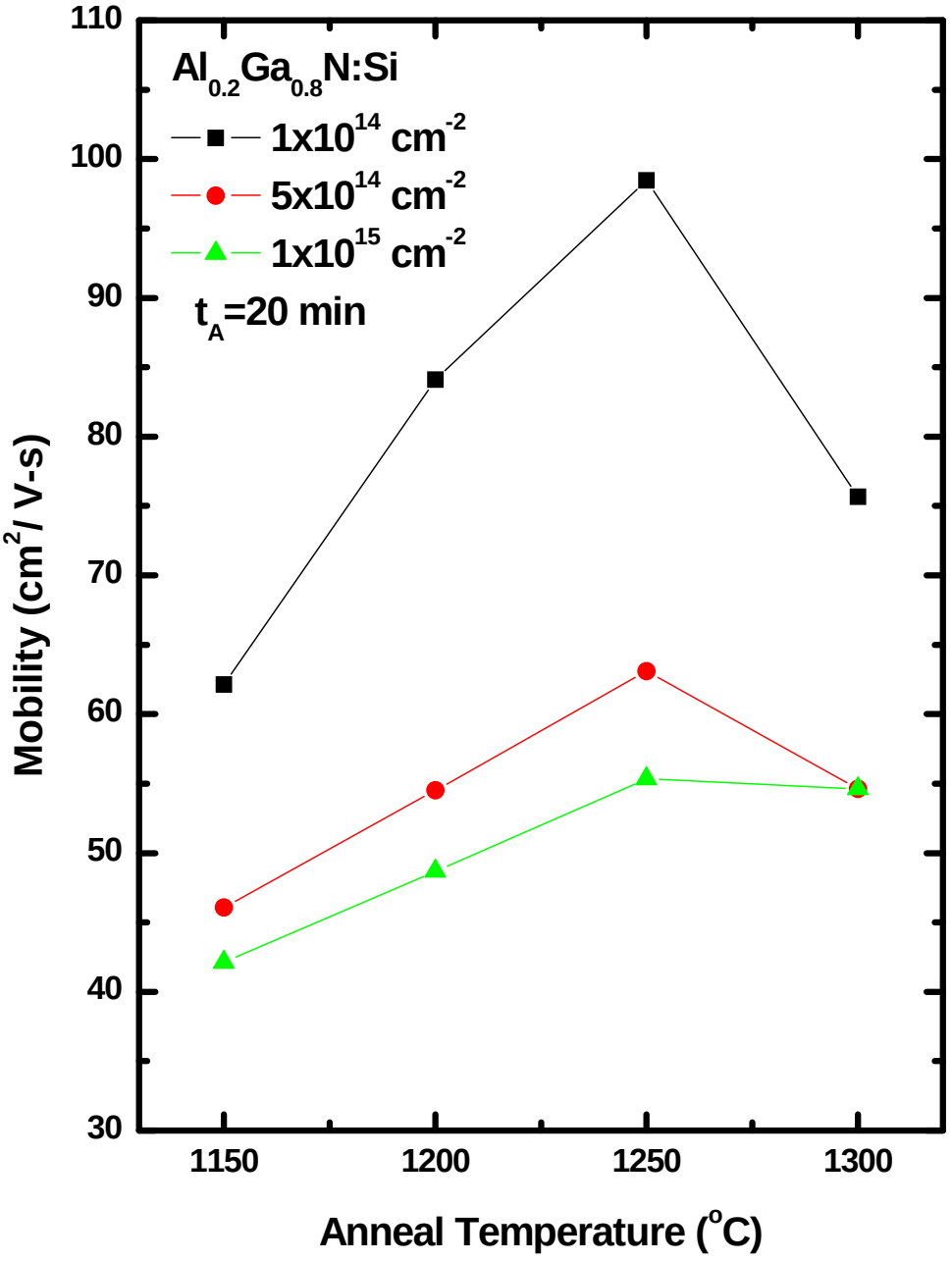

Figure 5.21. The room temperature mobility values obtained from Hall measurements on $Al_{0.2}Ga_{0.8}N$ implanted at room temperature with silicon at 200 keV with doses of $1x10^{14}$, $5x10^{14}$, and $1x10^{15}$ cm^{-2} and annealed from 1150 to 1300 ºC for 20 minutes in a nitrogen ambient.

1250 ºC. After being annealed at 1300 ºC the mobility for the samples implanted with this silicon dose decreases to 76 $cm^2/V{\cdot}s$, slightly lower than the mobility obtained for the samples annealed at 1200 ºC. The samples implanted with silicon doses of $5x10^{14}$ and $1x10^{15}$ cm^{-2} show a linear increase in mobility as the temperature is raised from 1150 to 1250 ºC, with the mobilities of the samples implanted with $5x10^{14}$ cm^{-2} silicon ions being higher for any given anneal temperature. The peak mobilities for the samples implanted with the two highest silicon doses are 63 and 55 $cm^2/V{\cdot}s$, respectively. After being annealed at 1300 ºC, the mobilities for the $Al_{0.2}Ga_{0.8}N$ implanted with these silicon doses drop to 54 $cm^2/V{\cdot}s$. The decrease in the mobility for the $Al_{0.2}Ga_{0.8}N$ annealed at 1300 ºC is caused by impurity scattering becoming dominant over defect scattering, considering the peak activation for each of the samples was achieved after annealing at 1300 ºC. This implies that lattice damage recovery was complete after annealing at 1250 ºC, whereas for the $Al_{0.1}Ga_{0.9}N$ this occurred at 1200 ºC.

The observed mobilities, in this study, are similar to those reported by others. Ryu *et al*. observed mobilities of are 64 and 62 $cm^2/V{\cdot}s$ for $Al_{0.18}Ga_{0.82}N$ implanted with doses $5x10^{14}$and $1x10^{15}$ cm^{-2} silicon ions and annealed for 25 minutes at 1200 ºC (35). They also reported a mobility of 76 $cm^2/V{\cdot}s$ for $Al_{0.24}Ga_{0.76}N$ implanted with a silicon dose of $1x10^{14}$ cm^{-2} after being annealed at 1300 ºC for 20 minutes. Chitwood observed mobilities of 28 and 50 $cm^2/V{\cdot}s$ for $Al_{0.25}Ga_{0.75}N$ implanted with doses of $5x10^{14}$ and $1x10^{15}$ cm^{-2} silicon ions after annealing for 2 minutes at 1350 ºC (47). The mobilities for the $Al_{0.2}Ga_{0.8}N$ implanted with silicon doses of $5x10^{14}$ and $1x10^{15}$ cm^{-2} are comparable to others findings however, the mobilities obtained for the samples implanted with a dose of $1x10^{14}$ cm^{-2} silicon ions are much higher than those reported to date.

Temperature-Dependent Hall Effect Measurements

Temperature-dependent Hall Effect measurements were taken on the $Al_{0.2}Ga_{0.8}N$ samples that were annealed at 1200 and 1300 ºC for 20 minutes in flowing nitrogen to determine the nature of the carriers as a function of temperature as well as to determine the ionization energy of the implanted silicon ions. The sheet carrier concentrations as a function of temperature from 10 to 700 K for the samples implanted with each of the three silicon doses and annealed at 1200 and 1300 ºC for 20 minutes are shown in Figure 5.22. The carrier concentrations for all the $Al_{0.2}Ga_{0.8}N$ implanted with each of the silicon doses remain relatively constant as the temperature increased from 10 to 50 K. The samples implanted with the two lower doses of $1x10^{14}$ and $5x10^{14}$ cm^{-2} silicon ions experience a decrease in carrier concentration beginning at 50 K and reaching a minimum at 100 and 160 K, respectively, before increasing to a higher carrier concentration at 700 K. The samples implanted with a silicon dose of $1x10^{15}$ cm^{-2} have a relatively constant carrier concentration, only increasing slightly over the measured temperature range and also reaching a higher carrier concentration at 700 K. The temperature independent nature of the carrier concentration is similar to that seen for the $Al_{0.1}Ga_{0.9}N$ samples and indicates that the implanted silicon ions have formed a degenerate impurity band in the band gap. The critical doping density of $Al_{0.2}Ga_{0.8}N$ calculated from equation 2.18 is found to be $2.35x10^{18}$ cm^{-3}. The predicted peak carrier concentrations determined from TRIM calculations for the three implantation doses of $1x10^{14}$, $5x10^{14}$, and $1x10^{15}$ cm^{-2} silicon ions are $5.63x10^{18}$, $2.82x10^{19}$, and $5.63x10^{19}$ cm^{-3}, respectively. All three implanted doses have volume carrier concentrations that exceed the critical Mott concentration, which explains the degenerate nature of the samples.

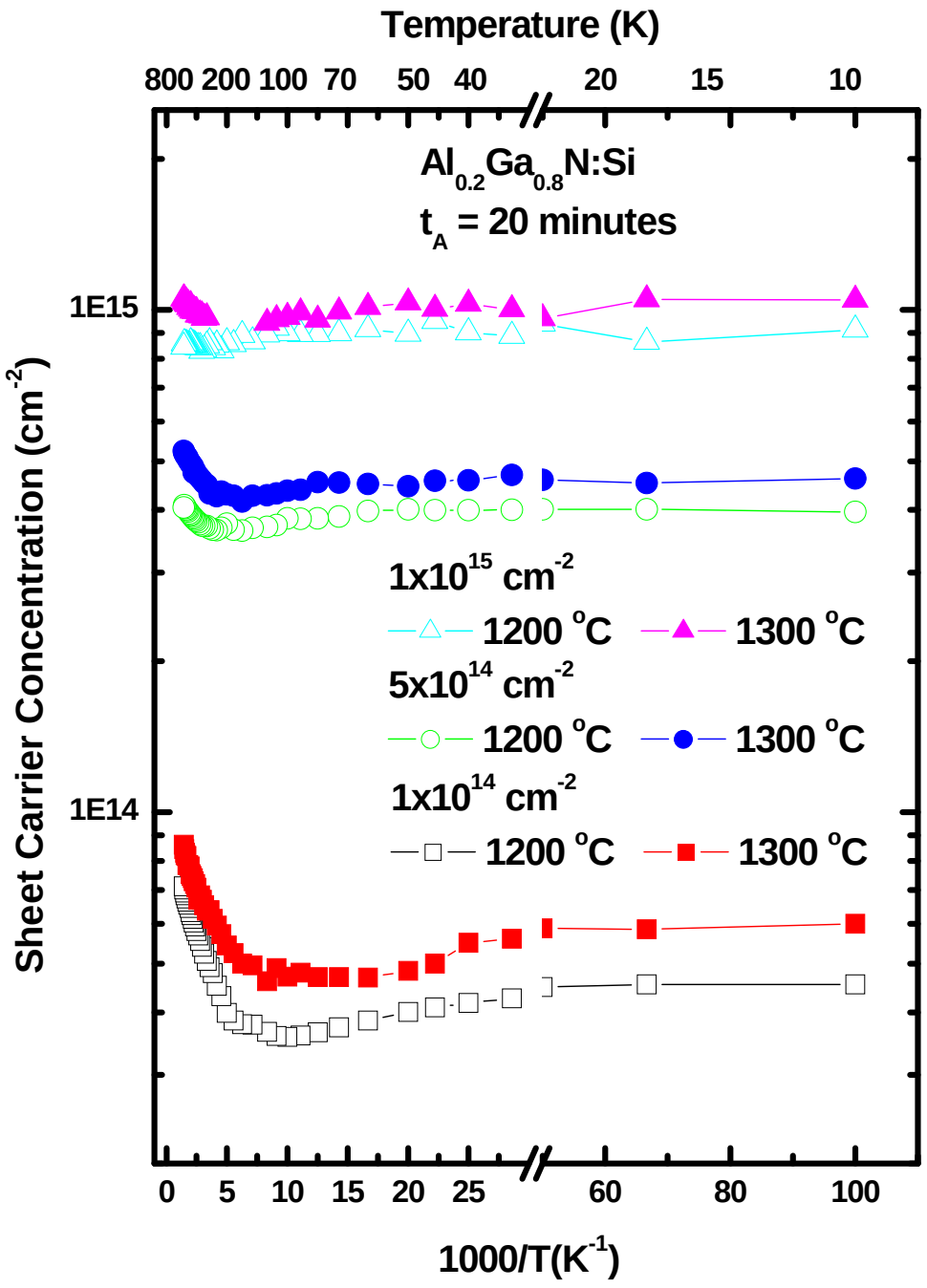

Figure 5.22. Temperature-dependent sheet carrier concentrations of $Al_{0.2}Ga_{0.8}N$ determined from Hall Effect measurements taken from 10 to 700 K. The $Al_{0.2}Ga_{0.8}N$ was implanted with three different doses of Si ions at 200 keV and annealed at 1200 and 1300 °C for 20 minutes in a flowing nitrogen environment.

The $Al_{0.2}Ga_{0.8}N$ samples implanted with $1x10^{14}$ and $5x10^{14}$ silicon ions undergo a larger dip in the carrier concentration as the temperature is increased than the $Al_{0.1}Ga_{0.9}N$. The samples implanted with the highest silicon dose have the most temperature independent carrier concentration as would be expected since this dose creates the most degenerate samples. The carrier concentration for the samples implanted with the lower doses dip between 100 and 500 K signifying the presence of a multi-channel conduction band, one being the degenerate layer and the other the non-degenerate layer due to an approximate Gaussian distribution of the carrier concentration, similar to that reported by Look *et al*. (37). The samples implanted with $1x10^{15}$ cm^{-2} silicon ions also have a slight dip in the carrier concentration which occurs at higher temperatures. Degenerate samples yield ionization energies lower than the actual energy due to the enhanced effects of impurity screening as the donor concentration is increased (72). Therefore, the silicon ionization energy for $Al_{0.2}Ga_{0.8}N$ can not be determined from the samples in this study.

The temperature-dependent hall mobilities for these samples are shown in Figure 5.23. The $Al_{0.2}Ga_{0.8}N$ implanted with the different silicon doses all exhibit a peak in their mobility curve slightly below 300 K. The sample implanted with $1x10^{14}$ cm^{-2} silicon ions has the highest mobilities of 82 and 101 $cm^2/V{\cdot}s$ after being annealed for 20 minutes at 1200 and 1300 ºC, respectively. The samples implanted with $5x10^{14}$ cm^{-2} silicon ions have peak mobilities of 52 and 67 $cm^2/V{\cdot}s$ after being annealed at 1200 and 1300 ºC, respectively, which are slightly higher than those of the samples implanted with a dose of $1x10^{15}$ cm^{-2} silicon ions. The samples implanted with the highest silicon dose have mobilities of 40 and 57 $cm^2/V{\cdot}s$ following a 20 minutes anneal at 1200 and 1300 ºC, respectively. The mobility curves for all the Si-implanted $Al_{0.2}Ga_{0.8}N$ increase as the sample temperature is increased to about 250 K at which point the mobility begins to

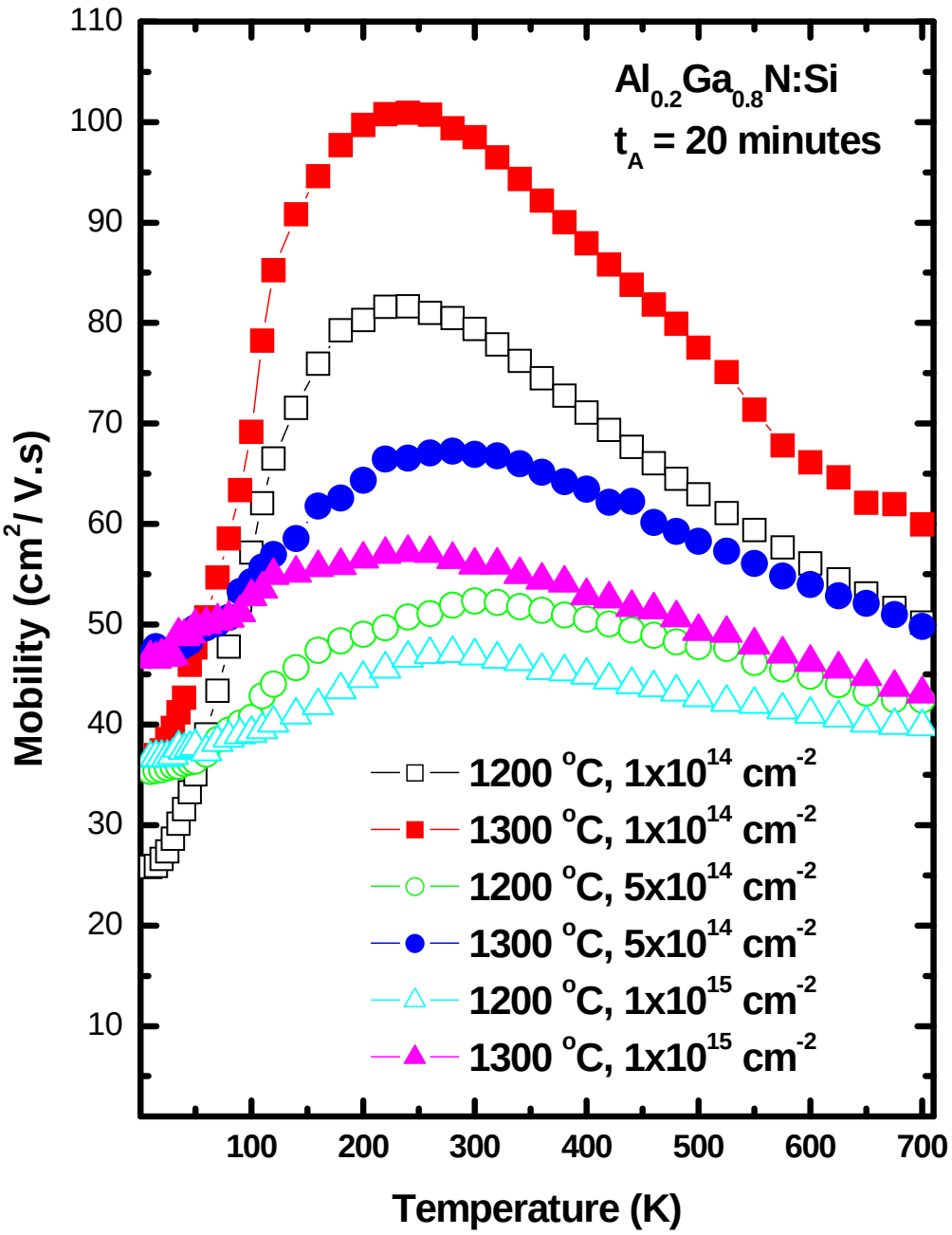

Figure 5.23. Temperature-dependent Hall mobilities taken from 10 to 700 K for $Al_{0.2}Ga_{0.8}N$ implanted at room temperature with three different doses of silicon ions at 200 keV and annealed at 1200 and 1300 ºC for 20 minutes.

decline. The mobility curves become more temperature independent as the implanted silicon dose is increased, exposing the increasingly degenerate nature of the samples. The degeneracy can also be noticed by the relatively high mobilities observed at 10 K, where the mobility of a non-degenerate material would approach zero. The mobility for the samples implanted with doses of $1x10^{14}$, $5x10^{14}$, and $1x10^{15}$ cm^{-2} silicon ions and annealed at 1200 ºC are 25.9, 35.3, and 36.6 $cm^2/V{\cdot}s$, respectively, when the samples temperature is 10 K. These mobilities are all lower than the those for the samples annealed at 1300 ºC, which are 35.6, 46.9, and 46.7 $cm^2/V{\cdot}s$ for the three doses, respectively. The degenerate impurity band causes the low temperature mobility to be temperature independent and is seen here to increase with doping level and also anneal temperature. The temperature-dependent mobility curve of the samples implanted with $1x10^{14}$ cm^{-2} silicon ions most resembles that which is predicted for a non-degenerate sample. The mobility curves for the samples implanted with the higher silicon doses are more flat as would be expected by a degenerate sample.

Figure 5.24 shows the temperature-dependent resistivity of the $Al_{0.2}Ga_{0.8}N$ samples annealed at 1200 and 1300 ºC for all three implanted silicon doses. The resistivity of the $Al_{0.2}Ga_{0.8}N$ decreases significantly as the implanted silicon dose is increased due to an increase in the carrier concentration. The samples implanted with $1x10^{14}$ cm^{-2} silicon ions have a large decrease in resistivity at high temperatures which is related to the rapid increase in the mobility seen at this temperature range. The resistivity of the samples implanted with the higher silicon doses are more temperature independent. The samples for all three implanted silicon doses show a relative temperature independent resistivity from 10 to 50 K and then they begin to slowly decline to a minimum around 240-380 K before increasing again as the sample temperature is raised

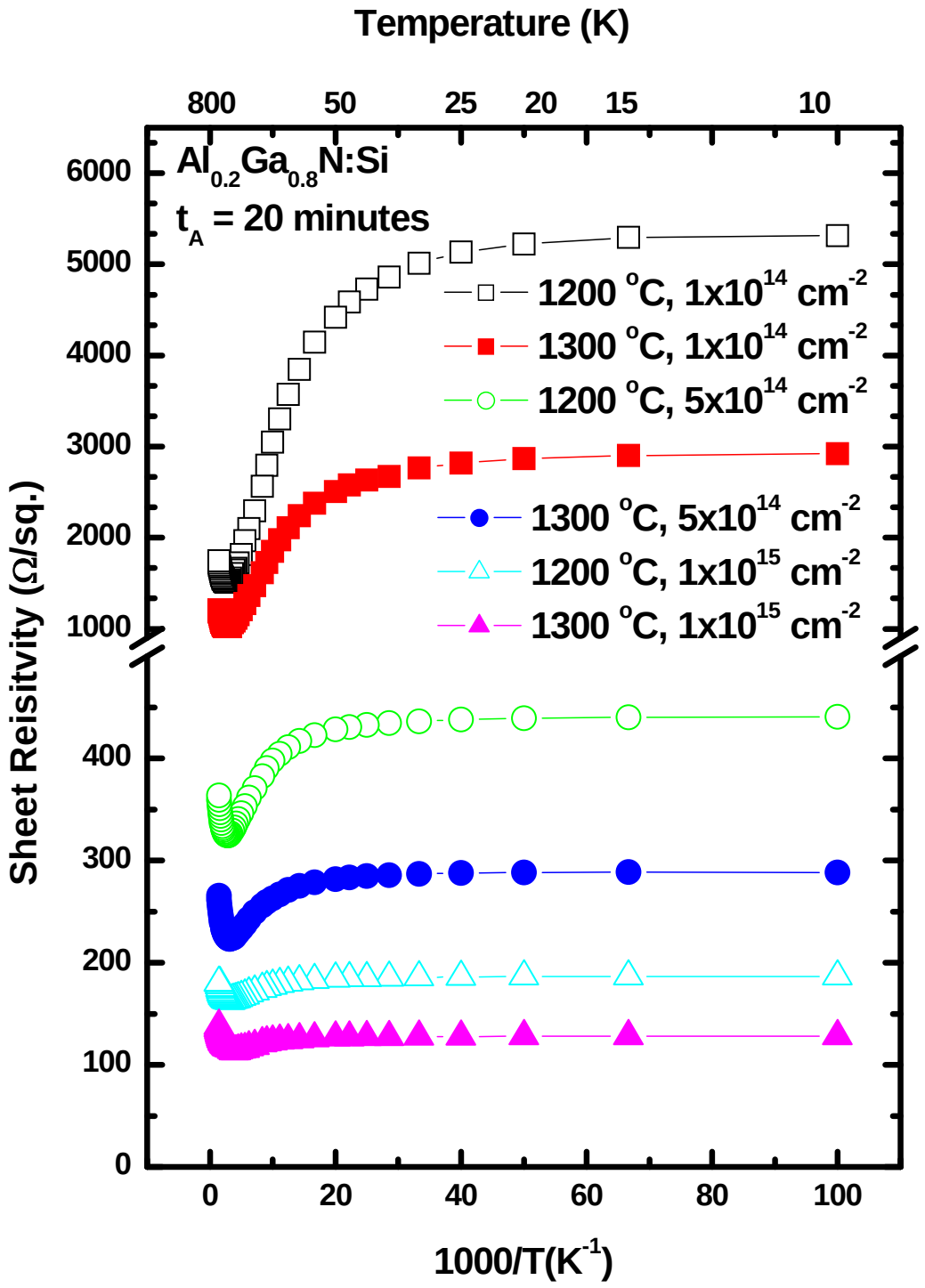

Figure 5.24. Temperature-dependent resistivity values calculated from Hall measurements taken from 10 to 700 K for $Al_{0.2}Ga_{0.8}N$ that had been implanted with $1x10^{14}$, $5x10^{14}$, and $1x10^{15}$ cm^{-2} silicon ions at 200 keV and annealed at 1200 and 1300°C for 20 minutes in flowing nitrogen.

to 700 K. The increase in the resistivity for high temperatures is a result of the dramatic decrease in the mobility at this temperature range which results from an increase in ionized impurity scattering. The bend in the resistivity around 300 K for each dose is a manifestation of the resistivity's dependence on the mobility, which is dependant on different scattering mechanisms at different temperatures and thus changes considerably with temperature.

Low Temperature Cathodoluminescence Measurements

Cathodoluminescence measurements were taken at an electron energy of 10 keV with 50 μA of source current, the temperature in the chamber was 7.4 K, and the slits on the spectrometer were 200 μm both at the entrance and the exit. The range scanned was 1800 to 7000 Å with a step size of 2 Å and an integration time of 0.1 second.

To gauge the level of damage recovery in the implanted samples, the behavior of the unimplanted samples must first be observed. The spectrum of the unimplanted samples shown as a function of anneal temperature are given in Figure 5.25. The features of the CL spectra for the unimplanted samples remain undamaged even after annealing at 1300 ºC showing a good (D^o,X) peak. However none of the annealed samples have an intensity as high as that of the as-grown sample, whose CL spectrum has been reduced by a factor of 80. The as-grown $Al_{0.2}Ga_{0.8}N$ has a (D^o,X) peak that is 30 times that of the unimplanted samples that had been annealed. The CL spectra for the as-grown sample and those annealed at 1200 and 1300 ºC show a strong neutral-donor-bound exciton (D^o,X) peak at 3.90 eV. The spectrums of the samples annealed at 1200 and 1300 ºC have been reduced by a factor of 4. The sample annealed for 20 minutes at 1150 ºC has a

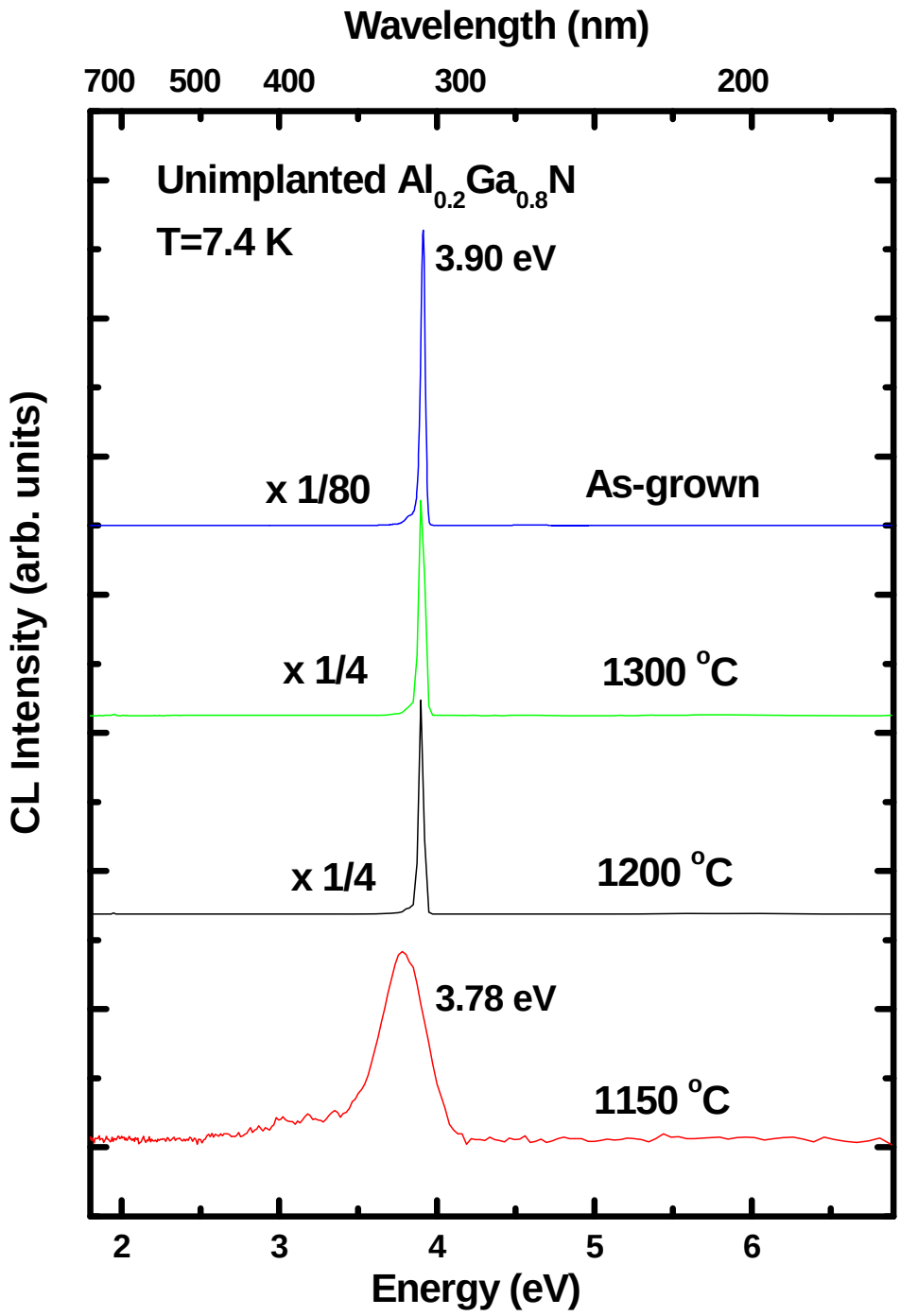

Figure 5.25. CL spectra taken at 7.4 K for unimplanted $Al_{0.2}Ga_{0.8}N$ both as-grown and annealed at 1150, 1200, and 1300 °C for 20 minutes in flowing nitrogen.

broad peak with the weakest intensity centered at 3.78 eV. The reasons for the redshifting and broadening of the peak are unclear. It seems that the low annealing temperatures have more detrimental effects on the optical properties of the as-grown material than higher temperature annealing. However, the spectra for the unimplanted $Al_{0.1}Ga_{0.9}N$ did not exhibit any broadening. In fact, the intensity of the (D^o,X) peak increased as the anneal temperature was increased from 1100 to 1150 ºC, and decreased upon further elevation of the anneal temperature.

The low temperature CL spectra for the Si-implanted $Al_{0.2}Ga_{0.8}N$ annealed for 20 minutes at 1300 ºC are shown in Figure 5.26. The spectrum of the unimplanted sample and that of sample implanted with $1x10^{14}$ cm^{-2} silicon ions have been reduced by a factor of 2. The spectra of all the samples show a sharp (D^o,X) peak at 3.90 eV. The (D^o,X) intensity for the samples implanted with $5x10^{14}$ and $1x10^{15}$ cm^{-2} silicon ions are similar to each other and much weaker than the peak for the sample implanted with $1x10^{14}$ cm^{-2} silicon ions and the unimplanted sample. The decrease in intensity of the (D^o,X) peak could be due to the increased donor concentration as the implanted silicon dose is increased. The sample implanted with a dose of $1x10^{14}$ cm^{-2} silicon ions show the strongest (D^o,X) peak at 3.90 eV matching the intensity of the unimplanted sample. The CL spectra for the $Al_{0.2}Ga_{0.8}N$ do not exhibit a broad yellow band (YL) as was seen in the spectra of the $Al_{0.1}Ga_{0.9}N$. The samples implanted with $5x10^{14}$ cm^{-2} silicon ions show a similar spectrum to the samples implanted with the lowest silicon dose, only the intensity of the (D^o,X) peak is much weaker. The features of the spectrum for the samples implanted with $1x10^{15}$ cm^{-2} silicon ions are similar to the samples implanted with the other silicon doses however, the peak energy is slightly shifted to higher energies at 3.95 eV, probably due to the effects of band filling.

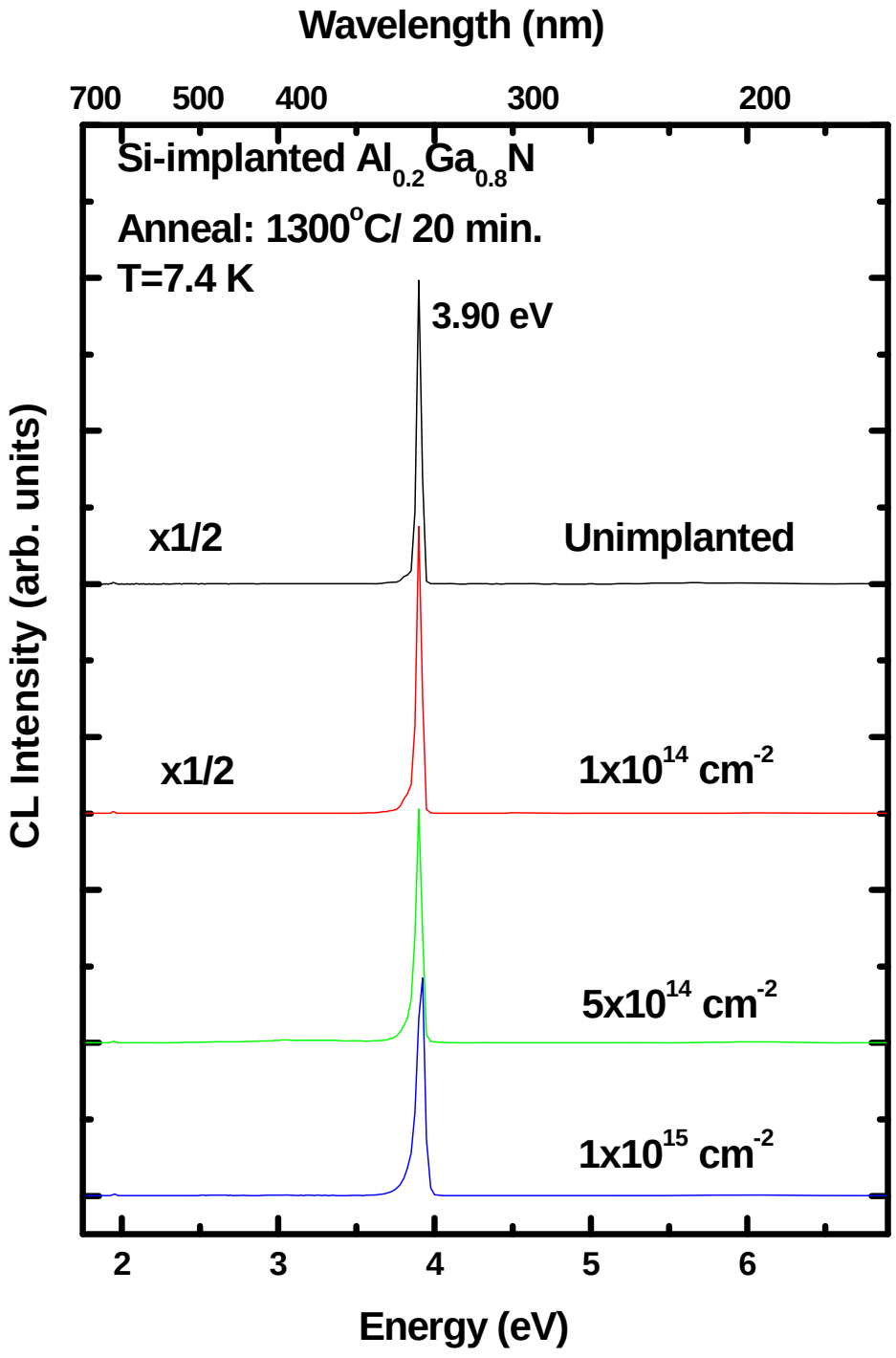

Figure 5.26. CL spectra taken at 7.4 K for $Al_{0.2}Ga_{0.8}N$ implanted at room temperature with silicon ions at 200 keV with doses of $1x10^{14}$, $5x10^{14}$, and $1x10^{15}$ cm^{-2} and annealed at 1300 °C for 20 minutes in flowing nitrogen.

The near band edge broadening on the low energy side of the (D^o,X) peak for the sample implanted with $1x10^{15}$ cm^{-2} silicon ions is due to band tailing effects. These effects are barely noticeable for the samples implanted with the lower silicon doses. The Si-implanted doses exceed the Mott concentration of the material which results in random band-edge effects and band tailing. Only the sample implanted with the highest dose of $1x10^{15}$ cm^{-2} silicon ions has a volume carrier concentration high enough for band filling to occur, which is seen as broadening of the (D^o,X) peak towards higher energies. The effects of band filling and band tailing are not as noticeable in the CL spectra for the $Al_{0.2}Ga_{0.8}N$ as they are for the $Al_{0.1}Ga_{0.9}N$. This is due to the increase in the Mott concentration as the Al mole fraction of the material is increased.

The low temperature CL spectra for the $Al_{0.2}Ga_{0.8}N$ implanted with $1x10^{14}$ cm^{-2} silicon ions and annealed for 20 minutes at various temperatures are shown in Figure 5.27. All of the anneal temperatures produce a (D^o,X) peak in the CL spectra centered at 3.90 eV that broadens as the temperature is decreased. The CL spectra for the samples annealed at 1200 and 1300 ºC have been reduced by a factor of twenty, while the spectra for the sample annealed at 1150 ºC was reduced by a factor of two. The samples implanted with this dose exhibit their best spectra after being annealed at 1300 ºC. The intensity of this spectrum is only slightly higher than the intensity of the sample annealed at 1200 ºC. The spectra improve as the anneal temperature is increased except in the case of the sample annealed at 1250 ºC in which the intensity is noticeably decreased and evidence of the YL band, seen in the $Al_{0.1}Ga_{0.9}N$, emerges. The CL intensity of the samples increases as the anneal temperature is increased signifying successive improvement in the crystal lattice with each increase in the anneal temperature.

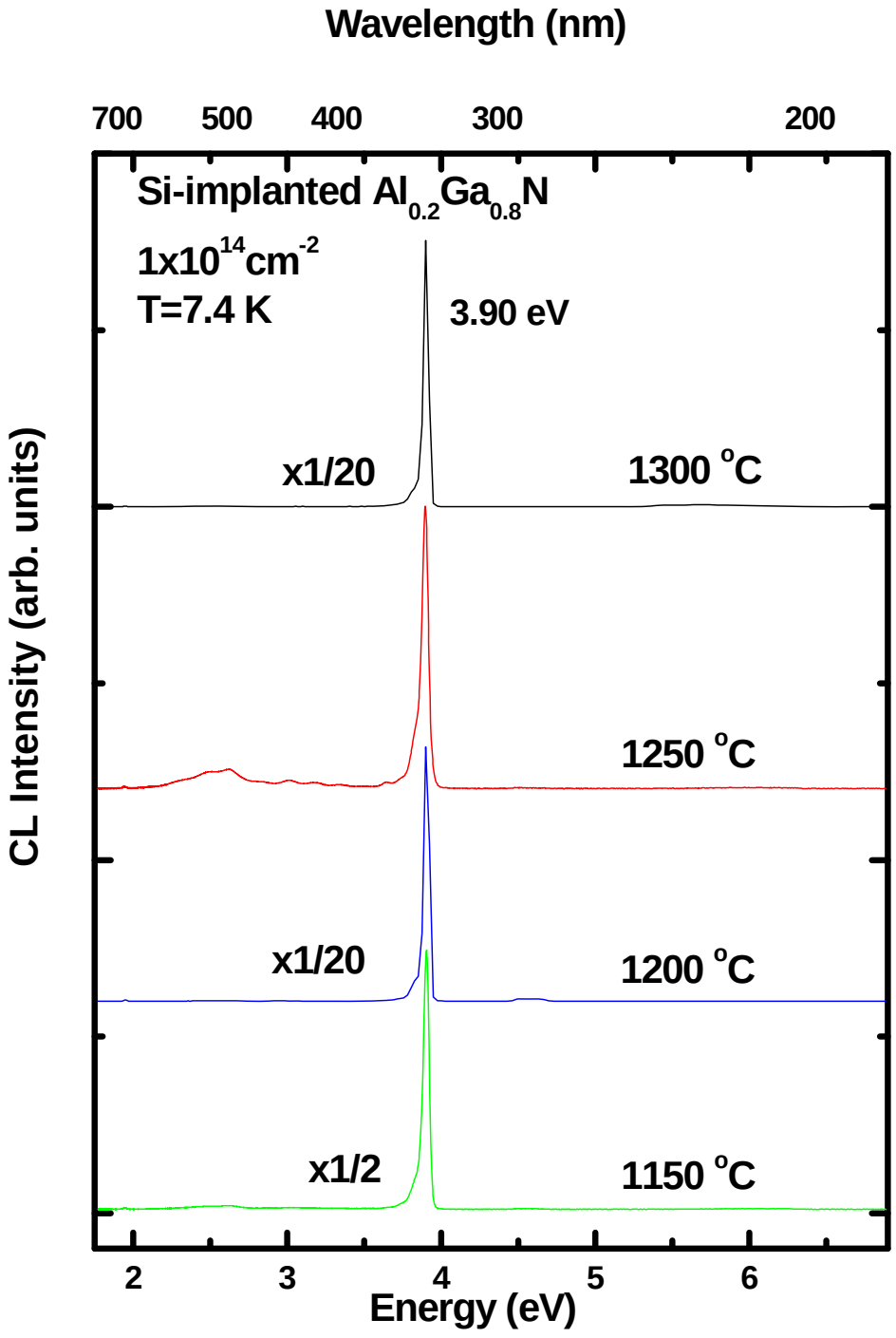

Figure 5.27. CL spectra taken at 7.4 K for $Al_{0.2}Ga_{0.8}N$ implanted at room temperature with silicon ions at 200 keV in a dose of $1x10^{14}$ cm^{-2} and annealed at various temperatures for 20 minutes in flowing nitrogen.

The (D^o,X) peak is weak for the samples annealed at 1150 ºC but it increases rapidly as the anneal temperature is increased. An anneal temperature of 1250 ºC produced unusually low CL intensity with unknown reason, however an anneal temperature of 1300 ºC produced and excellent peak signifying that the majority of the anneal damage had been restored as did the 1200 ºC anneal. The increase in intensity of the (D^o,X) peaks observed for all anneal temperatures except 1250 ºC indicate that more of the implanted silicon ions have become electrically active with an increase in anneal temperature.

These samples all exhibit their peak carrier concentration after being annealed at 1300 ºC; however the peak mobility occurred for the samples annealed at 1250 ºC. The decline in mobility was attributed to an increase in ionized impurity scattering, which occurred since the gain in mobility from the decrease in defect scattering had minimized (suggesting that the lattice defects had been repaired). Considering this information, the considerably low intensity of the CL spectrum from the sample annealed at 1250 ºC is completely unexpected and could be due to experimental error. Otherwise, these CL spectra agree very well with the electrical activation results obtained from Hall effect measurements for the samples implanted with this silicon dose. The sharpness and strong intensity of the (D^o,X) peak for the sample annealed at 1300 ºC correlate well with the high activation efficiencies obtained for this sample. The exciton peak and high mobilities observed on the samples implanted with $1x10^{14}$ cm^{-2} silicon ions indicate excellent implantation damage recovery following a 20 minute anneal at 1300 ºC in flowing nitrogen.

The CL spectra of the samples implanted with a silicon dose of $5x10^{14}$ cm^{-2} are shown in Figure 5.28. The spectra of the samples annealed at 1150, 1250, and 1300 ºC have all been reduced by a factor of 5. These samples exhibit their strongest (D^o,X) peak after being annealed at 1150 ºC for 20 minutes. The spectrum of the sample annealed at 1200 ºC has the weakest and broadest peak, without an apparent reason. As the anneal temperature is increased to 1250 and 1300 ºC, the intensity of the (D^o,X) peak increases significantly, almost matching the intensity of the sample annealed at 1150 ºC. Although, the CL spectra for the samples annealed at 1150 ºC is very strong, the peak electrical activation efficiency occurred after the samples were annealed at 1300 ºC. The spectrum of the samples annealed at 1300 ºC also exhibits excellent recovery of the (D^o,X) peak, and is close in intensity and sharpness to the sample annealed at 1150 ºC. The CL spectra for the $Al_{0.2}Ga_{0.8}N$ implanted with $5x10^{14}$ cm^{-2} silicon ions do not have any yellow luminescence. All the spectra exhibit a (D^o,X) peak with slight broadening on the low energy side due to band tailing effects.

The CL spectra of the samples implanted with the highest silicon dose of $1x10^{15}$ cm^{-2} and annealed for 20 minutes at various temperatures are shown in Figure 5.29. All the samples show recovery of the (D^o,X) centered at 3.90 eV and no emergence of yellow luminescence. As the anneal temperature is increased the intensity of the (D^o,X) peak increases significantly, except in the case of the sample annealed at 1250 ºC. This spectrum exhibits the weakest intensity and broadest peak of all the anneal temperatures without clear reason. The intensity of the peak for the samples annealed at 1300 ºC is at least 5 times more intense than the samples annealed at the lower anneal temperatures. All the spectra show considerable broadening both towards low and high energies, which

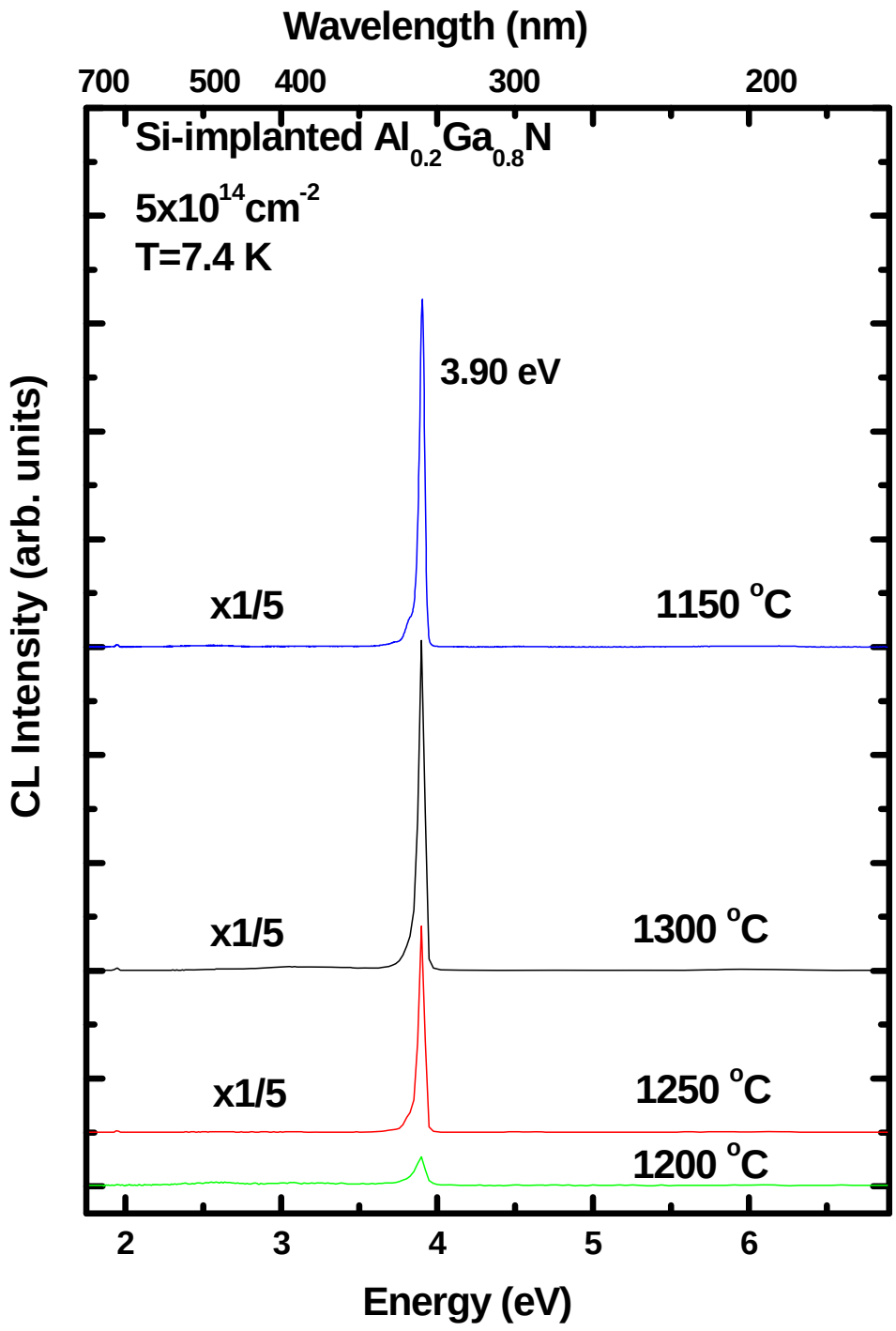

Figure 5.28. CL spectra taken at 7.4 K for $Al_{0.2}Ga_{0.8}N$ implanted at room temperature with silicon ions at 200 keV in a dose of $5x10^{14}$ cm^{-2} and annealed at various temperatures for 20 minutes in flowing nitrogen.

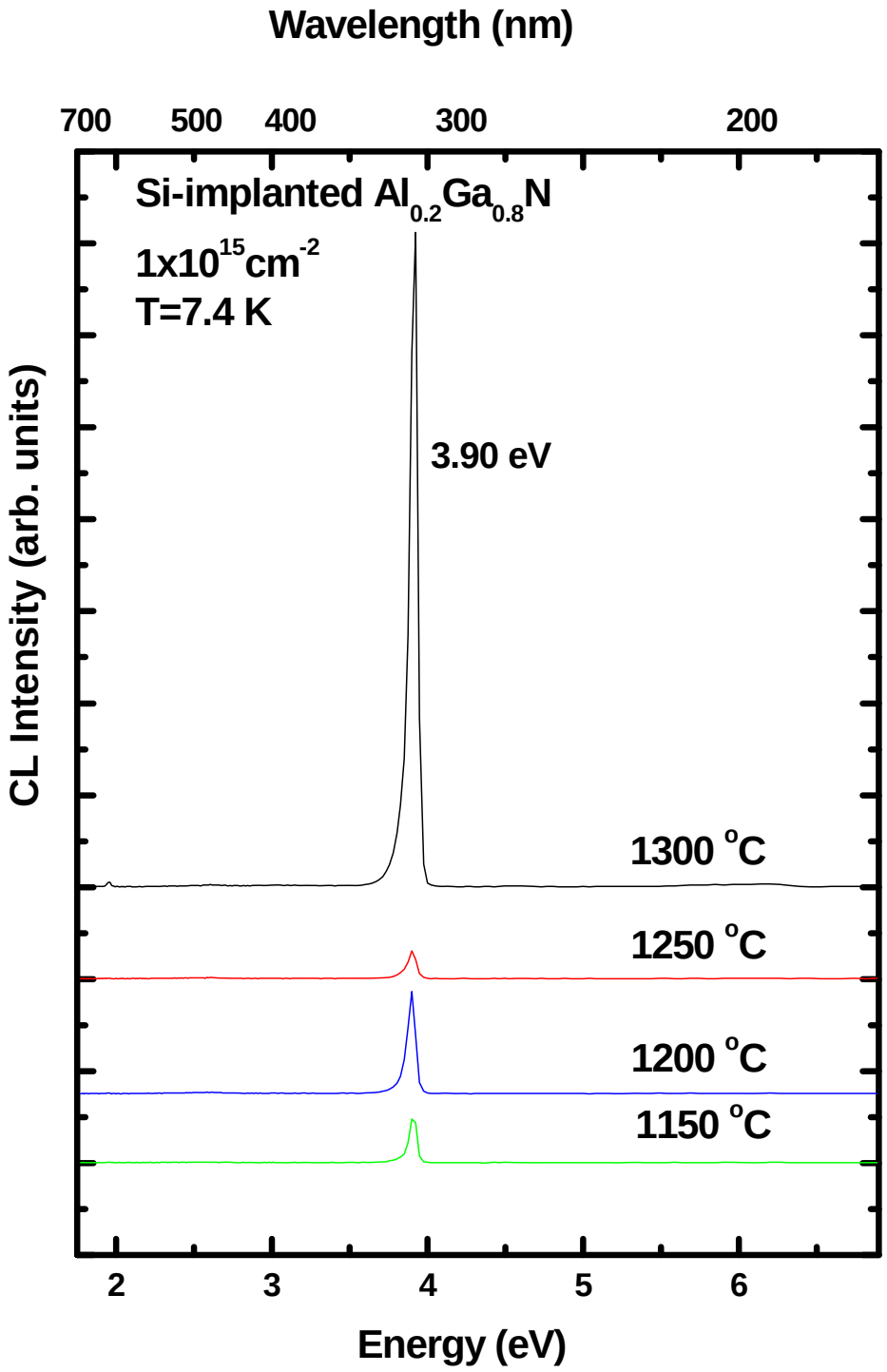

Figure 5.29. CL spectra taken at 7.4 K for $Al_{0.2}Ga_{0.3}N$ implanted at room temperature with silicon ions at 200 keV in a dose of $1x10^{15}$ cm^{-2} silicon ions and then annealed at various temperatures for 20 minutes in flowing nitrogen.

correlates well with the temperature-dependant data that suggests the samples implanted with this dose are highly degenerate.

The CL spectrum of the samples implanted with the latter two higher silicon doses exhibit their most intense (D^o,X) peak after being annealed at 1300 ºC for 20 minutes, indicating a greater level of damage recovery. This anneal temperature also produced the highest activation efficiency and lowest resistivity. The considerable decrease in intensity of the samples annealed at 1200 and 1250 ºC, respsectively is curious considering that the electrical data does not show any adverse behavior for this anneal temperature.

Silicon Implanted $Al_{0.3}Ga_{0.7}N$

Literature on implanted $Al_{0.3}Ga_{0.7}N$ is limited. Chitwood implanted $1x10^{15}$ cm^{-2} silicon ions into MBE grown $Al_{0.3}Ga_{0.7}N$ and achieved 42 % activation after annealing at 1300 ºC for 2 minutes in flowing nitrogen (47). She also attempted lower implanted silicon doses but the material quality was poor with visible cracks so that it was impossible to collect any electrical data. Good quality high Al concentration $Al_xGa_{1-x}N$ epilayers have only become available in recent years (49-50). The MEMOCVD $Al_{0.3}Ga_{0.7}N$ in this study had excellent surface morphology before and after the high temperature annealing.

There are no reported ionization energies for silicon implanted $Al_{0.3}Ga_{0.7}N$. Hwang *et al*. calculated the donor ionization energy of $Al_xGa_{1-x}N$ from a simple hydrogen model using low-frequency dielectric constants and found that it increases from 34 meV to 90 meV as the Al mole fraction is increased from 0 to 1 (51). The theoretical

ionization energy for Si in $Al_{0.3}Ga_{0.7}N$, assuming a linear increase with Al concentration, would then be on the order of 50 meV for a non-degenerate sample. The implanted silicon doses of $1x10^{14}$, $5x10^{14}$, and $1x10^{15}$ cm^{-2} correspond to peak volume carrier concentrations of $5.66x10^{18}$, $2.83x10^{19}$ and $5.66x10^{19}$ cm^{-3}, respectively in $Al_{0.3}Ga_{0.7}N$ which all exceed the Mott concentration of $2.67x10^{18}$ cm^{-3}, calculated from equation 2.18, for this material. Therefore, the implanted samples will be degenerate and the ionization energy for silicon in $Al_{0.3}Ga_{0.7}N$ can not be determined from the samples used in this study.

Room Temperature Hall Effect Measurements

The MEMOCVD grown $Al_{0.3}Ga_{0.7}N$ was capped with 500Å of AlN and then implanted at room temperature with Si ions at 200 keV in three different doses. The Si doses were $1x10^{14}$, $5x10^{14}$, and $1x10^{15}$ cm^{-2} which corresponds to effective doses of $9.87x10^{13}$, $4.94x10^{14}$, and $9.87x10^{14}$ cm^{-2}, respectively after accounting for the AlN encapsulant. The samples were annealed from 1150 to 1350 ºC for 20 minutes in a nitrogen environment. The samples exhibited slight edge damage on the surface after being annealed at 1350 ºC. Room temperature Hall effect measurements were conducted to determine sheet carrier concentrations for the samples and the results are shown in Figure 5.30. The unimplanted samples, both as-grown and annealed, were highly resistive making it impossible to collect any meaningful data. Thus, the silicon electrical activation was calculated using the measured carrier concentration with no corrections made for the background carriers.

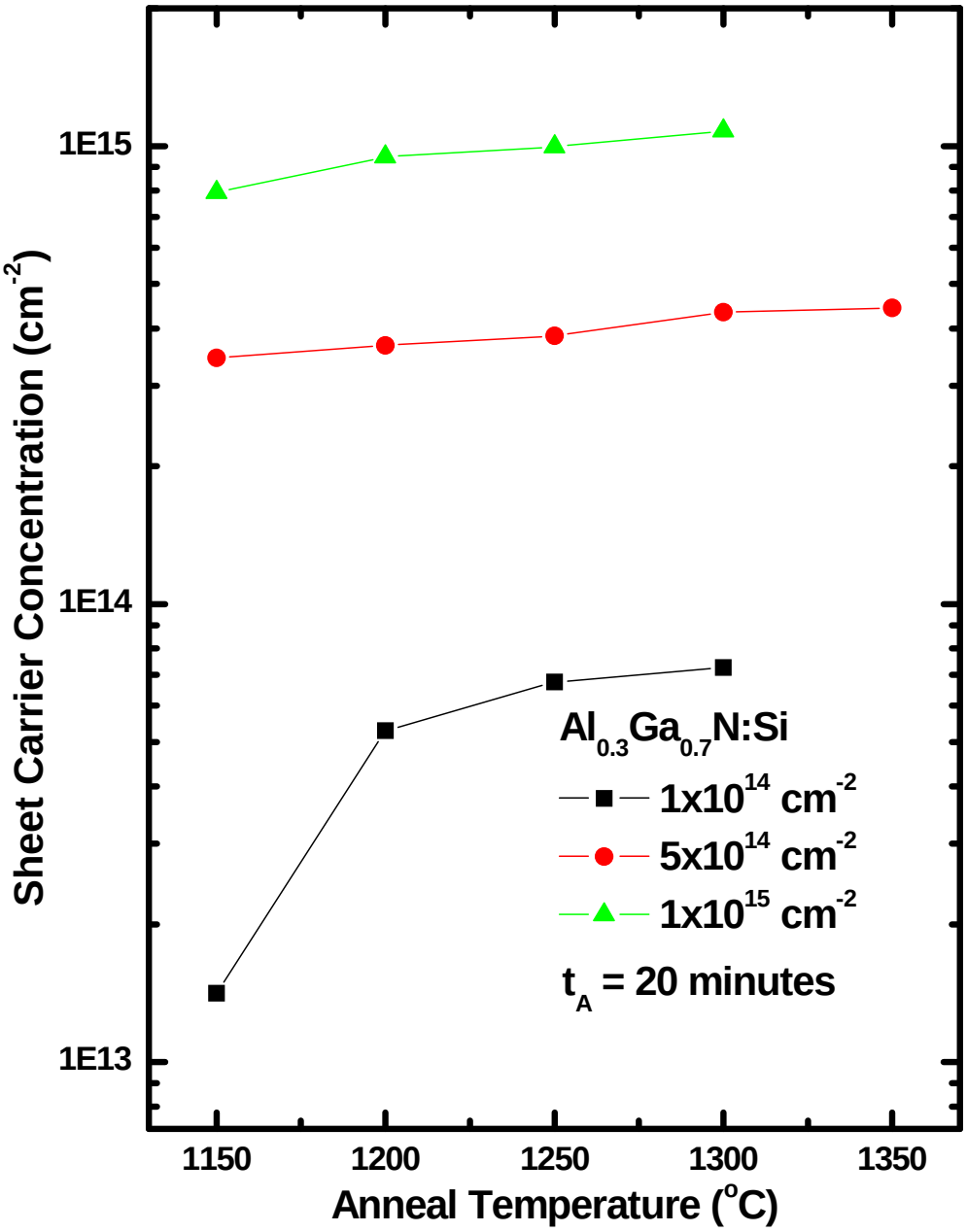

Figure 5.30. Room temperature sheet carrier concentrations for $Al_{0.3}Ga_{0.7}N$ implanted at room temperature with silicon ions at 200 keV with doses of $1x10^{14}$, $5x10^{14}$, and $1x10^{15}$ cm^{-2} and annealed from 1150 to 1350 °C for 20 minutes in flowing nitrogen.

The sheet carrier concentrations for $Al_{0.3}Ga_{0.7}N$ implanted with each silicon dose respond by increasing linearly to an increase in the anneal temperature and exhibit a small amount of change in magnitude over the given temperature range. The only exception is the sample implanted with $1x10^{14}$ cm^{-2} silicon ions which exhibits a large increase as the anneal temperature is raised from 1150 to 1200 ºC. Thus, the samples implanted with the lowest silicon dose show the most dramatic change in carrier concentration as the anneal temperature is raised, from $1.4x10^{13}$ to $6.7x10^{13}$ cm^{-2} for temperatures 1150 and 1300 ºC, respectively. The carrier concentrations for the $Al_{0.3}Ga_{0.7}N$ implanted with doses of $5x10^{14}$ and $1x10^{15}$ cm^{-2} silicon ions exhibit similiar dependence on the anneal temperature. For both samples, the carrier concentration increases steadily as the anneal temperature is raised from 1150 to 1300 and 1350 ºC, respectively. The maximum carrier concentration for the samples implanted with $5x10^{14}$ cm^{-2} silicon ions was $4.43x10^{14}$ cm^{-2} after annealing at 1350 ºC for 20 minutes in a flowing nitrogen ambient. The $Al_{0.3}Ga_{0.7}N$ implanted with a dose of $1x10^{15}$ cm^{-2} silicon ions reaches a maximum carrier concentration of $1.08x10^{15}$ cm^{-2} after being annealed for 20 minutes at 1300 ºC.

The dependence of the carrier concentration on the anneal temperature is very similar for the $Al_{0.1}Ga_{0.9}N$, $Al_{0.2}Ga_{0.8}N$ and $Al_{0.3}Ga_{0.7}N$ samples. For all the Al mole fractions, the samples implanted with the higher silicon doses exhibit only a small variation with the anneal temperature. Only the samples implanted with $1x10^{14}$ cm^{-2} silicon ions show any appreciable change in carrier concentration and just between anneal temperatures of 1150 and 1200 ºC. The peak carrier concentrations for both Al mole fractions were achieved after annealing at 1300 ºC for 20 minutes, with the $Al_{0.2}Ga_{0.8}N$ having higher carrier concentrations at any given ion dose. The $Al_{0.3}Ga_{0.7}N$ implanted

with $5x10^{14}$ cm^{-2} silicon ions have carrier concentrations have a 17% decrease in carrier concentration from the $Al_{0.2}Ga_{0.8}N$ implanted with this dose and annealed at 1300 ºC for 20 minutes, which are 20% lower than the carrier concentrations of the $Al_{0.1}Ga_{0.9}N$ samples that were annealed for 20 minutes at 1250 ºC. The $Al_{0.3}Ga_{0.7}N$ implanted with $1x10^{15}$ cm^{-2} silicon ions show a 10% decrease in carrier concentration over those obtained for the $Al_{0.2}Ga_{0.8}N$ under the same anneal conditions. The $Al_{0.2}Ga_{0.8}N$ sample also shows a 10% improvement over the $Al_{0.1}Ga_{0.9}N$ implanted with this dose and annealed at 1150 ºC. In general, the carrier concentrations of the $Al_xGa_{1-x}N$ with Al concentrations of 10 to 30% all exhibit similar dependencies on the anneal temperature. The annealing temperature that produces the highest carrier concentration increases as the Al mole fraction of the material is increased.

The silicon electrical activation of these samples is closely related to the carrier concentration and follows the same trends with the anneal temperature as mentioned above. The electrical activation for the $Al_{0.3}Ga_{0.7}N$, shown in Figure 5.31, was calculated using the effective dose and room temperature sheet carrier concentrations. The higher the implanted silicon dose the higher the activation efficiency for anneal temperatures up to 1350 ºC. The silicon electrical activation for the samples implanted with $1x10^{14}$ cm^{-2} silicon ions exhibits the most improvement over the given temperature range, increasing from 14% to 74% after being annealed for 20 minutes at 1150 and 1300 ºC, respectively. The $Al_{0.3}Ga_{0.7}N$ implanted with the lowest silicon dose experienced the lowest activation efficiencies but also showed the best response to an increase in anneal temperature, indicating that a further increase in the temperature may result in higher activation. This behavior is consistent with the $Al_{0.1}Ga_{0.9}N$ and $Al_{0.2}Ga_{0.8}N$ implanted with this silicon dose. The samples implanted with a dose of $5x10^{14}$ cm^{-2} silicon ions have a significant

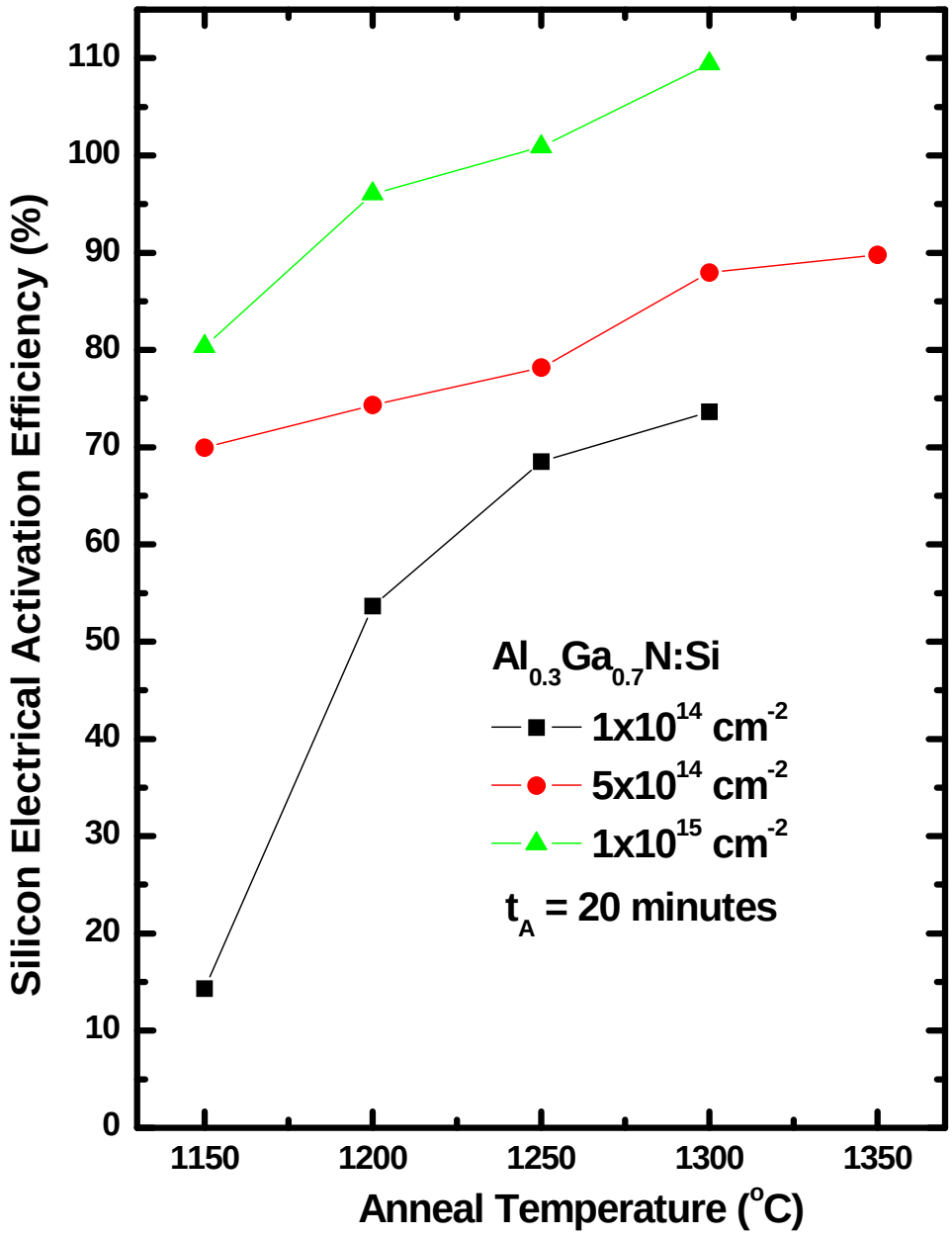

Figure 5.31. Silicon electrical activation efficiency for $Al_{0.3}Ga_{0.7}N$ calculated from the room temperature Hall measurements for implanted silicon doses of $1x10^{14}$, $5x10^{14}$, and $1x10^{15}$ cm^{-2} and annealed for 20 minutes from 1150 to 1350 °C.

70% activation efficiency after being annealed for 20 minutes at 1150 ºC and steadily increases to a maximum of 90% following the 1350 ºC anneal. The $Al_{0.3}Ga_{0.7}N$ implanted a silicon dose of $1x10^{15}$ cm^{-2} reaches 100% activation after being annealed at 1300 ºC for 20 minutes in a nitrogen ambient. The $Al_{0.2}Ga_{0.8}N$ samples implanted with the same dose reach 100% activation under the same annealing conditions, while the maximum activation for the $Al_{0.1}Ga_{0.9}N$ samples was 94% after a 40 minute anneal at 1200 ºC. The samples implanted with the highest silicon dose exhibited activations of 109% after the 1300 ºC anneal. An electrical activation over 100% could be the result of over dose implantation or underestimating the effective dose. The $Al_xGa_{1-x}N$ with 10 and 20% Al mole fractions implanted with this silicon dose also reached 100% activation under various annealing conditions. As seen with the $Al_xGa_{1-x}N$ with Al mole fractions of 10 and 20%, the $Al_{0.3}Ga_{0.7}N$ samples implanted with the highest silicon dose are also more readily activated than those implanted with the lower silicon doses, which is illustrated in Figure 5.32.

Based on the activation efficiency, the optimal anneal temperature for the $Al_{0.3}Ga_{0.7}N$ implanted with doses of $1x10^{14}$ and $5x10^{14}cm^{-2}$ silicon ions the may be higher than 1300 and 1350 ºC, respectively. However, 100% activation was achieved for the sample implanted with the higher silicon dose of $1x10^{15}$ cm^{-2} after annealing at 1300 ºC for 20 minutes. The optimal anneal temperature is dose dependent, with lower implanted doses requiring higher temperatures to attain the activations that the high dose implanted samples achieve at lower anneal temperatures, as was seen for both the $Al_{0.1}Ga_{0.9}N$ and $Al_{0.2}Ga_{0.8}N$.

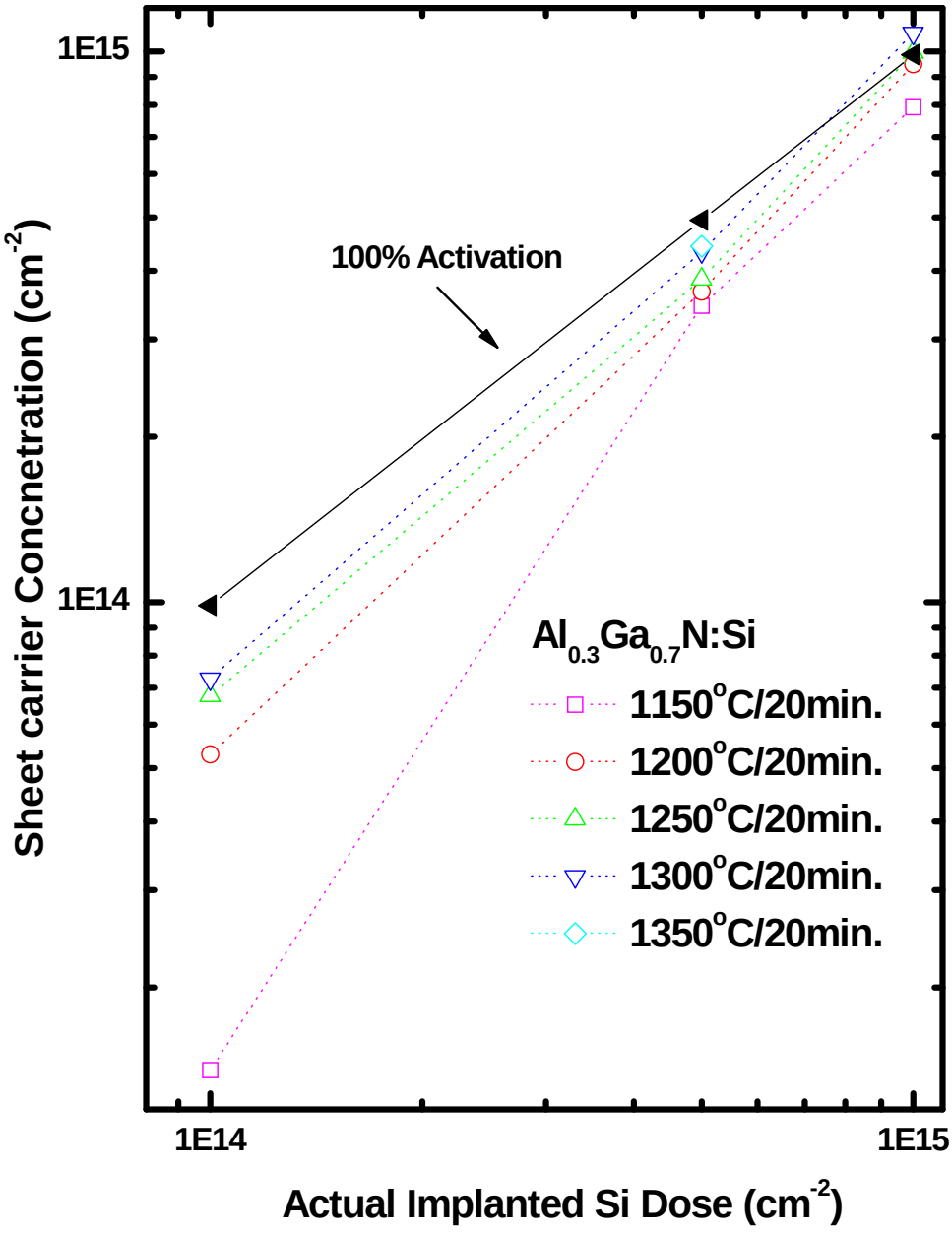

Figure 5.32. The room temperature sheet carrier concentrations versus the actual implantation dose for $Al_{0.3}Ga_{0.7}N$ implanted at room temperature with silicon at 200 keV with doses of $1x10^{14}$, $5x10^{14}$, and $1x10^{15}$ cm^{-2} and annealed from 1150 to 1350 °C for 20 minutes in a nitrogen ambient.

The resistivities for all the implanted $Al_{0.3}Ga_{0.7}N$ are shown in Figure 5.33. The low samples implanted with $1x10^{14}$ cm^{-2} silicon ions have a resistivity of 2.57 kΩ/□ which is 4 and 8 times higher than the samples implanted with $5x10^{14}$ and $1x10^{15}$ cm^{-2} when annealed at 1150 ºC for 20 minutes. The resistivity for the samples implanted with the lowest silicon dose falls about 1.3 kΩ/□ as the anneal temperature is increased to 1300 ºC. As seen with the $Al_{0.1}Ga_{0.9}N$ and $Al_{0.2}Ga_{0.8}N$, the resistivity of all the samples decreases as the anneal temperature is increased, with the samples implanted with the highest silicon dose showing the least improvement and the samples implanted with the lowest silicon dose the highest, which is consistent with the carrier concentration. The measured resistivities of the higher silicon dose implanted $Al_{0.3}Ga_{0.7}N$ are almost all below 400 Ω/□. The samples implanted with $5x10^{14}$ cm^{-2} silicon ions show a rapid decrease in resistivity as the anneal temperature is increased from 1150 to 1200 ºC and then begins to decreases linearly as the anneal temperature is brought up to 1350 ºC. The resistivity for the samples implanted with this dose drop from 666 Ω/□ to 221 Ω/□ as the anneal temperature is raised from 1150 to 1350 ºC. The samples implanted with $1x10^{15}$ cm^{-2} silicon ions showed a slightly linear decrease in resistivity as the anneal temperature is increased from 1150 to 1300 ºC dropping from 291 Ω/□ to 95 Ω/□, respectively.

The resistivity of the implanted $Al_{0.3}Ga_{0.7}N$ for each silicon dose is similar to the resistivity of the corresponding silicon dose in $Al_{0.2}Ga_{0.8}N$ and $Al_{0.1}Ga_{0.9}N$ samples. However, the overall values of the resistivity have decreased from the previous mole fractions. Of all the Al concentrations investigated thus far the $Al_{0.3}Ga_{0.7}N$ sample implanted with $1x10^{15}$ cm^{-2} silicon ions and annealed at 1300ºC for 20 minutes has the lowest resistivity of 95 Ω/□. The anneal temperature that produces the lowest resistivity

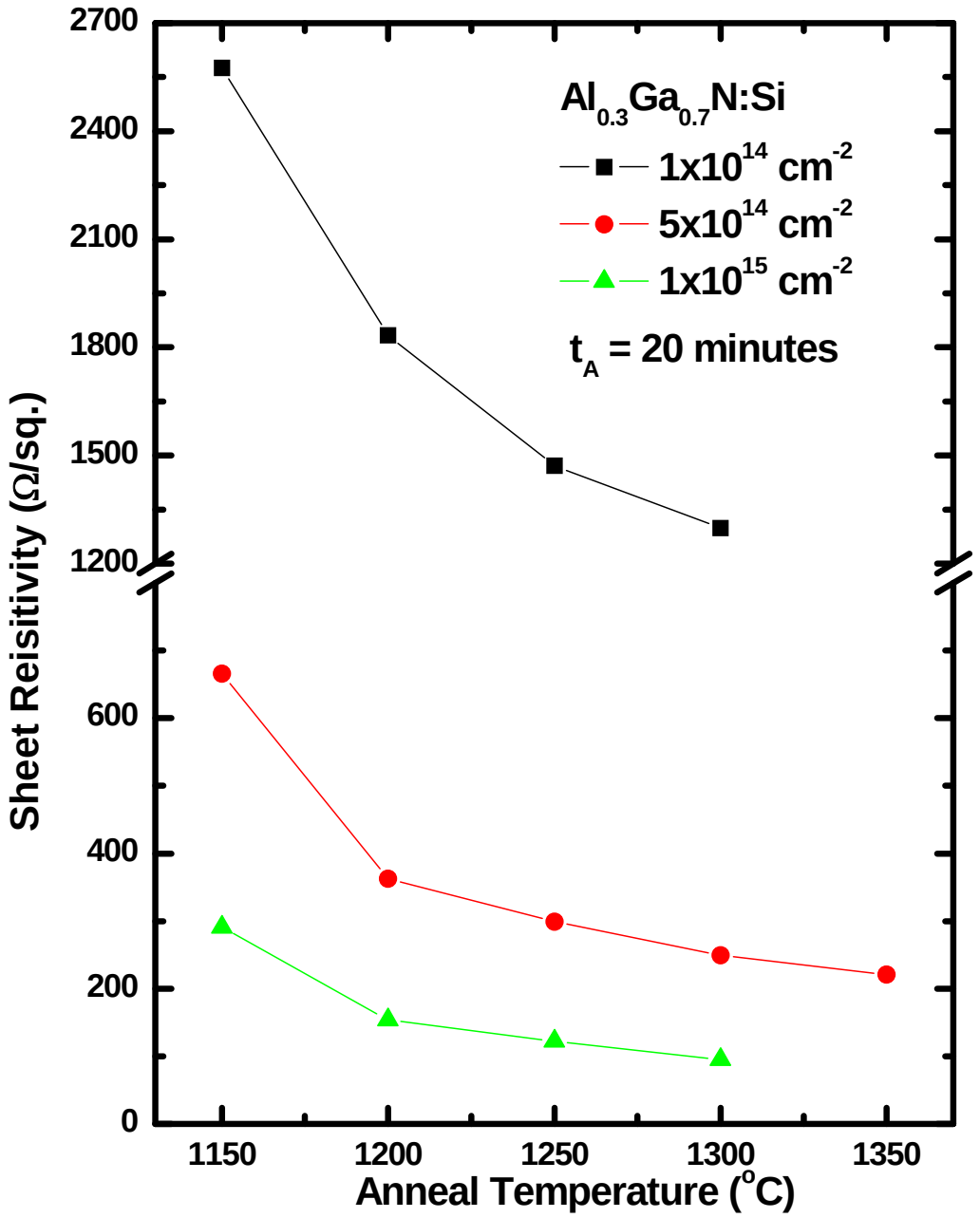

Figure 5.33. Room temperature resistivity measurements taken under zero magnetic field for $Al_{0.3}Ga_{0.7}N$ implanted at room temperature with silicon at 200 keV with doses of $1x10^{14}$, $5x10^{14}$, and $1x10^{15}$ cm^{-2} and annealed from 1150 to 1350 °C for 20 minutes in a nitrogen ambient.

in the $Al_{0.3}Ga_{0.7}N$ corresponds to the anneal temperature that creates a maximum in carrier concentration, and thus activation for all of the implanted doses.

Room temperature mobility values for Si-implanted $Al_{0.3}Ga_{0.7}N$ are shown in Figure 5.34. The mobility increases as the anneal temperature is increased up to 1350 ºC for each of the implanted samples despite the increased effects of ionized impurity scattering. The peak activation for each of the samples was achieved after annealing at 1300 ºC or 1350 ºC, which corresponds to the anneal temperature that produces the peak mobility for each of the samples suggesting that lattice recovery may not be complete after annealing at these temperatures. In general, the mobility increases as the implanted silicon dose is increased. However, the reverse it true for the samples annealed at 1150 ºC. The samples implanted with $5x10^{14}$ and $1x10^{15}$ cm^{-2} silicon ions have mobilities that are very close to one another, and after being annealed at 1300 ºC the samples implanted with $1x10^{15}$ cm^{-2} silicon ions have a higher carrier concentration. The samples implanted with $1x10^{14}$ cm^{-2} show a dramatic rise in mobility from 21 $cm^2/V{\cdot}s$ to 64 $cm^2/V{\cdot}s$ as the temperature is increased from 1150 to 1200 ºC and then begins to increase linearly as the temperature is raised to 1300 ºC. The mobility for the low-dose implanted $Al_{0.3}Ga_{0.7}N$ annealed at 1150 ºC decreased more than 40 $cm^2/V{\cdot}s$ from that of the $Al_xGa_{1-x}N$ with Al concentrations of 10 and 20%. After being annealed at 1300 ºC the mobility for these samples peaks at 76 $cm^2/V{\cdot}s$.

The mobility for the samples implanted with a dose of $5x10^{14}$ silicon ions increase throughout the temperature span, more rapidly between the 1150 and 1250 ºC anneal. These samples reach a peak mobility of 64 $cm^2/V{\cdot}s$ after being annealed for 20 minutes at 1350 ºC. The $Al_{0.1}Ga_{0.9}N$ and $Al_{0.2}Ga_{0.8}N$ implanted with $5x10^{14}$ cm^{-2} silicon ions had slightly lower peak mobilities of 63 and 55 $cm^2/V{\cdot}s$, respectively. The mobility of the

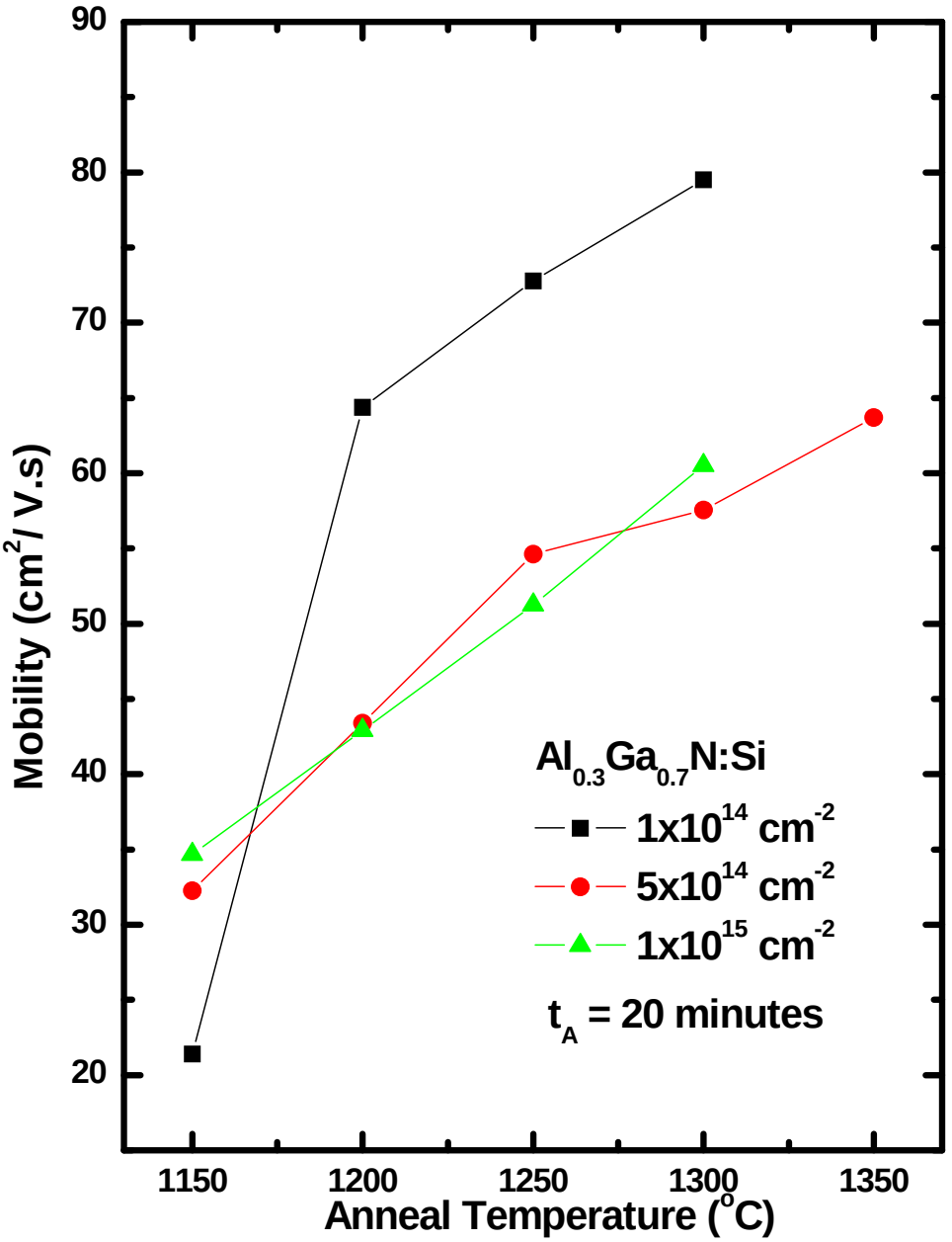

Figure 5.34.The room temperature mobility values calculated from Hall measurements on $Al_{0.3}Ga_{0.7}N$ implanted at room temperature with silicon at 200 keV with doses of $1x10^{14}$, $5x10^{14}$, and $1x10^{15}$ cm^{-2} and annealed from 1150 to 1350 ºC for 20 minutes in a nitrogen ambient.

samples implanted with $1x10^{15}$ cm^{-2} silicon ions increases linearly as the temperature is raised from 1150 to 1300 ºC, reaching a peak mobility of 61 $cm^2/V \cdot s$. The mobilities for the $Al_{0.1}Ga_{0.9}N$ and $Al_{0.2}Ga_{0.8}N$ implanted with the same silicon dose are higher, at 90 and 76 $cm^2/V \cdot s$, respectively. The mobilities for the $Al_{0.3}Ga_{0.7}N$ are slightly lower than the mobilities of t he $Al_{0.1}Ga_{0.9}N$ and $Al_{0.2}Ga_{0.8}N$. However, the mobilities obtained for the $Al_{0.3}Ga_{0.7}N$ are much higher than those observed by Chitwood of 35 and 38 $cm^2/V \cdot s$ after annealing at 1300 and 1350 ºC for two minutes (47).

The Si-implanted $Al_{0.3}Ga_{0.7}N$ samples behaved much like the $Al_xGa_{1-x}N$ with the Al mole fractions of 10 and 20%, with all three implanted silicon doses achieving high electrical activation efficiency. The samples implanted with the lowest silicon dose had the worst electrical activation and resistivity (74%, 1.3 kΩ/□) however, it had the highest mobility values of 80 $cm^2/V \cdot s$. The samples implanted with a silicon dose of $5x10^{14}$ cm^{-2} reached an activation of 90% after being annealed for 20 minutes at 1300 ºC with considerably lower resistivity and mobility values of 221 Ω/□ and $64 cm^2/V \cdot s$, respectively. The $Al_{0.3}Ga_{0.7}N$ implanted with the highest silicon dose had the best activation of 100% and the best resistivity of 95 Ω/□ following the 1300 ºC anneal for 20 minutes. The mobility for this dose was $61 cm^2/V \cdot s$.

To improve the silicon electrical activation efficiency of the Si-implanted $Al_{0.3}Ga_{0.7}N$ samples the anneal time was extended from 20 to 40 minutes for a set anneal temperature of 1200 ºC. A comparison of the results obtained for both the 20 and 40 minute anneals at 1200 ºC are listed in Table 5.2. A temperature of 1200 ºC is more commercially viable and therefore more practical for incorporation into device manufacturing techniques. Extending the anneal time had mixed affects on all of the physical aspects determined from Hall effect measurements. The carrier concentrations

and therefore activation efficiency of the all the implanted samples increased following the 40 minute anneal. The electrical activation efficiency also increased more with each successive dose. The resistivity of the samples implanted with $1x10^{14}$ silicon ions increases 10%, which is related to a decrease in the mobility for these samples. The samples implanted with $1x10^{14}$ cm^{-2} silicon ions exhibit a small increase in the sheet carrier concentration which causes a 3% increase in electrical activation efficiency bringing it up to 56.7%. The mobility for the samples implanted with this silicon dose decreases from 64.4 $cm^2/V{\cdot}s$ to 54.1 $cm^2/V{\cdot}s$, due to an increase in ionized impurity scattering thus suggesting that the lattice damage has been mostly repaired. The electrical activation for the samples implanted with $5x10^{14}$ cm^{-2} silicon ions increases 8% to 86% after the 40 minute anneal. The resistivity for the samples implanted with this dose decreases 17% to 300.5 Ω/□ due to the increase in the carrier concentration and mobility for these samples. The mobility for the samples implanted with $5x10^{14}$ cm^{-2} silicon ions increase 11% to 48.9 $cm^2/V{\cdot}s$ after the extended time anneal despite an increase in ionized impurity scattering indicating that the lattice damage is not fully recovered. The samples implanted with $1x10^{15}$ cm^{-2} silicon ions have an activation of 96% following a 20 minute anneal at 1200 ºC, extending the anneal time to 40 minutes resulted in an increase in the activation to 100%.

The resistivity for these samples decreases less than 35 Ω/□. The mobility increased slightly for the samples implanted with a silicon dose of $1x10^{15}$ cm^{-2} between the two anneal times from 43 $cm^2/V{\cdot}s$ to 47 $cm^2/V{\cdot}s$. Like the $Al_{0.3}Ga_{0.7}N$ implanted with $5x10^{14}$ cm^{-2} silicon ions, these samples show an increase in the mobility regardless of an increase in ionized impurity scattering suggesting that the lattice damage is not fully recovered.

Table 5.2. Room temperature Hall Effect results for $Al_{0.3}Ga_{0.7}N$ implanted at room temperature with Si ions at 200 keV in three doses and annealed at 1200 ºC for 20 or 40 minutes in flowing nitrogen.

Dose (cm^{-2})	Time (min.)	Carrier Concentration (cm^{-2})	Activation (%)	Resistivity (Ω/□)	Mobility ($cm^2/V \cdot s$)
$1x10^{14}$	20	$5.27x10^{13}$	53.65	1838.4	64.39
$1x10^{14}$	40	$5.60x10^{13}$	56.74	2035	54.1
$5x10^{14}$	20	$3.97x10^{14}$	74.35	362.55	43.91
$5x10^{14}$	40	$4.25x10^{14}$	86.11	300.52	48.9
$1x10^{15}$	20	$9.48x10^{14}$	96.07	153.56	42.89
$1x10^{15}$	40	$1.00x10^{15}$	100	120.67	47.34

All the samples showed an increase in activation from extending the anneal time to 40 minutes; however the improvement was not always significant enough to achieve an activation better than that achieved at higher annealing temperatures. The samples implanted with $1x10^{14}$ cm^{-2} silicon ions are the only samples not to exhibit a higher activation after being annealed at 1200 ºC for forty minutes than being annealed at 1250 ºC for 20 minutes. The samples implanted with $1x10^{14}$ cm^{-2} silicon ions responded to extending the anneal time with a 3% increase in activation efficiency while the activation increased about 15% after annealing at 1250 ºC for 20 minutes over the activation achieved for the samples annealed at 1200ºC for 20 minutes. The activation efficiency for the $Al_{0.3}Ga_{0.7}N$ samples implanted with $5x10^{14}$ cm^{-2} silicon ions was 86% after being annealed for 40 minutes at 1200 ºC, which is similar to the 88% activation achieved for these samples after being annealed for 20 minutes at 1300 ºC. The samples implanted

with a silicon dose of $1x10^{15}$ cm^{-2} have an activation of 100% after being annealed at 1200 ºC for 40 minutes and 1250 ºC for 20 minutes, which is a 4% increase from the samples annealed at 1200 ºC for 20 minutes. These results are similar to those of the $Al_{0.1}Ga_{0.9}N$ which all showed considerable improvement of all the physical characteristics after the 1200 ºC anneal for 40 minutes, except the mobility.

The Si-implanted $Al_{0.3}Ga_{0.7}N$ samples all achieved high silicon electrical activation efficiency above 70% for each dose. The samples implanted with the lowest silicon dose had the lowest overall activation, reaching 74% following a 20 minute anneal at 1300 ºC, which was not improved upon by extending the anneal time to 40 minutes. The samples implanted with $5x10^{14}$ cm^{-2} silicon ions reached an activation of 90% after being annealed for 20 minutes at 1350 ºC, which was comparable to the 86% activation achieved after annealing for 40 minutes at 1200 ºC. The samples implanted with the highest silicon dose had the best activation of 100% following the 1200 ºC anneal for 40 minutes and the 1250 ºC anneal for 20 minutes. The samples implanted with this dose also had considerable activation, 96%, following the 1200 ºC anneal for 20 minutes. Lowering the anneal temperature and lengthening the anneal time benefited the electrical activation of all the samples but had mixed results on the resistivity and mobility. Lower resistivities and higher mobilities where achieved after annealing at higher temperatures.

Temperature-Dependent Hall Effect Measurements

Temperature-dependent Hall effect measurements were taken on the $Al_{0.3}Ga_{0.7}N$ that were annealed at 1200 and 1300 ºC for twenty minutes in flowing nitrogen to

determine the nature of the carriers as a function of temperature. The sheet carrier concentrations as a function of temperature from 10 to 700 K for the samples implanted with each of the three silicon doses and annealed at 1200 and 1300 ºC for 20 minutes are shown in Figure 5.35. The carrier concentrations for all the implanted silicon doses remain relatively constant as the samples temperature is increased from 10 to 50 K. The carrier concentration for the samples implanted with the two lower silicon doses of $1x10^{14}$ and $5x10^{14}$ cm^{-2} begins to decrease around 50 K, reaching a minimum at 120 K and 140K, respectively, and then begins to increase to a higher carrier concentration at 700 K. The samples implanted with a dose of $1x10^{15}$ cm^{-2} silicon ions have a relatively constant carrier concentration that increases slightly over the measured temperature range.

The $Al_{0.3}Ga_{0.7}N$ implanted with the highest silicon dose has the most temperature independent carrier concentration, as would be expected considering this silicon dose produces the most degenerate samples. The temperature independent nature of the carrier concentration is similar to that seen for the $Al_xGa_{1-x}N$ with Al compositions of 20 and 30% also implanted with this dose. This behavior is a result of the implanted silicon ions forming a degenerate impurity band within the band gap. The $Al_{0.3}Ga_{0.7}N$ samples implanted with all three doses have volume carrier concentrations that exceed the Mott concentration of $2.7x10^{18}$ cm^{-3}, which defines the point at which the material takes on metallic characteristics. The samples implanted with $1x10^{14}$ cm^{-2} silicon ions exhibit properties most like a non-degenerate material since their volume concentration is close to the Mott concentration and the Gaussian distribution of the implanted ions. The $Al_{0.3}Ga_{0.7}N$ samples implanted with $1x10^{14}$ silicon ions undergo a larger drop in carrier concentration than the $Al_{0.1}Ga_{0.9}N$ and $Al_{0.2}Ga_{0.8}N$, since the implanted doses are static

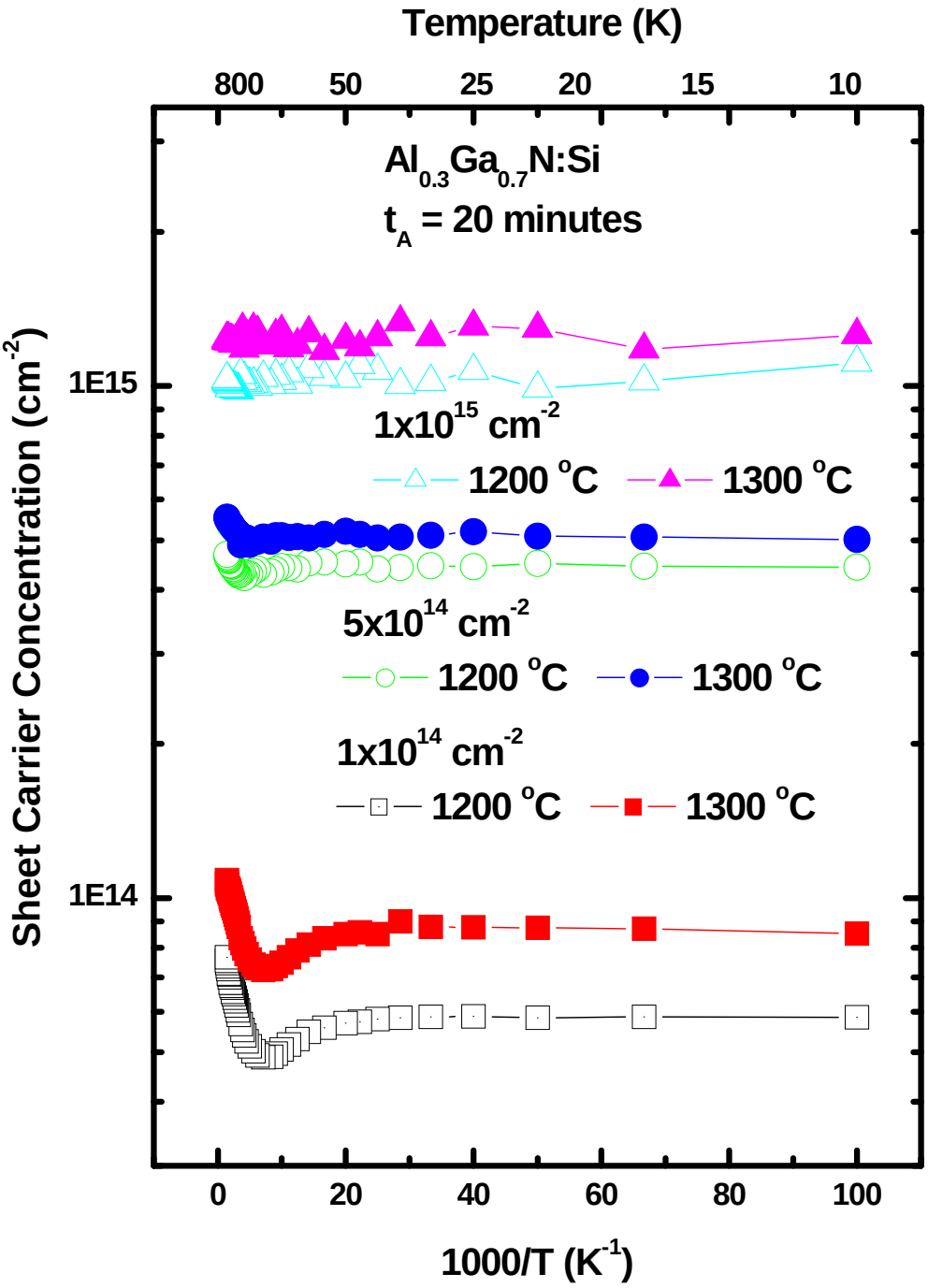

Figure 5.35. Temperature-dependent sheet carrier concentrations of $Al_{0.3}Ga_{0.7}N$ determined from Hall Effect measurements taken from 10 to 700 K. The $Al_{0.3}Ga_{0.7}N$ was implanted with three different doses of Si ions at 200 keV and annealed at 1200 °C and 1300 °C for 20 minutes in a flowing nitrogen environment.

and the Mott concentration increases as the Al mole fraction is increased. The dip in carrier concentration for the samples implanted with the lowest silicon dose is indicative of the formation of a multi-channel conduction band, one being the impurity band and the other the non-degenerate n-type layer which results from the Gaussian distribution of the implanted silicon ions (37). Samples that are degenerate yield ionization energies lower than the actual energy. Impurity screening acts to reduce the donor ionization energy and its effects are enhanced by an increase in the concentration of ionized donors. Therefore, the silicon ionization energy for $Al_{0.3}Ga_{0.7}N$ can not be accurately estimated from the samples in this study. However, Hwang *et al*. calculated from a simple hydrogen model that the ionization for $Al_{0.3}Ga_{0.7}N$ would be on the order of 50 meV.

The temperature-dependent Hall mobilities for the $Al_{0.3}Ga_{0.7}N$ are shown in Figure 5.36. All the samples exhibit a peak in their mobility curve below 300 K. The samples implanted with the lowest silicon dose exhibit a mobility of 55 $cm^2/V{\cdot}s$ after being annealed at 1200 ºC. The peak mobilities for the samples implanted with $5x10^{14}$ cm^{-2} silicon ions are 41 and 49 $cm^2/V{\cdot}s$, after being annealed at 1200 and 1300 ºC, respectively. The mobilities for the samples implanted with the highest dose are slightly lower at 42 and 54 $cm^2/V{\cdot}s$ for the two anneal temperatures, respectively. The mobility curves for all the samples increase as the temperature is increased up to about 250 K, at which point the mobility begins to decline. The mobility curves are more temperature independent for the samples implanted with the higher silicon doses, exposing the increasingly degenerate nature of the samples. However, the mobility curves for the $Al_{0.1}Ga_{0.9}N$ and $Al_{0.2}Ga_{0.8}N$ are much more flat. This degeneracy can also be noticed by the relatively high mobilities at 10 K where the mobility of a non-degenerate sample would approach zero. The mobility for the samples implanted with silicon doses of

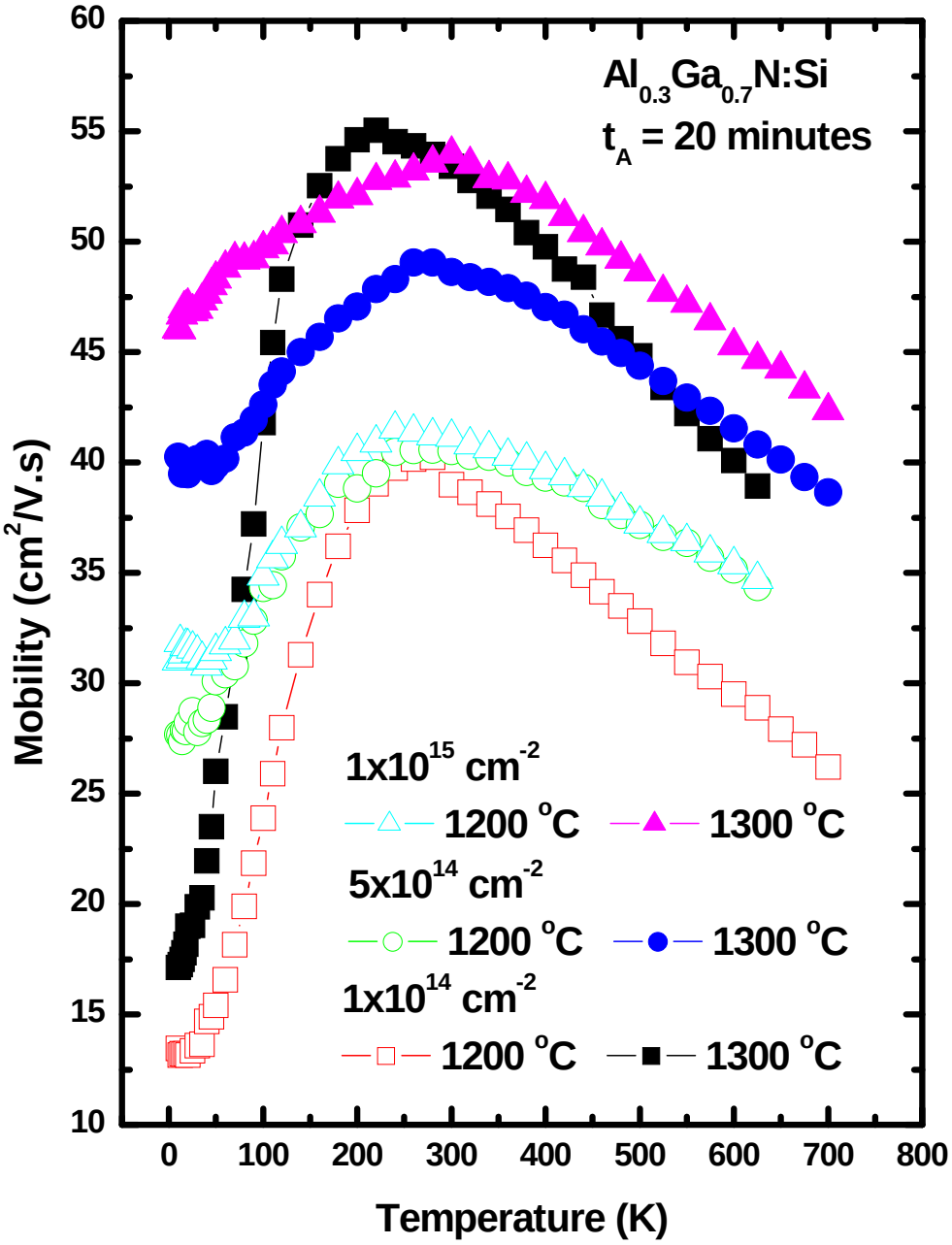

Figure 5.36. Temperature-dependent Hall mobilities taken from 10 to 700 K for $Al_{0.3}Ga_{0.7}N$ implanted at room temperature with silicon at 200 keV in three different doses and annealed at 1200 and 1300 ºC for 20 minutes.

$1x10^{14}$, $5x10^{14}$, and $1x10^{15}$ cm^{-2} and annealed at 1200 ºC are 17, 28, and 31$cm^2/V{\cdot}s$ at a temperature of 10 K. The mobilities for the samples annealed at 1200 ºC are all lower than the mobilities for the samples annealed at 1300 ºC, except for the samples implanted $1x10^{14}$ cm^{-2} silicon ions. The mobilities for the samples annealed at 1300 ºC are 13, 40, and 46 $cm^2/V{\cdot}s$ for the three doses, respectively. The degenerate impurity band causes the low temperature mobility to be temperature independent and is seen here to increase with doping level and also anneal temperature. The $Al_{0.3}Ga_{0.7}N$ samples implanted with a dose of $1x10^{14}$ cm^{-2} silicon ions exhibit a temperature-dependent mobility curve that most resembles that which is predicted for a non-degenerate sample and more so than the 10 and 20% $Al_xGa_{1-x}N$ samples. The mobility curves for the $Al_{0.1}Ga_{0.9}N$ and $Al_{0.2}Ga_{0.8}N$ implanted with a dose of $1x10^{15}$ cm^{-2} silicon ions are more flat and temperature-independent than the curves for the $Al_{0.3}Ga_{0.7}N$. Also, the mobility of the lower Al mole fraction material clearly increases as the silicon dose is decreased, which is not the case here. The $Al_{0.3}Ga_{0.7}N$ samples implanted with $5x10^{14}$ and $1x10^{15}$ cm^{-2} silicon ions and annealed at 1200 and 1300 ºC have higher mobilities than the samples implanted with $1x10^{14}$ cm^{-2} silicon ions and annealed at 1200 ºC.

The temperature-dependent resistivities of the $Al_{0.3}Ga_{0.7}N$ samples annealed at 1200 and 1300 ºC for all three implantation doses are shown in Figure 5.37. The samples annealed at the higher temperatures have considerably lower resistivities due to the increased carrier concentrations obtained at the elevated annealing temperatures. The resistivity decreases significantly as the implantation dose is increased and also becomes more temperature-independent which again is a result of the increased carrier concentration. All three implantation doses show a relative temperature-independent

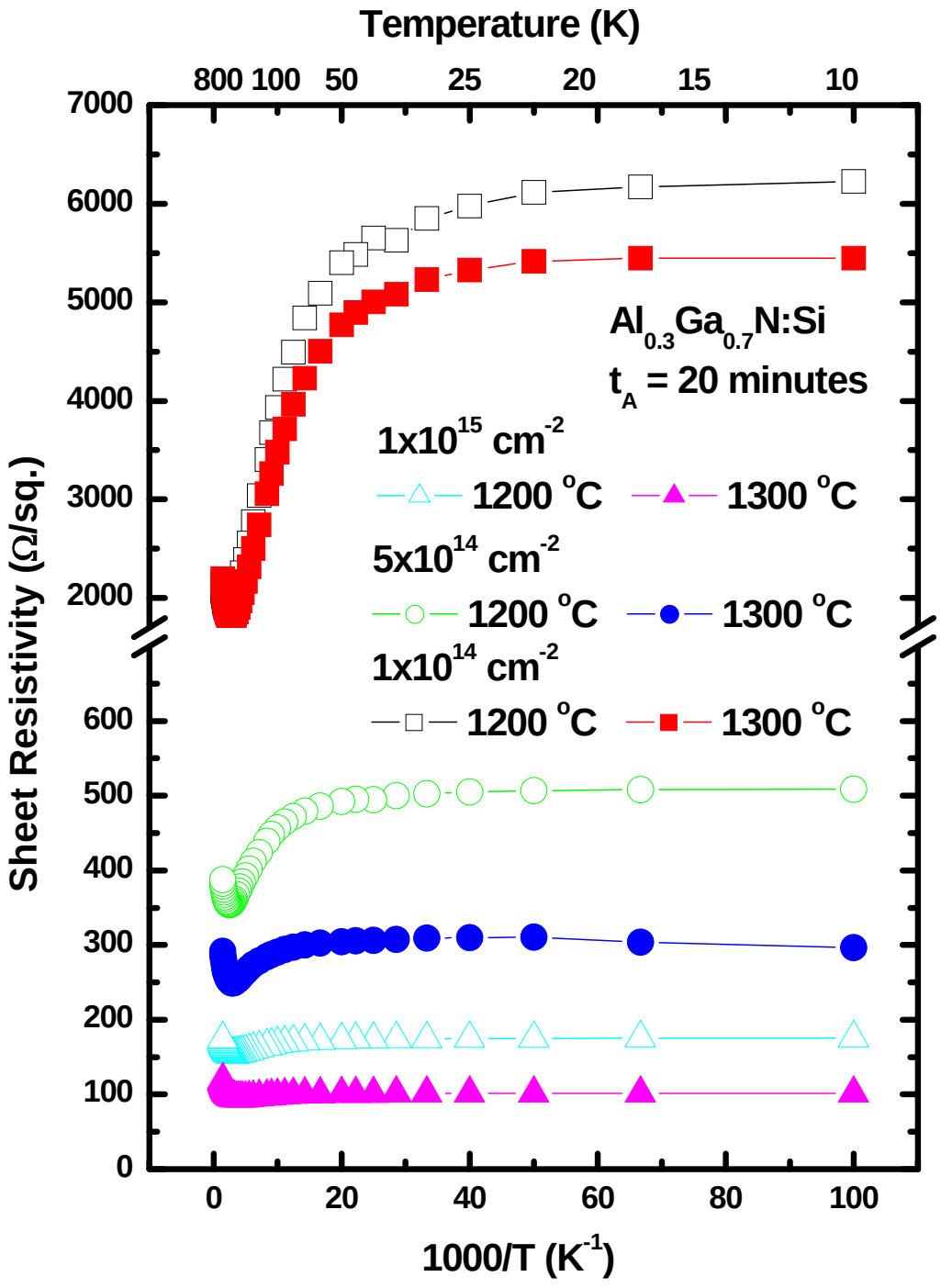

Figure.5.37. Temperature-dependent resistivity values calculated from Hall measurements taken from 10 to 700 K for $Al_{0.3}Ga_{0.7}N$ that had been implanted at room temperature with silicon ions at 200 keV with doses of $1x10^{14}$, $5x10^{14}$, and $1x10^{15}$ cm^{-2} and annealed at 1200 and 1300°C for 20 minutes in flowing nitrogen.

resistivity from 10 to 50 K before the resistivity slowly begins to decline to a minimum around 240-380 K at which point the resistivity begins to increase as the samples temperature is raised to 700 K. The dip in the resistivity curve for the samples implanted with $1x10^{14}$ cm^{-2} silicon ions is the most exaggerated while, the drop in the resistivity of the samples implanted with a silicon dose of $1x10^{15}$ cm^{-2} is almost unnoticeable. The decline in the resistivity curves around 300 K are a result of the rapid increase in the carrier concentration as the sample temperature is increased. The resistivity begins to increase at higher temperatures due to the decrease in the mobility as ionized impurity scattering becomes dominant. The resistivities curves for the $Al_{0.3}Ga_{0.7}N$ are similar is shape and value to those of the $Al_{0.1}Ga_{0.9}N$ and $Al_{0.2}Ga_{0.8}N$. In all three cases, the samples annealed at 1300 ºC have lower resistivities than the samples annealed at 1200 ºC. The implanted silicon dose has the most profound effect on the resistivity of the samples. Increasing the implanted silicon dose causes the resistivity of the material to decrease significantly and also causes the resistivity to become more temperature-independent.

Low Temperature Cathodoluminescence Measurements

Cathodoluminescence measurements were taken with an electron energy of 10 keV with 50 μA of source current, the temperature in the chamber was 7.4 K, and the slits on the spectrometer were 400 μm both at the entrance and the exit. The range scanned was 1800 to 7000 Å with a step size of 2 Å with an integration time of 0.1 second.

The spectrum of the unimplanted samples shown as a function of anneal temperature are given in Figure 5.38. To gauge the effects of the annealing on the

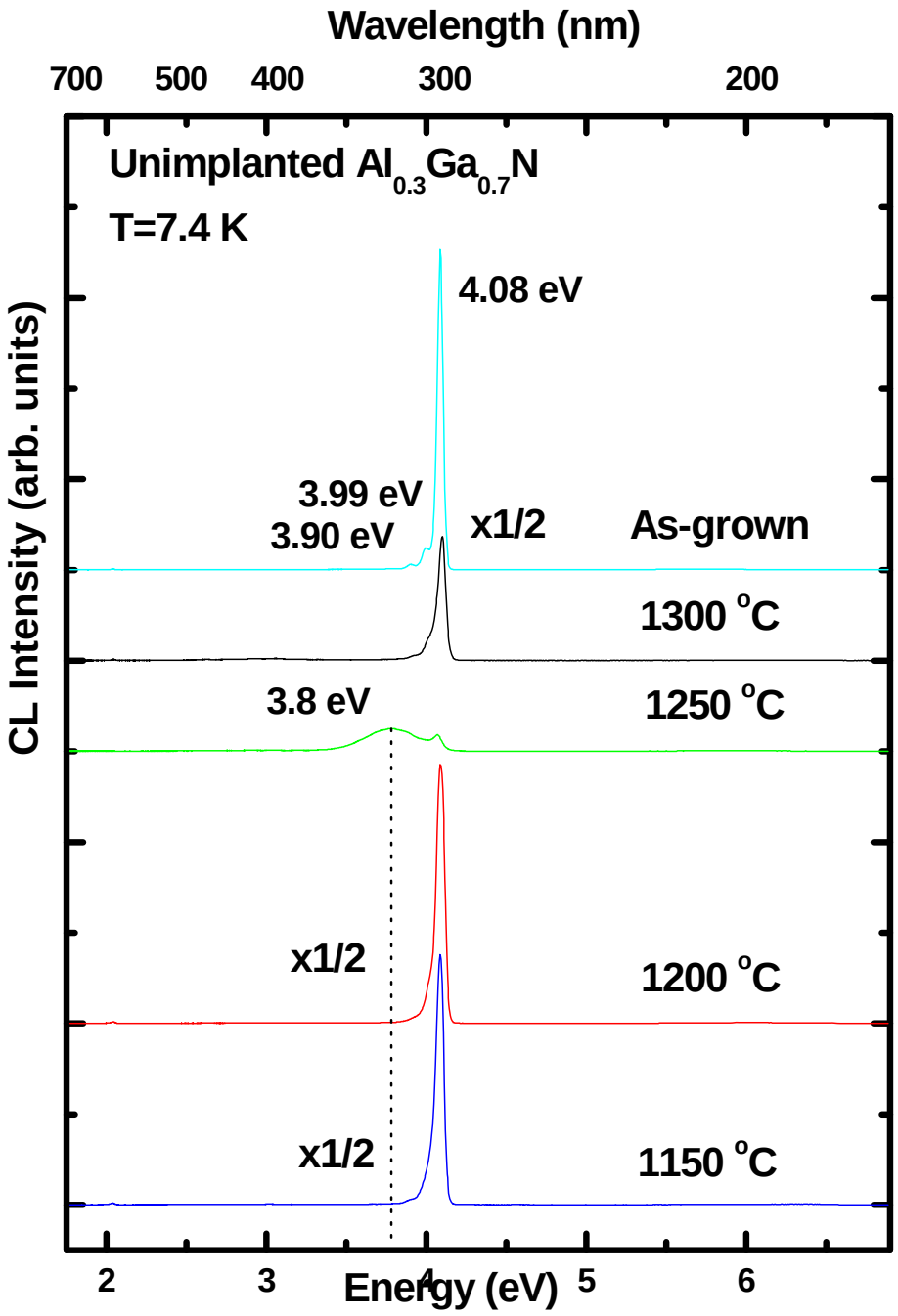

Figure 5.38.CL spectra taken at 7.4 K for unimplanted $Al_{0.3}Ga_{0.7}N$ that have been anneal at 1150, 1200, 1250 and 1350 °C for 20 minutes in flowing nitrogen and also an as-grown sample.

implanted samples, the behavior of the unimplanted samples must first be analyzed. The CL spectra for all the unimplanted samples all show a good neutral-donor-bound exciton (D^o,X) peak at 4.08 eV, except for the sample annealed at 1250 ºC. Nepal *et al*. identify a dominant peak at 4.27 eV in un-doped $Al_{0.38}Ga_{0.62}N$ which they attribute to localized exciton transitions (61). The spectra for the as-grown sample and the samples annealed at 1150 and 1200 ºC have been reduced by a factor of 2, to enhance the features of the spectra for the samples annealed at 1250 and 1300 ºC. The spectrum for the as-grown sample also has two small peaks at 3.99 and 3.90 eV which can be attributed to etalon effects. At first, the intensity of the (D^o,X) peak increases as the anneal temperature is increased up to 1200 ºC. The samples annealed at 1150 and 1200 ºC have CL spectra that closely resemble that of the as-grown sample in both intensity and sharpness. Further increasing the anneal temperature to 1250 ºC causes the (D^o,X) peak intensity to weaken considerably and a broad extension at 3.8 eV, most likely caused by defects created during the high temperature anneal. This broad emission centered around 3.8 eV is only evident in the sample annealed at 1250 ºC. Increasing the anneal temperature up to 1300 ºC recovers the (D^o,X) peak however, it still has a much weaker intensity than the as-grown sample. The unimplanted $Al_{0.3}Ga_{0.7}N$ respond better to low temperature annealing rather than high temperature annealing, indicating some annealing damage may occur for this Al mole fraction after annealing at 1250 ºC or higher.

The low temperature CL spectra for the Si-implanted $Al_{0.3}Ga_{0.7}N$ annealed for 20 minutes at 1300 ºC are shown in Figure 5.39. All of the spectra show a (D^o,X) peak at 4.08 eV, with a slight broadening toward lower energies. The implanted samples all exhibit a more intense (D^o,X) peak than that of the unimplanted sample, however the unimplanted sample's spectrum annealed at this temperature is highly reduced from that

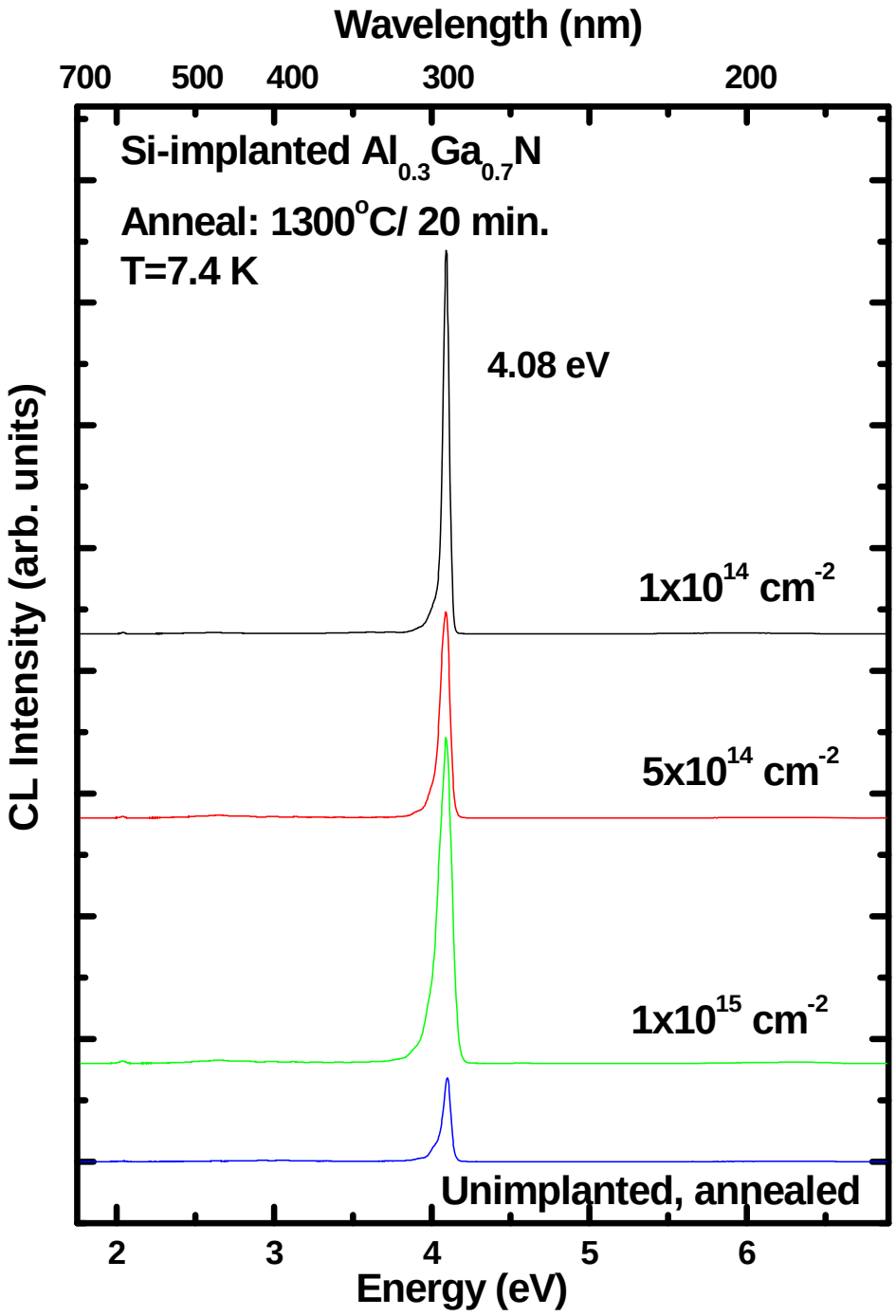

Figure 5.39. CL spectra taken at 7.4 K for $Al_{0.3}Ga_{0.7}N$ that have been anneal at 1300 ºC for 20 minutes in flowing nitrogen.

of the as-grown sample. The intensity of the (D^o,X) peak does not increase as the implanted silicon is decreased as it had in the previous Al mole fraction material. The $Al_{0.3}Ga_{0.7}N$ samples implanted with a silicon dose of $5x10^{14}$ cm^{-2} have a lower intensity than the samples implanted with the other silicon dose. The spectra of the $Al_{0.3}Ga_{0.7}N$, like those of the $Al_{0.2}Ga_{0.8}N$, do not show the broad yellow band (YL) that was seen in the spectra of the $Al_{0.1}Ga_{0.9}N$. The (D^o,X) peak broadens towards lower energy as the implanted silicon dose is increased from $1x10^{14}$ to $1x10^{15}$ cm^{-2}.

The near band edge broadening on the low energy side of the (D^o,X) peak, seen primarily in the spectra for the sample implanted with $1x10^{15}$ cm^{-2} silicon ions, is due mainly to band tailing effects. The implanted silicon doses exceed the Mott concentration of $Al_{0.3}Ga_{0.7}N$, which can result in band-edge effects such as band filling and band tailing. Band filling, seen in the CL spectrum as broadening of the (D^o,X) peak towards higher energies, occurs in highly-doped semiconductors when the Fermi energy moves toward very close to the conduction band or into the conduction band, thus allowing for transitions to occur at higher energies than the band gap. Only the sample implanted with a silicon dose of $1x10^{15}$ cm^{-2} has a volume carrier concentration high enough for noticeable band filling to occur.

The low temperature CL spectra for the $Al_{0.3}Ga_{0.7}N$ implanted with $1x10^{14}$ cm^{-2} silicon ions and annealed for 20 minutes at various temperatures are shown in Figure 5.40. All of the anneal temperatures produce spectra with a good (D^o,X) peak centered at 4.08 eV, except for the sample that was annealed at 1200 ºC. The peak for this sample has shifter to 4.0 eV. The spectra for the as-grown sample and the sample annealed at 1150 ºC had to be reduced 150^{th} of their original size. The samples annealed at 1250 and

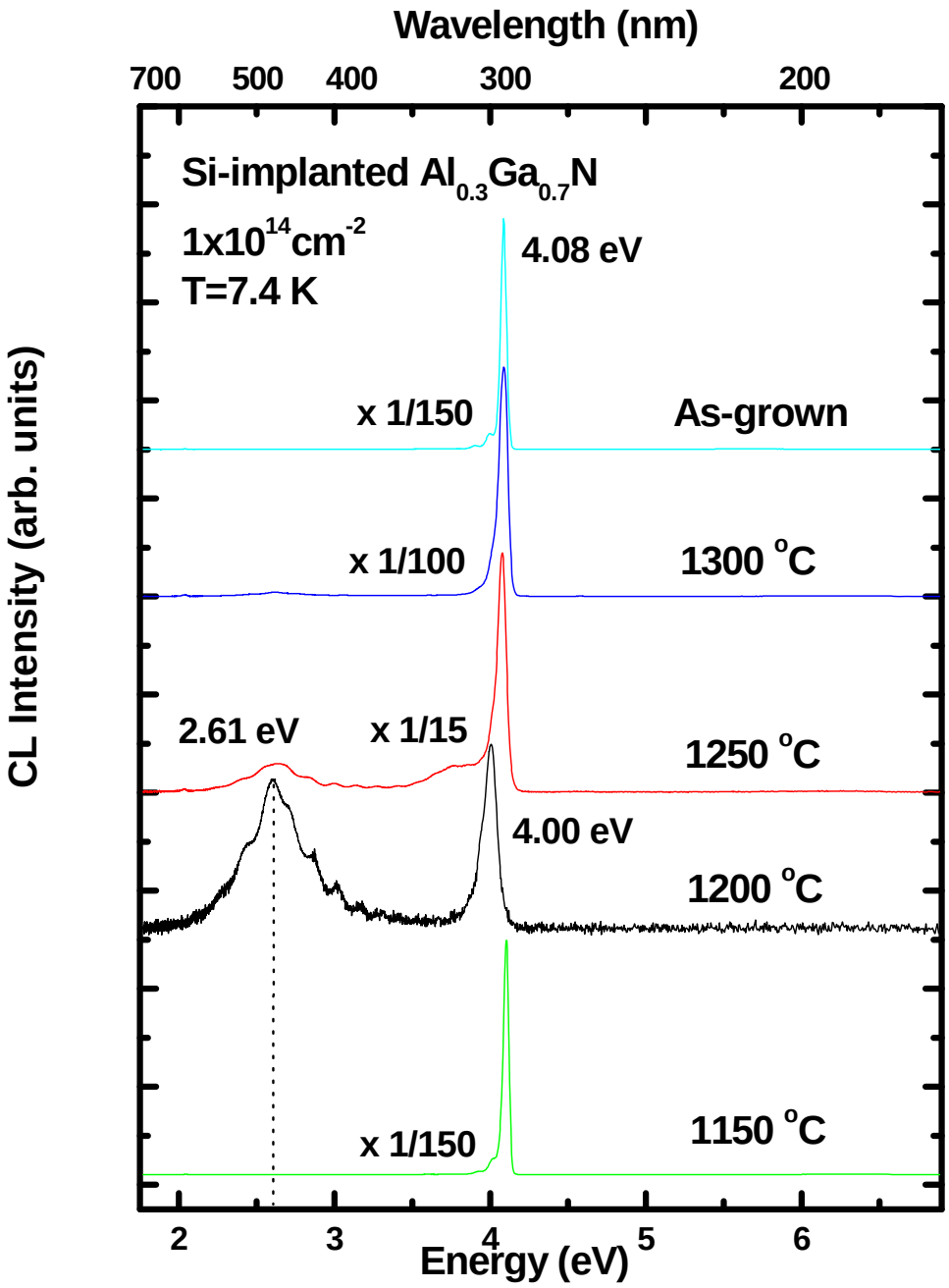

Figure 5.40. CL spectra taken at 7.4 K for $Al_{0.3}Ga_{0.7}N$ that has been implanted with $1x10^{14}$ cm^{-2} silicon ions and annealed at various temperatures for 20 minutes in flowing nitrogen.

1300 ºC also had to be reduced, but only by a factor of 15 and 100, respectively. Like the unimplanted $Al_{0.3}Ga_{0.7}N$, these samples exhibit their most intense (D^o,X) peak following the 1150 ºC. The intensity of the (D^o,X) peak for this temperature is only slightly less than that of the as-grown sample. Increasing the anneal temperature to 1200 ºC has detrimental effects on the spectra, the intensity of the (D^o,X) peak decreases and a broad luminescence, similar to the YL band seen in the $Al_{0.1}Ga_{0.9}N$, emerges. The intensity of the (D^o,X) peak and the intensity with the broad band luminescence centered at 2.61 eV are almost equal. The CL spectra improve considerably as the anneal temperature is raised to 1300 ºC. The sample annealed at 1250 ºC exhibits the YL band that has a much reduced intensity from that of the sample that was annealed at 1200 ºC. The 2.61 eV band is most likely related to implanted related defects, such as transitions from a silicon donor to an aluminum vacancy, that are activated at higher anneal temperatures. The spectra for the sample annealed at 1250 ºC also has a large broad shoulder off the low energy side of the (D^o,X) peak that is similar to the broad emission in the spectra for the unimplanted sample annealed at this temperature. The unimplanted sample annealed at 1250 ºC has a broad luminescence centered at 3.7 eV that could be related to damage caused during the anneal. Further increasing the anneal temperature to 1300 ºC produces a spectra with a sharp (D^o,X) peak and no YL band, similar to the spectrum of the unimplanted sample. The intensity of the (D^o,X) peak for the $Al_{0.3}Ga_{0.7}N$ samples implanted with a silicon dose of $1x10^{14}$ cm^{-2} increases as the anneal temperature is increased from 1200 to 1300 ºC, signifying successive improvement in the crystal lattice with each increase in the anneal temperature. The spectrum of the sample annealed at 1150 ºC has the best recovery of the (D^o,X) peak however, this sample has the lowest activation efficiency. An anneal temperature of 1200 ºC produced significantly reduced

intensity with no apparent reason, however the carrier concentration for this sample increased 73% over that of the sample annealed at 1150 ºC. An anneal temperature of 1300 ºC produced an excellent peak signifying that the majority of the implantation induced damage had been restored and most of the silicon ions have been activated. The increase in intensity of the (D^o,X) peaks observed for the anneal temperatures of 1200, 1250, and 1300 ºC indicate that more of the implanted silicon ions have become electrically active as the anneal temperature was increased. The CL spectra agree very well with the electrical activation results obtained from Hall Effect measurements for the $Al_{0.3}Ga_{0.7}N$ implanted with this silicon dose. The sharpness and strong intensity of the peak for the sample annealed at 1300 ºC correlate well with the high activation and mobility values obtained on this sample. The (D^o,X) peak and the high mobilities observed on the these samples indicate excellent implantation damage recovery after annealing at 1300 ºC for 20 minutes in flowing nitrogen.

Figure 5.41 shows the CL spectra of the $Al_{0.3}Ga_{0.7}N$ implanted with a silicon dose of $5x10^{14}$ cm^{-2} and annealed for 20 minutes at various temperatures. All the spectrum have a (D^o,X) peak at 4.08 eV with a small shoulder on the low energy side. The sample annealed at 1150 ºC produces a good (D^o,X) peak that is only slightly more intense peak than the samples annealed at 1200 and 1300 ºC. The intensity of the spectrum of the sample annealed at 1200 ºC is much reduced, like the $Al_{0.3}Ga_{0.7}N$ samples implanted with a silicon dose of $1x10^{14}$ cm^{-2}, for unknown reasons. The samples implanted with $5x10^{14}$ cm^{-2} silicon ions exhibit their strongest (D^o,X) peak after being annealed at 1250 ºC for 20 minutes, which is more intense than the as-grown sample. However, the sample annealed at 1300 ºC for 20 minutes again shows a diminished intensity for unknown reasons. The spectrum of the sample annealed at 1350 ºC closely resembles that of the

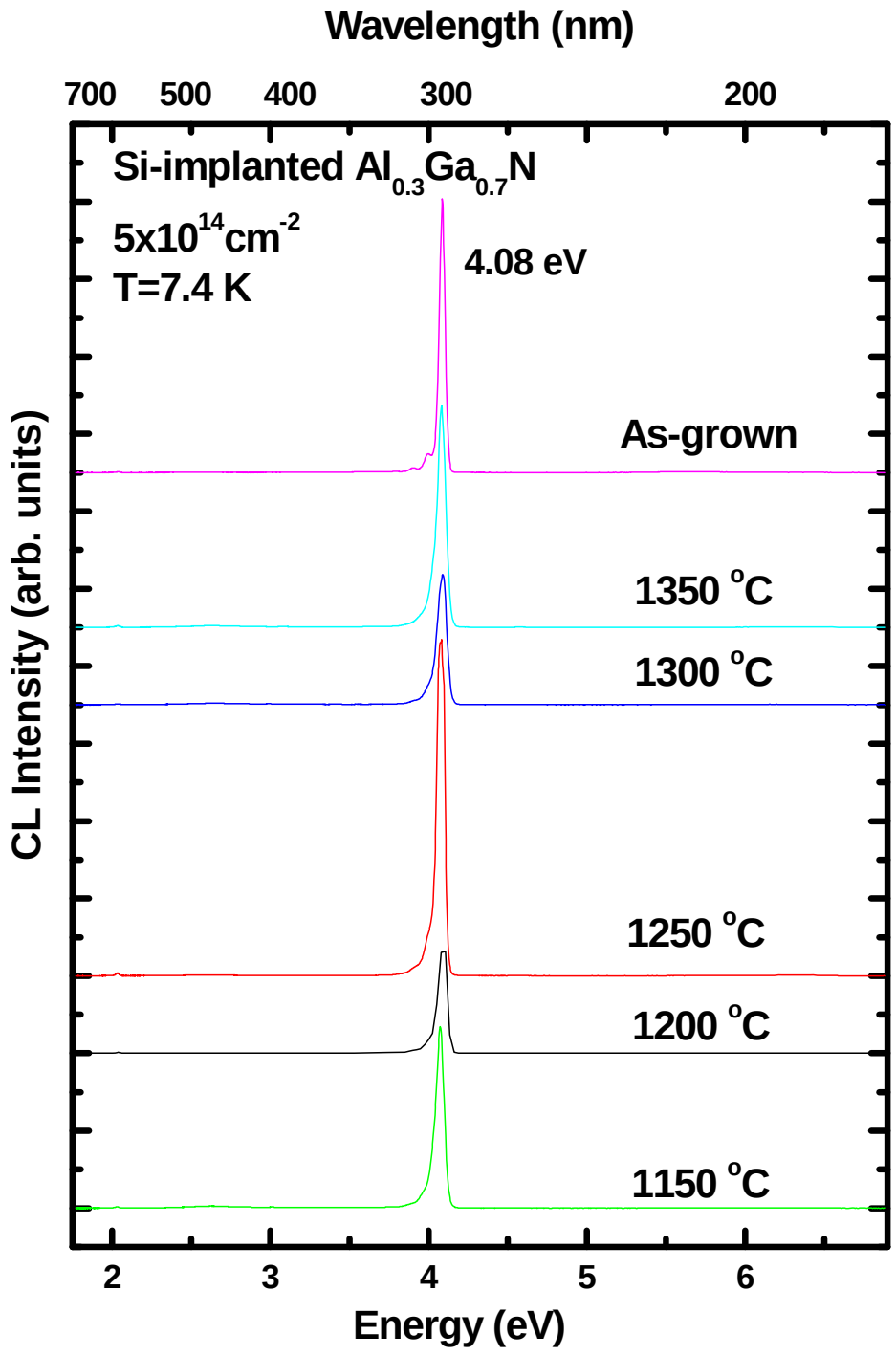

Figure 5.41. CL spectra taken at 7.4 K for $Al_{0.3}Ga_{0.7}N$ that has been implanted with $5x10^{14}$ cm^{-2} silicon ions and annealed at various temperatures for 20 minutes in flowing nitrogen.

as-grown sample in both intensity and sharpness. The $Al_{0.2}Ga_{0.8}N$ samples implanted with this dose also display their best (D^o,X) peak at lower anneal temperatures. The intensity of the (D^o,X) peak swamps out the broad band luminescence centered at 2.61 eV, that is present in the samples annealed at 1250, 1300 and 1350 ºC. This luminescence becomes more intense as the anneal temperature is increased. The samples annealed at lower temperatures do not have any broad band luminescence. The $Al_{0.3}Ga_{0.7}N$ samples implanted with $1x10^{14}$ cm^{-2} silicon ions and annealed at 1200 and 1250 ºC also exhibit this luminescence only it decreases ad the anneal temperature is increased and is not present in the spectrum of the sample annealed at 1300 ºC.

The CL spectra of the samples implanted with the highest silicon dose of $1x10^{15}$ cm^{-2} and annealed for 20 minutes at various temperatures are shown in Figure 5.42. The CL spectra exhibit the same dependence on the anneal temperature as the samples implanted $5x10^{14}$ cm^{-2} silicon ions. All the spectra have a (D^o,X) peak at 4.08 eV that slightly broadens on the lower energy side. The (D^o,X) peak for the sample annealed at 1250 ºC has the strongest intensity, which is stronger than the as-grown sample, however it has broadened both toward high and low energies due to band filling and band tailing effects. The samples annealed at 1150 and 1300 ºC have about the same intensity however, the sample annealed at 1300 ºC has a much broader peak due to the enhance effects of band tailing. The intensity of the peak increases as does the full width half max of the peak upon extending the anneal temperature from 1150 to 1250 ºC. The spectrum of the sample annealed at 1200 ºC has been increased 100 times of its original size. This spectrum shows a broad and weak peak centered at 4.0 eV and broad band centered at 2.61 eV, similar to the spectrum of the $Al_{0.3}Ga_{0.7}N$ sample implanted with $1x10^{14}$ cm^{-2} silicon ions and annealed at this temperature. The spectrum for the samples annealed at

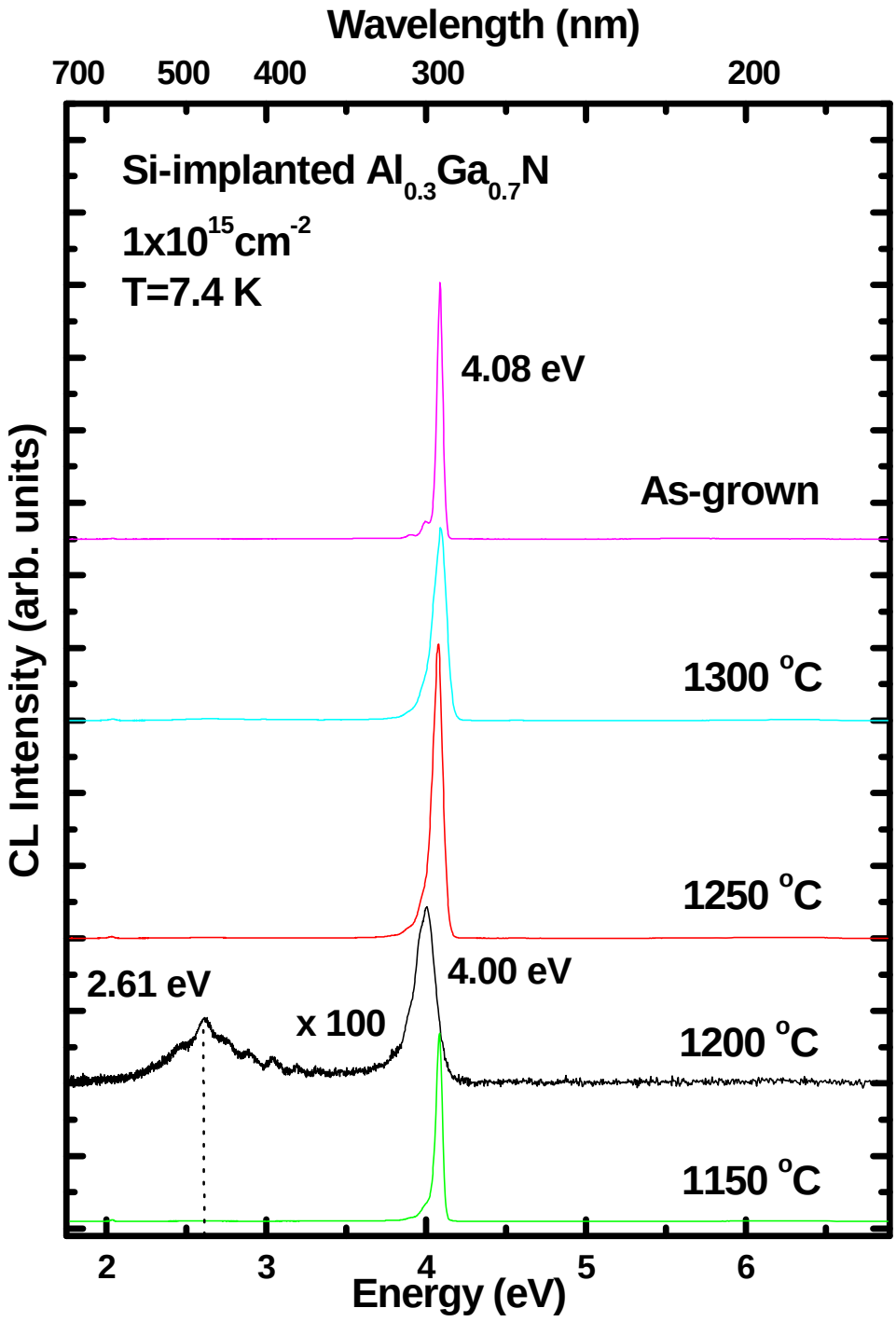

Figure 5.42. CL spectra taken at 7.4 K for $Al_{0.3}Ga_{0.7}N$ that has been implanted with $1x10^{15}$ cm^{-2} silicon ions and annealed at various temperatures for 20 minutes in flowing nitrogen.

1250 and 1300 ºC also exhibit a broad luminescence at 2.61 eV that has a much reduced intensity than the (D^o,X) peaks for these spectra and are not visible. This broad band luminescence decreases as the anneal temperature is increased.

The spectra for the $Al_{0.3}Ga_{0.7}N$ samples that were implanted with all three doses and annealed at 1200 ºC all experience a significant decrease in intensity for no obvious reason. As the anneal temperature was increased, this was the lowest anneal temperature to produce the 2.61 eV band for the samples implanted with $1x10^{14}$ and $1x10^{15}$ cm^{-2} silicon ions, which also corresponds to the temperature that the carrier concentration experiences its largest increase. This band has been suggested to be related to a silicon donor and a deep acceptor (44). The 2.61 eV band does not emerge for the samples implanted with $5x10^{14}$ cm^{-2} silicon ions until they were annealed at 1250 ºC. These samples experience the diminished intensity of the sample annealed at 1200 ºC and also again for the samples annealed at 1300 ºC, which corresponds to the temperatures that he carrier concentration increases the most. This could be considered the temperature required to excite the lattice enough for incorporation of the silicon ions to take place.

Silicon Implanted $Al_{0.4}Ga_{0.6}N$

Electrical and optical properties of Si-implanted $Al_xGa_{1-x}N$ with Al concentrations of 40 and 50% have not been reported in the literature. However, there is literature that addresses the effects of silicon doping on high Al mole fraction ($x > 0.5$) $Al_xGa_{1-x}N$. Hwang *et al*. investigated the effects of silicon doping on $Al_{0.65}Ga_{0.35}N$ that had a room temperature carrier concentration of $8.0x10^{19}$ cm^{-3} and mobility of 18 $cm^2/V{\cdot}s$ (51). Temperature-dependent Hall measurements on this sample exhibited no change with the increasing temperature, indicating the sample was degenerate. Nakarmi *et al*.

investigated $Al_{0.67}Ga_{0.33}N$ epilayers grown on AlN/sapphire templates by MOCVD and found that these epilayers exhibited n-type conductivity due to an unidentified shallow donor at 88 meV, which they believe to be oxygen (33). The $Al_{0.67}Ga_{0.33}N$ had a room temperature resistivity around 85 Ω/□ and a low electron mobility of about 2 $cm^2/V{\cdot}s$. They suggest the low mobility could be due to large alloy scattering and the increased effective mass of the electrons due to the high Al content of the material. Zhu *et al*. investigated Si-doped $Al_{0.7}Ga_{0.3}N$ epilayers grown by MOCVD on sapphire substrates (52). The Si-doping resulted in a carrier concentration of $6.0x10^{19}$ cm^{-3} that exhibited ionization energy of 10 meV.

There are no reported ionization energies for silicon implanted $Al_{0.4}Ga_{0.6}N$. Hwang *et al*. calculated, from a simple hydrogen model, the donor ionization energy of $Al_xGa_{1-x}N$ increases with increasing Al mole fraction from 34 meV for GaN to 90 meV for AlN, when low-frequency dielectric constants are used (51). Assuming the ionization energy increases linearly with Al concentration, the ionization energy for silicon in $Al_{0.4}Ga_{0.6}N$ would be on the order of 56 meV for a non-degenerate sample. The implanted silicon doses of $1x10^{14}$, $5x10^{14}$, and $1x10^{15}$ cm^{-2} correspond to peak volume carrier concentrations of $5.71x10^{18}$, $2.85x10^{19}$, and $5.71x10^{19}$ cm^{-3}, which all exceed the Mott concentration of $2.36x10^{18}$ cm^{-3} for $Al_{0.4}Ga_{0.6}N$, which was calculated using equation 2.18. Therefore, the empirical ionization energies determined for the $Al_{0.4}Ga_{0.6}N$ will underestimate the true ionization energy.

Room Temperature Hall Effect Measurements

The MEMOCVD grown $Al_{0.4}Ga_{0.6}N$ was capped with 500Å of AlN and implanted at room temperature with three different doses of silicon ions at 200 keV. The

silicon doses were $1x10^{14}$, $5x10^{14}$, and $1x10^{15}$ cm^{-2} which correspond to effective doses of $9.9x10^{13}$, $4.54x10^{14}$, and $9.9x10^{14}$ cm^{-2}, respectively when accounting for the AlN encapsulant. The samples were annealed from 1150 to 1350 ºC for 20 minutes in a nitrogen environment. All the samples had excellent mirror-like surface morphology even after the anneal at 1350 ºC. Room temperature Hall effect measurements were conducted to determine sheet carrier concentrations for the samples and are shown in Figure 5.43. The unimplanted samples, both as-grown and annealed, were highly resistive making it impossible to collect any meaningful data. Thus, the electrical activation efficiency was calculated using the measured carrier concentration with no correction for the background carriers.

In general, the sheet carrier concentrations for the $Al_{0.4}Ga_{0.6}N$ samples implanted with each silicon dose increase as the anneal temperature is increased. The only exceptions are for the samples implanted with $1x10^{15}$ cm^{-2} silicon ions that were annealed at 1300 and 1350 ºC. The samples implanted with $1x10^{14}$ cm^{-2} silicon ions exhibits a large increase in carrier concentration as the anneal temperature is raised from 1150 to 1200 ºC and then increases more slowly as the anneal temperature is brought up to 1350ºC. This is much like the behavior of the lower Al mole fraction $Al_xGa_{1-x}N$ that had been implanted with this dose, only the increase is more exaggerated for the $Al_{0.3}Ga_{0.7}N$ and $Al_{0.4}Ga_{0.6}N$ samples. The samples implanted with this silicon dose increase in carrier concentration from $6.6x10^{13}$ to $9.8x10^{13}$ cm^{-2} as the anneal temperature is increased from1150 to 1350 ºC. The carrier concentrations for the $Al_{0.4}Ga_{0.6}N$ samples implanted with a dose of $5x10^{14}$ silicon ions has the largest increase as the anneal temperature is raised from 1150 to1200 ºC and then levels off as the temperature is increased to 1350 ºC. A maximum carrier concentration of $4.8x10^{14}$ cm^{-2} was obtained for the samples

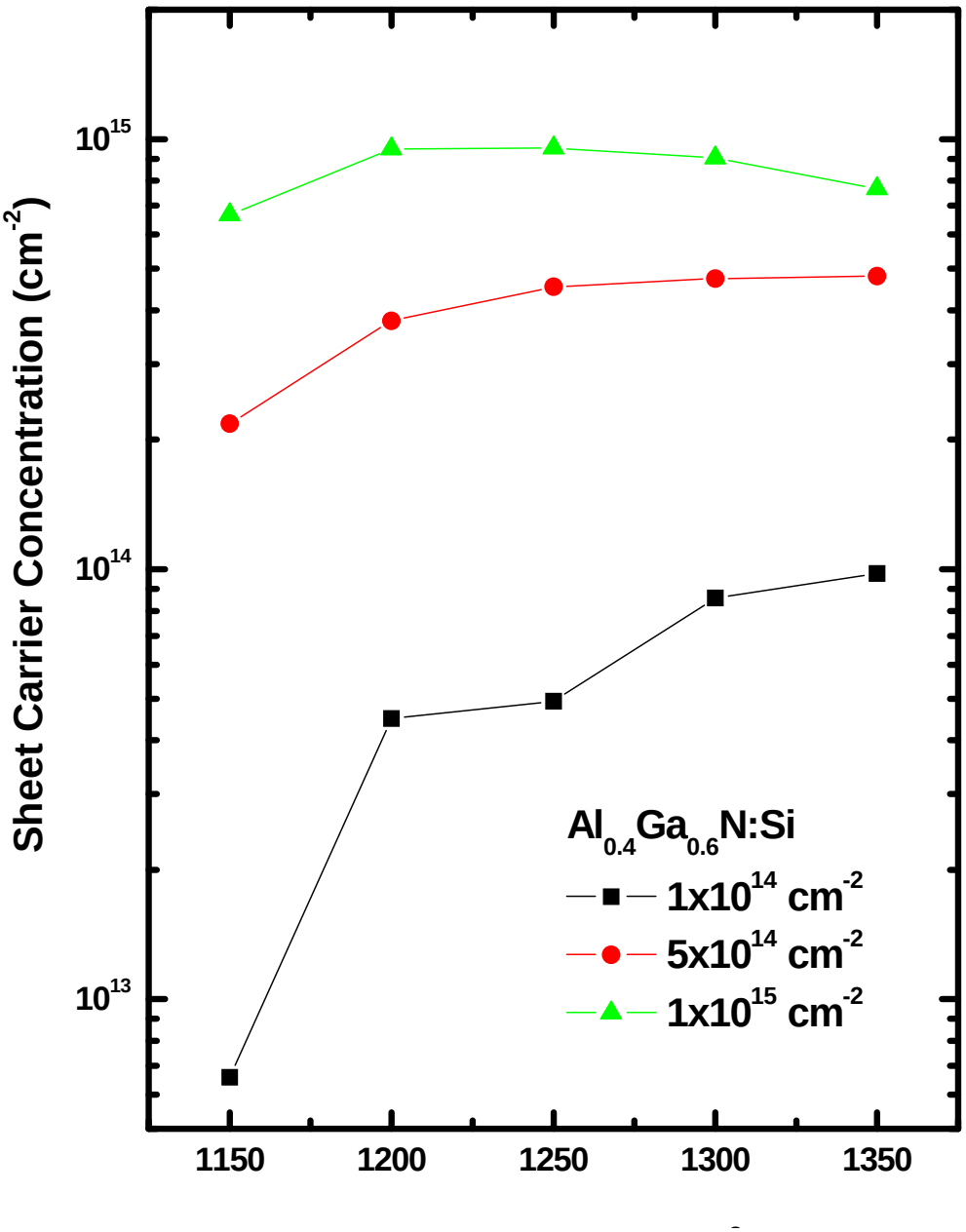

Figure 5.43. Room temperature sheet carrier concentrations for $Al_{0.4}Ga_{0.6}N$ implanted at room temperature with silicon ions at 200 keV with doses of $1x10^{14}$, $5x10^{14}$, and $1x10^{15}$ cm^{-2} and annealed from 1150 to 1350 ºC for 20 minutes in flowing nitrogen.

implanted with a silicon dose of $5x10^{14}$ cm^{-2} following a 20 minute anneal at 1350 ºC. The carrier concentrations for the $Al_{0.4}Ga_{0.6}N$ implanted with a dose of $1x10^{15}$ cm^{-2} silicon ions increases as the temperature is raised from 1150 to 1250 ºC and then shows a slight decline as the anneal temperature is further increased to 1350 ºC. The $Al_{0.4}Ga_{0.6}N$ implanted with a silicon dose of $1x10^{15}$ cm^{-2} reaches a maximum carrier concentration of $9.55x10^{14}$ cm^{-2} after being annealed for 20 minutes at 1250 ºC. The $Al_{0.1}Ga_{0.9}N$ samples implanted with the highest silicon dose also had a decline in the carrier concentration after being annealed at higher temperatures of 1200 and 1250 ºC.

Figure 5.44 shows the electrical activation for the $Al_{0.4}Ga_{0.6}N$ that was calculated using the effective doses and room temperature sheet carrier concentrations. The silicon electrical activation of these samples is closely related to the carrier concentration and follows the same trends with the anneal temperature as mentioned above. The $Al_{0.4}Ga_{0.6}N$ implanted with all three silicon doses exhibit excellent activation above 90% after the high temperature anneal. The samples implanted with $1x10^{14}$ cm^{-2} silicon ions have activation efficiencies that increase as the anneal temperatures are increased up to 1350 ºC. The activation of the $Al_{0.4}Ga_{0.6}N$ implanted with $5x10^{14}$ cm^{-2} silicon ions increases rapidly as the anneal temperature is raised from 1150 to 1250 ºC and then steadies off and slowly increases as the anneal temperature is raised to 1350 ºC. The electrical activation for the samples implanted with $1x10^{15}$ cm^{-2} silicon ions peaks for the sample annealed at 1250 ºC and then begins to decline for the samples that were annealed at higher temperatures. The decrease in activation efficiency could be due to out diffusion of silicon or compensating acceptor-like defects that were created during the higher temperature anneals. However, the activation of the $Al_{0.4}Ga_{0.6}N$ implanted with this silicon dose still has a significant activation of 78% after being annealed at 1350 ºC.

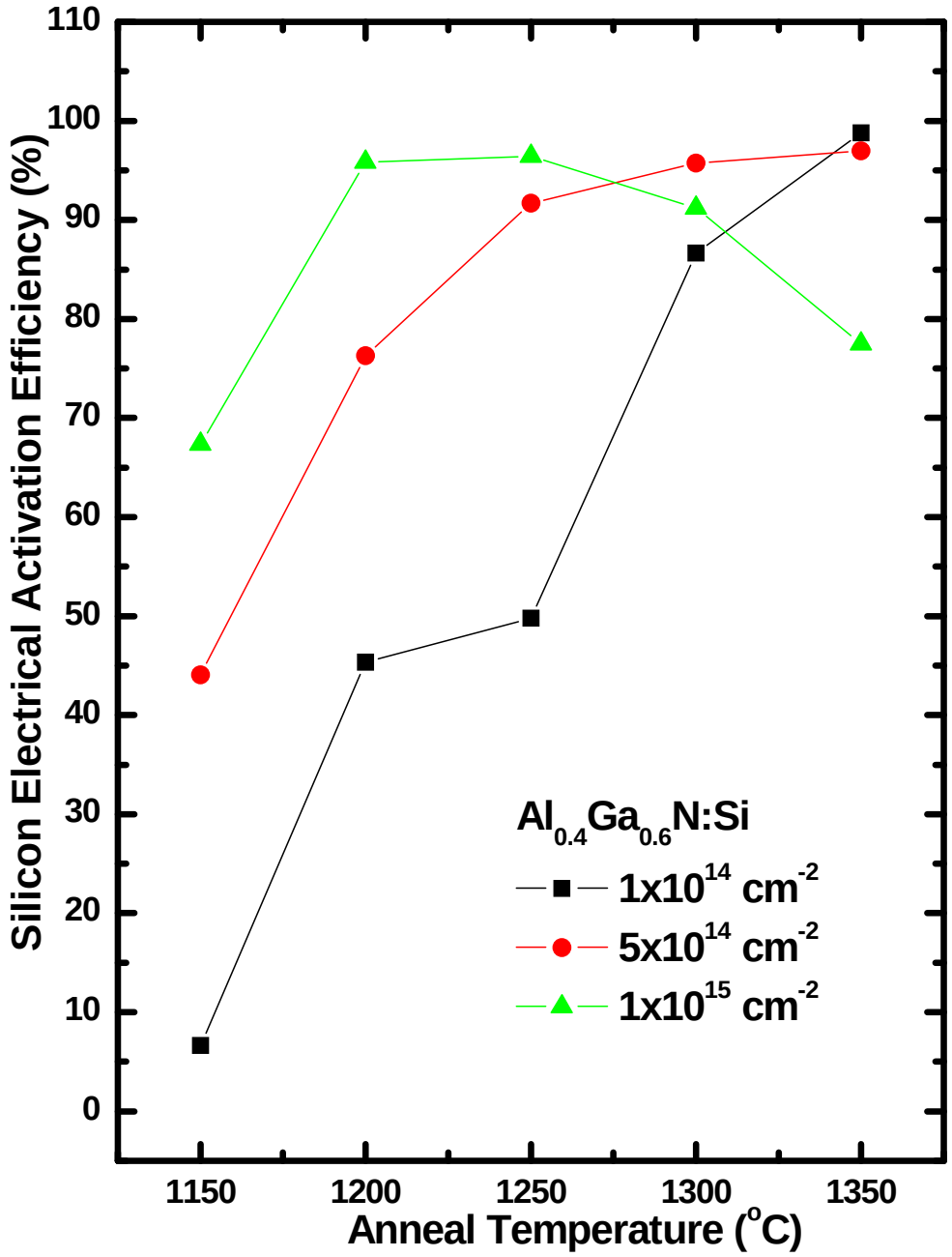

Figure 5.44. Silicon electrical activation efficiency for $Al_{0.4}Ga_{0.6}N$ calculated from the room temperature Hall measurements for Si-implanted doses of $1x10^{14}$, $5x10^{14}$, and $1x10^{15}$ cm^{-2} and annealed from 1150 to 1350 °C for 20 minutes.

This activation is higher than that for the samples implanted with this silicon dose and annealed at 1150 ºC which is of 67 %.

The samples implanted with $1x10^{14}$ cm^{-2} silicon ions exhibit the most improvement over the given temperature range, increasing from 6% to 99% after being annealed for 20 minutes at 1150 ºC and 1350 ºC, respectively. The $Al_{0.4}Ga_{0.6}N$ implanted with this silicon dose had the lowest activations but showed the best response to an increase in the anneal temperature, indicating that a further increase in the anneal temperature or time may result in higher activation. This behavior is consistent with the $Al_xGa_{1-x}N$ samples with Al concentrations from 10 to 30% that were implanted with this silicon dose. The activation efficiencies of the $Al_{0.4}Ga_{0.6}N$ implanted with a dose of $5x10^{14}$ cm^{-2} silicon ions reach a peak activation of 97%, for the sample that was annealed at 1350 ºC for 20 minutes. The peak activation efficiency for the $Al_{0.2}Ga_{0.8}N$ implanted with this dose was 100% after being annealed at 1300 ºC for 20 minutes. The $Al_{0.1}Ga_{0.9}N$ and $Al_{0.3}Ga_{0.7}N$ samples implanted with this silicon dose achieved lower peak activations for various annealing conditions. The maximum activation for the $Al_{0.1}Ga_{0.9}N$ samples implanted with $5x10^{14}$ cm^{-2} silicon ions was 94% after a 40 minute anneal at 1200 ºC, while the activation for the $Al_{0.3}Ga_{0.7}N$ was considerably lower at 88% for the sample annealed at 1300 ºC for 20 minutes. The $Al_{0.4}Ga_{0.6}N$ implanted with the highest silicon dose of $1x10^{15}$ cm^{-2} reaches 96% activation after being annealed at 1250 ºC for 20 minutes in a nitrogen ambient. The activation efficiencies of the $Al_xGa_{1-x}N$, with Al concentrations from 10 to 30%,

implanted with the same silicon dose all reach 100% after being annealed at various temperatures. All of the implanted silicon doses are readily activated in $Al_{0.4}Ga_{0.6}N$, which is illustrated in Figure 5.45. Considerably lower anneal temperatures

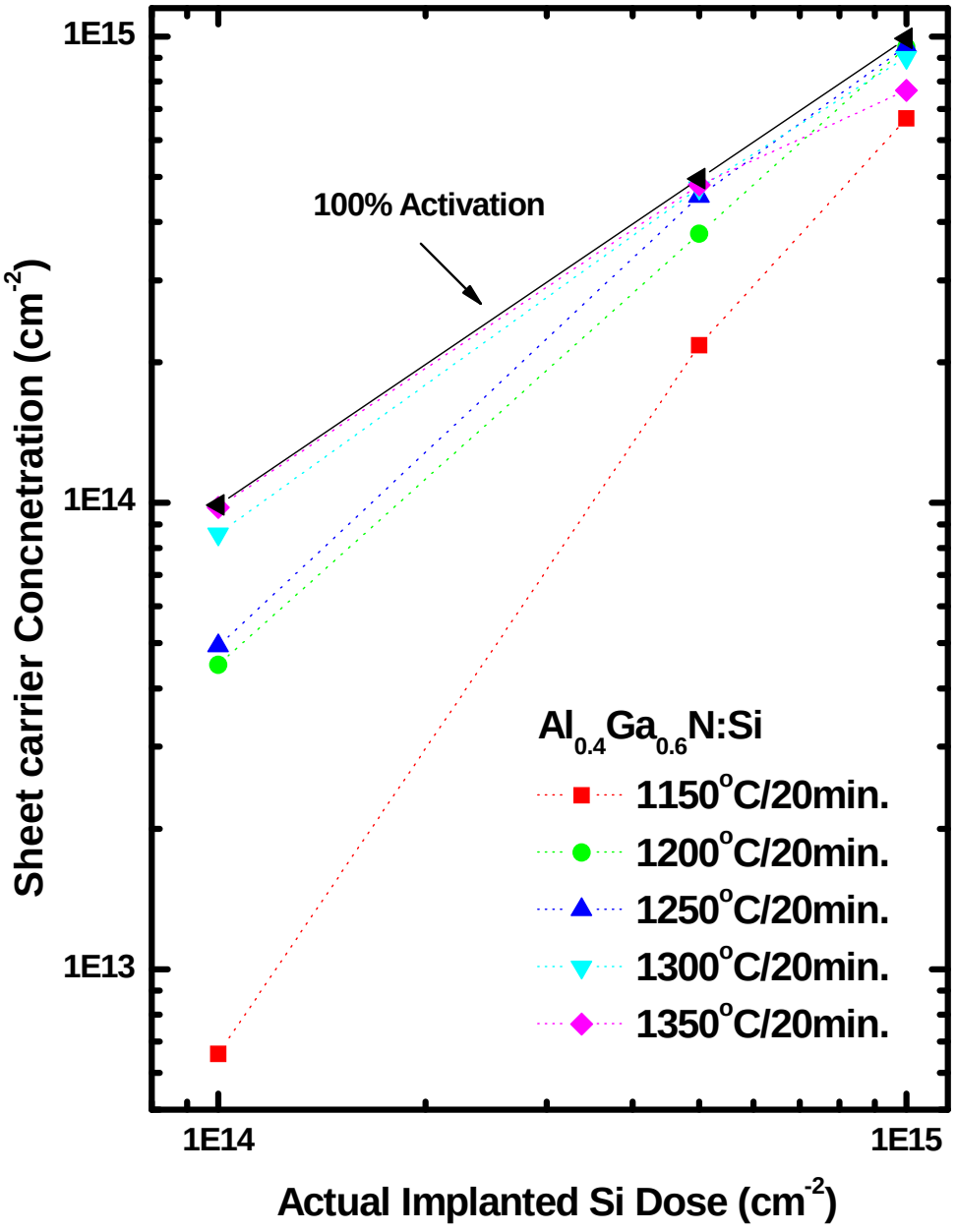

Figure 5.45. The room temperature sheet carrier concentrations versus the actual implantation dose for $Al_{0.4}Ga_{0.6}N$ implanted at room temperature with silicon ions at 200 keV with doses of $1x10^{14}$, $5x10^{14}$, and $1x10^{15}$ cm^{-2} and annealed from 1150 ºC to 1350 ºC for 20 minutes in a nitrogen ambient.

were required to achieve a high activation efficiency in the samples implanted with $1x10^{15}$ cm^{-2} silicon ions than in the samples implanted with the lower silicon doses. The $Al_{0.4}Ga_{0.6}N$ is the only material to have an activation efficiency above 85% for the samples implanted with a dose of $1x10^{14}$ cm^{-2} silicon ions.

The optimal annealing temperature based solely on the results of activation efficiency is found to be dose dependant in the $Al_{0.4}Ga_{0.6}N$, as it was for the $Al_xGa_{1-x}N$ with lower Al mole fractions. The lower the implanted silicon dose the higher the annealing temperature required to achieve high electrical activation. The samples implanted with the lower silicon doses of $1x10^{14}$ and $5x10^{14}$ cm^{-2} have an optimal anneal temperature of 1350, while the optimal anneal temperature for the samples implanted with $1x10^{15}$ cm^{-2} silicon ions is 1250 ºC.

The resistivities of the Si-implanted $Al_{0.4}Ga_{0.6}N$ implanted with each silicon dose and annealed for 20 minutes at various temperatures are shown in Figure 5.46. The samples implanted with $1x10^{14}$ cm^{-2} silicon ions exhibit the largest measured resistivity 181 kΩ/□, which is 118 and 487 times higher than the samples implanted with $5x10^{14}$ and $1x10^{15}$ cm^{-2} silicon ions when annealed at 1150 ºC for 20 minutes. The resistivity for these samples falls about 180 kΩ/□ as the anneal temperature is increased to 1350 ºC. As seen in the $Al_xGa_{1-x}N$ with lower Al mole fractions the resistivity of all the samples decreases as the anneal temperature is increased due to the increase in the carrier concentration and mobility as the temperature is increased. The $Al_{0.4}Ga_{0.6}N$ implanted with $5x10^{14}$ cm^{-2} silicon ions show a rapid decrease in resistivity as the anneal temperature is increased from 1150 to 1200 ºC and then decreases linearly as the anneal temperature is raised to 1350 ºC. The resistivity for the samples implanted with this dose drops from 1.5 kΩ/□ to 213 Ω/□ after being annealed at 1150 and 1350 ºC. The

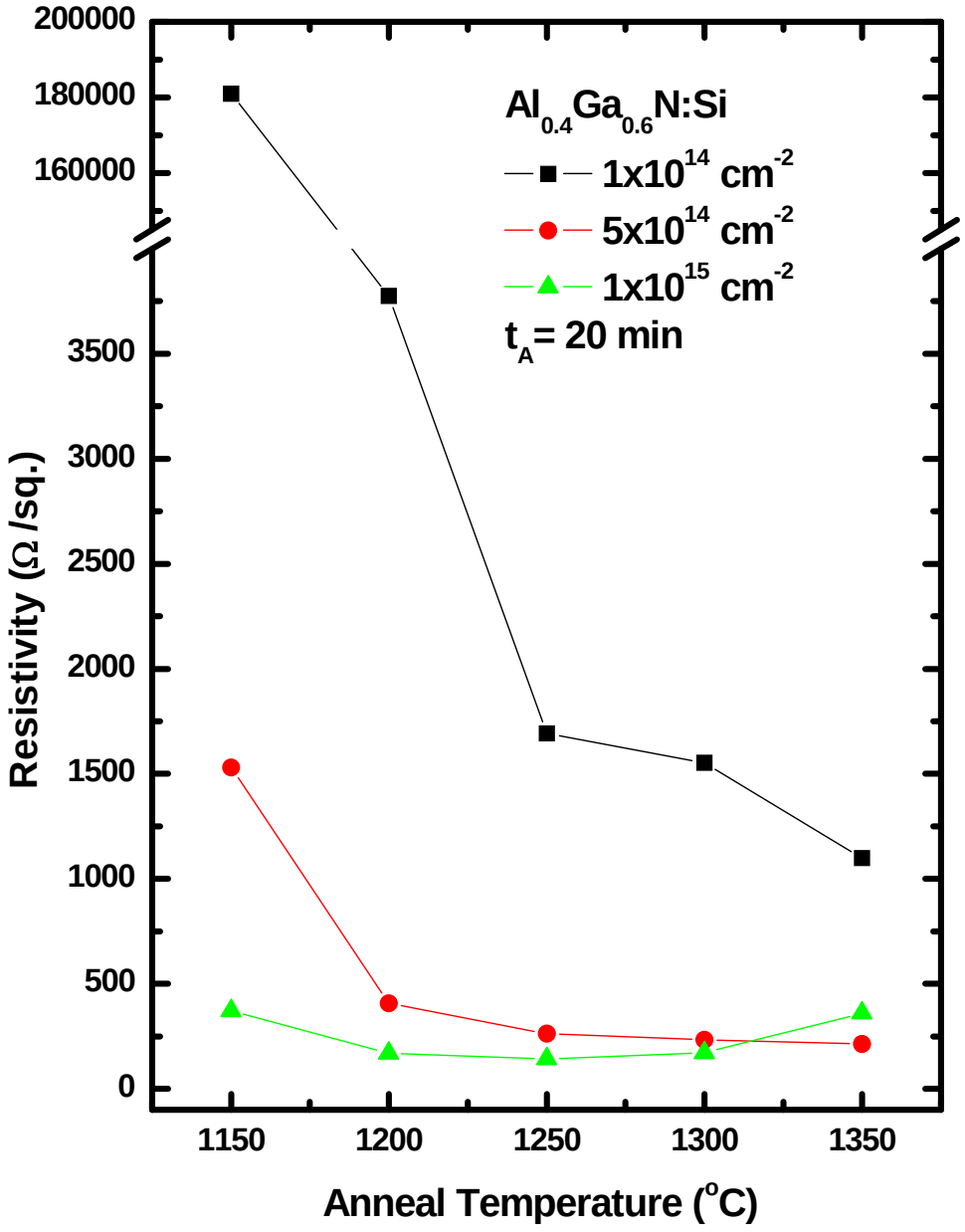

Figure 5.46. Room temperature resistivity measurements taken under zero magnetic field for $Al_{0.4}Ga_{0.6}N$ implanted at room temperature with silicon ions at 200 keV with doses of $1x10^{14}$, $5x10^{14}$, and $1x10^{15}$ cm^{-2} and annealed from 1150 ºC to 1350 ºC for 20 minutes in a nitrogen ambient.

$Al_{0.4}Ga_{0.6}N$ implanted with $1x10^{15}$ cm^{-2} silicon ions show a decrease in resistivity as the anneal temperature is increased from 1150 to 1250 ºC, dropping from 371 Ω/□ to 143 Ω/□, respectively. The resistivity of these samples increases slightly as the anneal temperature is increased above 1250 ºC due to the decrease in the carrier concentration of these samples at the higher temperature anneals. As expected, the samples experience their lowest resistivity at the same anneal temperature that produces a maximum in carrier concentration, and thus activation. The dependence of the resistivity on the anneal temperature is similar for all the $Al_xGa_{1-x}N$ investigated. The magnitudes of the resistivity slightly increase, for the samples implanted with each of the silicon doses, for each of the Al mole fractions of $Al_xGa_{1-x}N$ investigated.

Room temperature mobilities for the Si-implanted $Al_{0.4}Ga_{0.6}N$ are shown in Figure 5.47 as a function of anneal temperature. The mobility of the samples implanted with $1x10^{14}$ and $5x10^{14}$ cm^{-2} silicon ions increase with anneal temperature up to 1350 ºC, despite the increase in ionized impurity scattering. The samples implanted with $1x10^{14}$ cm^{-2} silicon ions do not exhibit the largest mobility as they have for the $Al_xGa_{1-x}N$ with lower Al concentrations. The $Al_{0.4}Ga_{0.6}N$ implanted with $5x10^{14}$ cm^{-2} silicon ions have a higher mobility for any given anneal temperature. The samples implanted with $1x10^{14}$ cm^{-2} silicon ions show a dramatic rise in mobility from 5 $cm^2/V{\cdot}s$ to 40 $cm^2/V{\cdot}s$ as the anneal temperature is increased from 1150 to 1200 ºC, and then increases steadily as the temperature is raised to 1350 ºC. After being annealed at 1350 ºC the mobility for the sample implanted with this dose peaks 58 $cm^2/V{\cdot}s$, which is lower than the peak mobility of the $Al_xGa_{1-x}N$ samples implanted with this same dose that had lower Al mole fractions. The mobility for the samples implanted with a dose of $5x10^{14}$ cm^{-2} silicon ions increase throughout the temperature span. The greatest increase in mobility for these samples

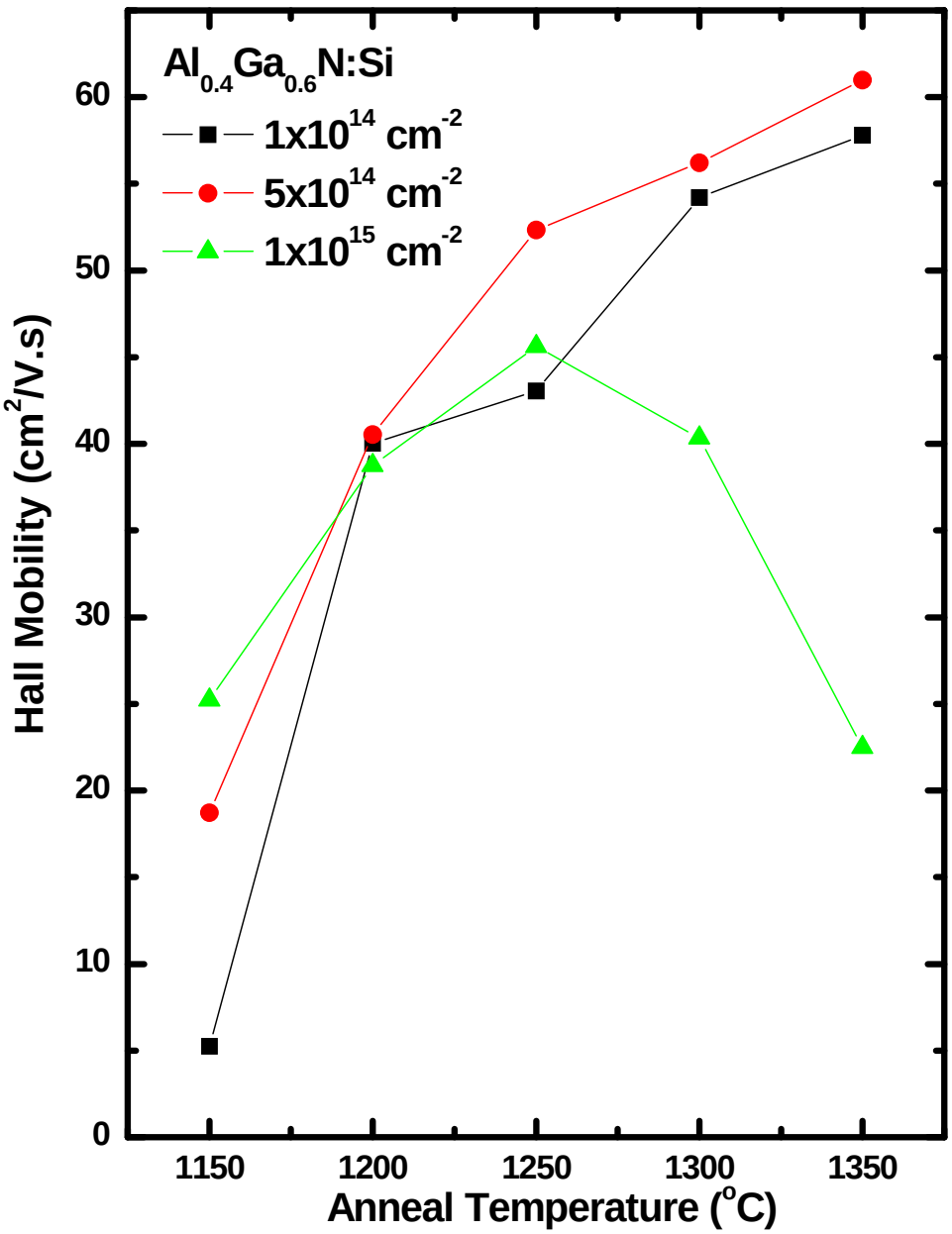

Figure 5.47. The room temperature mobilities calculated from Hall effect measurements on $Al_{0.4}Ga_{0.6}N$ implanted with at room temperature with silicon at 200 keV with doses of $1x10^{14}$, $5x10^{14}$, and $1x10^{15}$ cm^{-2} and annealed from 1150 ºC to 1350 ºC for 20 minutes in a nitrogen ambient.

occurs for the samples annealed from 1150 to 1250 ºC. The $Al_{0.4}Ga_{0.6}N$ implanted with this dose reaches a peak mobility of 61 $cm^2/V \cdot s$ after being annealed for 20 minutes at 1350 ºC, which is only slightly less than the $Al_{0.3}Ga_{0.7}N$ sample implanted with the same dose and annealed under the same conditions. The mobility of the samples implanted with $1x10^{15}$ cm^{-2} silicon ions increase linearly as the temperature is raised from 1150 to 1250 ºC reaching a peak mobility of 45 $cm^2/V \cdot s$. A further increase in the anneal temperature causes a decline in the mobility and activation for these samples, therfore the decrease in the mobility is not due to an increase in ionized impurity scattering. The decrease in the mobility can most likely be attributed to an increase in defect scattering due to damage caused from the high temperatures of the anneal. The mobilities for the $Al_{0.1}Ga_{0.9}N$, $Al_{0.2}Ga_{0.8}N$ and $Al_{0.3}Ga_{0.7}N$ samples implanted with the same dose are all higher at 90, 76 and 61 $cm^2/V \cdot s$, respectively. The magnitude of the mobility for the $Al_{0.4}Ga_{0.6}N$ is not as large as it was for the $Al_xGa_{1-x}N$ with lower Al mole fractions which could be due to an increase in the effective mass as the Al mole fraction is increased (33).

The mobility of the $Al_{0.4}Ga_{0.6}N$ implanted with the lower two silicon doses increases as the anneal temperature is increased despite the increased effects of ionized impurity scattering, indicating that lattice damage is still being repaired even at anneal temperatures up to 1350 ºC. The samples implanted with the highest silicon dose exhibit an increase in the mobility with activation for annealing temperatures up to 1250 ºC, however they both decline as the anneal temperature is increased, thus indicating that before the lattice damage could be repaired annealing damage became a dominating factor. This is the first time this behavior has been seen.

To improve the electrical activation efficiency of the implanted silicon in the $Al_{0.4}Ga_{0.6}N$ the anneal time was extended from 20 to 40 minutes for a set anneal temperature of 1200

ºC. A comparison of the results obtained for both the 20 and 40 minute anneals at 1200 ºC are listed in Table 5.3. Extending the anneal time had positive affects on all of the physical aspects determined from Hall effect measurements. The carrier concentrations and therefore activation energy of the all the implanted samples increased following the 40 minute anneal. The resistivity of all the implanted samples decreases as does the mobility, except for the $Al_{0.4}Ga_{0.6}N$ implanted with $5x10^{14}$ cm^{-2} silicon ions, which show a slight decease in mobility after being annealed for 40 minutes. The samples implanted with $1x10^{14}$ cm^{-2} silicon ions exhibit a significant 20% increase in the electrical activation efficiency going from 45 to 66% after the 20 and 40 minute anneals, respectively. The resistivity drops 40% to 2142 Ω/□ for the samples implanted with the lowest silicon dose after being annealed for 40 minutes at 1200 ºC. The mobility for these samples increases slightly from 40.0 $cm^2/V{\cdot}s$ to 44.5 $cm^2/V{\cdot}s$, despite an increase in ionized impurity scattering. The samples implanted with $5x10^{14}$ cm^{-2} silicon ions exhibit a 20% increase in the electrical activation bringing it up to 100% following the 40 minute anneal. The resistivity of these samples decreases 22% to 316 Ω/□. The $Al_{0.4}Ga_{0.6}N$ implanted with this dose were the only samples to show a decrease in mobility due to an increase in ionized impurity scattering when the anneal time was extended to 40 minutes. The mobility for the samples implanted with $5x10^{14}$ cm^{-2} silicon ions decreases only slightly from 40.5 to 37.9 $cm^2/V{\cdot}s$. The $Al_{0.4}Ga_{0.6}N$ implanted with a dose of $1x10^{15}$ cm^{-2} silicon ions have an activation of 96% following a 20 minute anneal at 1200 ºC, extending the anneal time to 40 minutes resulted in an insignificant increase in the activation of 0.4%. The resistivity for these samples decreases about 6 %, which is less than 10 Ω/□. The mobility for the samples implanted with the highest silicon dose had a negligible increase from 38.7 to 41.1 $cm^2/V{\cdot}s$ after extending the anneal time to 40 minutes.

Table 5.3. Room temperature Hall effect results for $Al_{0.4}Ga_{0.6}N$ implanted at room temperature with silicon ions at 200 keV in three doses and annealed at 1200 ºC for 20 or 40 minutes.

Dose (cm^{-2})	Time (min.)	Carrier Concentration (cm^{-2})	Activation (%)	Resistivity (Ω/□)	Mobility ($cm^2/V{\cdot}s$)
$1x10^{14}$	20	$4.49x10^{13}$	45.37	3775.4	40.03
$1x10^{14}$	40	$6.55x10^{13}$	65.96	2141.8	44.5
$5x10^{14}$	20	$3.78x10^{14}$	76.29	407.76	40.53
$5x10^{14}$	40	$5.02x10^{14}$	101.11	315.96	37.89
$1x10^{15}$	20	$9.49x10^{14}$	95.86	169.61	38.74
$1x10^{15}$	40	$9.56x10^{15}$	96.27	159.21	41.05

All the samples showed an increase in activation from extending the anneal time to 40 minutes; however the improvement was not always significant enough to achieve an activation better than that obtained at a higher anneal temperature. The $Al_{0.4}Ga_{0.6}N$ implanted with $1x10^{15}$ cm^{-2} silicon ions are the only samples not to show a higher activation after being annealed at 1200 ºC for forty minutes than being annealed at 1250 ºC for 20 minutes. However, the activation of these samples is roughly 96% after being annealed for 20 minutes at 1200 and 1250 ºC and also after the 1200 ºC anneal for 40 minutes. The activation of the $Al_{0.4}Ga_{0.6}N$ implanted with $1x10^{14}$ cm^{-2} silicon ions was 66% after being annealed at 1200 ºC for 40 minutes. This is higher than the 50% activation achieved after annealing at 1250 ºC for 20 minutes. However, it was not as high as the 87% activation of these samples after being annealed at 1300 ºC for 20 minutes. The $Al_{0.4}Ga_{0.6}N$ implanted with $5x10^{14}$ cm^{-2} silicon ions had an increased

activation of 100% after being anneal for 40 minutes at 1200 ºC, which is slightly higher than the 96% activation achieved for these samples after being annealed for 20 minutes at 1300 ºC. These results are similar to those of the $Al_{0.1}Ga_{0.9}N$ and $Al_{0.3}Ga_{0.7}N$, which all showed considerable improvement in electrical activation after the 1200 ºC anneal for 40 minutes.

The Si-implanted $Al_{0.4}Ga_{0.6}N$ samples all achieved a high electrical activation efficiency above 95%. Unlike the $Al_xGa_{1-x}N$ with lower Al concentrations, the samples implanted with the highest silicon dose had the lowest activation. The peak activation efficiency for the samples implanted with $1x10^{15}$ cm^{-2} silicon ions was 96% after being annealed for the 20 minutes at 1200 or 1300 ºC, and also after annealing for 40 minutes at 1200 ºC. The samples implanted with a dose of $5x10^{14}$ cm^{-2} silicon ions reached an activation of 100% after being annealed for 40 minutes at 1200 ºC, which was comparable to the 97% activation achieved after annealing at 1350 for 20 minutes. The samples implanted with the lowest silicon dose had an activation of 99% following the 1350 ºC anneal for 20 minutes. Lowering the anneal temperature and lengthening the anneal time benefited the electrical activation of all the samples however it did not always improve the activation as much as increasing the anneal temperature.

The silicon implanted $Al_{0.4}Ga_{0.6}N$ samples began to deviate in behavior from the lower Al mole fraction $Al_xGa_{1-x}N$. All the implanted silicon doses in the $Al_{0.4}Ga_{0.6}N$ were readily activated. The $Al_xGa_{1-x}N$ with Al mole fractions from 10 to 30% all achieved an activation below 85% for the samples implanted with $1x10^{14}$ cm^{-2} silicon ions. For the $Al_xGa_{1-x}N$ with lower Al concentrations, the peak activation efficiency increased slightly as the implanted silicon dose is increased. The $Al_{0.4}Ga_{0.6}N$, however, have a higher activation for the samples implanted with $1x10^{14}$ cm^{-2} silicon ions than it

does for the samples implanted with $5x10^{14}$ cm^{-2} silicon ions. Also, the mobility for the $Al_{0.4}Ga_{0.6}N$ is not as dependent on the implanted silicon dose as it was for the $Al_xGa_{1-x}N$ with Al mole fractions from 10 to 30%.

Temperature-Dependent Hall Effect Measurements

Temperature-dependent Hall Effect measurements were taken on the samples annealed at 1200 and 1300 ºC for twenty minutes in flowing nitrogen to determine the nature of the carriers as a function of temperature. The sheet carrier concentrations, as a function of the temperature from 10 to 700 K, for the samples implanted with each of the three silicon doses and annealed at 1200 and 1300 ºC for 20 minutes are shown in Figure 5.48. The carrier concentrations for all the Si-implanted samples remain relatively constant as the sample temperature is increased from 10 to 50 K. The samples implanted with a dose of $1x10^{15}$ cm^{-2} silicon ions are the most temperature independent, as has been the case for the $Al_xGa_{1-x}N$ with lower Al mole fractions. The carrier concentration of the samples implanted with the two lower doses of $1x10^{14}$ and $5x10^{14}$ cm^{-2} silicon ions decreases to a minimum around 110 K and then increases to a maximum at 700 K. The carrier concentration curve for the samples implanted with a dose of $1x10^{14}$ cm^{-2} silicon ions and annealed at 1200 ºC show a noticeable increase in carrier concentration from 30 to 80 K before declining to a minimum that has not been seen in the curves for any other sample. The reason for this behavior is not clear at present.

The samples implanted with the highest silicon dose have the most temperature-independent carrier concentration, as would be expected considering it is the most degenerate of all the samples. The temperature-independent nature of the carrier concentration is similar to that seen for the $Al_xGa_{1-x}N$ with Al concentrations from 10 to

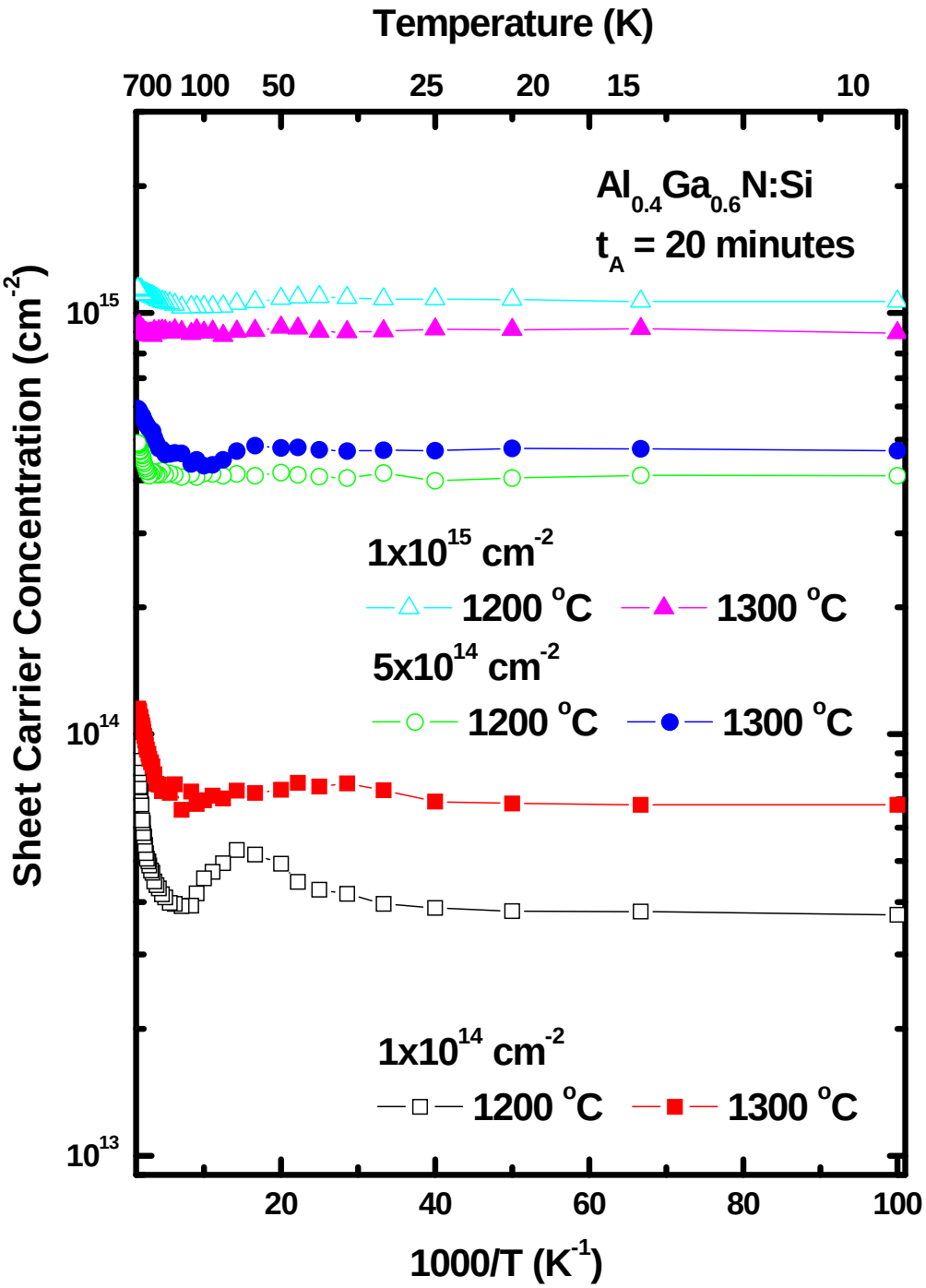

Figure 5.48. Temperature-dependent sheet carrier concentrations of $Al_{0.4}Ga_{0.6}N$ determined from Hall effect measurements taken from 10 to 700 K. The $Al_{0.4}Ga_{0.6}N$ was implanted with three different doses of Si ions at 200 keV and annealed at 1200 and 1300 °C for 20 minutes in a flowing nitrogen environment.

30%, and indicates that the implanted silicon ions have formed a degenerate impurity band in the band gap of the $Al_{0.4}Ga_{0.6}N$. All three of the implanted silicon doses correspond to volume carrier concentrations that exceed the Mott concentration of the material. The samples implanted with $1x10^{14}$ cm^{-2} silicon ions exhibit properties most like a non-degenerate semiconductor and therefore undergo a larger drop in carrier concentration than the samples implanted with the other doses. This dip in carrier concentration signifies the presence of a multi-channel conduction band, caused from the Gaussian profile of the implanted silicon ions (37,68). Impurity screening acts reduce the donor ionization energy and its effects are enhanced by an increase in the concentration of ionized donors, consequently degenerate samples yield ionization energies lower than the actual ionization energy. Therefore, the silicon ionization energy for $Al_{0.4}Ga_{0.6}N$ can not be accurately estimated from the samples in this study. However, Hwang *et al*. calculated from a simple hydrogen model that the ionization for $Al_{0.3}Ga_{0.7}N$ would be on the order of 56 meV (51).

The temperature-dependent Hall mobilities for these samples are shown in Figure 5.49. All of the mobility curves increases as the temperature is increased up to about 250-300 K, due to the decreased effects of phonon scattering. As the temperature is increased further the mobility begins to decline due to the increased effects of ionized impurity scattering. The samples implanted with each of the three silicon doses exhibit a peak in their mobility curve at or slightly below 300 K. The samples annealed at 1300 ºC have mobilities that are higher than the mobilities observed for the samples annealed at 1200 ºC for all the implanted silicon doses. The peak mobilities for the samples annealed

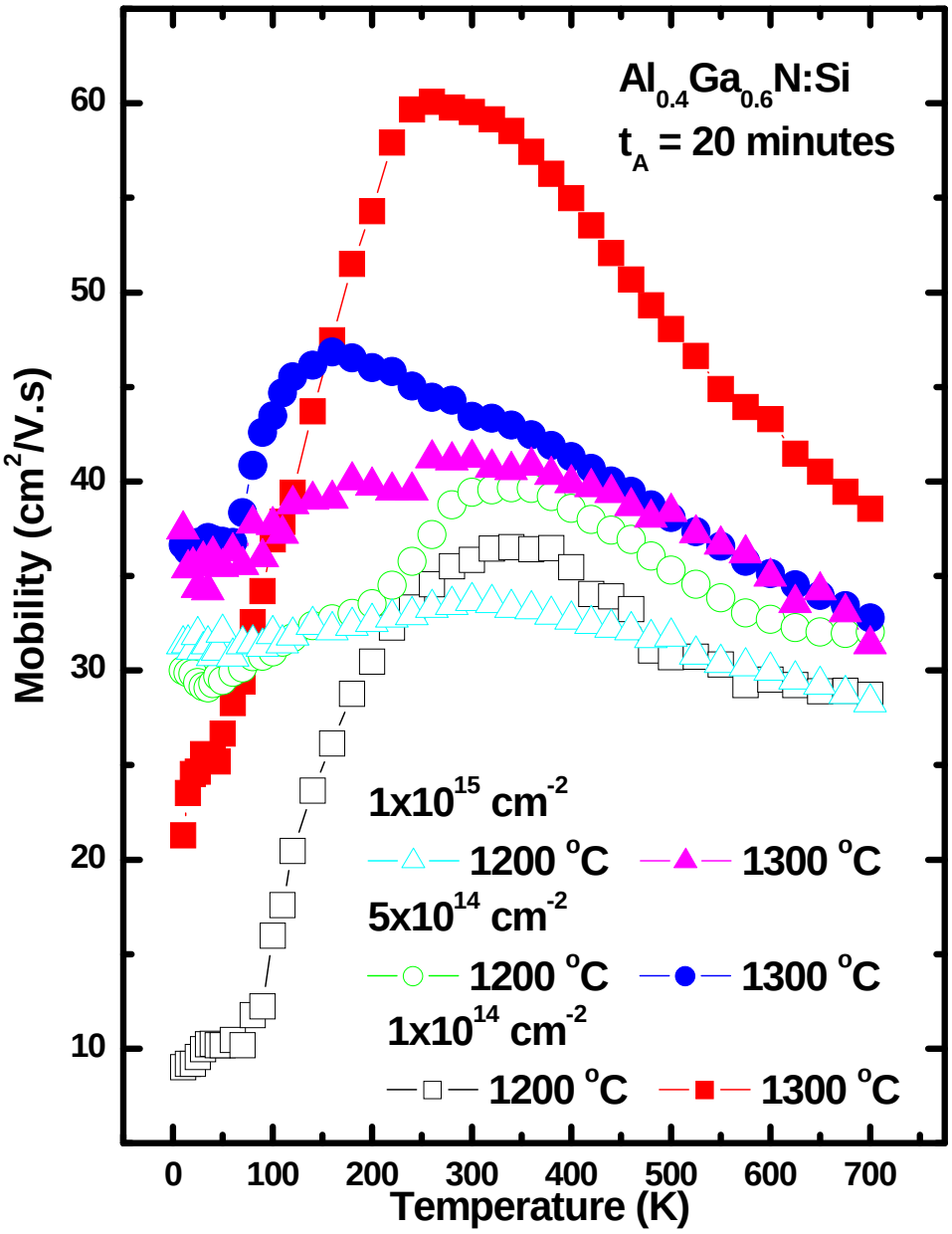

Figure 5.49. Temperature-dependent mobilities calculated from Hall effect measurements taken from 10 to 700 K for $Al_{0.4}Ga_{0.6}N$ implanted at room temperature with Si ions at 200 keV in three different doses and annealed at 1200 and 1300 ºC for 20 minutes.

at 1300 ºC occur at lower sample temperatures than the mobilities for the samples annealed at 1200 ºC. As the implanted silicon dose is increased, the mobility curves become more temperature-independent. The sample implanted with $1x10^{14}$ cm^{-2} silicon ions and annealed at 1300 ºC has the highest mobility of 60 $cm^2/V{\cdot}s$ at 260 K. The peak mobilities for the samples implanted with $5x10^{14}$ cm^{-2} are 40 and 57 $cm^2/V{\cdot}s$ which are slightly lower than those of the samples implanted with the highest dose, 42 and 34 $cm^2/V{\cdot}s$, for anneal temperatures or 1200 and 1300 ºC, respectively. The degeneracy of the Si-implanted $Al_{0.4}Ga_{0.6}N$ can be noticed by the relatively high mobilities at 10 K where the mobility of a non-degenerate sample would approach zero. The mobility at 10K for the samples implanted with silicon doses of $1x10^{14}$, $5x10^{14}$, and $1x10^{15}$ cm^{-2} and annealed at 1200 ºC are 9, 30, and 31 $cm^2/V{\cdot}s$. The mobilities for the samples annealed at 1300 ºC are all higher than those of the samples annealed at 1200 ºC. The mobilities for the samples annealed at 1300 ºC are 21, 37, and 37 $cm^2/V{\cdot}s$ for the three implanted silicon doses, respectively. The degenerate impurity band causes the low temperature mobility to be temperature-independent and is seen here to increase with doping level and also anneal temperature.

The temperature-dependent mobility curve for the samples implanted with $1x10^{14}$ cm^{-2} silicon ions most resembles that which is predicted for a non-degenerate sample, more so for the $Al_{0.4}Ga_{0.6}N$ than for the $Al_xGa_{1-x}N$ with Al mole fractions of 10 to 30%. The $Al_{0.1}Ga_{0.9}N$ and $Al_{0.2}Ga_{0.8}N$ had mobility curves that were more flat and temperature-independent for the samples implanted with $5x10^{14}$ and $1x10^{15}$ cm^{-2} silicon ions than they are for the $Al_{0.4}Ga_{0.6}N$. Also, the lower Al mole fraction material had mobilities that clearly increased with decreasing implanted silicon dose, which is not the case here. The

samples implanted with $5x10^{14}$ and $1x10^{15}$ cm^{-2} silicon ions and annealed at 1200 and 1300 ºC have higher mobilities than the samples implanted with $1x10^{14}$ cm^{-2} silicon ions and annealed at 1200 ºC.

Figure 5.50 shows the temperature-dependent resistivities of the Si-implanted $Al_{0.4}Ga_{0.6}N$ samples that were annealed at 1200 and 1300 ºC. The higher anneal temperature of 1300 ºC produced considerably lower resistivities, except for the samples implanted with $1x10^{15}$ cm^{-2} silicon ions which has the same resistivity for both anneal temperatures. The resistivity decreases significantly and becomes more temperature-independent as the implanted silicon dose is increased, which is consistent with the carrier concentration. All of the Si-implanted $Al_xGa_{1-x}N$ shows a relatively temperature-independent resistivity from 10 to 50 K before slowly declining to a minimum around 240-380 K and then increases up through 700 K. The drop in the resistivity for the samples implanted with $1x10^{14}$ cm^{-2} silicon ions is the most pronounced, while the dip in resistivity for the samples implanted with $1x10^{15}$ cm^{-2} silicon ions is almost unnoticeable. The decrease in the resistivity curves is a manifestation of the rapid increase in the mobility as the temperature is increased. This is overtaken by the large increase in the carrier concentration at higher temperatures that causes an increase in phonon scattering that causes the mobility to decrease.

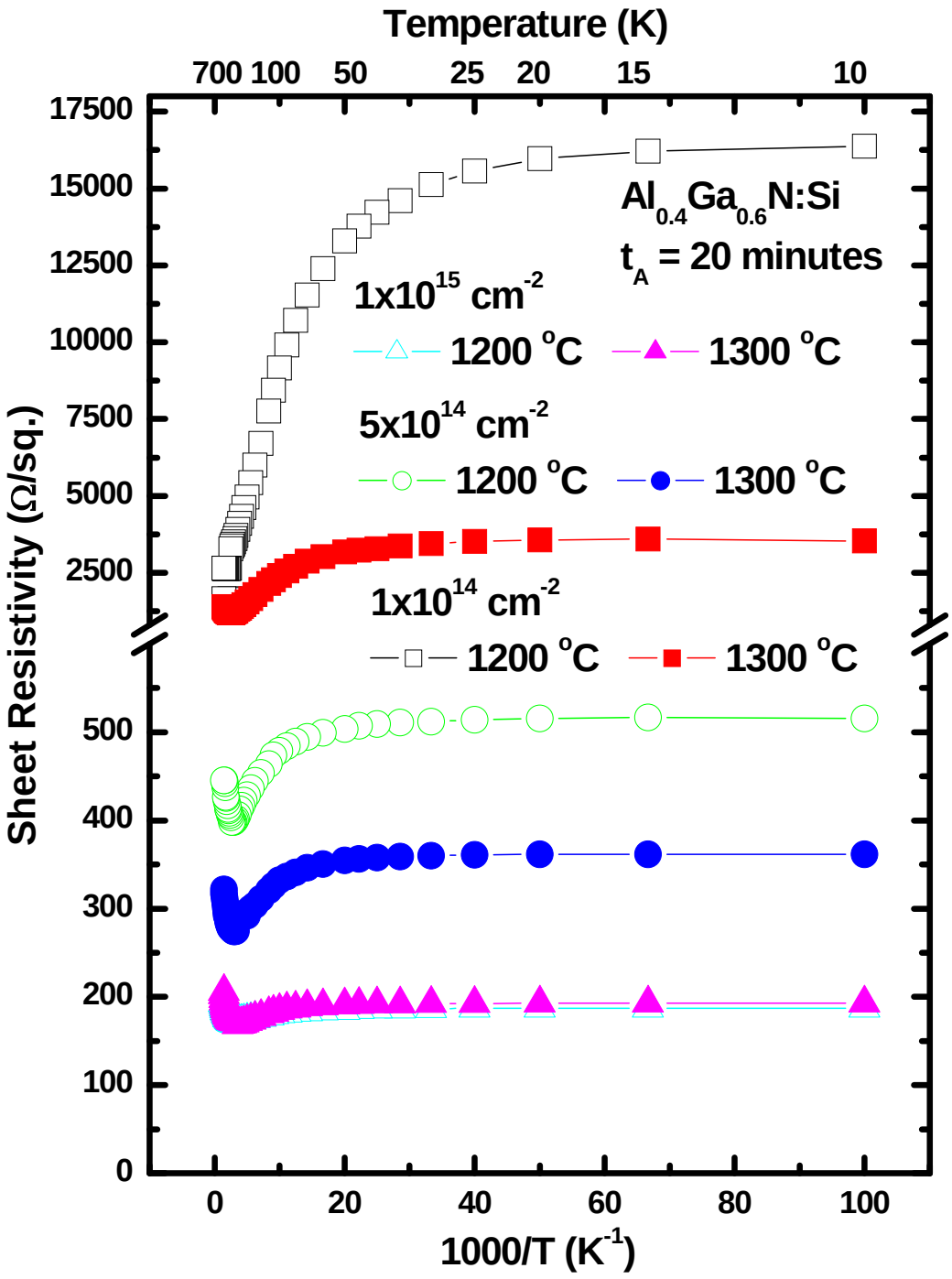

Figure 5.50. Temperature-dependent resistivity calculated from Hall effect measurements taken from 10 to 700 K for $Al_{0.4}Ga_{0.6}N$ that had been implanted at room temperature with silicon ions at 200 keV with doses of $1x10^{14}$, $5x10^{14}$, and $1x10^{15}$ cm^{-2} and annealed at 1200 and 1300°C for 20 minutes in flowing nitrogen.

Low Temperature Cathodoluminescence Measurements

Cathodoluminescence measurements were taken at an electron energy of 10 keV with 50 μA of source current, the temperature in the chamber was 7.4 K, and the slits on the spectrometer were 400 μm both at the entrance and the exit. The range scanned was 1800 to 7000 Å at a step size of 2 Å with an integration time of 0.1 second.

The spectrum of the unimplanted samples shown as a function of anneal temperature are shown in Figure 5.51. To gauge the effects of annealing on the implanted samples the behavior of the unimplanted samples must first be observed. The CL spectrum for the as-grown sample has a strong neutral donor bound exciton peak at 4.41 eV. The spectra of the as-grown sample exhibits two phonon coupled replicas separated by 80 meV on the low energy side of the (D^o,X) peak at 4.33 and 4.25 eV (49). Annealing the as-grown material changes the luminescence properties immensely. The spectrum of the sample annealed at 1200 ºC has been reduced by a factor of 3. This spectrum has a very intense broad peak centered at 3.78 eV and also shows the development of some peaks on the low energy side of the peak at 3.78 eV. Increasing the temperature to 1250 ºC causes the 3.78 eV peak to decrease in intensity and the lower energy peaks that began to emerge in the spectra for the sample annealed at 1200 ºC are considerably enhanced. The energies of these peaks are 3.75, 3.64, 3.53, 3.41, 3.29, 3.17, 3.05, 2.92, 2.78, and 2.64 eV. The spacing in between the peaks increases slightly from 110 to 140 meV as the energy of the peaks decreases. The CL spectra for the samples annealed at 1300 ºC show no evidence of this broad luminescence instead it had an excellent (D^o,X) peak centered at 4.41 eV with two phonon replicas at 4.33 and 4.25 eV, as seen in the spectrum of the as-grown sample. The spectrum for the sample annealed at 1300 ºC was more intense than the as-grown sample and the spectrum had to be reduced

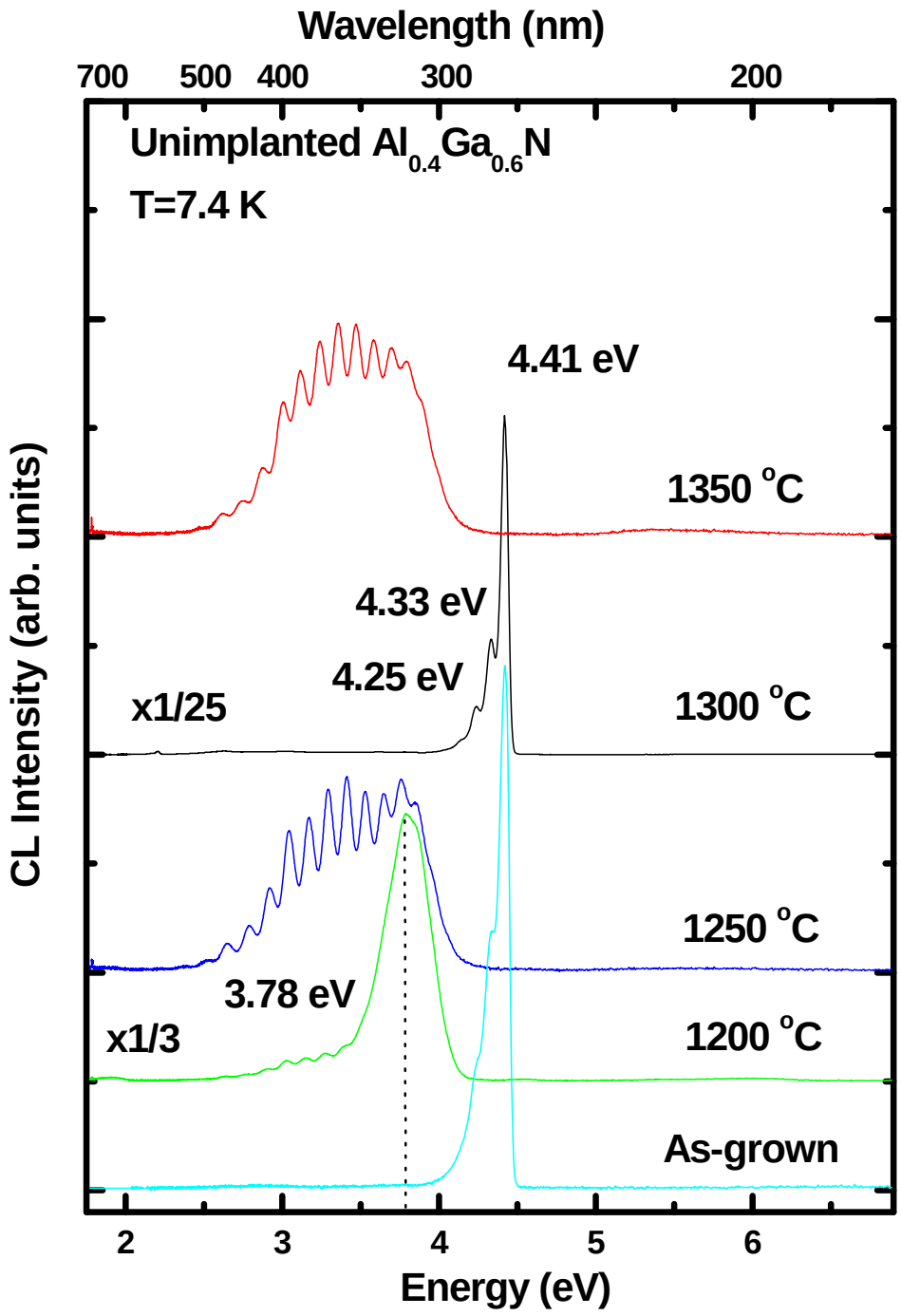

Figure 5.51. CL spectra taken at 7.4 K for unimplanted $Al_{0.4}Ga_{0.6}N$ that have been anneal at 1200, 1250, 1300, and 1350 °C for 20 minutes in flowing nitrogen.

by a factor 25. Further increasing the anneal temperature to 1350 ºC produces a CL spectrum that resembles that of the samples annealed at 1250 ºC in that there was no evidence of the (D^o,X) peak only a broad luminescence that consisted of 10 individual peaks. Similar oscillations were seen by Lee *et al*. for Mg-doped $Al_xGa_{1-x}N$ with Al mole fractions from less than 0.1. They observed the same oscillations and attributed the peak at 3.3 eV to be a free electron transitioning to a Mg acceptor and the other peaks to be interference patterns (76). They also observed that the peak position of the free electron to Mg acceptor transition blueshifts from 3.30 to 3.35 as the Al mole fraction of the material was increased from 0.05 to 0.09. This luminescence is obviously not due to Mg acceptors, but it could be related to reduction of the crystalline quality with increasing Al content which can increase the number of Al vacancies that act as deep acceptors in $Al_xGa_{1-x}N$ (44). The spectra for the samples annealed at all of the temperatures except 1300 ºC exhibit this lower energy luminescence.

The low temperature CL spectra for the Si-implanted $Al_{0.4}Ga_{0.6}N$ annealed for 20 minutes at 1300 ºC are shown in Figure 5.52. All of the spectra show a (D^o,X) peak at 4.41 eV and two phonon coupled replicas separated by 80 meV on the low energy side of the (D^o,X) peak at 4.33 and 4.25 eV (49). The intensities of the (D^o,X) peak for the unimplanted sample and the sample implanted with $1x10^{14}$ cm^{-2} silicon ions are much stronger than those of the other implanted samples and their spectrums have been decreased by a factor of 5. The sample implanted with a dose of $1x10^{14}$ cm^{-2} silicon ions has a (D^o,X) peak with higher intensity than the unimplanted sample, indicating excellent recovery of the lattice damage and incorporation of the implanted silicon ions. The samples implanted with a dose of $5x10^{14}$ cm^{-2} silicon ions have a CL spectrum that has broadened due to band tailing effects from the increased carrier concentration. The

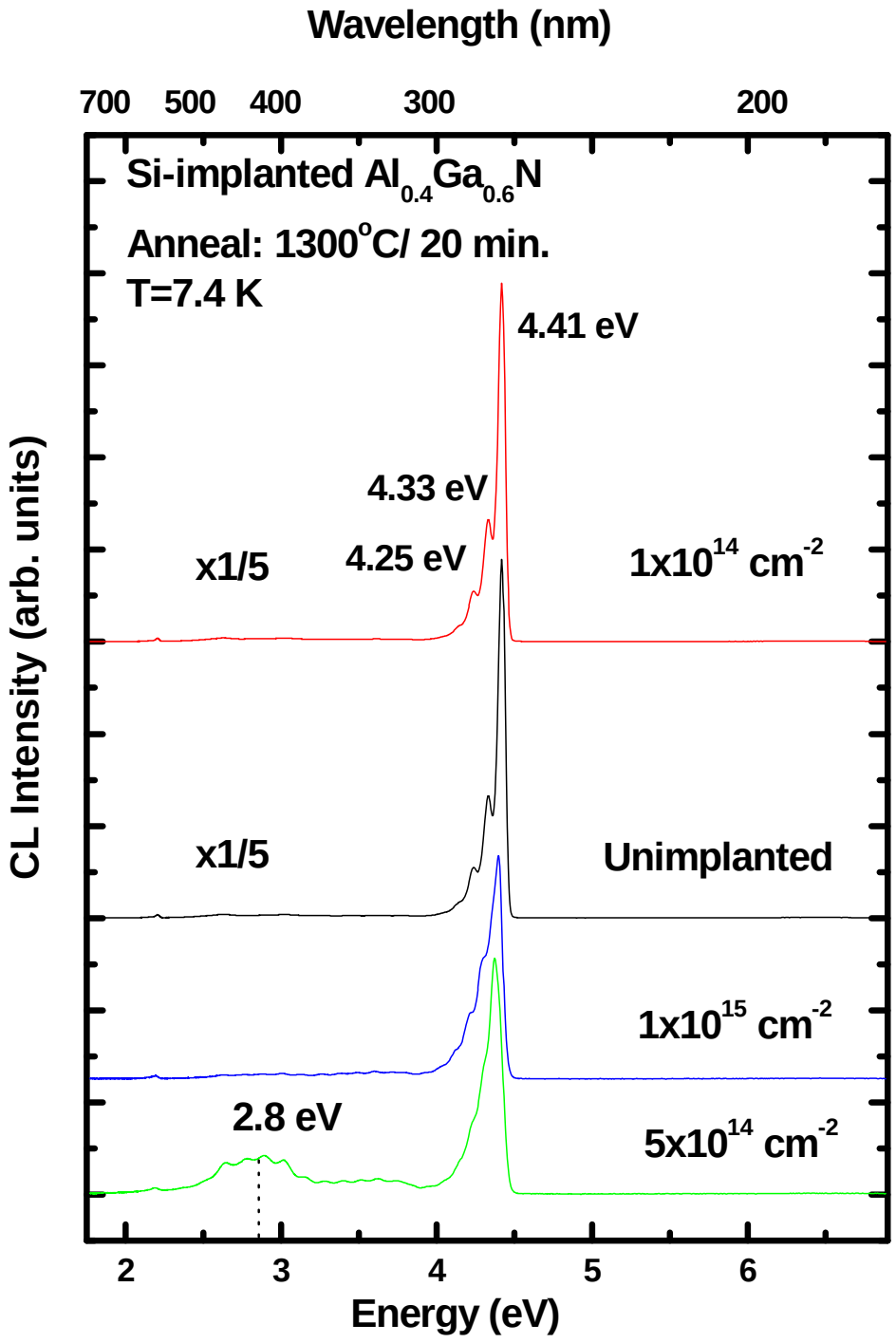

Figure 5.52. CL spectra taken at 7.4 K for $Al_{0.4}Ga_{0.6}N$ that have been anneal at 1300 ºC for 20 minutes in flowing nitrogen.

spectrum for this sample also shows a broad band of luminescence centered around 2.8 eV that could be similar to the luminescence observed for the unimplanted samples. The sample implanted with $1x10^{15}$ cm^{-2} silicon ions has a also has a broadened (D^o,X) peak with evidence of the two phonon replicas, but does not exhibit the broad band luminescence centered around 2.8 eV. Like the $Al_xGa_{1-x}N$ with lower Al mole fractions the intensity of the (D^o,X) peak decreased as the implanted dose was increased. However, the sample implanted with $5x10^{14}$ cm^{-2} silicon ions have the most degraded optical properties.

The low temperature CL spectra for the $Al_{0.4}Ga_{0.6}N$ implanted with $1x10^{14}$ cm^{-2} silicon ions and annealed for 20 minutes at various temperatures are shown in Figure 5.53. All of the anneal temperatures produced a good (D^o,X) peak centered at 4.41 eV and evidence of two phonon coupled replicas separated by 80 meV on the low energy side of the (D^o,X) peak at 4.33 and 4.25 eV (49) in their CL spectra.

The spectra for the samples annealed at 1200 and 1250 ºC are very similar, only the sample annealed at 1250 ºC has a more intense (D^o,X) peak. The phonon peaks for the samples implanted with this dose and annealed at 1200 and 1250 ºC are clearly identifiable. However, as the anneal temperature is increased the carrier concentration increases, thus increasing the effects of band tailing causing the peaks to broaden and merge together, as seen in the spectra for the samples annealed at higher temperatures. The intensity of the (D^o,X) peak increases as the anneal temperature is increased, except for the sample annealed at 1300 ºC which shows diminished intensity for unknown reasons. However, as seen in the previous figure, the spectra for the samples annealed at 1300 ºC shows a sharp (D^o,X) peak that has similar intensity as the as-grown sample. None of the samples implanted with $1x10^{14}$ cm^{-2} silicon ions exhibit any broad

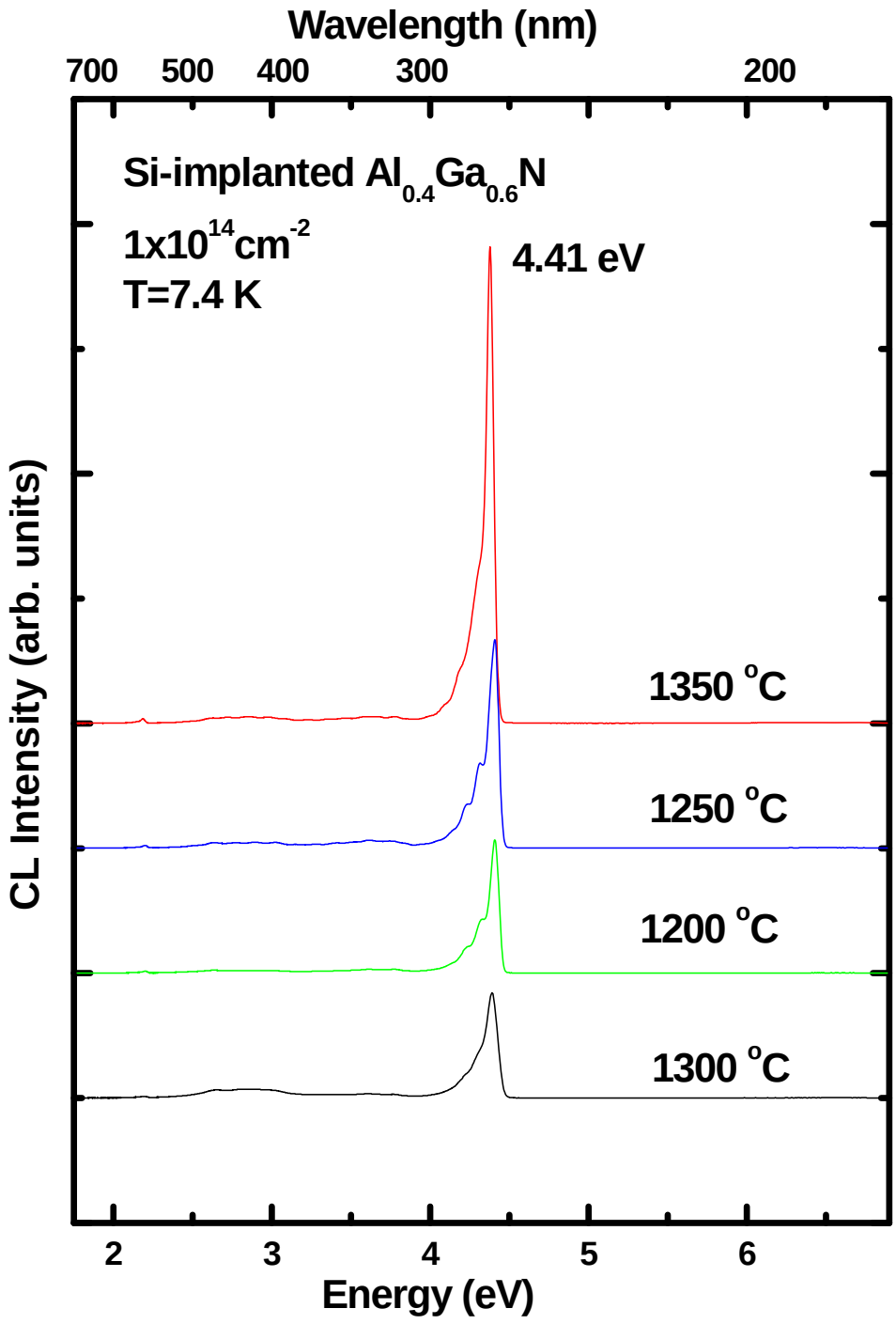

Figure 5.53. CL spectra taken at 7.4 K for $Al_{0.4}Ga_{06}N$ that has been implanted with $1x10^{14}$ cm^{-2} silicon ions and annealed for 20 minutes at various temperatures in flowing nitrogen.

luminescence at lower energies, as was seen for the $Al_{0.1}Ga_{0.9}N$. The intensity of the (D^o,X) peak increases as the anneal temperature is increased from 1200 to 1350 ºC, signifying successive improvement in the crystal lattice with each increase in the anneal temperature. The increase in intensity of the (D^o,X) peaks observed for the samples annealed at temperatures of 1200, 1250, and 1350 ºC indicate that more of the implanted silicon ions have become electrically active as the anneal temperature was increased.

These CL spectra agree very well with the electrical activation results obtained from Hall effect measurements for the samples implanted with this silicon dose. The strong intensity of the (D^o,X) peak and the band tailing effects seen in the spectra of the sample annealed at 1350 ºC anneal correlate well with the high activation obtained for this sample. The (D^o,X) peak and the high mobilities observed on the samples implanted with the lowest silicon dose indicate excellent recovery of the radiation damage caused during the ion implantation after annealing at 1350 ºC for 20 minutes in flowing nitrogen.

The CL spectra of the samples implanted with a silicon dose of $5x10^{14}$ cm^{-2} and annealed for 20 minutes at various temperatures are shown in Figure 5.54. Not all of the spectrum have the (D^o,X) peak at 4.41 eV and the phonon related peaks. The sample annealed at 1200 ºC exhibit a strong (D^o,X) peak along with some weak luminescence centered around 2.8 eV that could be similar to the broad emission in the spectra for the unimplanted samples. Increasing the anneal temperature to 1250 ºC causes the peak position to shift to 4.37 eV however there is still evidence of the phonon replicas. This spectrum has an increased broad luminescence centered at 2.8 eV. Nam *et al*. attribute the origin of this luminescence to the be the same as that of the yellow luminescence found in GaN at 2.15 eV, which is still under debate, however it is generally accepted to

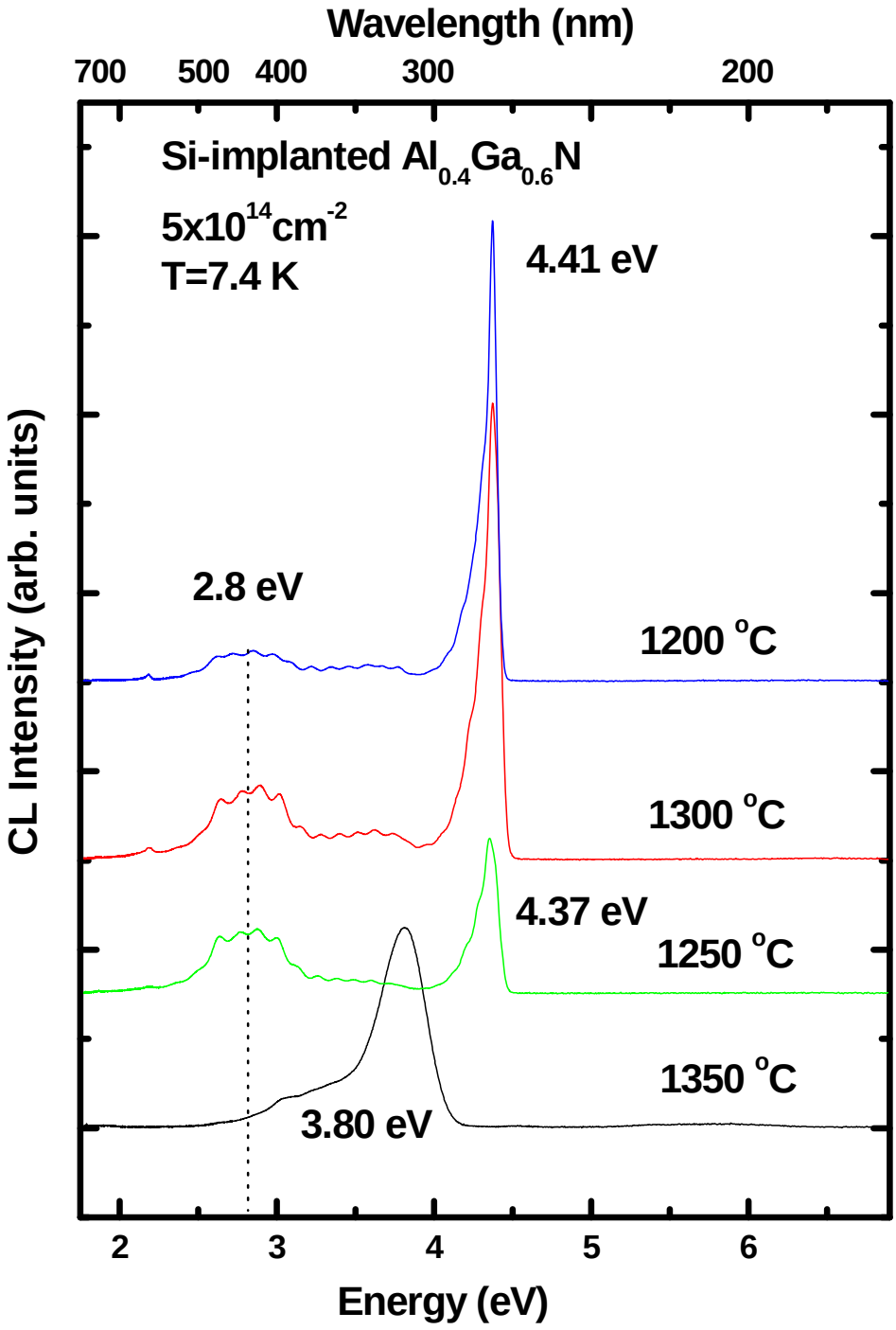

Figure 5.54. CL spectra taken at 7.4 K for $Al_{0.4}Ga_{0.6}N$ that was implanted with $5x10^{14}$ cm^{-2} silicon ions and annealed at various temperatures for 20 minutes in flowing nitrogen.

be related to a donor acceptor pair transition with a shallow donor and deep acceptor that could be an aluminum vacancy or vacancy complex (44). The (D^o,X) peak in the spectra for the samples annealed at 1300 ºC is similar in intensity and shape to the sample annealed at 1200 ºC. However, the intensity of the broad luminescence centered at 2.8 eV is more enhanced for the sample annealed at 1300 ºC. The sample annealed at 1350 ºC has a unique spectrum with a broad peak centered at 3.8 eV that has a shoulder that extends out to 3.3 eV. This is similar to a peak reported by McFall *et al*, who observed a donor bound acceptor pair (DAP) peak at 3.82 eV in Si-doped $Al_{0.5}Ga_{0.5}N$ and a phonon replica at 3.72 eV (49).

The CL spectra indicate that for the samples implanted with this silicon dose were generally recovered from the ion implantation induced damage. The silicon electrical activation for these samples gradually increased as the anneal temperature was increased to 1350 ºC. However, there is only a 1% difference in the activation between the samples annealed at 1300 and 1350 ºC. Electrical efficiencies for the samples implanted with $5x10^{14}$ cm^{-2} silicon ions increases dramatically as the anneal temperature is raised from 1200 to 1300 ºC.

The CL spectra of the samples implanted with the a silicon dose of $1x10^{15}$ cm^{-2} and annealed for 20 minutes at various temperatures are shown in Figure 5.55. The samples annealed from 1200 to 1300 ºC all have a (D^o,X) peak centered at 4.41 eV, whose intensity increases as the anneal temperature is increased. The spectrum for the sample annealed at 1350 ºC does not have any features in common with the spectra of the other samples. The samples annealed at 1200 ºC show a weak peak that has red shifted to 4.33 eV and the broad luminescence at 2.8 eV, which is similar to the spectrum of the $Al_{0.4}Ga_{0.6}N$ sample implanted with $5x10^{14}$ cm^{-2} silicon ions and annealed at 1250 ºC. The

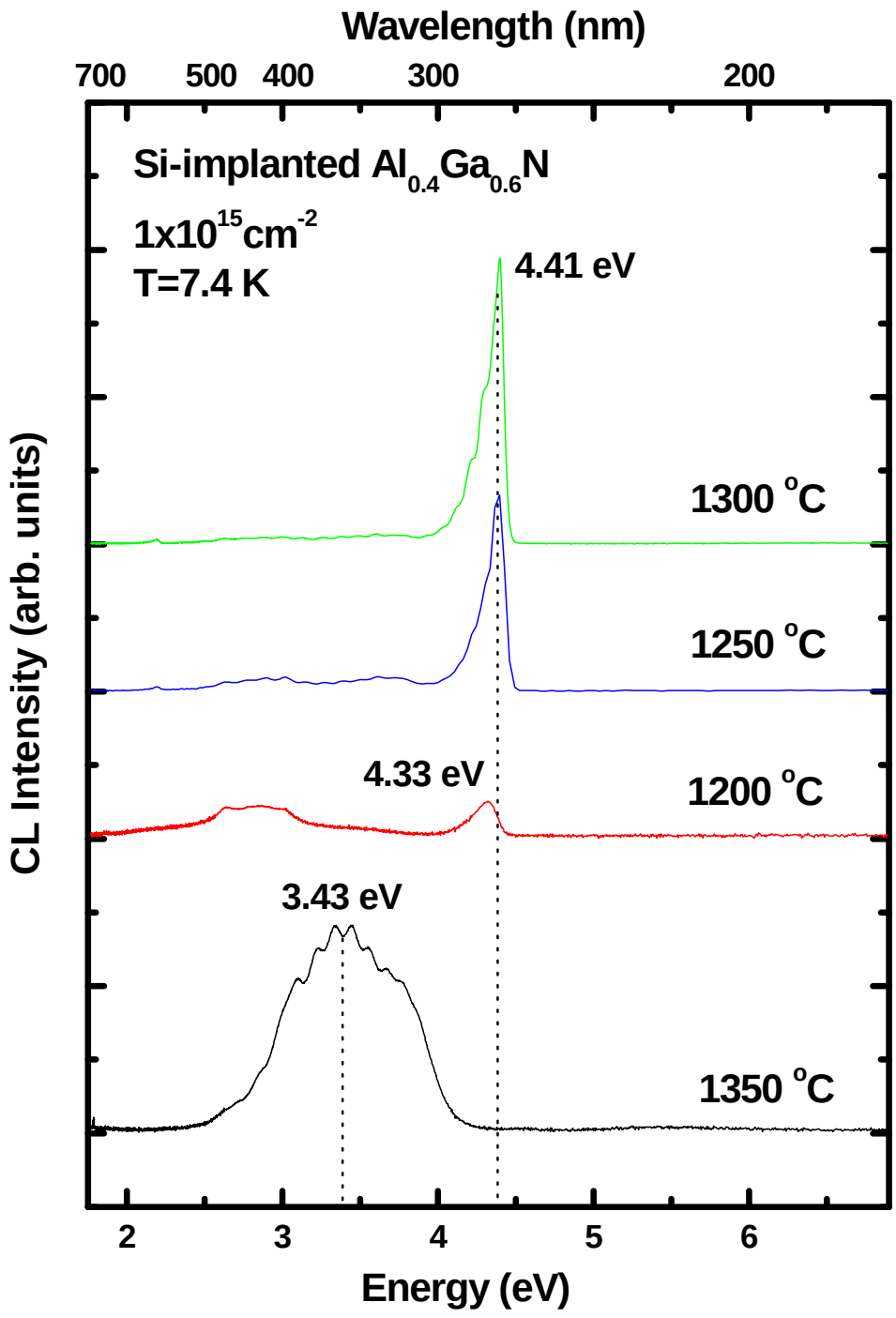

Figure 5.55. CL spectra taken at 7.4 K for $Al_{0.4}Ga_{0.6}N$ that was implanted with $1x10^{15}$ cm^{-2} silicon ions and annealed at various temperatures for 20 minutes in flowing nitrogen.

sample annealed at 1250 ºC shows recovery of the (D^o,X) peak at 4.41 eV and the has a broad shoulder for the lower energy phonon replicas. The peak has broadened considerably towards the lower energy due to band tailing effects, and the two low energy peaks are seen as shoulder peaks. The spectra for the sample annealed at 1300 ºC has the strongest (D^o,X) peak with the two low energy peaks seen as shoulders. The spectra for the sample annealed at 1350 ºC shows a broad band luminescence that is centered at 3.43 eV. This sample has a spectrum similar to that of the $Al_{0.4}Ga_{0.6}N$ sample implanted with $5x10^{14}$ cm^{-2} silicon ions and annealed at 1350 ºC, only what was seen as a broad, wide shoulder has now developed into an etalon effect of the donor acceptor pair peak identified by Mcfall *et al*. at 3.82 eV (49). This type of luminescence was also seen in the spectra for the unimplanted samples that were annealed at this temperature suggesting that is could be caused from anneal related damage.

Silicon Implanted $Al_{0.5}Ga_{0.5}N$

In the last few years the emerging importance of high mole fraction $Al_xGa_{1-x}N$ for device applications has become prevalent sparking an increase in research regarding silicon doping of $Al_xGa_{1-x}N$ with Al concentrations 50% or above. Yoshitaka *et al*. investigated the effects of Si-doping on $Al_xGa_{1-x}N$ and AlN alloys. $Al_xGa_{1-x}N$ with Al concentrations above 50% were found to exhibit a sharp decrease in the electron concentration and a spike in resistivity by 5 orders of magnitude (53). Silicon was found to act as a donor over the entire range of Al content however; there is an upper Si-doping limit at which n-type conduction is obtained that decreases with increasing Al content. Additional silicon ions form an acceptor state that compensates the silicon donors producing a highly resistive material (53). They reported that the ionization energy of

$Al_xGa1_{-x}N$ with Al concentration less than 0.49 slowly increases from 8.1 to 12 meV as the Al concentration was increased. When the Al content is greater than 0.49, the ionization energy increases at a greater rate going from 12 meV for $Al_{0.49}Ga_{0.51}N$ to 86 meV for AlN.

There are no reported ionization energies for Si-implanted $Al_{0.5}Ga_{0.5}N$. The ionization energy can be extracted from Hwang *et al*. who determined that the donor ionization energy of $Al_xGa_{1-x}N$ increases with increasing Al mole fraction from 34 meV for GaN to 90 meV for AlN, by using hydrogen atom model (51). Assuming the ionization energy increases linearly the ionization energy for Si in $Al_{0.5}Ga_{0.5}N$ would then be on the order of 61 meV for a non-degenerate sample. The implanted silicon doses of $1x10^{14}$, $5x10^{14}$, and $1x10^{15}$ cm^{-2} correspond to peak volume carrier concentrations of $5.78x10^{18}$, $2.89x10^{19}$ and $5.78x10^{19}$ cm^{-3}, which all exceed the Mott concentration of $4.16x10^{18}$ cm^{-3} for $Al_{0.5}Ga_{0.5}N$. The Si-implanted $Al_{0.5}Ga_{0.5}N$ samples will be degenerate and therefore will underestimate the actual ionization energies.

Room Temperature Hall Effect Measurements

The MEMOCVD grown $Al_{0.5}Ga_{0.5}N$ was capped with 500Å of AlN and implanted at room temperature with silicon ions at 200 keV in three different doses. The silicon doses were $1x10^{14}$, $5x10^{14}$, and $1x10^{15}$ cm^{-2} and the effective doses are $9.93x10^{13}$, $4.96x10^{14}$, and $9.93x10^{14}$ cm^{-2}, respectively after taking into account the 500Å AlN cap. The samples were annealed from 1200 to 1350 ºC for 20 minutes in a nitrogen environment. All the samples had excellent surface morphology following the anneal at 1350 ºC. Room temperature Hall effect measurements were conducted to determine sheet carrier concentrations for the samples and are shown in Figure 5.56. The

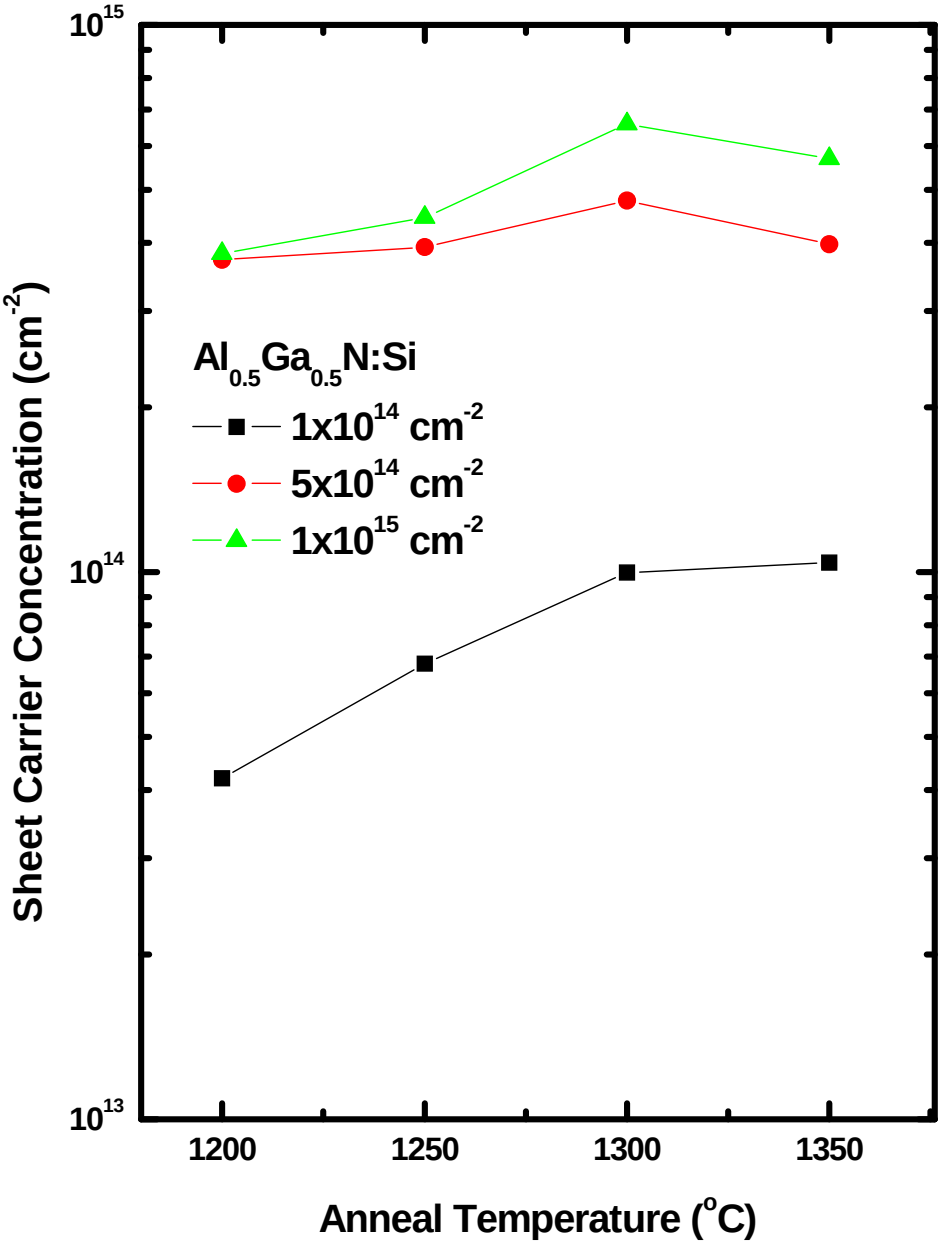

Figure 5.56. Room temperature sheet carrier concentrations for $Al_{0.5}Ga_{0.5}N$ implanted at room temperature with silicon ions at 200 keV with doses of $1x10^{14}$, $5x10^{14}$, and $1x10^{15}$ cm^{-2} and annealed from 1200 to 1350 ºC for 20 minutes in flowing nitrogen.

unimplanted samples, both as-grown and annealed, were highly resistive making it impossible to collect any meaningful data. Thus, the silicon electrical activation was calculated using the measured room temperature carrier concentration with no correction for the background carriers.

The room temperature sheet carrier concentrations for the samples implanted with $1x10^{14}$ cm^{-2} silicon ions behave differently from the samples implanted with the other silicon doses. The carrier concentration for the $Al_{0.5}Ga_{0.5}N$ implanted with a dose of $1x10^{14}$ cm^{-2} silicon ions increases linearly as the anneal temperature is raised from 1200 to 1300 ºC. The carrier concentration begins to saturate for the samples annealed at 1350 ºC. Like the $Al_xGa_{1-x}N$ with the lower Al mole fractions, these samples also show the most dramatic change in carrier concentration as the anneal temperature is increased. The carrier concentrations for the $Al_{0.5}Ga_{0.5}N$ implanted with $1x10^{14}$ cm^{-2} silicon ions increases from $4.2x10^{13}$ to $1.04x10^{14}$ cm^{-2} as the anneal temperature is raised from 1200 to 1350 ºC, respectively. The carrier concentrations for the $Al_{0.5}Ga_{0.5}N$ implanted with $5x10^{14}$ and $1x10^{15}$ cm^{-2} silicon ions have a similar dependence on the anneal temperature. The carrier concentration for these samples increases slightly as the anneal temperature is raised from 1200 to 1250 ºC. The increase in carrier concentration is more significant when the anneal temperature is raised to 1300 ºC for these samples. The samples implanted with both silicon doses exhibit their peak carrier concentrations after being annealed at 1300 ºC for 20 minutes in a nitrogen environment. The carrier concentration decreases for the samples implanted with $5x10^{14}$ and $1x10^{15}$ cm^{-2} silicon ions after being annealed at 1350 ºC. The carrier concentration for the $Al_{0.5}Ga_{0.5}N$ implanted with a dose of $5x10^{14}$ cm^{-2} silicon ions reaches a maximum carrier concentration of $4.8x10^{14}$ cm^{-2} while the sample implanted with $1x10^{15}$ cm^{-2} reaches a maximum carrier concentration of

$6.6x10^{14}$ cm^{-2}. The carrier concentrations for the $Al_{0.5}Ga_{0.5}N$ implanted with a dose $1x10^{15}$ cm^{-2} silicon ions are considerably lower than those of achieved for the $Al_xGa_{1-x}N$ with the lower Al mole fractions. However, the carrier concentrations for the $Al_{0.1}Ga_{0.9}N$ and $Al_{0.4}Ga_{0.6}N$ samples implanted with this silicon dose also declined as the anneal temperatures reached their upper range.

The silicon electrical activation is closely related to the carrier concentration and has the same trends with the anneal temperature as mentioned above. The electrical activations for the $Al_{0.5}Ga_{0.5}N$ were calculated using the effective doses and room temperature sheet carrier concentrations and the results are shown in Figure 5.57. Unlike the $Al_xGa_{1-x}N$ with lower Al mole fractions, the $Al_{0.5}Ga_{0.5}N$ exhibit excellent activation for the samples implanted with $1x10^{14}$ cm^{-2} silicon ions. The samples implanted with this dose experience higher silicon activation as the anneal temperatures are increased from 1200 to 1350 ºC. The samples implanted with $1x10^{14}$ cm^{-2} silicon ions reach 100% activation after being annealed for 20 minutes at 1300 ºC and 104% following the 1350 ºC anneal. Activation efficiency greater than 100% is unrealistic and could be due to an underestimate of the effective dose. This is the best activation for samples implanted with this dose for all the Al concentrations of $Al_xGa_{1-x}N$ investigated. The activation efficiency for the samples implanted with $5x10^{14}$ and $1x10^{15}$ cm^{-2} silicon ions peak after being annealed at 1300 ºC. The activation efficiency for these samples declines as the anneal temperature is raised to 1350 ºC. The samples implanted with $5x10^{14}$ cm^{-2} silicon ions experience a peak activation of 96% following the anneal at 1300 ºC for 20 minutes. The activation of the samples implanted with this dose and annealed at 1350 ºC drops to 80%, which is the same as the activation achieved for the samples annealed at 1250 ºC. The activation efficiencies of the samples implanted with the highest silicon dose of

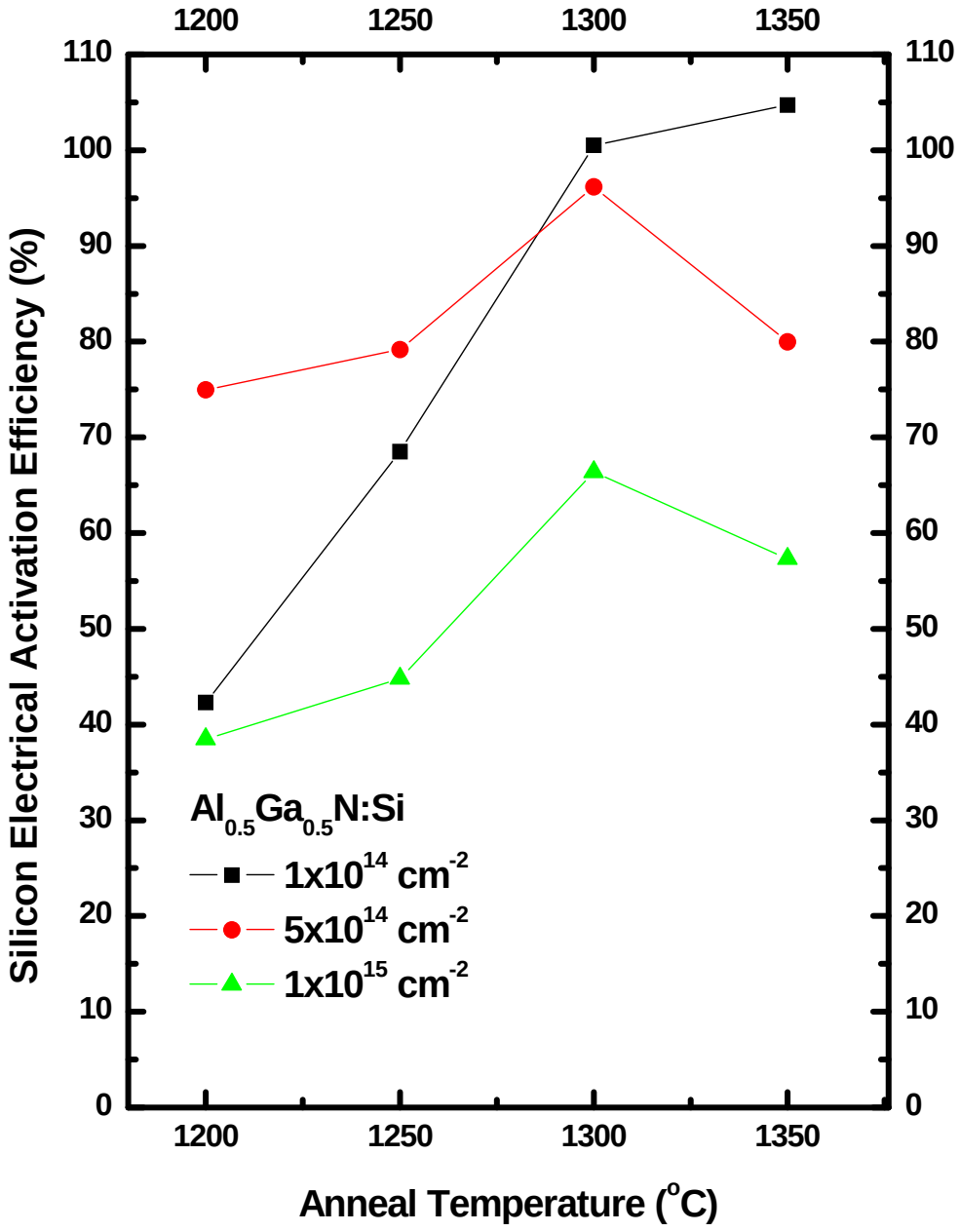

Figure 5.57. Electrical activation efficiency, for $Al_{0.5}Ga_{0.5}N$ implanted at room temperature with silicon ions at 200 keV with doses of $1x10^{14}$, $5x10^{14}$, and $1x10^{15}$ cm^{-2} and annealed from 1200 to 1350 °C for 20 minutes.

$1x10^{15}$ cm^{-2} reaches 66% after being annealed at 1300 ºC for 20 minutes in a nitrogen ambient. The samples implanted with the highest silicon dose had the lowest activation efficiencies and increasing the anneal temperature to 1350 ºC caused the activation for these samples to decline. Thus, the optimal anneal temperature for the $Al_{0.5}Ga_{0.5}N$ implanted with a dose of $1x10^{15}$ cm^{-2} silicon ions is less then 1350 ºC and an anneal time of 20 minutes is insufficient.

This behavior is inconsistent with the $Al_xGa_{1-x}N$ samples with lower Al mole fractions implanted with $1x10^{15}$ cm^{-2} silicon ions, which all had activation efficiencies higher than 96% under various annealing conditions. This decline in activation could be related to the upper silicon doping limit referred to by Yoshitaka *et al*. at which point the silicon ions begin to act as acceptors (53). All of the implanted samples show considerable activation efficiencies in $Al_{0.5}Ga_{0.5}N$ however, the activation increases as the implantation dose is decreased as is illustrated in Figure 5.58, which is a shift in behavior from the $Al_xGa_{1-x}N$ with lower Al concentrations.

Based on the electrical activation efficiencies of the implanted silicon the optimal anneal temperature for the Si-implanted $Al_{0.5}Ga_{0.5}N$ is 1300 ºC. The samples implanted with $1x10^{14}$ and $5x10^{14}$ cm^{-2} silicon ions reach activations of 100% and 96% after being annealed at this temperature for 20 minutes. The $Al_{0.5}Ga_{0.5}N$ implanted with a dose of $1x10^{15}$ cm^{-2} silicon ions has a lower activation of 66% at this temperature however, further increasing the anneal temperature to 1350 ºC has negative effects on the activation, indicating that extending the anneal time at 1300 ºC could improve the activation. The optimal anneal temperature for the Si-implanted $Al_{0.5}Ga_{0.5}N$ was not as dependent on the implanted as it was for the $Al_xGa_{1-x}N$ with lower Al concentrations.

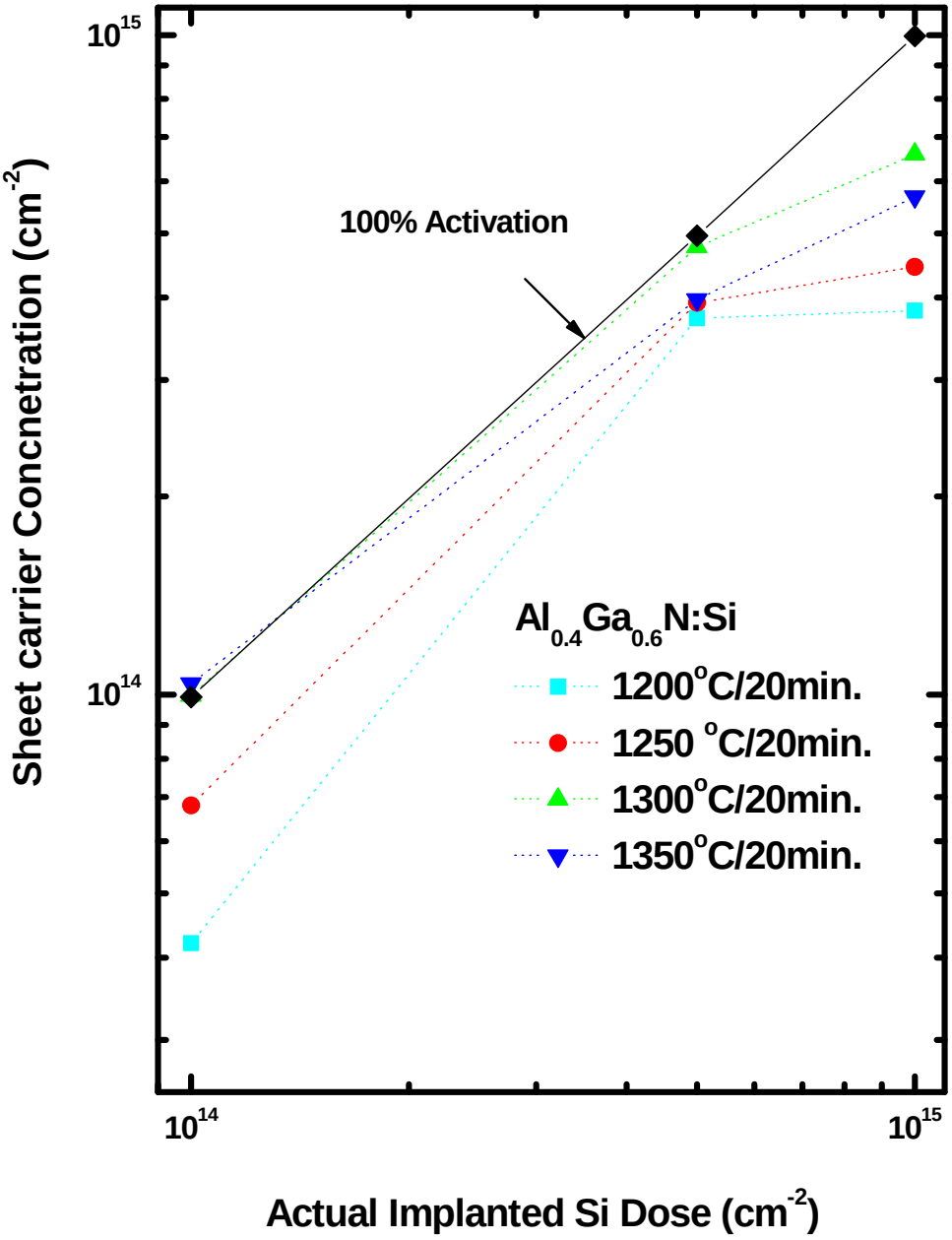

Figure 5.58. The room temperature sheet carrier concentrations versus the actual implanted silicon dose for $Al_{0.5}Ga_{0.5}N$ implanted at room temperature with silicon ions at 200 keV with doses of $1x10^{14}$, $5x10^{14}$, and $1x10^{15}$ cm^{-2} and annealed from 1200 to 1350 ºC for 20 minutes in a nitrogen ambient.

The resistivities for the Si-implanted $Al_{0.5}Ga_{0.5}N$ that have been annealed for 20 minutes at various temperatures are shown in Figure 5.59. The sample implanted with $1x10^{14}$ cm^{-2} silicon ions has a resistivity of 6.6 kΩ/□ which is 10 times higher than the resistivity of the samples implanted with $5x10^{14}$ and $1x10^{15}$ cm^{-2} silicon ions when annealed at 1200 ºC for 20 minutes. The resistivity for the samples implanted with the lowest silicon dose falls about 5.5 kΩ/□ as the anneal temperature is increased to 1350 ºC. Unlike the $Al_xGa_{1-x}N$ with lower Al mole fractions, only the resistivity of the samples implanted with $1x10^{14}$ cm^{-2} silicon ions decrease as the anneal temperature is increased, due to the increase in the carrier concentration. The resistivity for the samples implanted with $5x10^{14}$ and $1x10^{15}$ cm^{-2} silicon ions decreases as the anneal temperature is increased from 1200 to 1300 ºC, but then the resistivity increases for the samples annealed at 1350 ºC due to a decrease in the carrier concentration. The resistivity for $Al_{0.5}Ga_{0.5}N$ implanted with $1x10^{14}$ cm^{-2} silicon ions decreases from 6.6 kΩ/□ to 1.1 kΩ/□ as the anneal temperature is raised from 1200 to 1350 ºC, respectively. The lowest resistivity for the $Al_{0.5}Ga_{0.5}N$ implanted with $5x10^{14}$ cm^{-2} silicon ions is of 362 Ω/□ and occurred for the samples annealed at 1300 ºC. The samples implanted with $1x10^{15}$ cm^{-2} silicon ions showed a slightly linear decrease in resistivity as the anneal temperature is increased from 1250 to 1300 ºC dropping from 674 Ω/□ to 270 Ω/□, respectively. However the resistivity for the samples implanted with this dose and annealed at 1350 ºC increases to 352 Ω/□.

The anneal temperature that produces the lowest resistivity corresponds to the temperature at which the samples have a maximum in carrier concentration, and thus activation for all of the implanted silicon doses, as expected. The dependence of the resistivity on the anneal temperature of the Si-implanted $Al_{0.5}Ga_{0.5}N$ are similar to the

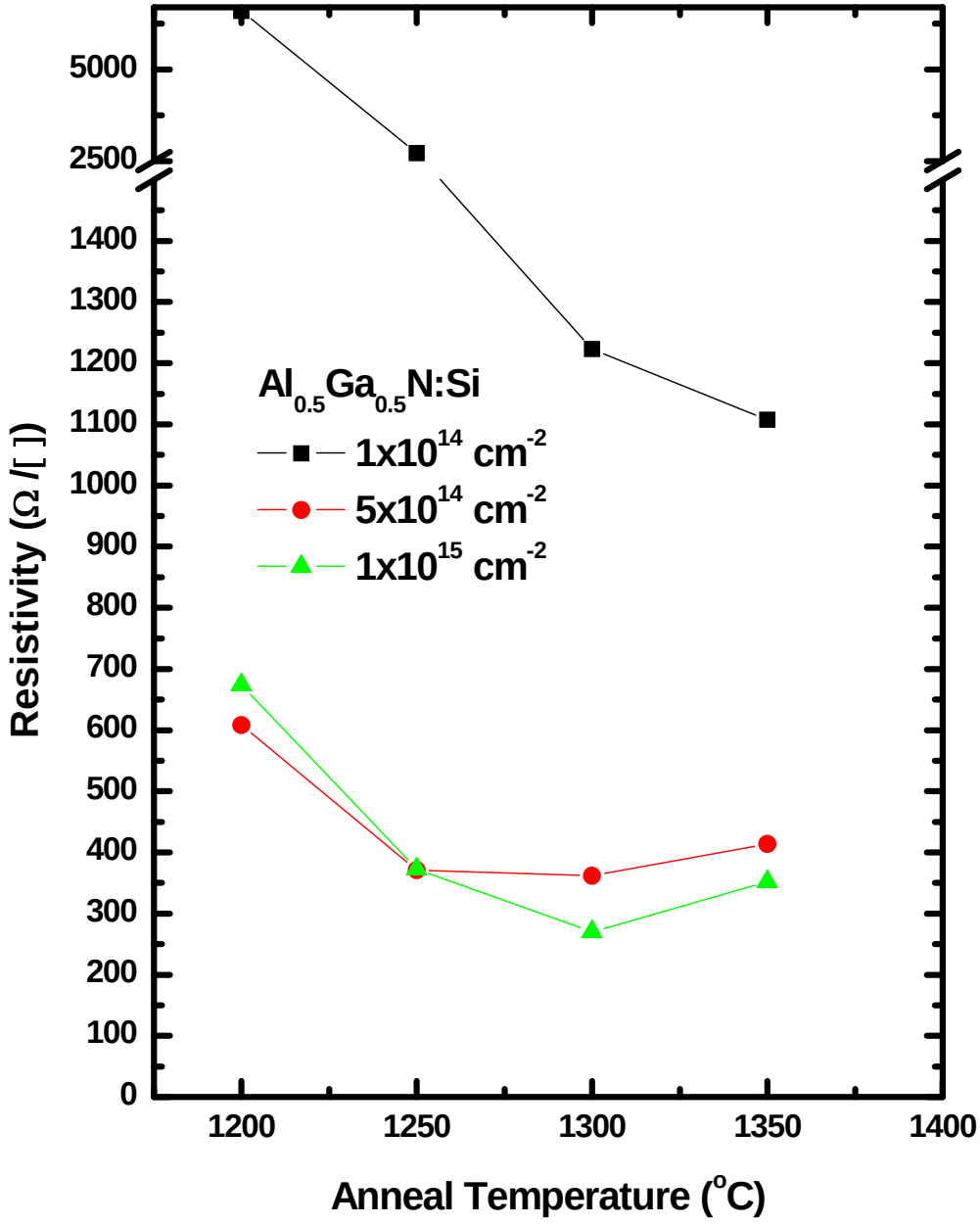

Figure 5.59. Room temperature resistivity measurements taken under zero magnetic field for $Al_{0.5}Ga_{0.5}N$ implanted at room temperature with silicon ions at 200 keV with doses of $1x10^{14}$, $5x10^{14}$, and $1x10^{15}$ cm^{-2} and annealed from 1200 to 1350 °C for 20 minutes in a nitrogen ambient.

dependence observed in $Al_xGa_{1-x}N$ with lower Al concentrations. However, the magnitude of the resistivity is higher, for samples implanted with each silicon dose, in $Al_{0.5}Ga_{0.5}N$ than for the $Al_xGa_{1-x}N$ with lower Al concentrations.

The room temperature mobilities for all the Si-implanted $Al_{0.5}Ga_{0.5}N$ annealed for 20 minutes at various temperatures are shown in Figure 5.60. The mobility increases as the anneal temperature is increased from 1200 to 1350 ºC for the samples implanted with doses of $1x10^{14}$ silicon ions, despite an increase in ionized impurity scattering. The mobility for the samples implanted with and $1x10^{15}$ cm^{-2} silicon ions also increases as the anneal temperature is increased. The carrier concentration for the sample implanted with the highest silicon dose decreases after being annealed at 1350 ºC, thus decreasing the effects of ionized impurity scattering causing the mobility to increase. The mobility of the $Al_{0.5}Ga_{0.5}N$ implanted with $5x10^{14}$ cm^{-2} silicon ions increases as the anneal temperature is raised from 1200 to 1250 ºC, where is reaches a peak of 43 $cm^2/V{\cdot}s$. Further increasing the anneal temperature to 1300 ºC causes the mobility to decrease to 36 $cm^2/V{\cdot}s$ which could be caused by an increase in ionized impurity scattering. The samples implanted with this dose and annealed at 1350 ºC show a slight increase in the mobility to 38 $cm^2/V{\cdot}s$ due to the decreased effects of ionized impurity scattering, however this mobility is not as high as it was for the samples annealed at 1250 ºC. The $Al_{0.5}Ga_{0.5}N$ implanted with a dose of $1x10^{15}$ cm^{-2} silicon ions exhibit a large increase in mobility as the anneal temperature is raised from 1200 to 1250 ºC. The mobility for these samples levels off as the anneal temperature is increased further to 1350 ºC. The peak mobility for the samples implanted with the highest silicon dose was of 35 $cm^2/V{\cdot}s$ which occurred for the sample annealed at 1350 ºC for 20 minutes. The sample implanted with

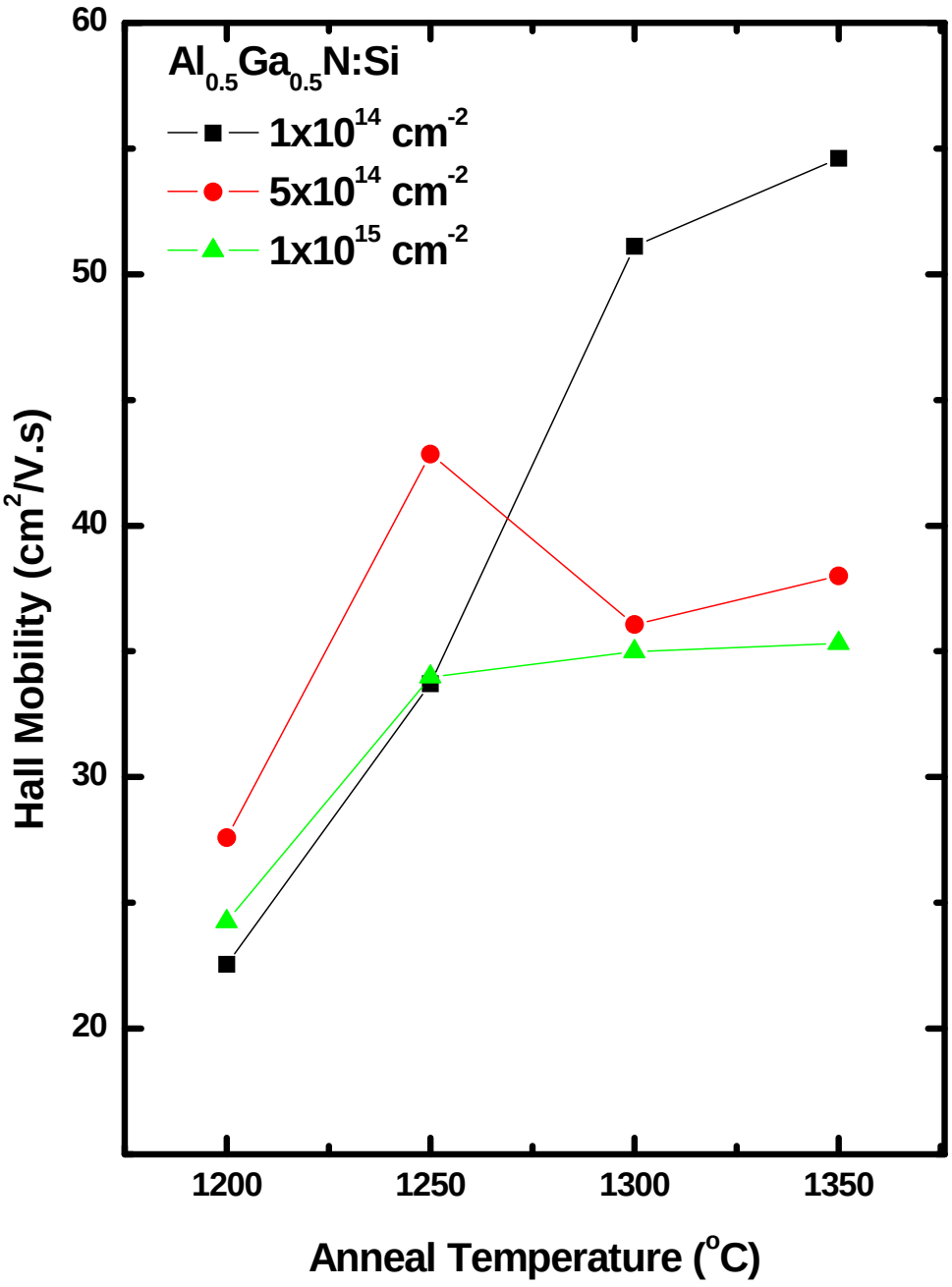

Figure 5.60. The room temperature mobilities calculated from Hall effect measurements on $Al_{0.5}Ga_{0.5}N$ implanted at room temperature with silicon ions with doses of $1x10^{14}$, $5x10^{14}$, and $1x10^{15}$ cm^{-2} and annealed from 1200 ºC to 1350 ºC for 20 minutes in a nitrogen ambient.

$1x10^{14}$ cm^{-2} silicon ions shows a dramatic rise in mobility from 23 $cm^2/V \cdot s$ to 55 $cm^2/V \cdot s$ as the temperature is increased from 1200 to 1350 ºC.

The mobility for the $Al_{0.5}Ga_{0.5}N$ is dose dependent, as it has been for all of the $Al_xGa_{1-x}N$ investigated, with the lower doses having higher mobilities. The samples implanted with a dose of $1x10^{14}$ cm^{-2} silicon ions achieved their peak activation after annealing at 1350 ºC, which corresponds to the anneal temperature for the peak mobility. Indicating that with each successive increase in the anneal temperature more lattice damage is recovered and more of the implanted silicon ions are activated. The samples implanted with silicon doses of $5x10^{14}$ and $1x10^{15}$ cm^{-2} experience their peak activation at different anneal temperatures than their peak mobilities, suggesting that most of the implantation induced damage had been repaired since the effects of ionized impurity scattering are dominant over those of defect scattering. The samples implanted with the lowest silicon dose exhibit the largest mobility, as they have for all the $Al_xGa_{1-x}N$ samples with lower Al mole fractions, except for the $Al_{0.4}Ga_{0.6}N$ samples. The peak mobilities for the Si-implanted $Al_{0.5}Ga_{0.5}N$ are lower than those of the lower Al mole fraction samples which is lost likely related to the increased effective mass as the Al mole fraction is increased (33).

To improve the electrical activation efficiency of the Si-implanted $Al_{0.5}Ga_{0.5}N$ the anneal time was extended from 20 to 40 minutes for a set anneal temperature of 1200 ºC. A comparison of the results obtained for both the 20 and 40 minute anneals at 1200 ºC are listed in Table 5.4. The $Al_{0.5}Ga_{0.5}N$ implanted with a dose of $1x10^{14}$ cm^{-2} silicon ions were not included in the study based on the low activation efficiency achieved after annealing at 1200 ºC and the poor results obtained from the samples implanted with a silicon dose of $1x10^{15}$ cm^{-2}, which also had a low activation after the 20 minute anneal at

1200 ºC. Complete activation has been shown to be achievable for the Si-implanted $Al_{0.5}Ga_{0.5}N$ however, an anneal temperature of 1200 ºC appears to be too low for this to take place.

Extending the anneal time to 40 minutes had positive affects on all of the physical aspects determined from the Hall effect measurements. The carrier concentrations, and therefore activation energies, of the samples implanted with $5x10^{14}$ and $1x10^{15}$ cm^{-2} silicon ions increased only slightly for the samples annealed for 40 minutes as opposed to those annealed for 20 minutes. The samples implanted with $5x10^{14}$ cm^{-2} silicon ions exhibit less than a 5% increase in the electrical activation efficiency going from 75% to 80% for the 40 minute anneal. The mobility for the samples implanted with this dose increase significantly from 27.6 to 39.6 $cm^2/V{\cdot}s$ regardless of the increase in ionized impurity scattering. The resistivity for these samples decreases 30% by extending the anneal time, as expected. The electrical activation for the samples implanted with $1x10^{15}$ cm^{-2} silicon ions increases 5% bringing it up to 44% after the 40 minute anneal. The resistivity for the samples implanted with this silicon dose and annealed for 40 minutes is almost half that of the samples annealed for 20 minutes. The mobility for the $Al_{0.5}Ga_{0.5}N$ implanted with $1x10^{15}$ cm^{-2} silicon ions increases from 24.3 to 40.7 $cm^2/V{\cdot}s$ after the extended time anneal, despite the increase in ionized impurity scattering. This is the highest mobility obtained for an $Al_{0.5}Ga_{0.5}N$ sample implanted with $1x10^{15}$ cm^{-2} silicon ions.

All the samples showed an increase in activation from extending the anneal time to 40 minutes; however the improvement was not always significant enough to achieve an activation better than that achieved at a higher annealing temperature. The samples implanted with a dose of $5x10^{14}$ cm^{-2} silicon ions, as well as the samples implanted with $1x10^{15}$ cm^{-2} silicon ions, have the same activation for the samples annealed at 1200 ºC

Table 5.4. Room temperature Hall effect results for $Al_{0.5}Ga_{0.5}N$ implanted at room temperature with silicon ions at 200 keV in three doses and annealed at 1200 ºC for 20 or 40 minutes nitrogen ambient.

Dose (cm^{-2})	Time (min.)	Carrier Concentration (cm^{-2})	Activation (%)	Resistivity (Ω/□)	Mobility ($cm^2/V{\cdot}s$)
$5x10^{14}$	20	$3.72x10^{14}$	74 .98	607.89	27.59
$5x10^{14}$	40	$3.96x10^{14}$	79.76	428.93	39.55
$1x10^{15}$	20	$3.82x10^{14}$	38.47	674	24.26
$1x10^{15}$	40	$4.39x10^{15}$	44.21	349.93	40.66

for 40 minutes and 1250 ºC for 20 minutes. Despite having the same activation the other physical properties of the $Al_{0.5}Ga_{0.5}N$, such as resistivity and mobility, do not respond to the lengthened anneal time the same way. The resistivity of the samples implanted with $5x10^{14}$ cm^{-2} silicon ions and annealed at 1250 ºC have a 58 Ω/□ lower resistivity and a 3 $cm^2/V{\cdot}s$ higher mobility than the samples implanted with this dose and annealed at 1200 ºC for 40 minutes. The $Al_{0.5}Ga_{0.5}N$ implanted with $1x10^{15}$ cm^{-2} silicon ions exhibit the opposite behavior, the samples annealed at 1200 ºC for 40 minutes have a lower resistivity and a higher mobility than the samples implanted with this dose and annealed at 1250 ºC for 20 minutes. The resistivity of the samples implanted with this dose and annealed for 40 minutes is lower by 22 Ω/□ and the mobility increases by 7 $cm^2/V{\cdot}s$ over the samples annealed at 1250 ºC for 20 minutes.

The $Al_{0.5}Ga_{0.5}N$ implanted with a dose of $5x10^{14}$ and $1x10^{15}$ cm^{-2} silicon ions reach their peak activation efficiencies after being annealed for 20 minutes at 1300 ºC.

Their peak activations for the samples annealed at this temperature are 16% and 20% higher than the activations achieved for the samples annealed at 1200 ºC for 40 minutes. Annealing the $Al_{0.5}Ga_{0.5}N$ at 1200 ºC for 40 minutes did not significantly increase the activation efficiency of the implanted samples as it had for the $Al_xGa_{1-x}N$ with lower Al concentrations. An anneal temperature of 1200 ºC does not appear to be high enough for complete activation of the implanted silicon to occur in $Al_{0.5}Ga_{0.5}N$.

The Si-implanted $Al_{0.5}Ga_{0.5}N$ implanted with a doses of $1x10^{14}$ and $5x10^{14}$ cm^{-2} achieved high electrical activation efficiency above 95% for the samples annealed at 1300 ºC for 20 minutes. The samples implanted with the lowest silicon dose had the best activation of 100% and the activation for the samples implanted with $5x10^{14}$ cm^{-2} silicon ions was only slightly lower at 96%. The samples implanted with the highest silicon dose of $1x10^{15}$ cm^{-2} had the lowest peak activation efficiency of 66% for the samples annealed at 1300 ºC for 20 minutes. The Si-implanted $Al_{0.5}Ga_{0.5}N$ samples deviate in behavior from the $Al_xGa_{1-x}N$ material with lower Al mole fractions. The $Al_{0.5}Ga_{0.5}N$ samples are the only $Al_xGa_{1-x}N$ samples to achieve higher activation efficiencies for the samples implanted the lowest silicon dose than the samples implanted with the highest silicon dose. The peak activation for the $Al_xGa_{1-x}N$ with Al concentrations of 10 to 40% increases as the implanted silicon dose increases, except for the $Al_{0.4}Ga_{0.6}N$ which had excellent activation for all three implanted silicon doses. The opposite is true for the $Al_{0.5}Ga_{0.5}N$ which exhibit a decrease in activation as the implanted silicon dose in increased.

Temperature-Dependent Hall Effect Measurements

Temperature-dependent Hall effect measurements were taken on the samples annealed at 1200 and 1300 ºC for twenty minutes in flowing nitrogen to determine the nature of the carriers as a function of temperature. The sheet carrier concentrations as a function of temperature from 10 to 700 K for the samples implanted with each of the three silicon doses and annealed at 1200 and 1300 ºC for 20 minutes are shown in Figure 5.61. The carrier concentrations for all the Si-implanted $Al_{0.5}Ga_{0.5}N$ remain relatively constant as the temperature is raised from 10 to 50 K. Above 50 K the carrier concentrations, for all the samples, begin to decrease reaching a minimum around 110-320 K and the increase to a higher carrier concentration at 700 K. The $Al_{0.5}Ga_{0.5}N$ implanted with $1x10^{15}$ cm^{-2} silicon ions are the most temperature-independent, as has been the case for all the $Al_xGa_{1-x}N$ studied. However, unlike the $Al_xGa_{1-x}N$ with lower Al concentrations these samples experience a noticeable dip in the carrier concentration for all of the implanted silicon doses. The carrier concentration for the sample implanted with a dose of $1x10^{14}$ cm^{-2} silicon ions and annealed at 1300 ºC noticeably increases from 30 to 80 K before it dips to a minimum at 150 K.

The samples implanted with the highest silicon dose have the most temperature-independent carrier concentrations as has been seen for the $Al_xGa_{1-x}N$ with Al concentrations of 10 to 40%. However, the $Al_xGa_{1-x}N$ with lower Al concentrations had a much more temperature-independent nature to the carrier concentration, than the $Al_{0.5}Ga_{0.5}N$ samples. This can be attributed to the increase in the Mott concentration as the Al concentration of the material is increased. Nonetheless, the carrier concentrations still indicate that the implanted silicon ions have formed a degenerate impurity band

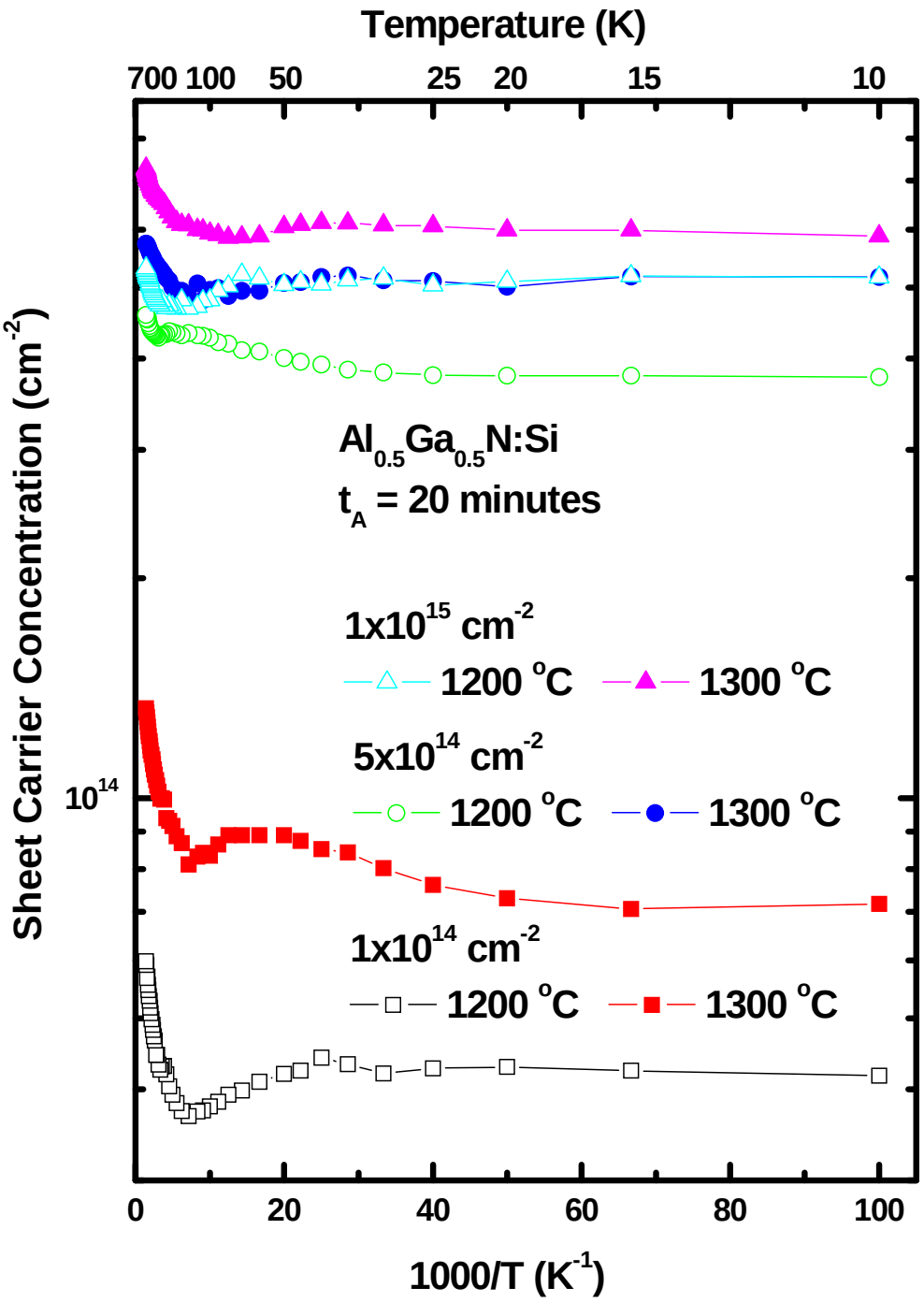

Figure 5.61. Temperature-dependent sheet carrier concentrations of $Al_{0.5}Ga_{0.5}N$ determined from Hall effect measurements taken from 10 to 700 K. The $Al_{0.5}Ga_{0.5}N$ was implanted with three different doses of Si ions at 200 keV and annealed at 1200 and 1300 °C for 20 minutes in a flowing nitrogen environment.

region in the band gap. All three of the implanted silicon doses in $Al_{0.5}Ga_{0.5}N$ correspond to volume carrier concentrations that exceed the Mott concentration. Like the $Al_xGa_{1-x}N$ with lower Al mole fractions, the samples implanted with $1x10^{14}$ cm^{-2} silicon ions exhibit properties most like that of a non-degenerate semiconductor. The dip in carrier concentrations of the Si-implanted $Al_{0.5}Ga_{0.5}N$ signifies the presence of a multi-channel conduction band, caused by the Gaussian profile of the implanted silicon ions (37,68). Degenerate samples yield ionization energies lower than the actual energy due to impurity screening. Impurity screening acts reduce the donor ionization energy and its effects are enhanced by an increase in the concentration of ionized donors. Therefore, the silicon ionization energy for $Al_{0.5}Ga_{0.5}N$ can not be accurately estimated from the samples in this study. However, Hwang *et al*. calculated from a simple hydrogen model that the ionization for $Al_{0.5}Ga_{0.5}N$ would be on the order of 61 meV.

The temperature-dependent Hall mobilities the Si-implanted $Al_{0.5}Ga_{0.5}N$ are shown in Figure 5.62. All of the samples exhibit a peak in their mobility curve around 320 K. The sample implanted with $1x10^{14}$ cm^{-2} silicon ions and annealed at 1300 ºC has the highest mobility of 52 $cm^2/V{\cdot}s$ after being annealed at 1300 ºC. The mobility of the samples implanted with this dose and annealed at 1200ºC are considerably lower. Only the samples implanted with the lowest silicon dose have higher mobilities for the samples annealed at 1300ºC, which is consistent with the room temperature data. The mobility curves become more temperature-independent as the implanted silicon dose is increased. The samples implanted with $5x10^{14}$ and $1x10^{15}$ cm^{-2} silicon ions have very similar temperature dependencies, especially in the high temperature regime. The peak mobilities for the samples implanted with $5x10^{14}$ cm^{-2} silicon ions are 27 and 31 $cm^2/V{\cdot}s$ after being annealed at 1200 and 1300ºC, respectively. The samples implanted with the

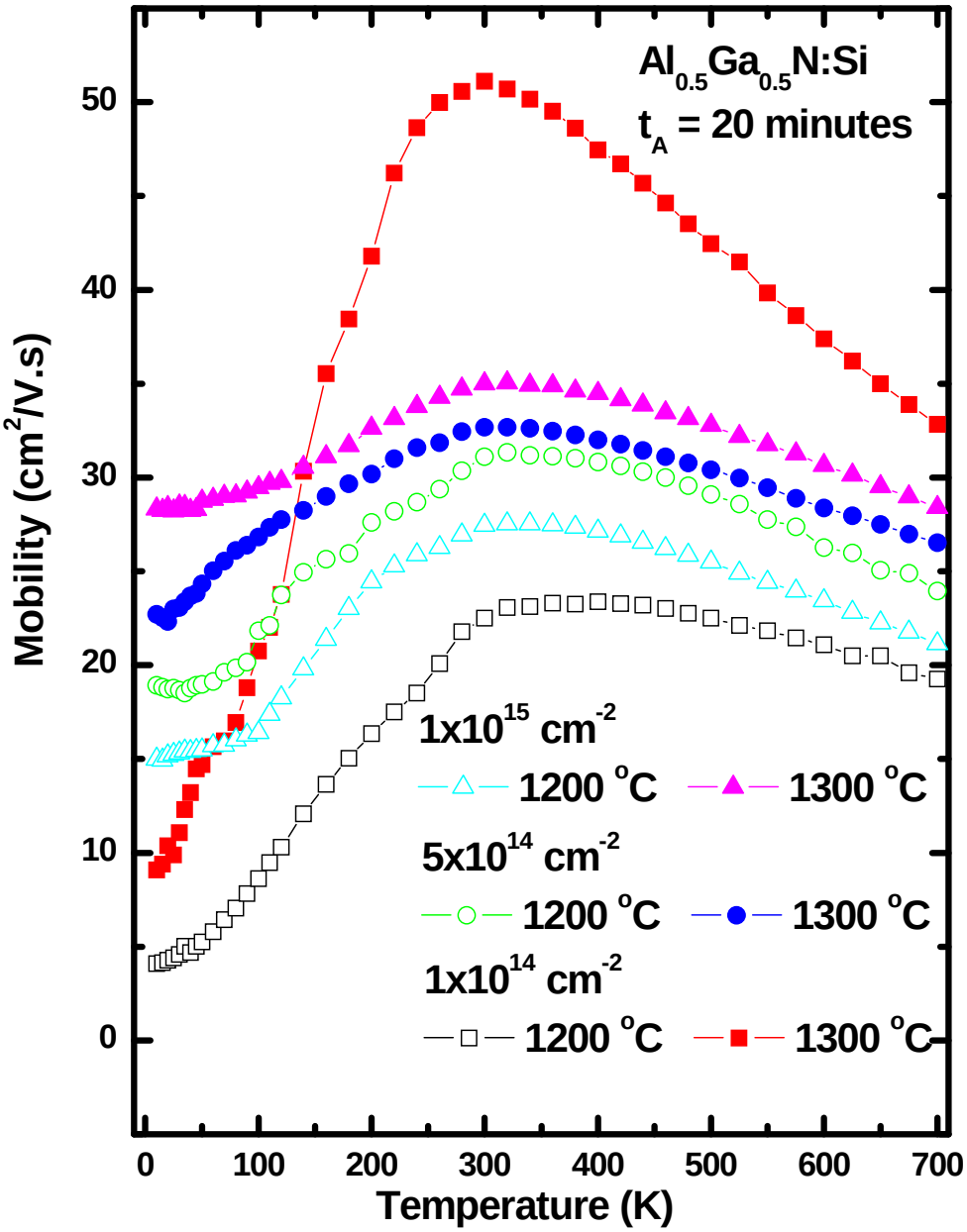

Figure 5.62. Temperature-dependent mobilities calculated from Hall effect measurements taken from 10 to 700 K for $Al_{0.5}Ga_{0.5}N$ implanted at room temperature with Si ions at 200 keV in three different doses and annealed at 1200 and 1300 ºC for 20 minutes.

highest silicon dose have peak mobilities of 27 and 35 $cm^2/V \cdot s$ for the two anneal temperatures, respectively. As seen in the $Al_xGa_{1-x}N$ with lower Al concentrations, the mobilities at 10 K increase as the implanted silicon is increased due to the degeneracy of the samples. The mobilities at 10 K for the samples implanted with $1x10^{14}$, $5x10^{14}$, and $1x10^{15}$ cm^{-2} silicon ions and annealed at 1200 ºC are 4, 15, and 18 $cm^2/V \cdot s$. The mobility for the samples that were annealed at 1300 ºC are 9, 23, and 28 $cm^2/V \cdot s$ for the three doses, respectively. The degenerate impurity region causes the low temperature mobility to be temperature-independent, more so for the samples implanted with $1x10^{15}$ cm^{-2} silicon ions. The temperature-dependent mobility of the samples implanted with $1x10^{14}$ cm^{-2} silicon ions most resembles that which is predicted for a non-degenerate sample, more so for the $Al_{0.5}Ga_{0.5}N$ than the $Al_xGa_{1-x}N$ with lower Al mole fractions due to the increase in the Mott concentration as the Al mole fraction is increased. The mobility curves for the $Al_{0.1}Ga_{0.9}N$ and $Al_{0.2}Ga_{0.8}N$ implanted with the higher silicon doses curves are more flat and temperature-independent than they are for the $Al_{0.5}Ga_{0.5}N$. Also, the lower Al mole fraction material had mobilities that clearly increased as the implanted silicon dose was decreased, which is not the case here. The samples implanted with $5x10^{14}$ and $1x10^{15}$ cm^{-2} silicon ions and annealed at 1200 and 1300 ºC have higher mobilities than the samples implanted with $1x10^{14}$ cm^{-2} silicon ions and annealed at 1200 ºC.

Figure 5.63 shows the temperature-dependent resistivity of the $Al_{0.5}Ga_{0.5}N$ samples annealed at 1200 and 1300 ºC for all three of the implanted silicon doses. The samples annealed at the higher temperature of 1300 ºC had larger resistivity, except for the samples that were implanted with a dose of $1x10^{15}$ cm^{-2} silicon ions which is consistent with the room temperature data. The resistivity decreases significantly as the

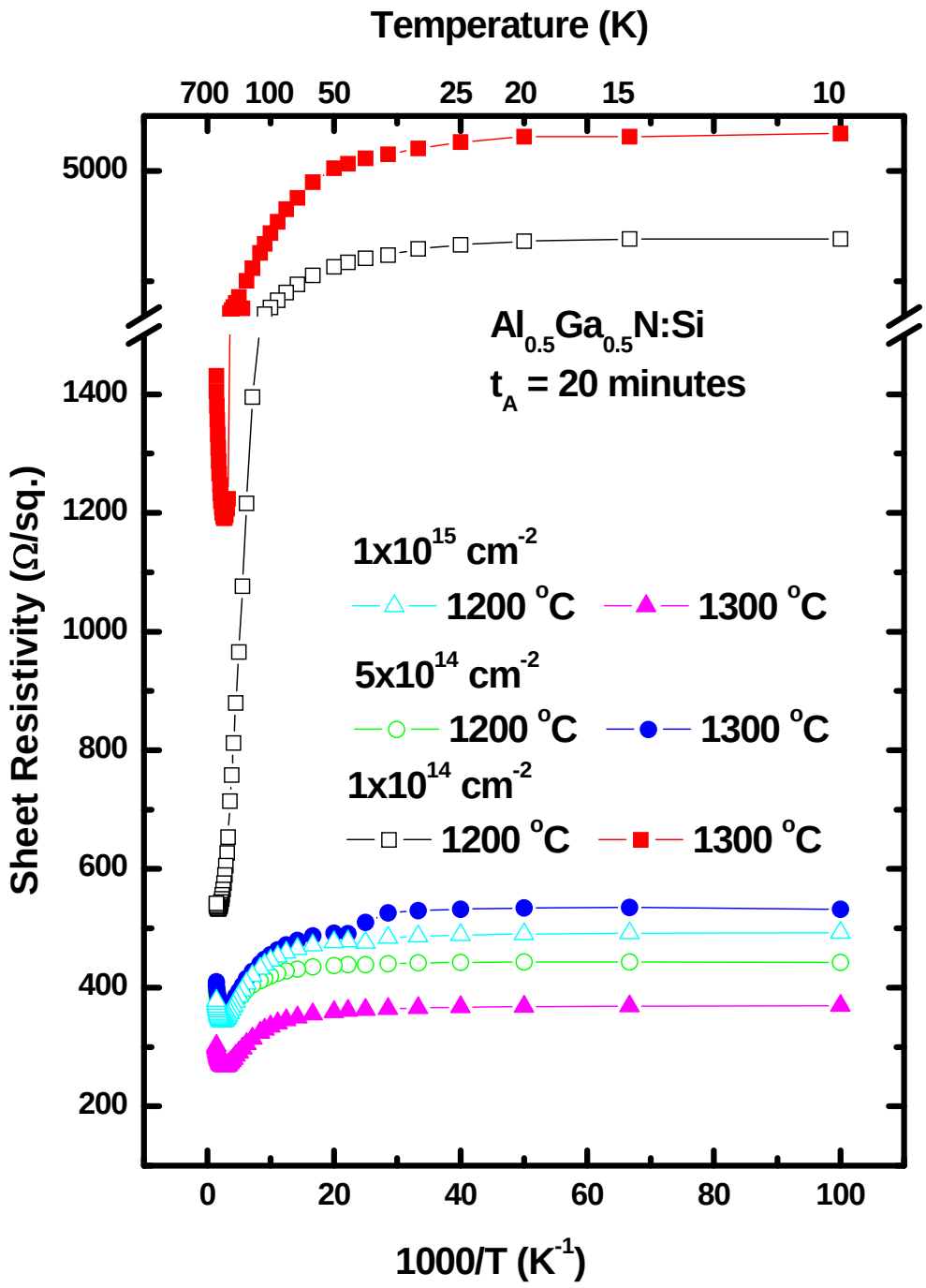

Figure 5.63. Temperature-dependent resistivity calculated from Hall effect measurements taken from 10 to 700 K for $Al_{0.5}Ga_{0.5}N$ that had been implanted at room temperature with silicon ions at 200 keV in does of $1x10^{14}$, $5x10^{14}$, and $1x10^{15}$ cm^{-2} and annealed at 1200 and 1300°C for 20 minutes in flowing nitrogen.

implantation dose is increased and also becomes more temperature-independent. The Si-implanted $Al_{0.5}Ga_{0.5}N$ show a relative temperature-independent resistivity from 10 to 50 K and then the resistivity slowly dips to a minimum around 380 K before beginning to increasing up through 700 K. The dip in the samples implanted with $1x10^{14}$ cm^{-2} silicon ions is the most exaggerated and the drop resistivity for the samples implanted with $1x10^{15}$ cm^{-2} silicon ions is significantly less noticeable. This dip in the resistivity is related to the dramatic increase in the carrier concentration and also the decline of the mobility.

Low Temperature Cathodoluminescence Measurements

Cathodoluminescence measurements were taken at an electron energy of 10 keV with 50 μA of source current, the temperature in the chamber was 7.4 K, and the slits on the spectrometer were 400 μm both at the entrance and the exit. The range scanned was 1800 to 7000 Å with a step size of 2 Å and an integration time of 0.1 second.

The spectrum of the unimplanted samples shown as a function of anneal temperature are given in Figure 5.64. To gauge the level of damage recovery in the implanted samples the behavior of the unimplanted samples must first be observed. The CL spectra for the as-grown sample shows a neutral-donor-bound exciton (D^o,X) peak at 4.59 eV followed by three peaks at 4.49, 4.42, and 4.35 eV due to etalon effects. The peak at 4.35 eV is more enhanced in the spectra of the implanted samples that it is for the as-grown samples. The spectrum also has a broad luminescence centered at 3.0 eV, similar to that seen in GaN, due to a deep impurity transition between a shallow donor and a deep acceptor. Nam *et al*. observed that as the peak positions in $Al_xGa_{1-x}N$ blue shifted from 3.42 to 5.96 eV with increasing Al mole fraction from zero to one, the deep

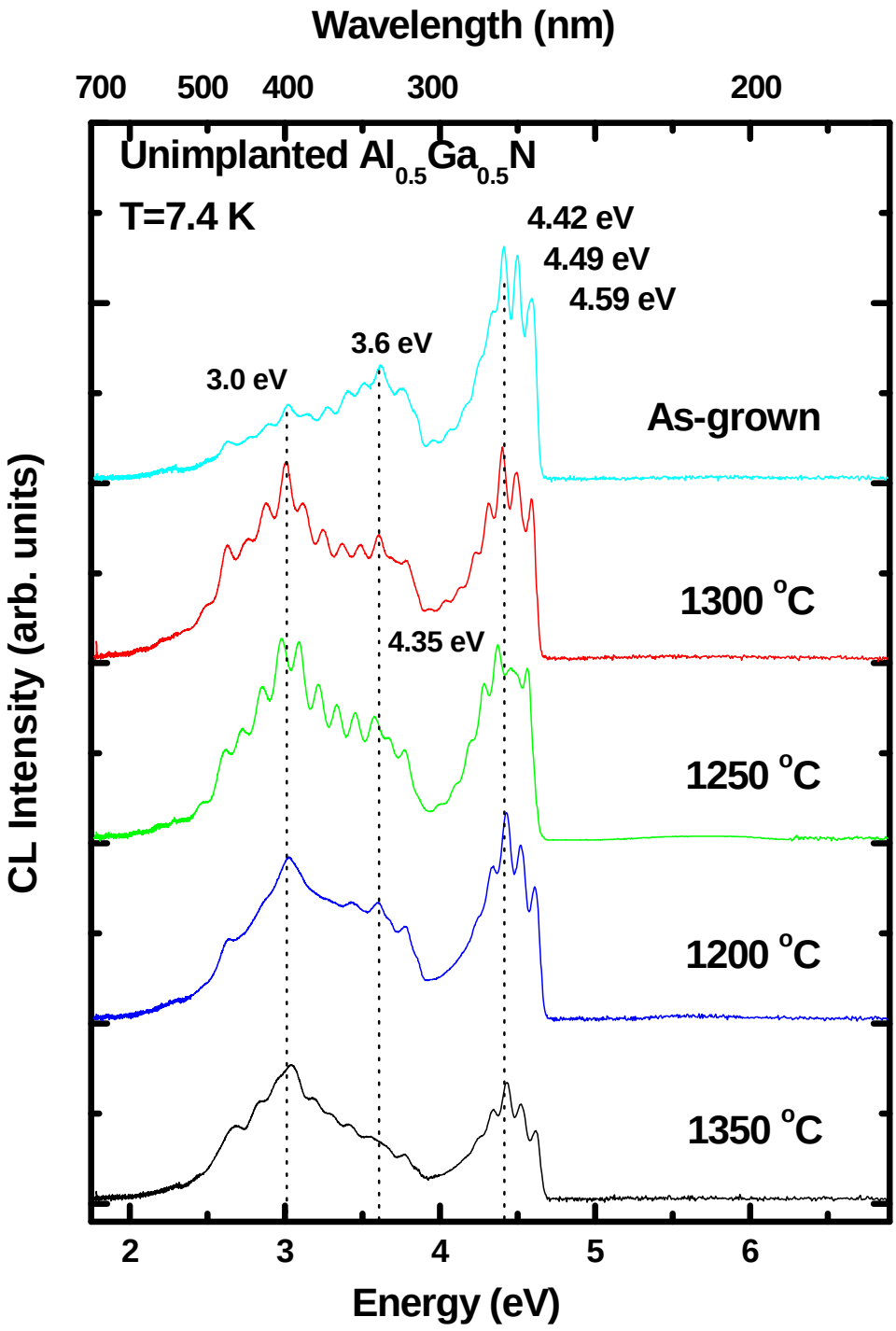

Figure 5.64. CL spectra taken at 7.4 K for unimplanted $Al_{0.5}Ga_{0.5}N$ that have been anneal at 1200, 1250, 1300, and 1350 ºC for 20 minutes in flowing nitrogen and also an as-grown sample.

impurity peaks also shifted from 2.15 eV (YL) in GaN to 3.90 eV (VL) for AlN (44). They attribute this luminescence to be related to an Al vacancy or an Al vacancy complex. The CL spectra also exhibit a broad luminescence centered around 3.6 eV that is the most prominent in the spectrum of the as-grown sample. The origin of this luminescence is unknown at this time but is most likely related to defects is the crystal caused from the large incorporation of Al atoms. The as-grown sample has the most intense (D^o,X) peak. As the anneal temperature is increased from 1200 to 1300 ºC, the intensity of the (D^o,X) peak increases however, annealing at 1350 ºC severely decreases the intensity of the (D^o,X) peak, most likely due to annealing related damage. The implanted samples show considerable amplification of the 3.0 eV and diminishing intensity of the 3.6 eV band compared to that of the as-grown sample. As the anneal temperature is increased from 1200 to 1300 ºC the 3.0 eV band intensifies and the peaks become more distinguished.

The low temperature CL spectra for the Si-implanted $Al_{0.5}Ga_{0.5}N$ annealed for 20 minutes at 1250 ºC are shown in Figure 5.65. All of the samples have a comparable spectrum with the unimplanted sample. The spectrum show a (D^o,X) peak at 4.59 eV followed by a several other peaks due to etalon effects. All of the spectra have a dominant luminescence centered at 3.0 eV that is attributed to deep impurity transitions most likely related to Al vacancy complexes (44). There is also an unknown luminescence centered at 3.6 eV that could be the result of as-grown defects from the Al composition of the sample. All of the spectra of the implanted $Al_{0.5}Ga_{0.5}N$ show an increase in the 3.0 eV band compared to the as-grown sample, with samples implanted with $1x10^{14}$ cm^{-2} silicon ions being the most profound. The unimplanted samples have the weakest intensity. The intensity of the spectra decrease as the implanted dose is

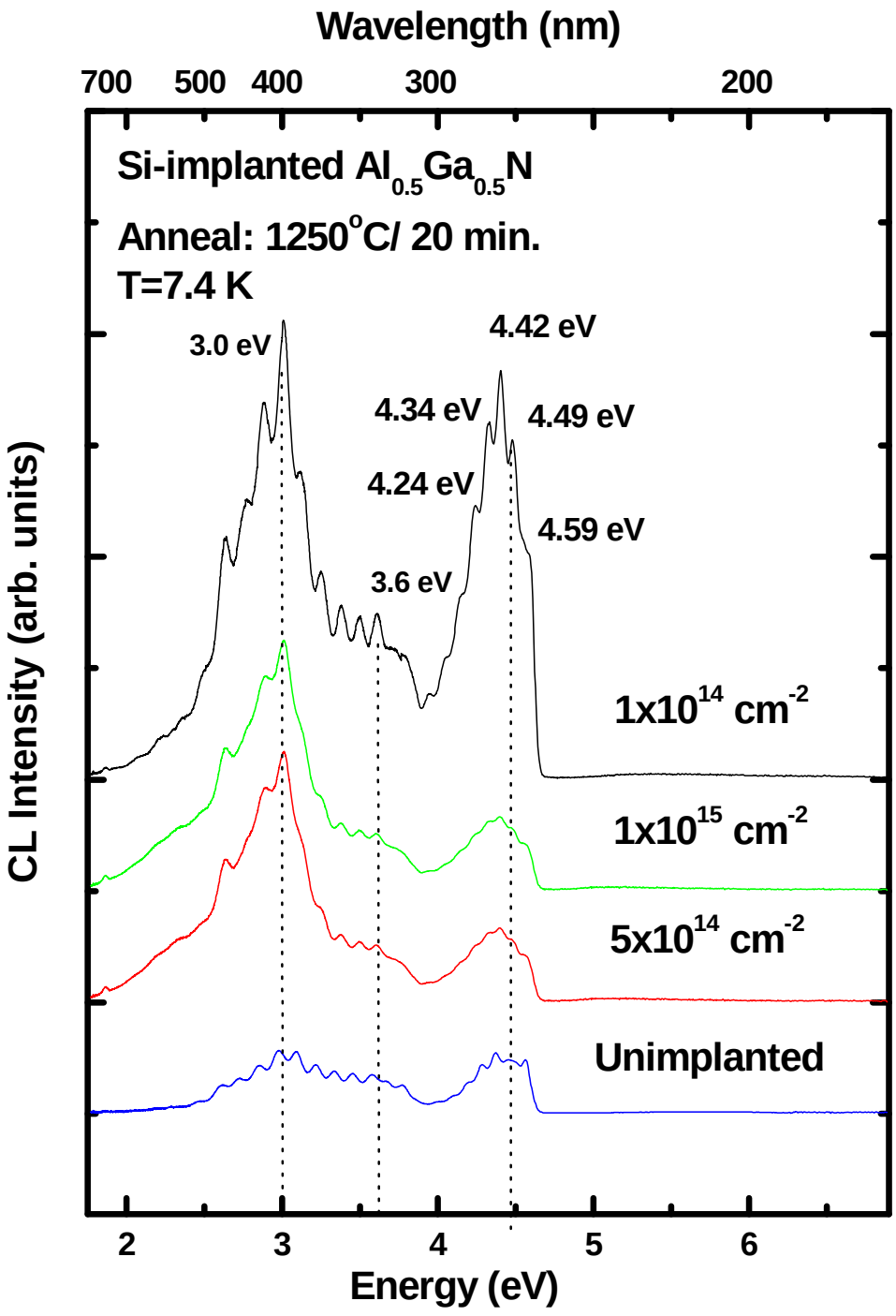

Figure 5.65. CL spectra taken at 7.4 K for Si-implanted $Al_{0.5}Ga_{0.5}N$ that have been anneal at 1250 ºC for 20 minutes in flowing nitrogen.

increased. The samples implanted with $1x10^{14}$ cm^{-2} silicon ions exhibit the most intense group of peaks and 3.0 eV band. The (D^o,X) peak appears as a shoulder off the high energy side of the 4.49 eV peak for this sample. The samples implanted with $5x10^{14}$ and $1x10^{15}$ cm^{-2} silicon ions have very similar spectrums that match in intensity and shape. For both samples, the peaks are not distinguishable; they have broadened into a luminescence centered at 4.42 eV due to the increase in the carrier concentration.

The low temperature CL spectra for the $Al_{0.5}Ga_{0.5}N$ implanted with $1x10^{14}$ cm^{-2} silicon ions annealed for 20 minutes at various temperatures are shown in Figure 5.66. All of the anneal temperatures result in spectra that exhibit the (D^o,X) peak and peaks due to etalon effects that are in the spectrum of the as-grown sample. The a (D^o,X) peak centered at 4.59 eV and the peaks due to etalon effects broaden as the temperature is increased from 1200 to 1350 ºC, as would be expected due to the increase in the number of ionized donors. As the anneal temperature is increased from 1200 to 1250 ºC the intensity of the peaks centered at 4.42 eV improves. All of the spectra have similar intensity, except for the samples annealed at 1350 ºC which has a weaker intensity that could have been caused by annealing related damage. The samples that were annealed at 1300 ºC exhibit a reduction in the intensity of these peaks however; the shape of this spectrum most resembles that of the as-grown sample. All the spectra also show the broad luminescence centered at 3.0 eV that is similar to the YL band observed in GaN samples. The intensity of the 3.0 eV luminescence increases as the anneal temperature is raised from 1200 to 1300 ºC and is more dominant in the implanted samples than the as-grown sample. All of the spectra have a weak luminescence centered at 3.6 eV that is most predominant in the spectrum of the as-grown sample. This broad luminescence is believed to be due to as-grown defects caused from the increasing Al mole fraction of the

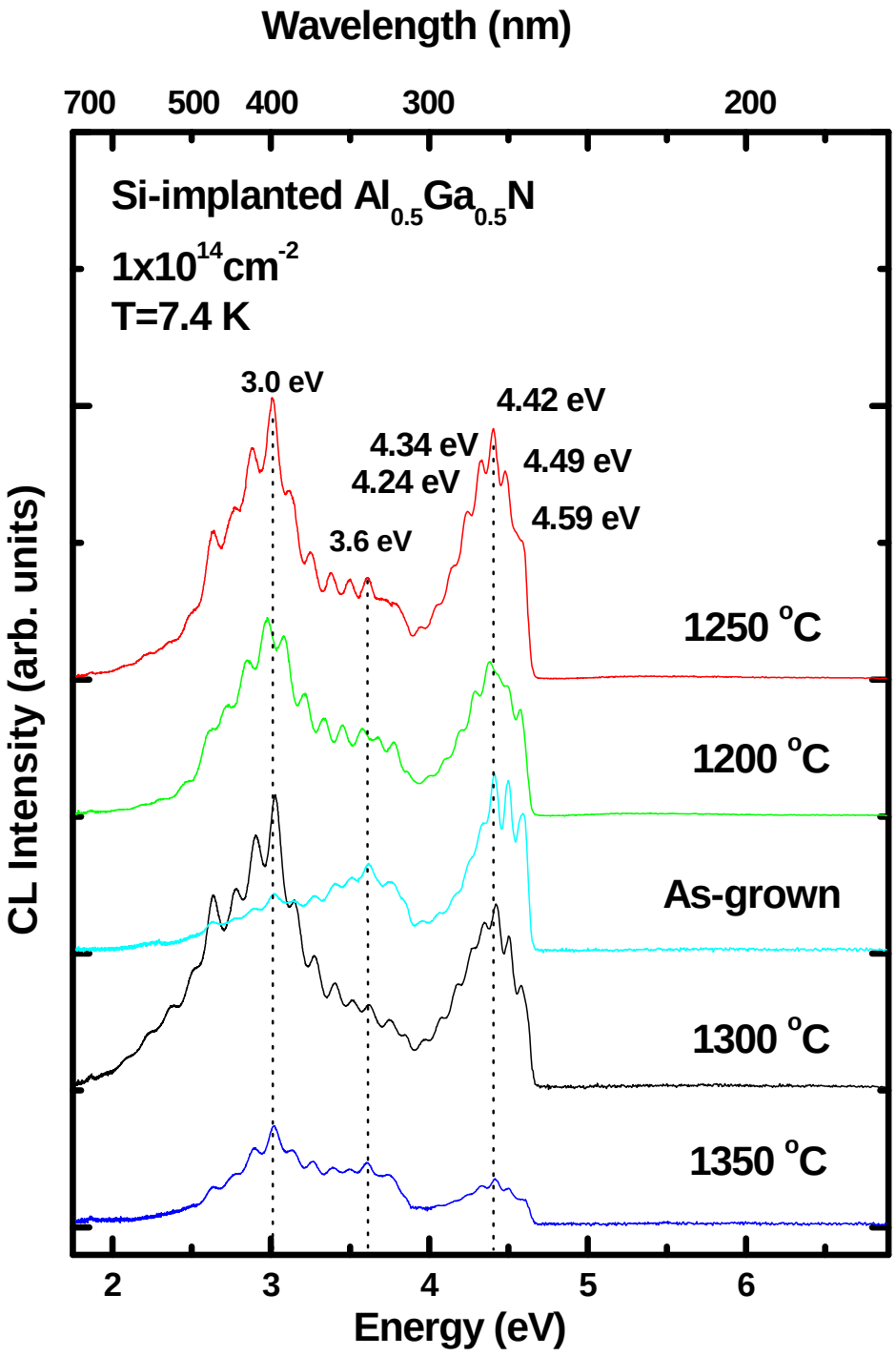

Figure 5.66. CL spectra taken at 7.4 K for $Al_{0.5}Ga_{05}N$ that has been implanted with $1x10^{14}$ cm^{-2} silicon ions and annealed at various temperatures for 20 minutes in flowing nitrogen.

material. The intensity of the 3.6 eV band for the samples annealed at 1200 and 1250 ºC remains the same as that of the as-grown sample. The intensity of this band deceases as the anneal temperature is increased up to 1350 ºC, indicating that an anneal temperatures of at least 1300 ºC are required to repair as-grown defects in $Al_{0.5}Ga_{0.5}N$.

The CL spectra of the samples implanted with a silicon dose of $5x10^{14}$ cm^{-2} silicon ions and annealed for 20 minutes at various temperatures are shown in Figure 5.67. All of the anneal temperatures result in spectra that exhibit the (D^o,X) peak and etalon effects that are in the spectrum of the as-grown sample. However, the (D^o,X) peak an phonon replicas are not as distinguishable for the implanted samples as they are for the as-grown sample. The a (D^o,X) peak centered at 4.59 eV and the etalon effect peaks broaden as the temperature is increased from 1200 to 1300 ºC, as would be expected due to the increase in the number of ionized donors. Initially, the intensity of these peaks increases as the anneal temperature is raised from 1200 to 1250 ºC, however increasing the anneal temperature further causes the intensity to diminish. All of the spectrums for the implanted samples have a dominant broad luminescence centered at 3.0 eV, which is enhanced compared to the as-grown sample, which is similar to the YL band observed in GaN samples (44). The 3.0 eV band for the sample annealed at 1250 ºC is orders of magnitude higher than that of the samples annealed at the other temperatures. The intensity of this band decreases for higher anneal temperature. All of the spectra have a weak luminescence centered at 3.6 eV that is most predominant in the spectrum of the as-grown sample. This broad luminescence is believed to be due to as-grown defects caused from the increasing Al mole fraction of the material. The intensity of the 3.6 eV band for the samples annealed at 1200 and 1300 ºC remains the same as that of the as-grown sample. The intensity of this band increases only for the sample annealed at 1250 ºC.

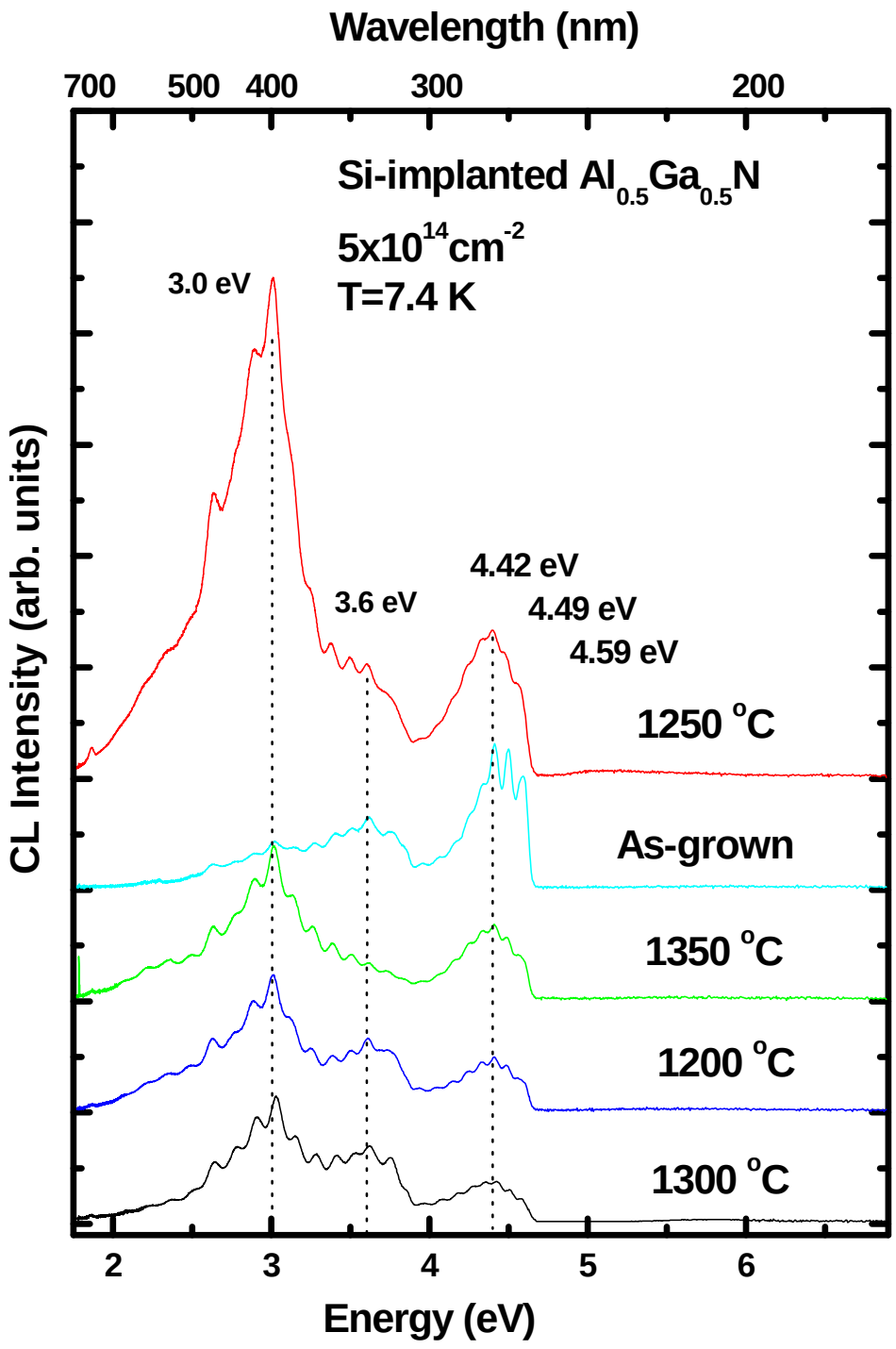

Figure 5.67. CL spectra taken at 7.4 K for $Al_{0.5}Ga_{0.5}N$ that has been implanted with $5x10^{14}$ cm^{-2} silicon ions and annealed at various temperatures for 20 minutes in flowing nitrogen.

The intensity of this band deceases as the anneal temperature is increased to 1350 ºC, indicating that an anneal temperatures of at least 1350 ºC are required to repair as-grown defects in $Al_{0.5}Ga_{0.5}N$. The electrical results for samples implanted with this silicon dose all steadily improve as the anneal temperature was increased from 1200 to 1300 ºC, which corresponds to a decrease of the 3.0 eV luminescence.

The CL spectra of the samples implanted with a dose of $1x10^{15}$ cm^{-2} silicon ions and annealed for 20 minutes at various temperatures are shown in Figure 5.68. All of the anneal temperatures result in spectra that exhibit the (D^o,X) peak and etalon effects that are in the spectrum of the as-grown sample. However, the (D^o,X) peak an phonon replicas are not as distinguishable for the implanted samples as they are for the as-grown sample. The a (D^o,X) peak centered at 4.59 eV and the etalon effect peaks broaden as the temperature is increased from 1200 to 1300 ºC, as would be expected due to the increase in the number of ionized donors. The spectra for the sample annealed at 1250 ºC had to be reduced by a factor of 5. The intensity of the (D^o,X) peak decreases as the anneal temperature is increased from 1200 to 1300 ºC and is no longer observable in the spectrum of the sample annealed at 1350 ºC. All of the spectrums for the implanted samples have a dominant broad luminescence centered at 3.0 eV, similar to the YL band observed in GaN samples, which is enhanced compared to the as-grown sample (44). The 3.0 eV band is not the dominant feature in the spectrum of the samples annealed at 1350 ºC, but rather the main feature is a luminescence centered around 2.5 eV. This band is present in all the spectra of the Si-implanted samples. Nam et al. also observed a luminescence band at 2.56 eV that was only observed in samples with Al mole fraction greater than 0.5, and increased as the Al mole fraction was increased (44). They attributed this impurity band to a DAP transition from shallow donor to an aluminum

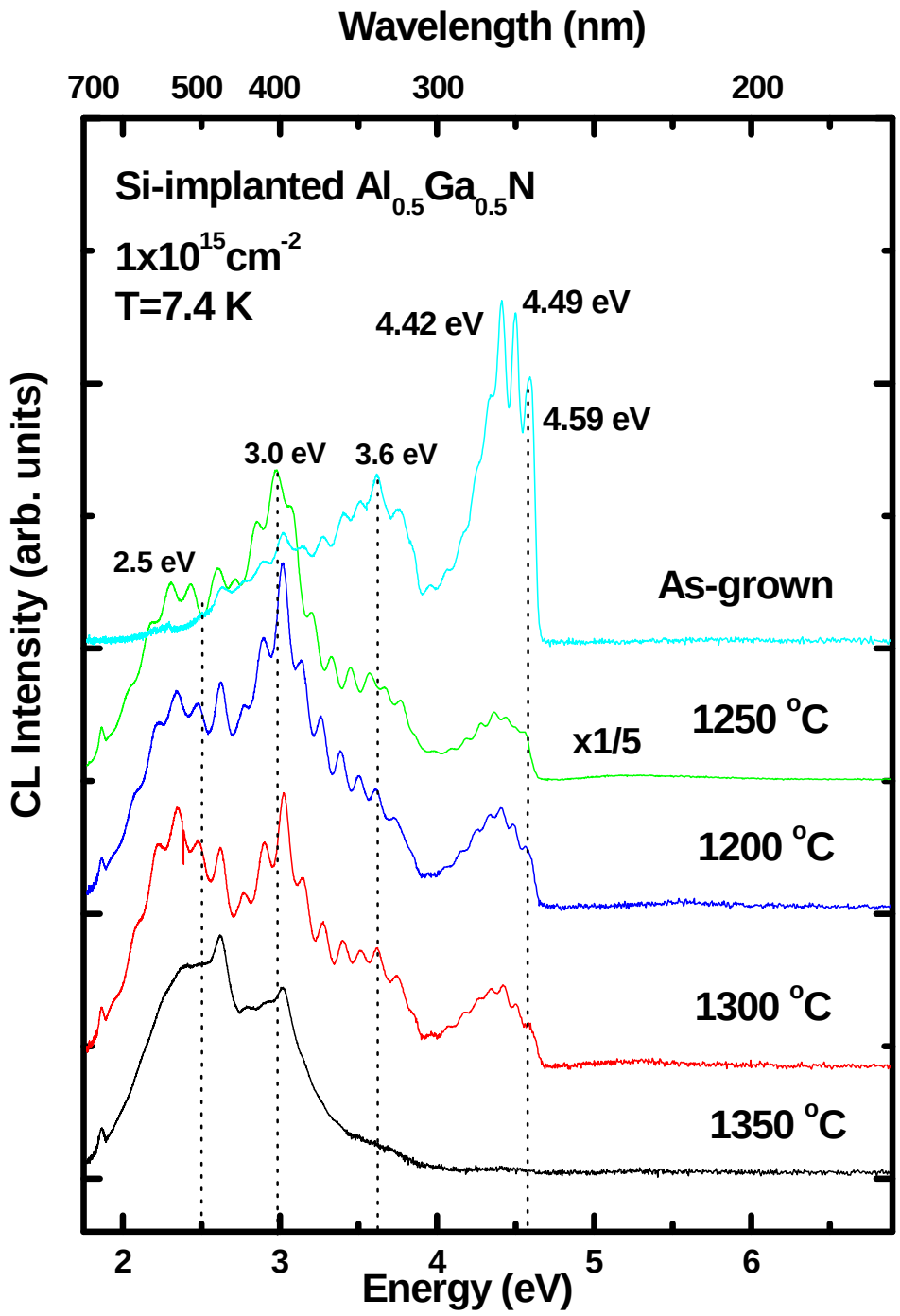

Figure 5.68. CL spectra taken at 7.4 K for $Al_{0.5}Ga_{0.5}N$ that has been implanted with $1x10^{15}$ cm^{-2} silicon ions and annealed at various temperatures for 20 minutes in flowing nitrogen.

vacancy $(V_{Al})^{3-}$, which acts as a deep acceptor. This luminescence was not observed in the $Al_{0.5}Ga_{0.5}N$ implanted with lower silicon doses or in the as-grown sample All of the spectra have a weak luminescence centered at 3.6 eV that is most predominant in the spectrum of the as-grown sample, except for the sample annealed at 1350 ºC. This broad luminescence is believed to be due to as-grown defects caused from the increasing Al mole fraction of the material. The 3.36 eV luminescence band decreases for all of the anneal temperatures, except for the samples annealed 1250 ºC for which it is considerably enhanced. The 3.36 eV band is not present in the spectra for the sample annealed at 1350 ºC, similar to the behavior of the $Al_{0.5}Ga_{0.5}N$ implanted with the lower silicon doses. The spectrum for the sample annealed at 1350 ºC has a different shape than the other spectra, as was seen in the $Al_{0.4}Ga_{0.6}N$ samples implanted with all three doses and annealed at this temperature.

Summary

The Si-implanted $Al_xGa_{1-x}N$ samples with Al mole fractions from 10 to 50% all achieved high activation efficiencies after a high temperature anneal treatment. The highest obtainable activation for each implanted sample are shown in Table 5.5 along with the anneal conditions and other physical properties.

Anneal conditions were determined for each Al mole fraction implanted with each silicon dose that produce greater than 95% activation in most samples. The activations and mobilities obtained for Si-implanted $Al_xGa_{1-x}N$, in this study, are higher than those reported (33-35, 47, 51-52).

Table 5.5. The electrical results obtained for the annealing conditions that produced the highest electrical activation efficiency for each silicon dose implanted into $Al_xGa_{1-x}N$.

	Silicon dose (cm^{-2})	Anneal Temp. (ºC)	Anneal Time (min.)	Activation (%)	Carrier Concentration (cm^{-2})	Mobility ($cm^2/V{\cdot}s$)	Resistivity ($\Omega/\square$)
$Al_{0.1}Ga_{0.9}N$	$1x10^{14}$	1200	40	73	$7.13x10^{13}$	101	792
	$5x10^{14}$	1200	40	94	$4.61\ x10^{14}$	70	190
	$1x10^{15}$	1200	40	100	$9.95\ x10^{14}$	64	96
$Al_{0.2}Ga_{0.8}N$	$1x10^{14}$	1300	20	83	$8.25\ x10^{13}$	76	1000
	$5x10^{14}$	1300	20	100	$5.33\ x10^{14}$	54	214
	$1x10^{15}$	1300	20	100	$9.92\ x10^{14}$	54	115
$Al_{0.3}Ga_{0.7}N$	$1x10^{14}$	1300	20	74	$7.27\ x10^{13}$	80	1298
	$5x10^{14}$	1300	20	88	$4.34x10^{14}$	58	249
		1350	20	90	$4.49\ x10^{14}$	64	221
	$1x10^{15}$	1200	40	100	$1.00\ x10^{14}$	47	121
		1300	20	100	$1.00\ x10^{14}$	61	95
$Al_{0.4}Ga_{0.6}N$	$1x10^{14}$	1350	20	99	$9.78x10^{13}$	58	1099
	$5x10^{14}$	1200	40	100	$5.02x10^{14}$	38	316
	$1x10^{15}$	1200	40	96	$9.56x10^{14}$	41	159
$Al_{0.5}Ga_{0.5}N$	$1x10^{14}$	1300	20	100	$9.98x10^{13}$	51	1223
	$5x10^{14}$	1300	20	96	$4.78x10^{14}$	36	362
	$1x10^{15}$	1300	20	66	$6.59x10^{14}$	35	270

VI. Conclusions

Ion implantation of silicon ions into $Al_xGa_{1-x}N$ with Al mole fractions of 0.1 to 0.5 was found to be a viable method of creating highly conductive n-type material. The implanted silicon ions were readily activated with a post implantation annealing treatment that resulted in a minimum of 66% activation efficiency of the implanted ions and in most cases close to 100% activation. The optimal annealing temperature was found to vary between 1200 and 1350 °C depending on the anneal time, ion dose, and Al mole fraction of the sample. The overall mobilities are weak in comparison to Si or GaAs; however they are higher than those reported in the literature for Si-implanted $Al_xGa_{1-x}N$ (33-35, 47, 51-52). Resistivity values lower then 100 Ω/□ were attainable.

The Si-implanted $Al_xGa_{1-x}N$ with Al concentrations of 10 to 30% were found to behave similarly to each other as well as GaN in that the higher implanted silicon doses are more readily activated than the lower implanted doses. As the Al mole fraction of the $Al_xGa_{1-x}N$ was increased up to 50% the trend reverses and higher activations are achieved for the samples implanted with the lower silicon doses, as is the case with gallium arsenide (GaAs). However, the $Al_{0.4}Ga_{0.6}N$ exhibit much less of a preference on the doping level and high activation efficiencies were achieved for all three silicon implanted doses. This phenomenon could be related to the elevated temperatures required to sufficiently repair lattice damage in the higher Al mole fraction material.

The annealing conditions for the implanted $Al_xGa_{1-x}N$ were varied in order to attain the best configuration of time and temperature that generates the highest activation of the implanted silicon ions as well as significant restoration of the crystal lattice configuration. The anneal temperature at which the majority of the ion implantation

induced lattice damage is repaired was found to increase as the Al mole fraction of the material was increased indicating that damage profile from the implantation increased as the Al mole fraction increased. Correlating the activation efficiency and mobility data for the $Al_{0.1}Ga_{0.9}N$ samples indicated that most of the lattice damage had been recovered after annealing at 1200°C, while this did not occur for the $Al_{0.2}Ga_{0.8}N$ samples until after annealing at 1250°C. Complete lattice recovery did not take place for the $Al_xGa_{1-x}N$ with higher Al mole fractions even after annealing at temperatures up to 1350°C. However, electrical activations of the implanted silicon were greater than 95% for most of the implanted doses.

The optimal annealing temperature for the $Al_xGa_{1-x}N$ with Al concentrations of 10 to 30% increases as the implanted silicon dose is decreased or the Al concentration of the material is increased. Optimal annealing conditions are easily identified for the samples implanted with a dose of $1x10^{15}$ cm^{-2} silicon ions however; the samples implanted with the lower silicon doses do not always achieve 100% activation. The $Al_{0.1}Ga_{0.9}N$ required the lowest temperatures to activate the implanted ions and therefore responded the best to a lengthened anneal time of 40 minutes at an anneal temperature of 1200 ºC. These are the annealing conditions for $Al_{0.1}Ga_{0.9}N$ and produce electrical activation efficiencies of 73, 94, and 100% for the $Al_{0.1}Ga_{0.9}N$ implanted with doses of $1x10^{14}$, $5x10^{14}$, and $1x10^{15}$ cm^{-2} silicon ions, respectively. For the Si-implanted $Al_{0.2}Ga_{0.8}N$ the optimal annealing conditions are 1300 ºC for 20 minutes, which generate electrical activation efficiencies of 100% for the samples implanted with the two higher silicon doses. The $Al_{0.2}Ga_{0.8}N$ implanted with the lowest silicon dose had an electrical activation of only 83%, even after annealing at 1300 ºC. An anneal temperature of 1300 ºC produced excellent

activation for the Si-implanted $Al_{0.2}Ga_{0.8}N$ however, this anneal temperature was not high enough to produce the same results for the $Al_{0.3}Ga_{0.7}N$ samples. This anneal temperature generated electrical activation efficiencies of 74, 88, and 100% for $Al_{0.3}Ga_{0.7}N$ implanted with doses of $1x10^{14}$, $5x10^{14}$, and $1x10^{15}$ cm^{-2} silicon ions, respectively. The electrical activations for the two lower implanted silicon doses for the $Al_{0.3}Ga_{0.7}N$ are much lower than those of the $Al_{0.2}Ga_{0.8}N$, indicating that a higher anneal temperature or longer anneal time may be required to achieve improved activation for these samples. Samples with all three Al mole fractions have their lowest electrical activations for the samples implanted with $1x10^{14}$ cm^{-2} silicon ions. These samples show no sign of saturation suggesting that higher anneal temperatures or longer anneal times may produce elevated activation efficiencies. The annealing conditions were found to be dependent on the implanted silicon dose as well as the Al concentration of the material, with lower doses and higher Al mole fractions requiring higher annealing temperatures.

The Si-implanted $Al_xGa_{1-x}N$ with Al concentrations of 40 and 50% shifts in behavior from that of the samples with lower Al concentrations, in that the lower silicon implanted doses are more readily activated. Although the $Al_{0.4}Ga_{0.6}N$ exhibits a high activation efficiency for the lowest implanted silicon dose, the anneal conditions are much more extreme (1350 ºC for 20 minutes) than those required to achieve 100 and 96% electrical activation for the two higher silicon implanted doses. The latter two activations were obtained after annealing the $Al_{0.4}Ga_{0.6}N$ implanted with doses of $5x10^{14}$ and $1x10^{15}$ cm^{-2} silicon ions at 1200 ºC for 40 minutes. By increasing the Al concentration to 40% the samples maintain the ability to readily activate the high dose implants and gain the ability to activate low doses as well. The $Al_{0.5}Ga_{0.5}N$ behaves as the $Al_{0.4}Ga_{0.6}N$ samples

however, the increase in Al content caused the materials ability to activate highest dose implants to diminish. Electrical activation efficiencies of 100 and 96% were obtained after annealing the $Al_{0.5}Ga_{0.5}N$ implanted with doses of $1x10^{14}$ and $5x10^{14}$ cm^{-2} silicon ions for 20 minutes at 1300 ºC. The $Al_{0.5}Ga_{0.5}N$ implanted with a dose of $1x10^{15}$ cm^{-2} has an electrical activation of only 66% after being annealed at the same conditions.

Optimal annealing conditions were identified for the Si-implanted $Al_xGa_{1-x}N$ as a function of implanted silicon dose and Al concentration. Based on the electrical activations the optimum annealing conditions appear to be 1200 ºC for 40 minutes or 1300 ºC for 20 minutes and dependent on the implantation dose and the Al mole fraction of the material. The $Al_xGa_{1-x}N$ with Al concentrations of 10 and 40% implanted with doses of $5x10^{14}$ and $1x10^{15}$ cm^{-2} silicon ions manifest their best electrical properties after being annealed for 40 minutes at 1200 ºC, while the remaining Al concentrations preferred the higher temperature anneal. The $Al_{0.4}Ga_{0.6}N$ is the transition point between the activation behavior of the lower Al concentration samples and that of the $Al_{0.5}Ga_{0.5}N$, allowing for easy activation of al three implanted silicon doses.

The electrical activation efficiencies obtained for the $Al_xGa_{1-x}N$ with Al mole fractions from 0.1 to 0.5 are higher than those reported in similar studies for all of the Al mole fractions investigated (32-36, 47-48, and 51-53). At least one dose had an activation of 100% for each Al mole fraction and in most cases each Al mole fraction had samples that had an activation efficiency around 95% for a second dose. The high activations were obtained at relatively low annealing temperatures of 1200 and 1300 ºC. The Si-implanted $Al_xGa_{1-x}N$ also had higher mobilities and lower resistivity than those in the aforementioned reports.

The electrical properties obtained from Hall Effect measurements, such as the carrier concentration, mobility and resistivity of the implanted silicon all change as a function of the Al concentration of the material. Graphs of these properties as a function of Al mole fraction can be found in Appendix B. In general, these properties all decrease as the implanted silicon dose is increased. However, increasing the Al content of the $Al_xGa_{1-x}N$ has differing effects on the mobility and the resistivity.

In general, the mobility increased as the anneal temperature was increased from 1100 to 1350 ºC. The mobility decreases as the Al mole fraction of the material is increased which is most likely due to the increase in the effective mass as the Al concentration is increased. The mobility also decreases as the implanted silicon dose is increased due to an increase in ionized impurity scattering. All of the Al mole fractions investigated exhibited an increase in mobility despite an increase in the activation indicating that a decrease in defect scattering has stronger effects on the mobility than an increase in impurity scattering. The $Al_xGa_{1-x}N$ for all the Al mole fractions exhibited the highest mobility for the samples implanted with a dose of $1x10^{14}$ cm^{-2} silicon ions. The highest mobility obtained at 300 K was 109 $cm^2/V{\cdot}s$ for an $Al_{0.1}Ga_{0.9}N$ sample that had been implanted with $1x10^{14}$ cm^{-2} silicon ions and annealed at 1200 ºC for 20 minutes in nitrogen ambient. This is the highest reported mobility for Si-implanted $Al_{0.1}Ga_{0.9}N$ however; the mobility is much lower than those observed in Si-implanted GaN (22). The peak mobility for the $Al_{0.5}Ga_{0.5}N$ implanted with a silicon dose of $1x10^{15}$ cm^{-2} is the lowest of all the samples at 35 $cm^2/V{\cdot}s$ after being annealed for 20 minutes at 1350 ºC. The mobility values obtained in this study are higher than those reported in the literature

for samples with similar Al compositions and implantation conditions, except for the 20% samples where Ryu *et al*. obtained slightly higher mobilities (35).

The resistivity for all the implanted samples decreases as the ion dose is decreased or as anneal temperature is increased from 1100 to 1350 ºC due to an increase in lattice damage recovery and in activation efficiency. The lowest resistivity obtained was 96 Ω/□, for an $Al_{0.1}Ga_{0.9}N$ sample that was implanted with $1x10^{15}$ cm^{-2} silicon ions and annealed at 1200 ºC for 40 minutes. The resistivities for the $Al_xGa_{1-x}N$ samples implanted with the highest silicon dose are under 270 Ω/□, while the samples implanted with $5x10^{14}$ cm^{-2} silicon ions have resistivities under 362 Ω/□. The resistivity of the $Al_xGa_{1-x}N$ samples implanted with a dose of $1x10^{14}$ cm^{-2} silicon ions are much larger, increasing from 792 to 1298 Ω/□ as the Al composition is increased from 10 to 30%, where it reaches a maximum. As the Al concentration is increased to 40% the resistivity declines to 1099 Ω/□ however, it increases again as the Al concentration is raised to 50%.

The temperature-dependent Hall shows that the samples are degenerate. The $Al_xGa_{1-x}N$ samples implanted with a dose of $1x10^{14}$ cm^{-2} silicon ions exhibit less of a temperature-independence than the samples implanted with the higher silicon doses. The Mott concentration for $Al_xGa_{1-x}N$ increases slightly as the Al mole fraction is increased, so that as the Al mole fraction is increased from 0.1 to 0.5 the samples implanted with the lower silicon doses become more temperature-dependent.

All the CL spectra for the Si-implanted $Al_xGa_{1-x}N$ have a dominant donor bound exciton peak whose energy shifts from 3.7 to 4.6 eV has the Al mole fraction is increased form 0.1 to 0.5. The implanted $Al_{0.1}Ga_{0.9}N$ samples have a broad yellow luminescence (YL) band centered around 2.4 eV, which is not visible for the $Al_{0.2}Ga_{0.8}N$. This broad

luminescence shifts to 3.6 eV for the $Al_{0.3}Ga_{0.7}N$ and is only visible for the samples implanted with $1x10^{14}$ and $1x10^{15}$ cm^{-2} silicon ions that were annealed at 1200 °C. The $Al_{0.4}Ga_{0.6}N$ samples have a very weak luminescence around 2.8 eV for the higher implanted silicon doses. The $Al_{0.5}Ga_{0.5}N$ samples have a large luminescence centered around 3.1 eV that is more intense than the donor bound exciton peak. The broad band luminescence is attributed to a transition between silicon donors and a deep acceptor that could possibly be an aluminum vacancy or aluminum vacancy complex (44).

The mobility, resistivity and the high electrical activations achieved in this study for the implanted $Al_xGa_{1-x}N$, when correlated with the temperature-dependent and cathodoluminescence data, conclude that $Al_xGa_{1-x}N$ is a well suited material for electronic and optical device applications. The fundamental properties can easily be modified with Si-implantation to create the desired material functionality required for different device purposes. This research will assist device engineers by offering enhanced insight into the silicon activation of implanted $Al_xGa_{1-x}N$ that will improve the performance of $Al_xGa_{1-x}N$ based devices that require ion implantation.

Recommendations for Future Research

1. Replace the AlN encapsulant. As the Al mole fraction of the material is increased the AlN capping layer becomes more difficult to remove.
2. Investigate the optical properties of the material with temperature and power dependant cathodoluminescence to determine the nature of broad luminescence features and their connection to the activation efficiency.
3. Anneal the $Al_{0.1}Ga_{0.9}N$ and $Al_{0.2}Ga_{0.8}N$ implanted with doses of $5x10^{14}$ and $1x10^{15}$ cm^{-2} silicon ions at lower temperatures than 1200 ºC extending the anneal time beyond 20 minutes to obtain significant electrical activation efficiencies.
4. Determine commercially viable annealing conditions for the $Al_xGa_{1-x}N$ implanted with a dose of $1x10^{14}$ cm^{-2} for Al concentrations of 10 to 30% and $Al_{0.5}Ga_{0.5}N$ implanted with a dose of $1x10^{15}$ cm^{-2} silicon ions.
5. Continue the investigation of Si-implanted $Al_xGa_{1-x}N$ with Al mole fractions of 0.6 to 1.

Appendix A

Hall Effect Measurements

Room Temperature Measurements – Sample Mounting

1. Use the green sample card kept in the cabinet by the HT system.
2. Place sample within the outline square on card
3. Place one of the four pressure probes on each contact.
4. Use the curve tracer (power on, memory 1, hit recall) to check the connections
5. Insert card into RT sample mount.
6. Connect the 4 yellow testing cables to the top of the sample probe.

Low Temperature Measurements – Sample Mounting

1. Turn on the soldering iron.
2. Get a wet paper towel from the restroom.
3. Use **indium** solder only. Place some on a glass slide.
4. The LT sample holder is brass with four gold wires kept in the drawer of the LT system. Make sure the sapphire plate is in place.
5. Check the wires on the samples holder, spare wire is kept in the drawer to the right of the desk.
6. Apply a small drop of rubber cement to the back of the sample using a sharpened cotton swap stick.
7. Mount the sample in the middle of the sapphire plate. Wait a few minutes for the rubber cement to dry.
8. With the soldering iron place a small amount of indium of each contact.
9. Attach the wires from the samples holder to the contacts on the sample.
10. Use the curve tracer to test the connection.
11. Place the samples holder on the samples mount and tighten in place with 2 screws.
12. Attached the cold shield with 2-4 brass screws
13. Attach the top cover so that the windows are opposite the windows of the cold shield; tighten in place with 4 screws.
14. Connect the 4 yellow testing cables to the side of the sample chamber.
15. Check that the temperature sensor cable is connected.
16. Check that the vacuum gauge is connected.
17. Connect the turbo pump.
18. Turn the turbo pump on and let it come up to speed.
19. Open the valve so that the turbo pumps on the chamber.
20. Carefully flip the sample chamber in between the magnets, making sure the helium lines do NOT rub against the mounting plate.
21. Wait for the chamber pressure to get below 10 microns. (~30 minutes)
22. Turn on water to the compressor. **NEVER** turn on water to full pressure, open valve enough to override the interlocks of the compressor.
23. Turn on compressor and wait for system to cool. (~45 minutes)

High Temperature Measurements – Sample Mounting

1. Place high temperature head on foam block
2. Make sure set screws are loose so that the sample can fit underneath the probes.
3. Place sample in the center of the copper sample holder.
4. Place one probe on a contact at a time by tightening the set screws.
5. Place the probes in a clockwise fashion careful not to knock the previous probe out of position.
6. Use the curve tracer to test the connection.
7. Carefully place the sample holder into the vacuum jacket and secure with clamp.
8. Connect the 4 yellow testing cables to the top of the sample chamber.
9. Connect the yellow thermocouple wire
10. Connect the heater cable.
24. Turn the turbo pump on and let it come up to speed.
11. Open the valve so that the turbo pumps on the chamber.
12. Wait for the chamber pressure to get below 10 microns. (~15 minutes)

System Start-up

1. Turn on water to magnets. **NEVER** turn on water to full pressure, open valve enough to override the interlocks of the magnets.
2. Checks to make sure the return water lines are open.
3. Check for water leaking from the connections at the back of the magnets.
4. Check the placement of the Gaussmeter.
5. Flip the switch on the front of the magnet power supply into stand by mode.
6. Make sure all the interlock lights are green. Hit the reset button if any are red.
7. Push the green button to power on the magnets.
8. Turn on equipment stack. (red button upper right side on cabinet)
9. Turn on the computer and log in with password Lake Shore.
10. Open the program from icon on desktop. (Hall Measurement System)
11. Make sure all equipment in functioning by checking the Systems Logs box in the program.

Taking Measurements

1. Choose a current to test the samples, one that works through the entire temperature range.
   - Click on the resistivity button at the top right corner of the program.
   - Choose high or low resistivity.
   - Select the contact configuration to test (12,12).
   - Select a current and click the measure button.
   - Monitor that the out put is in range and that there are no errors.
   - Check that the current works for all contact pairs. (23,23; 34,34; 14,14)
2. Check that the contacts are linear.

- Do an I-V test with the selected current chose a step that results is about 5 measurement points. (right click in the measurements box on the left and choose I-V measurement)
- Choose high or low resistivity based on the sample material.
- Choose default contact pairs, click ok.
- Click the Start button at the top of the program.

3. Create a program for RT, HT or LT measurements. (right click in the measurements box on the left and choose variable field of variable temperature measurement)
   - Select Hall and resistivity measurements
   - Select to calculate resistivity at zero field.
   - Select a magnetic field of 5 kG; choose a step of 1 kG.
   - Enter the chosen current both positive and negative.
   - Select high or low resistivity.
   - Enter the temperatures for measurement.

* Temperature-dependent measurements take ~5 hours.
* Room temperature measurements with different three currents take ~20 min.

Shut Down

1. Turn off the magnets. (red button)
2. Put the magnet power supply out of stand by mode. (toggle switch)
3. Turn off water to magnets.
4. Turn off compressor after LT measurements.
5. Turn of water to the compressor.
6. Close the HMS.exe program.
7. Turn off computer monitor or entire stack if not going to use for awhile.
8. Wait for systems to return to room temperature. (294 K)
9. Turn of vacuum pump. (ONLY if system is at room temperature)
10. Wait for sample chamber to pressurize.
11. Unplug the necessary cables to remove sample mount.
12. Remove sample.
13. Assemble the sample chamber to keep dust and contaminants out while not in use.

Cathodoluminescence Measurements

Mounting Sample

1. Prepare, at most 8 samples, by thoroughly cleaning the surface in the clean room with TCE, acetone, methanol, and DI water.
2. The sample holder is marked with a black line across the top and an "X" and a black line on the bottom. Two samples can be mounted on at the top and 6 can be mounted on the bottom row beginning at the "X". The samples mounted on the top (bottom) row should be mounted slightly above (below) the black line to unsure proper grounding.
3. Apply a small drop of rubber cement to the back of the sample using a sharpened cotton swap stick to the portion of the sample that will be placed above (below) the black line. Wait a few minutes for the rubber cement to dry.
4. There are 4 mounting screws inside the chamber. Make sure they are loose.
5. Slide the sample plated onto the 4 screws
6. Place the grounding bars on the screws and then tighten, making sure that the grounding bar makes contact with all the samples.
7. Close chamber door
8. When mounting a whole 2 inch wafer, do not use sample holder. Take out he 4 mounting screws. Place flat edge of wafer up leaving one of the mounting screws holes uncovered. Use this mounting screw to mount pne discharge bar.

System Start-up

1. Open vacuum line is open. (green in-line valve on the floor under table)
2. Turn on roughing pump by flipping breaker on the wall. (2^{nd} from right)
3. Check that power strips behind the computer are on.
4. Turn on power to turbo pump.
5. Turn on power to vacuum pressure moniter.
6. Plug the green switch on the back of the turbo pump.
7. Flip switch on small black box on the back of the table to begin pumping on the chamber. (On is to the right)
8. When chamber pressure is less than $1x10^{-2}$ (~10 minutes) turn on turbo pump. (Press start un Alcatel box)
9. When chamber pressure reads $1x10^{-3}$, turn on ion gauge. (Green light comes on)
10. Flip switch on black box to off. (towards the left)

Cooling

1. Turn on water (in-line valve on floor under table)
2. Turn on Lakeshore temperature controller.
3. Wait until chamber pressure is below $5x10^{-6}$.(~30 minutes)
4. Turn off ion gauge.
5. Check pressure reading on back of compressor.

6. Turn first switch on the right on the back of the compressor. Wait 10 seconds.
7. Flip the second switch. There is a 30 second built-in delay.
8. Flip the last switch to turn on the cold head. (It takes about one hour to cool)

Taking Measurements

1. Turn the key on gamma high voltage supply.
2. Turn on E-gun power. (green button)
3. Turn on High voltage (red button)
4. Turn on Source (red button)
5. Turn on Deflection (blue button)
6. Turn the E-gun energy knob the desired energy. (10keV)
7. Make sure ammeter on top of the spectrometer is on.
8. Slowly turn up the E-beam source current to 2.3 - 2.5 Amps, until the ammeter reads 50 μA. Takes ~30 minutes to stabilize.
9. Turn on PMT HV power supply. (push button, lower right)
10. Supply 1500 V to PMT (toggle switch, lower left)
11. Turn on computer and open the "Instrument Control" program. Select yes to both questions.
12. Check the slit openings on the spectrometer.
13. Check to make sure the program is set up to read from the correct slit openings.
14. Open the Faraday cup. Be gentle it is tricky. The current on the ammeter will drop.
15. Focus the beam on the samples using the X-Y control box.
16. Turn off the room lights to eliminate background noise.
17. Align the sample luminescence with the entrance slit on the spectrometer using two lenses.
18. Open shutter all the way.
19. Take spectrum.

Shut Down

1. Gradually turn down source current on E-gun.
2. Turn down the E-gun energy.
3. Turn off all buttons, 2 red, green and blue.
4. Turn the key on the high voltage source.
5. Turn off high voltage to PMT.
6. Close the shutter on spectrometer.
7. Cover lenses.
8. Turn off computer monitor.
9. Turn off compressor – 3 switches from left to right.
10. Wait for chamber to reach 294 K. (~12 hours)
11. Stop the turbo pump.
12. Pull green plug from back of turbo.
13. Wait for the system to pressurize. (~30 minutes)
14. Turn off Turbo pump.
15. Turn off roughing pump. (flip breaker)

Appendix B

This Appendix contains graphs of the activation efficiency, mobility, resistivity and donor bound exciton energy as a function of the Al mole fraction of the material to aid in the discussion in the conclusion. The plot of the donor bound exciton peak energy as a function of the Al mole fraction utilizes the calculated mole fractions from Equation 4.1, assuming a bowing parameter of one, that are given in Table 4.1. This is followed by plots of the activation efficiency, mobility and resistivity graphs for the $Al_xGa_{1-x}N$ samples implanted with the lowest silicon dose, and then those of the samples implanted with the higher silicon doses.

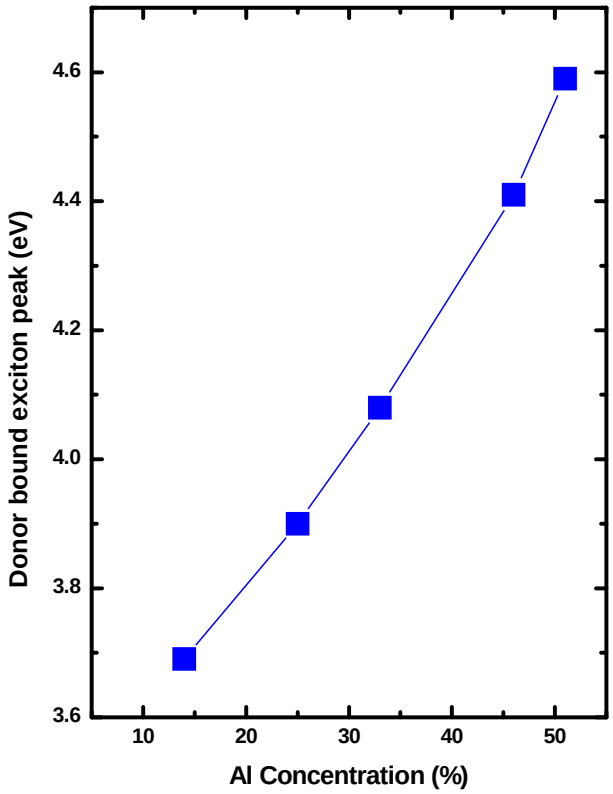

Silicon Dose: $1x10^{14}$ cm^{-2}

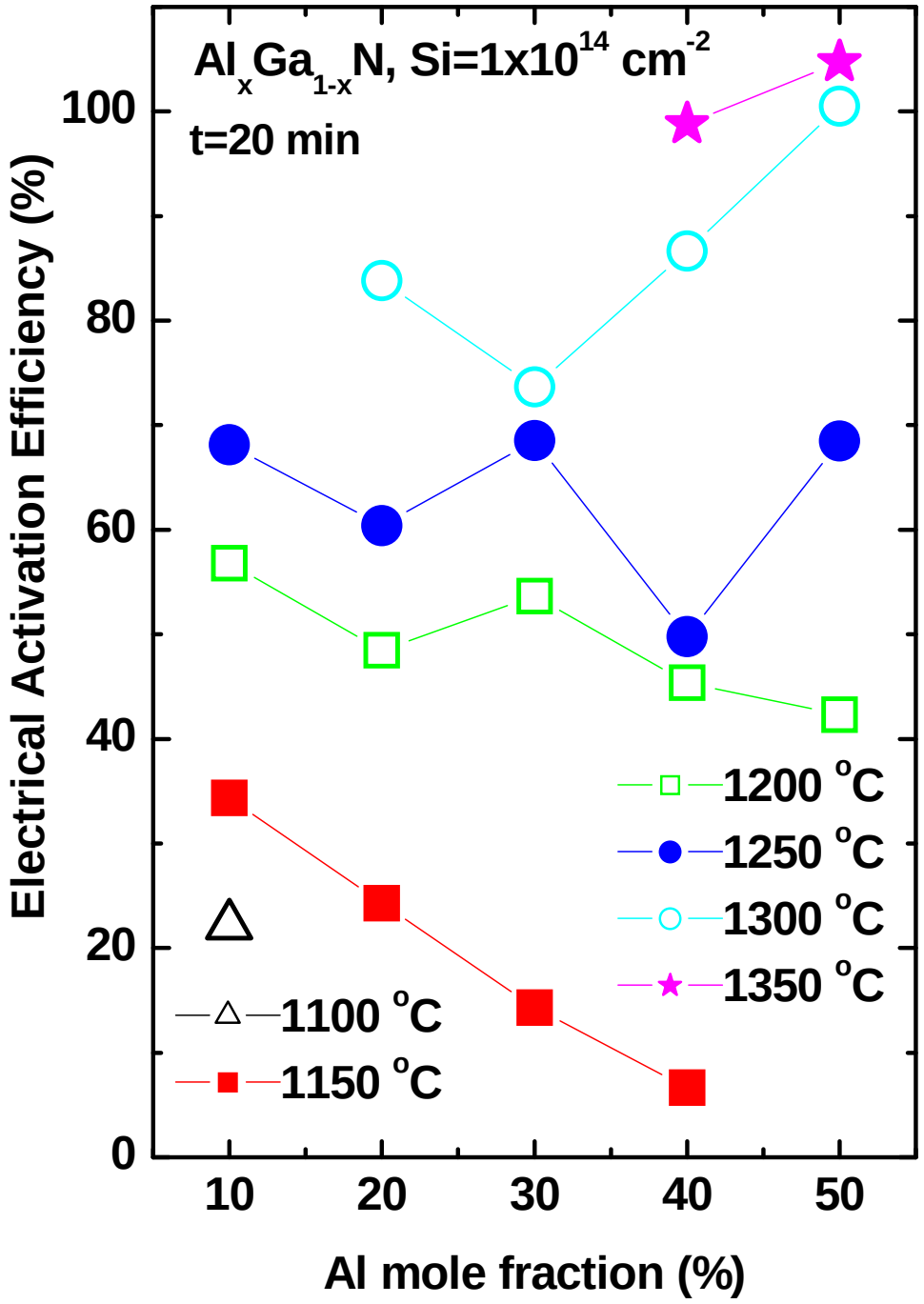

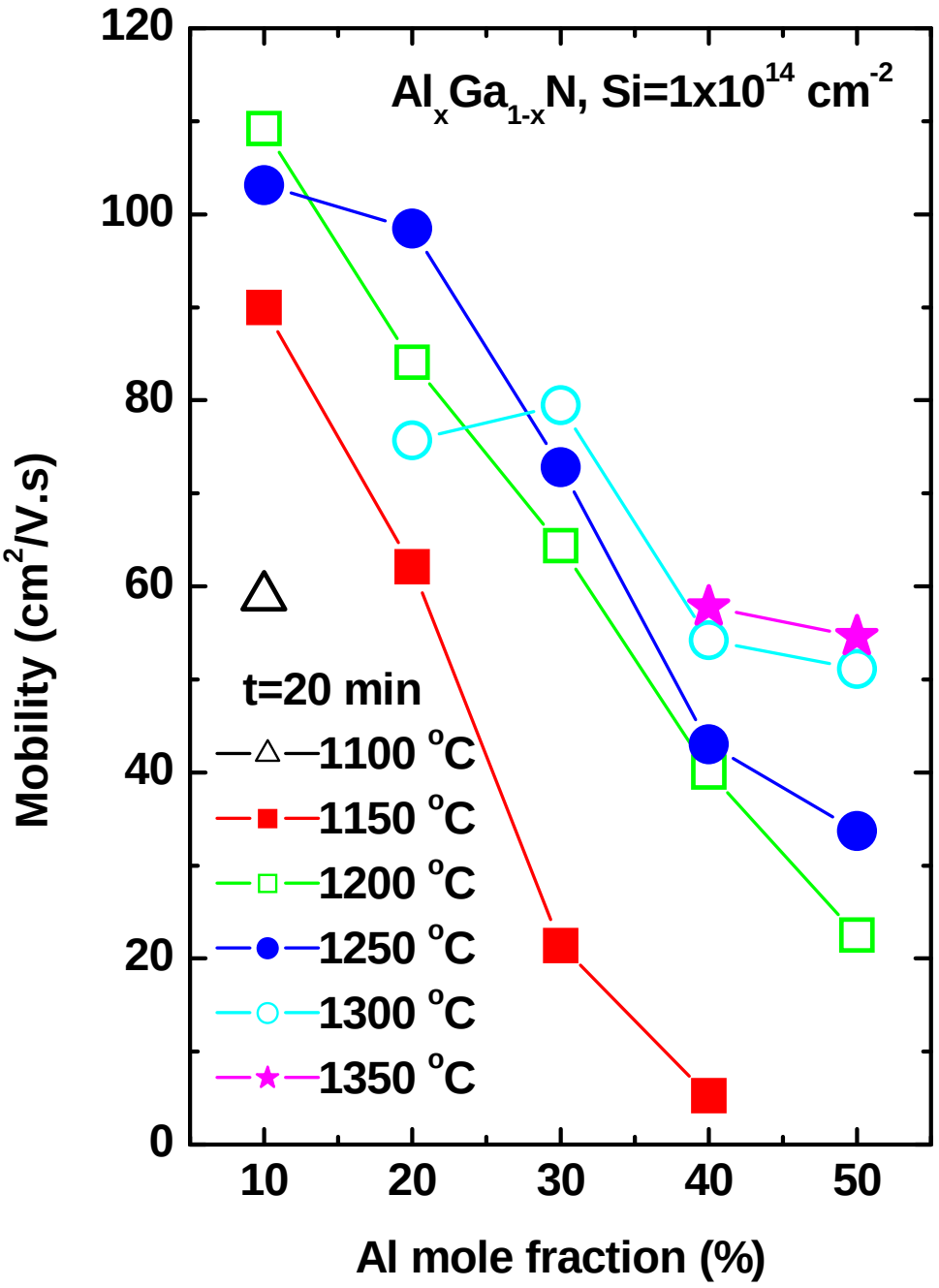
Al$_x$Ga$_{1-x}$N, Si=1x10^{14} cm^{-2}
Mobility (cm^2/V.s)
Al mole fraction (%)
t=20 min
1100 °C
1150 °C
1200 °C
1250 °C
1300 °C
1350 °C
0
20
40
60
80
100
120
10
20
30
40
50

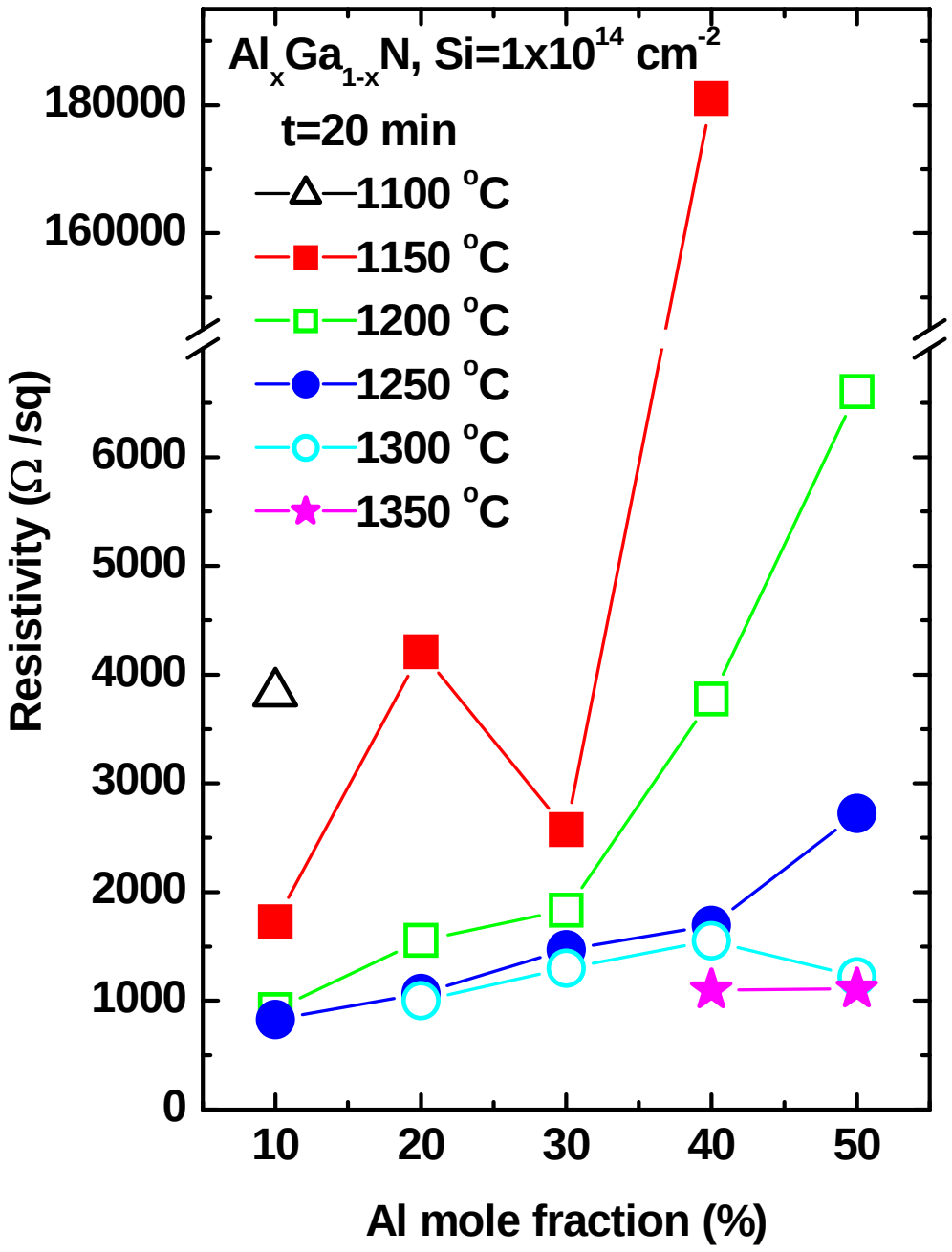
Al$_x$Ga$_{1-x}$N, Si=1x10^{14} cm^{-2}
t=20 min
1100 °C
1150 °C
1200 °C
1250 °C
1300 °C
1350 °C
Resistivity (Ω /sq)
180000
160000
6000
5000
4000
3000
2000
1000
0
10
20
30
40
50
Al mole fraction (%)

Silicon Dose: $5x10^{14}$ cm^{-2}

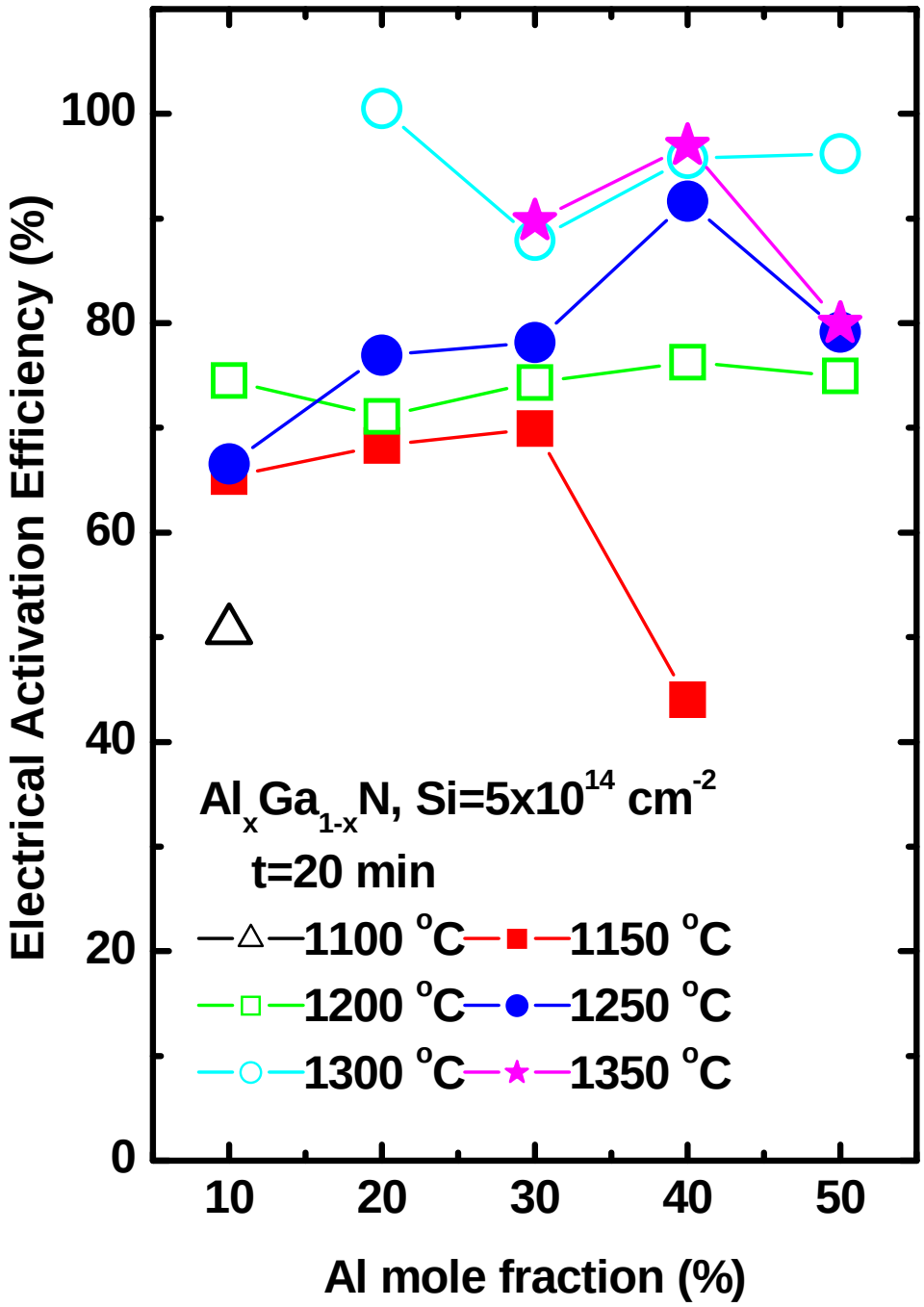

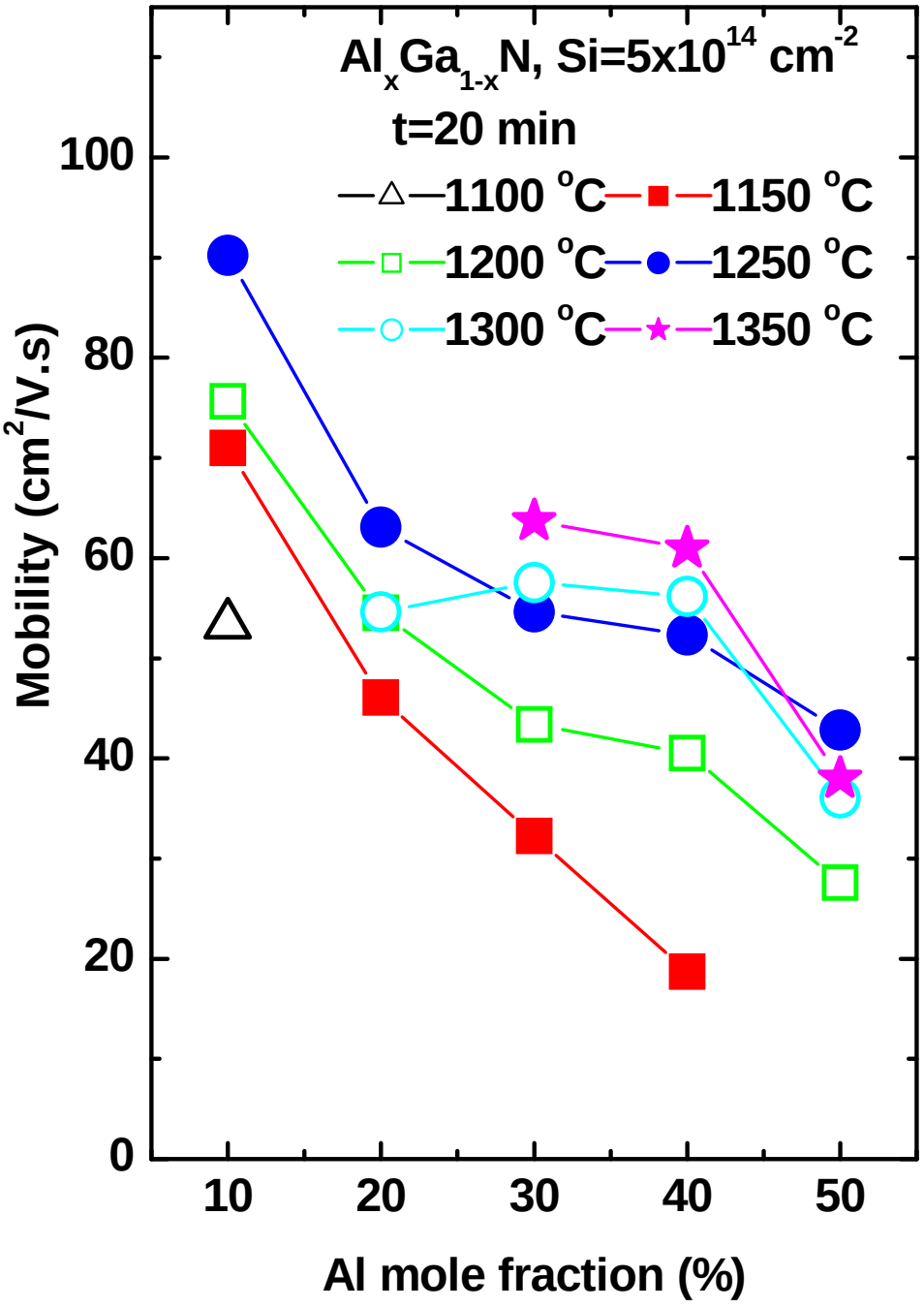
Al$_x$Ga$_{1-x}$N, Si=5x10^{14} cm^{-2}
t=20 min
1100 °C
1150 °C
1200 °C
1250 °C
1300 °C
1350 °C
Mobility (cm^2/V.s)
Al mole fraction (%)
0
20
40
60
80
100
10
20
30
40
50

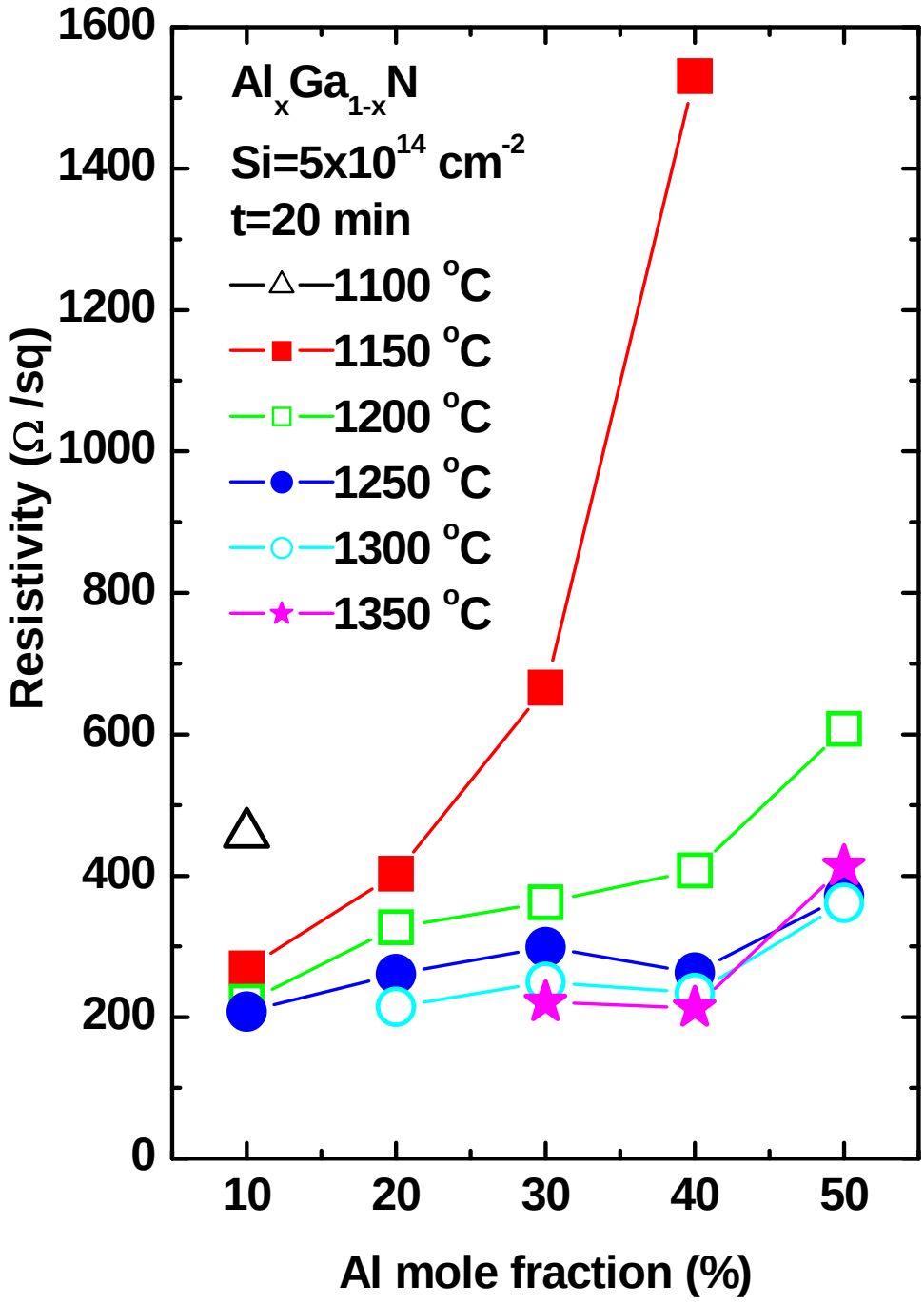
Al$_x$Ga$_{1-x}$N
Si=5x10^{14} cm^{-2}
t=20 min
1100 °C
1150 °C
1200 °C
1250 °C
1300 °C
1350 °C
Resistivity (Ω /sq)
Al mole fraction (%)
0
200
400
600
800
1000
1200
1400
1600
10
20
30
40
50

Silicon Dose: $1x10^{15}$ cm^{-2}

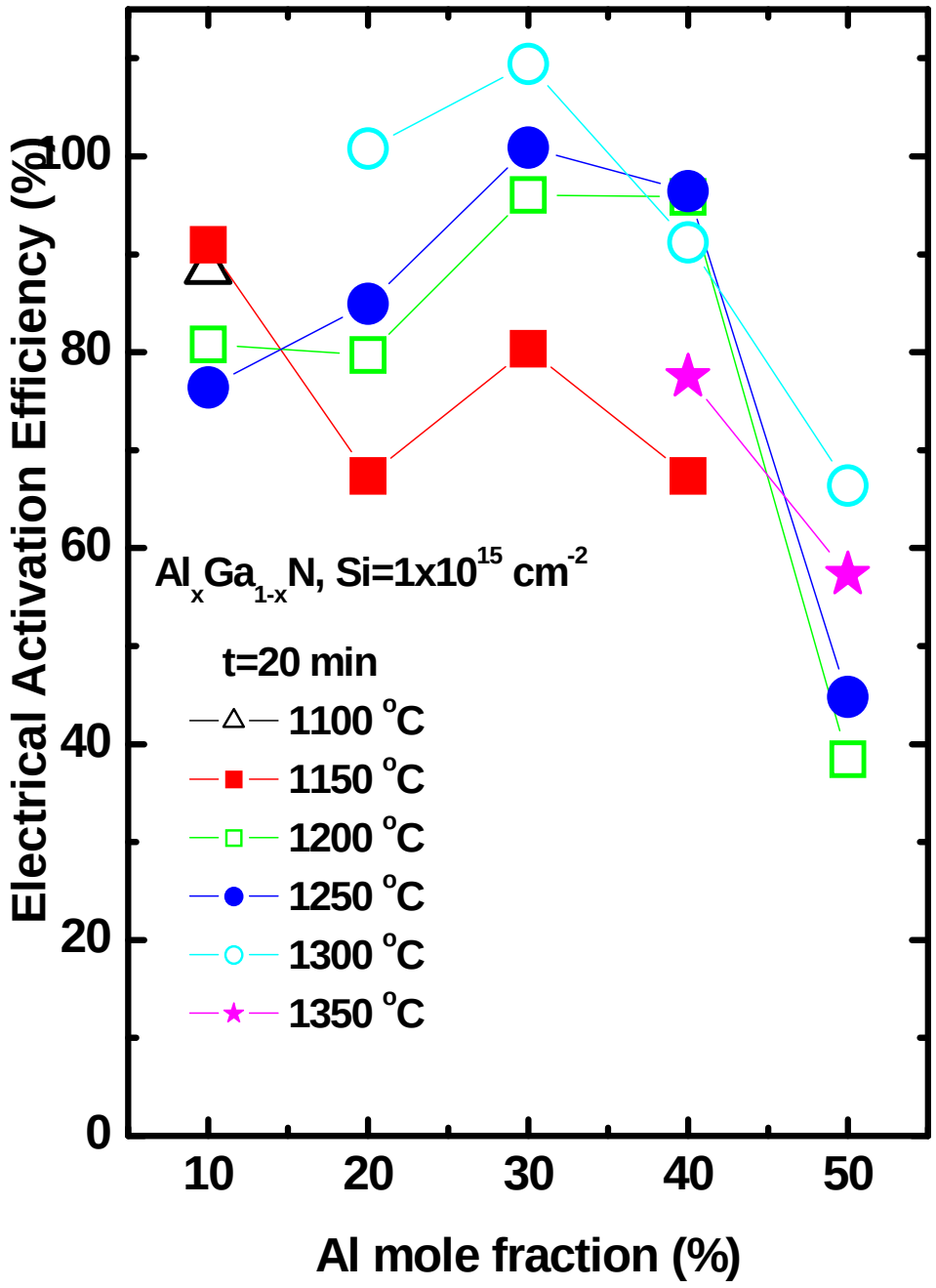

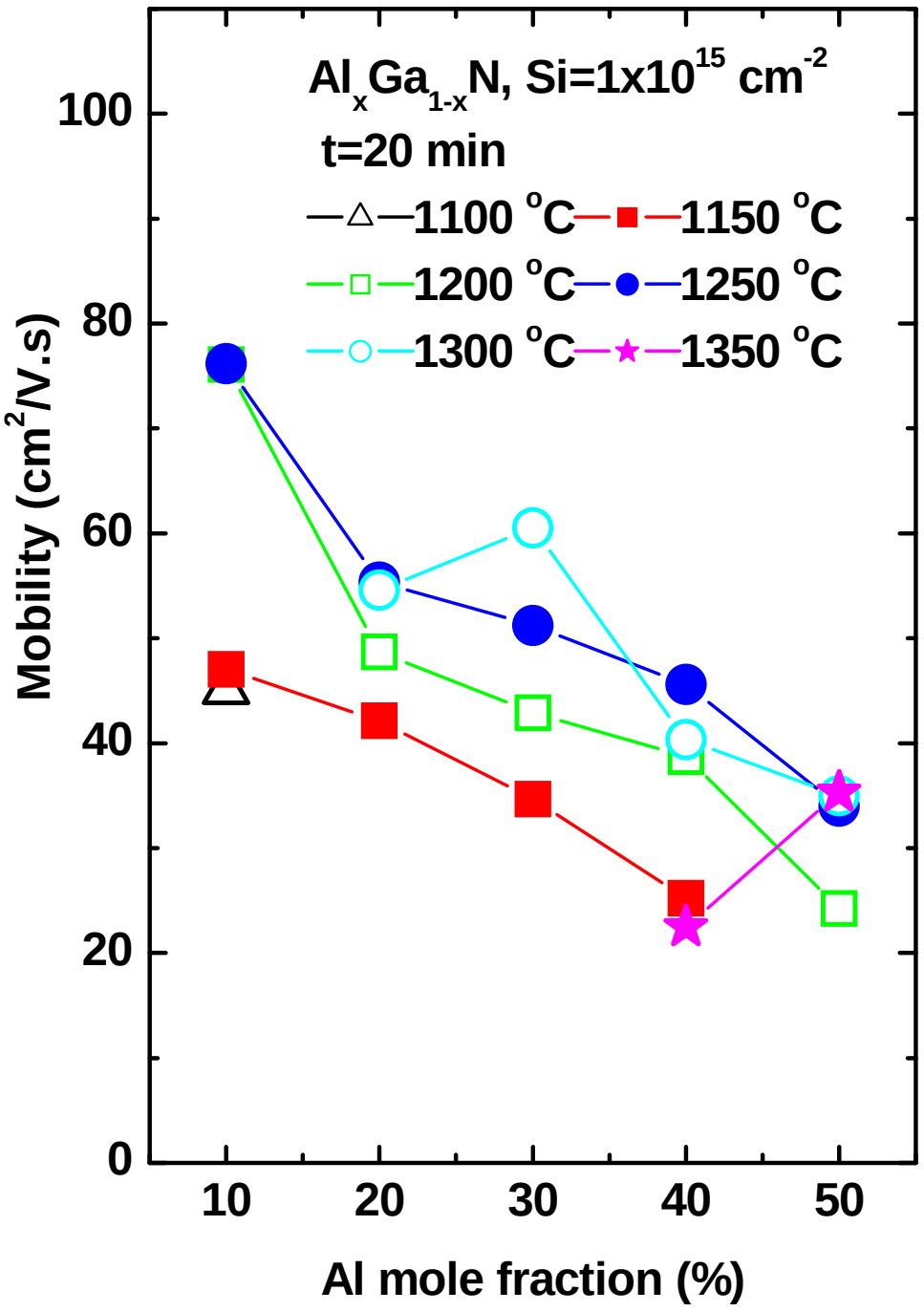
Al$_x$Ga$_{1-x}$N, Si=1x10^{15} cm^{-2}
t=20 min
1100 °C
1150 °C
1200 °C
1250 °C
1300 °C
1350 °C
Mobility (cm^2/V.s)
0
20
40
60
80
100
10
20
30
40
50
Al mole fraction (%)

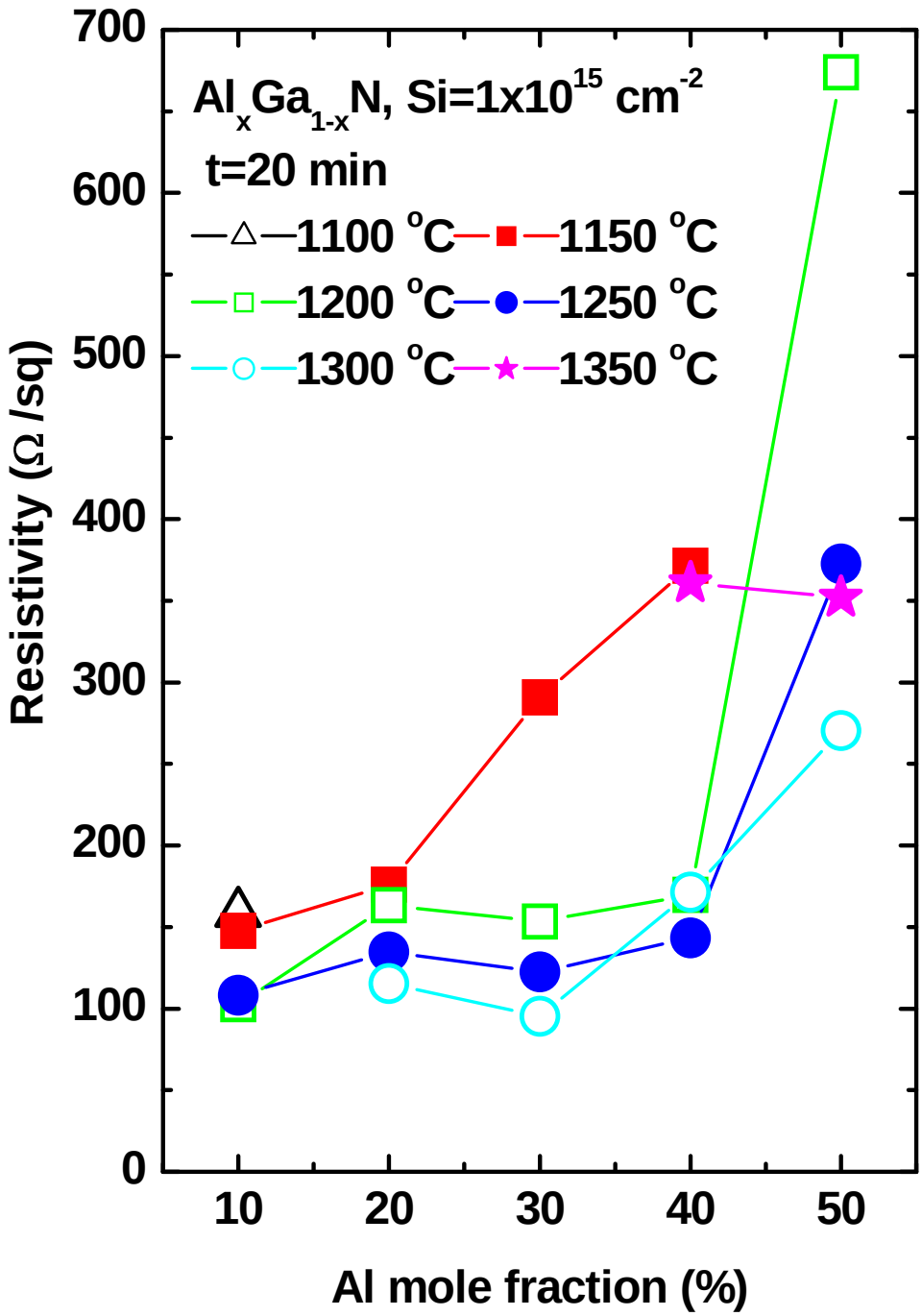
Al$_x$Ga$_{1-x}$N, Si=1x10^{15} cm^{-2}
t=20 min
1100 °C
1150 °C
1200 °C
1250 °C
1300 °C
1350 °C
Resistivity (Ω /sq)
Al mole fraction (%)
0
100
200
300
400
500
600
700
10
20
30
40
50

References

1. Houglum, Rodger J. Electronics: Concepts, Applications and History. Boston, Massachusetts: Breton Publishers (1985).

2. Wilson, A. H. Proceedings of the Royal Society A, 133:458 (1931).

3. Bhattacharya, Pallab, *Semiconductor Optoelectronic Devices Second Edition*. New Jersey: Prentice Hall (1997).

4. Neaman, Donald A. *Semiconductor Physics and Devices Basic Principles*. New York: McGraw-Hill (2003).

5. Aschroft, Neil and David Mermin. *Solid State Physics*. United States of America: Thompson Learning (1976).

6. Tolbert, Leon M., B. Ozpineci, S. K. Islam and M. S. Chinthavali. "Wide Band Gap Semiconductors for Utility Applications," *Power and Energy Systems*, 379: 80 (2003).

7. Materials for High Temperature Semiconductor Devices, the National Materials Advisory Board, Committee on Engineering and Technical Systems, National Research Council, NMAB-474, Washington D. C: National Academy Press (1995).

8. Nepal, N., L. Nakarmi, J. Y. Lin and H. X. Jiang. "Photoluminescence Studies of Impurity Transitions in AlGaN Alloys," *Applied Physics Letters*, 89: 092107 (2006).

9. Pavlidis, Dimitris. "Recent Advances in III-V Electronics," Electron Device Meeting, IEDM Technical Digest, IEEE International: 795-798 (2004).

10. Yu, Haijing, L. McCarthy, S. Rajan, S. Keller, S. Denbaars, J. Speck and U. Mishra. "Ion Implanted AlGaN-GaN HEMTs with Nonalloted Ohmic Contacts," *IEEE Electron Device Letters*, 26(5): 283-285 (2005).

11. Hui, Rongqing, Yueting Wan, Jing Li, Sixuan Jin, Jingyu Lin and Hongxing Jiang. "III-Nitride-Based Planar Lightwave Circuits for Long Wavelength Optical Communications," *IEEE Journal of Quantum Electronics*, 41(1): 100-110 (2005).

12. Scofield, James D. *Electrical Characterization of Intrinsic and Induced Deep Level Defects in Hexagonal Si*. PhD Dissertation, AFIT/DS/ENP/96-08. Graduate School of Management and Engineering, Air Force Institute of Technology (AU), Wright-Patterson AFB, OH, November 1996.

13. Zavada, J. M. and S. J. Pearton. “High Resistivity $Al_xGa_{1-x}N$ Layers Grown by MOCVD,” MIJ-NSR 1(36): (1997).

14. Baliga, B. J. “Power Semiconductor device Figure of Merit for High Frequency Applications” *IEEE Electron Device Letters*, 10(10): 455-457 (1989).

15. Nakarmi, M.L., N. Napal, J. Y Lin and H. X. Jiang. “Unitentionally doped n-type $Al_xGa_{1-x}N$ Epilayers,” *Applied Physics Letters*, 86: 261902 (2005).

16. Kim, Jong Kyu, E. Fred Schubert, Jeahee Cho, Cheolsoo, J. Y. Lin, H. X. Jiang and J. M. Zavada. “GaN Light Emitting Triodes for High-Efficiency Hole Injection,” *Journal of the Electrochemical Society*, 153(8): G734-G737 (2006).

17. Khizar, M., Z. Y. Fan, K. H. Kim, J. Y. Lin, and H. X. Jiang. “Nitride Deep-ultaviolet Light-emitting Diodes with Microlens Array,” *Applied Physics Letters*, 86: 172504 (2005).

18. Shakya, J., K. Knabe, K.H. Kim, J. Li, J. Y Lin and H. X. Jiang. “Polarization of III-nitride Blue and Ultraviolet Light Emitting Diodes,” *Applied Physics Letters*, 86: 091107 (2005).

19. Yu, Haijing, L. McCarthy, S. Rajan, S. Keller, S. Denbaars, J. Speck and U. Mishra. “Ion Implanted AlGaN-GaN HEMTs with Nonalloted Ohmic Contacts,” *IEEE Electron Device Letters*, 26(5): 283-285 (2005).

20. Miyoshi, Makoto, Masahiro Sakai, Hiroyasu Ishikawa, Takashi Egawa, Takashi Jimbo, Mitsuhiro Tanaka and Osamu Oda. “MOVPE Growth and Characterization of High Al Content AlGaN/GaN Heterostructures on 100 mm Diameter Sapphire Substrates,” *Journal of Crystal Growth*, 272: 293-299 (2004).

21. Lee, Jaesun, Dongmin Liu, Hyeongnam Kim and Wu Lu. “Post Annealing Efects on Device Performance of AlGaN/GaN HFETs,” *Solid-State Electronics*, 48: 1855-1859 (2004).

22. Fellows, James. *Electrical Activation studies of ion implanted GaN*, PhD Dissertation, AFIT/DS/ENP/02-2. Graduate School of Management and Engineering, Air Force Institute of Technology (AU), Wright-Patterson AFB, OH, November 2001.

23. van der Pauw, van der Pauw, L.J. (1958). "A method of measuring specific resistivity and Hall effect of discs of arbitrary shape, " *Philips Research Reports* 13: 1–9.

24. Yacobi, B. G. *Cathodoluminescence Microscopy of Inorganic Solids*. New York: Plenum Press (1990).

25. Fareed, Qhalid, R. Gaska, J. Mickevicius, G. Tamulatis, M. S. Shur, and M. A. Khan. "Migration Enhanced Metalorganic Chemical Vapor Deposition of Aln/GaN/InN Based Heterostructures," *Compound Semiconductor*, 21799: (2005).

26. F. Fedler, R. J. Hauenstein, H. Klausing, D. Mistele, O. Semchinova, J. Aderhold and J. Graul. "The Influence of V/III Ratio in the Initial Growth Stage on the Properties of GaN Epilayer deposited on low temperature AlN Buffer Layer," *Journal of Crystal Growth*, 303(2): 414-418 (2007).

27. Shan, W, J. W. Ager III, K. M. Yu, W. Walukiewicz, E. E. Haller, M.C. Martin, W. R. McKinney, and W. Yang. "Dependence of the Fundamental Band Gap of AlxGa1-xN on Alloy Composition and Pressure," *Journal of Applied Physics*, 85(12): 8505-8507 (1999).

28. Ziegler, J. F., J. P. Biersack and U. Littmark. *The Stopping and Range of Ions in Solids*, New York: Pergamon Press (1985).

29. Irokawa, Y., O. Ishiguro, T. Kachi, S. J. Pearton, F. Ren. "Implantation temperature dependence of Si activation in $Al_xGa_{1-x}N$," *Applied Physics Letters*, 88: 182106 (2006).

30. Kuckeyev, S. O. and J. S. Williams. "Structural disorder in ion-implanted AlGaN," *Applied Physics Letters*, 80: 5 (2002).

31. Kuckeyev, S. O., J. Williams, and C. Jagadish. "Ion Beam Defect Processes in group-III nitrides and ZnO," *Vacuum* 73: 93-104 (2004).

32. Zopler, .C, J. Han, S. Van Deusen, R. Buefeld, J. Jun, T. Suski, J. Baranowski, S. Pearton, and M. Crawford. "Recent Progress in implanting and annealing of GaN and $Al_xGa_{1-x}N$," *Materials Research Society Symposium Proceedings* 482: 979-980 (1998).

33. Nakarmi, M., N. Nepal, J.Y. Lin, H.X. Jiang. "Unintentionally doped n-type $Al_{0.67}Ga_{0.33}N$ Epiolayers," *Applied Physics Letters* 86: 261902 (2005).

34. Irokawa, Y., O. Ishiguro, T. Kachi, S. J. Pearton, F. Ren. "Activation characteristics of ion-implnated Si^+ in $Al_xGa_{1-x}N$," *Applied Physics Letters*, 86: 192102 (2005).

35. Ryu, Mee-Yi, Y.K. Yeo, M. Marciniak, T. Zens, E. Moore, R. Hengehold, T. Stiener. "Electrical and Optical Characterization Studies of Lower Dose Si-

Implanted $Al_xGa_{1-x}N$," *Journal of Electromagnetic Materials*, 35(4): 647-653 (2006).

36. Polyakov, A.Y, N. Smirnov, A. Govorkov, M. Milividskii, J. Redwing, M. Shin, M. Skowronski, D. Greve, and R. Wilson. "Properties of Si Donors and Persistent Photoconductivity in $Al_xGa_{1-x}N$," *Solid State Electronics* 42(4): 627-635 (1998).

37. Look, D.C. and R. J. Molnar. "Degenerate layer at GaN/sapphire Interface on Hall Effect Measurements," *Applied Physics Letters* 70: 3377, (1997).

38. Zhu, K., M. L. Nakarmi, K. Kim, J.Y. Lin, and H. X Jiang. "Silicon Doping Dependence of Highly Conductive n-type $Al_{0.7}Ga_{0.3}N$," *Applied Physics Letters* 85(20): 4669-4671 (2004).

39. Lee, Cheul-Ro, "N-type Doping Behavior of $Al_{0.15}Ga_{0.85}N$:Si with Various Si Incorporations," *Journal of Crystal Growth* 246: 25-30 (2002).

40. Zavada, J. M. and S. J. Pearton. "High Resistivity $Al_xGa_{1-x}N$ Layers Grown by MOCVD," MIJ-NSR 1, 36: (1997).

41. Glaser, E. R. "Optically Detected Magnetic Resonance in GaN Films Grown by OMVPE," *Physical Review B: Condensed Matter Material Physics* 51: 13326 (1995).

42. Ogino, T. and Masaharu Aoki. "Mechanism of Yellow Luminescence in GaN," *Japanese Journal of Applied Physics* 119: 2395-2405 (1980).

43. Polyakov, A. Y, M. Shin, J. A. Freitas, M. Showronski, D. W. Grere, R. J. Wilson. "On the Origin of Electrically Active Defects in $Al_xGa_{1-x}N$ Alloys Grown by OMVPE," *Journal of Applied Physics* 80: 6349 (1996).

44. Nam, K.B., M. L. Nakarmi, J.Y. Lin, and H. X. Jiang. "Deep Impurity Transitions Involvonig Cation Vacancies and Complexes in $Al_xGa_{1-x}N$ alloys," *Applied Physics Letters* 86: 222108 (2005).

45. Ryu, Mee-Yi, Y.K. Yeo, M. Marciniak, T. Zens, E. Moore, R. Hengehold, T. Stiener. "Electrical and Optical Characterization Studies of Lower Dose Si-Implanted $Al_xGa_{1-x}N$," *Journal of Electromagnetic Materials*, 35(4): 647-653 (2006).

46. Ryu, Mee-Yi, E. Chitwood, E. Claunch, Y. Yeo, R. Hengehold, J. Fellows, and T. Steiner. "Annealing studies of Si-Implanted $Al_{0.25}Ga_{0.75}N$," *Physics Stat Sol(c)* 1-4, (2003).

47. Chitwood, Elizabeth. *Electrical Activation Studies of $Al_xGa_{1-x}N$ and Co-implanted GaN*. MS thesis, AFIT/GAP/ENP/03-01. Graduate School of Management and Engineering, Air Force Institute of Technology (AU), Wright-Patterson AFB, OH, March 2003.

48. Nakano, Yoshitaka, Osamu Fujishima, T. Kachi, K. Abe, O. Eryu, K. Nakashima, and T. Jimbo. "n-Type Doping Characteristics of O-Implanted AlGaN," *Journal of the Electrochemical Society*, 151(12): G801-G804 (2005).

49. McFall, J. L., R. Hengehold, Y.K. Yeo, J. Van Nostrand and A. Saxler. "Optical Investigation of MBE Grown Si-doped $Al_xGa_{1-x}N$ as a Function of Nominal Al Mole fraction up to 0.5," *Journal of Crystal Growth*, 227-228: 458-465 (2001).

50. Touzi, C., F. Omnes, B. El Jani, P. Gibart. "LP MOVPE Gowth and Characterization of High Al Content $Al_xGa_{1-x}N$ Epilayers," *Journal of Crystal Growth* 279(1-2): 31-36 (2005).

51. Hwang, Jeonghyun, W. Schaff, L. Eastman, S. Bradley, L, Brillson, D. Look, J. Ku, W. Walukiewicz, M. Furis, and A. Cartwright. "Si Doping of High-Al-mole Fraction $Al_xGa_{1-x}N$ Alloys with rf Plasma-induced Molecular Beam Epitaxy," *Applied Physics Letters* 81(27): 5192-5194 (2002).

52. Zhu, K., M. Nakarmi, K. Kim, J. Lin and H. Jiang. "Silicon Doping Dependence of Highly Conductive n-type $Al_{0.7}Ga_{0.3}N$," *Applied Physics Letters* 85(20): 4669-4671 (2004).

53. Gil, Bernard. *Low-Dimensional Nitride Semiconductors*. New York: Oxford University Press (2002).

54. Madelung, Otfried. *Semiconductors: Data Handbook 3rd Edition*, New York: Springer Publishing, 2003.

55. Yu, Peter Y. *Fundamentals of Semiconductors: Physics and Material Properties*, New York: Springer Publishing, 2001.

56. Li, J. N. Oder, M. Nakarmi, J.Lin, and H. Jiang. "Optical and Electrical properties of Mg-Doped p-type $Al_xGa_{1-x}N$," *Applied Physics Letters* 80(7): 1210-1212 (2002).

57. Katsuragawa, Maki, S. Sota, M. Komori, C. Anbe, T. Takeuchi, H. Sakai, H. Amano, and I. Akasaki. "Thermal Ionization Energy of Si and Mg in $Al_xGa_{1-x}N$," *Journal of Crystal Growth* 189/190: 528-531 (1998).

58. Kuckeyev, S.O., J. Williams, J. Zou, C. Jagadish, G. Li. "The effects of ion mass, energy, dose, flux and irradiation temperature on implantation disorder in GaN," *Nuclear Instruments and Methods in Physics Research B* 178: 209-213 (2001).

59. Nam, K.B., M. L. Nakarmi, J.Y. Lin, and H. X. Jiang. "Unique Optical Properties of $Al_xGa_{1-x}N$ Alloys and Related Ultraviolet Emmitters," *Applied Physics Letters* 84: 5264-5266 (2004).

60. Nepal, N., J. Li, M. L. Nakarmi, J. Y. Lin and H. X. Jiang. "Exciton Localization in $Al_xGa_{1-x}N$ Alloys," *Applied Physics Letters* 88: 062103 (2006).

61. Nepal, N., J. Li, M. L. Nakarmi, J. Y. Lin and H. X. Jiang. "Temperature and Compositional Dependence of the Energy Band Gap of $Al_xGa_{1-x}N$ Alloys," *Applied Physics Letters* 87: 242104 (2005).

62. Furis, M., A. Cartwright, J. Hwang and W. Schaff. "Time Resolved Photoluminescence of Si-doped High AL Mole Fraction $Al_xGa_{1-x}N$ Epilayers Grown by Plasma-Enhanced Molecular Beam Epitaxy," *Material Research Society Symposium Proceedings* 798: Y5.45.1-5 (2004).

63. Look, D. C., H. Lu, W. J. Schaff, J. Jasinski and Z. Liliental-Weber. "Donor and Acceptor Concentrations in Degenerate InN," Applied Physics Letters 80(2): 258-260 (2002).

64. Bardwell, J. A., S. Haffouz, H. Tang, and R. Wang. "Electrical Characterization and Surface Morphology of Optimized Ti/Al/Ti/Au Ohmic Contacts for $Al_xGa_{1-x}N$/GaN HEMTs," *Journal of The Electrochemical Society* 153(8): G746-749 (2006).

65. Qiao, D., L. S. Yu, S. S. Lau, J. M. Redwing, J. Y. Lin and H. X. Jiang. " Dependance of Ni/ $Al_xGa_{1-x}N$ Schottky Barrier Height on Al Mole Fraction," *Journal of Applied Physics* 87(2): 801-804 (2000).

66. Lee, M. L., J. K. Sheu, L. S. Yeh, M.S. Tsai, C. J. Kao, C. J. Tun, S. J. Chang, and G. C. Chi. " GaN p-n Junction Diode Formed by Si Ion Implantation into p-GaN," *Solid-State Electronics* 46: 2179-2183 (2002).

67. Xing, H., D. S. Green, L. McCarthy, L. P. Smorchkova, P. Chavarkar, T. Mates, S. Keller, S. DenBaars, J. Speck and Umesh K. Mishra. "Progress in Gallium Nitride-based Bipolar Transistors," Bipolar/BiCMOS Circuits and Technology Meeting, Proceedings of the 2001:125-130 (2001).

68. Fellows, James A., Y. K. Yeo, Mee-Yi Ryu, and R. L. Hengehold. "Electrical and Optical Activation Studies of Si-Implanted GaN," *Journal of Electronic Materials* 34(8): 1157-1164 (2005).

69. Seghier, D., H. P. Gislason. "Effect of Hydrogenation on the Electrical Properties of n-type $Al_xGa_{1-x}N$," *Journal of Physics D: Applied Physics* 37: 10-12 (2004).

70. Piazza, Gianluca, P. J. Stephanou and A. P. Pisano. "AlN Contour-Mode Vibrating RF MEMS for Next Generation Wireless Communications," Solid State Device Research Conference, Proceedings of the 36th European: 61-64 (2006).

71. Sze, S. M. *Physics of Semiconductor Devices* (2nd Edition). New York: John Wiley & Sons, 1981.

72. Look, David C., *Electrical Characterization of GaAs Materials and Devices*. New York: John Wiley & Sons, 1989.

73. Shklovskii, B. I., and A. L. Efros, *Electrical Properties of Doped Semiconductors*. Berlin: Springer-Verlag, 1984.

74. Bradley, S.T., S. H. Goss, L. J. Brillson, J. Hwang, W. J. Schaff. "Deep level defects and doping of high Al mole fraction $Al_xGa_{1-x}N$," *Journal of Vacuum Science and Technology B* 21 (6): 2558-2563 (2003).

75. Hashizume, Tamotsu, and Hideki Hasegawa. "Effects of nitrogen deficiency on the electronic properties of $Al_xGa_{1-x}N$ surfaces subject to thermal and plasma radiation," *Applied Surface Science* 234 (1-4): 387-394 (2004).

76. Lee, Sung-Nam, JoongKon Son, Tan Sakong, Wonseok Lee, Hosun Peaek, Euijoon Yoon, Jiyoung Kim, Yong-Hoon Cho, Okhyun Nam, and Yongjo Park. "Investigation of optical and electrical properties of Mg-doped p-$In_xGa_{1-x}N$, p-GaN and p-$Al_xGa_{1-x}N$ grown by MOCVD," *Journal of Crystal Growth* 272: 455-459 (2004).

77. Christensen, N.E., and Gorczyca I. "Optical and structural properties of III-V nitrides under pressure," *Physics Review B*: 4397-4415 (1994).

78. Neilson, Karl Ove. "Accelerators with ion sources for heavy radioactive decay," Presented at the Conference for Applications of Ion Beams to Semiconductors Technology, Grenoble. May 1967. www.phys.au.dk/main/historie/giraf/home.htm

79. Ziegler, James F. *Ion Implantation – Science and Technology 2004 Edition*. New York: IIT Press, 2004.

80. Pearton, S. J. “ GaN: Processing, defects and devices,” *Journal of Applied Physics* 86(1): 1-78 (1999).

REPORT DOCUMENTATION PAGE

Form Approved

OMB No. 074-0188

1. REPORT DATE *(DD-MM-YYYY)*	**2. REPORT TYPE**	**3. DATES COVERED** *(From – To)*
12-2007	Doctoral Dissertation	Oct 2004 – Dec 2007

4. TITLE AND SUBTITLE

ELECTRICAL ACTIVATION STUDIES OF SILICON IMPLANTED ALUMINUM GALLIUM NITRIDE WITH HIGH ALUMINUM MOLE FRACTION

5a. CONTRACT NUMBER

5b. GRANT NUMBER

5c. PROGRAM ELEMENT NUMBER

6. AUTHOR(S)

Elizabeth A. Moore

5d. PROJECT NUMBER

5e. TASK NUMBER

5f. WORK UNIT NUMBER

7. PERFORMING ORGANIZATION NAME(S) AND ADDRESS(ES)

Air Force Institute of Technology
Graduate School of Engineering and Management (AFIT/EN)
2950 P Street, Building 640
WPAFB OH 45433-7765

8. PERFORMING ORGANIZATION REPORT NUMBER

AFIT/DS/ENP/08-D01

9. SPONSORING/MONITORING AGENCY NAME(S) AND ADDRESS(ES)

Air Force Office of Scientific Research
Dr. Don Silversmith
4015 Wilson Blvd.
Arlington, VA 22203

10. SPONSOR/MONITOR'S ACRONYM(S)

AFOSR/NE

11. SPONSOR/MONITOR'S REPORT NUMBER(S)

12. DISTRIBUTION/AVAILABILITY STATEMENT

APPROVED FOR PUBLIC RELEASE; DISTRIBUTION UNLIMITED.

13. SUPPLEMENTARY NOTES

14. ABSTRACT

This research demonstrates a method for producing highly conductive Si-implanted n-type aluminum gallium nitride ($Al_xGa_{1-x}N$) alloys, and represents a comprehensive analysis of the resulting material's electrical and optical properties as a function of Al mole fraction, anneal temperature, anneal time, and implantation dose. Highly conductive alloys are critical to the fabrication of devices operating in deep UV, high-temperature, high-power, and high-frequency environments, and thus this research is significant in regard to the application of such devices. The $Al_xGa_{1-x}N$ wafers of this study, with Al concentrations of 10 to 50%, were implanted at room temperature with silicon ions at energies of 200 keV with doses of $1x10^{14}$, $5x10^{14}$, and $1x10^{15}$ cm^{-2} and annealed from 1100 to 1350 ºC for 20 to 40 minutes in flowing nitrogen. Excellent activation was achieved for each of the implanted silicon doses for all of the five Al mole fractions studied, with most activation efficiencies above 90%. These activation efficiencies are the highest reported activations, to the best of my knowledge. The mobilities were found to decrease as the Al concentration of the $Al_xGa_{1-x}N$ was increased from 10 to 50% and also as the implanted silicon dose was increased. Typical mobilities ranged from 101 $cm^2/V{\cdot}s$ for the $Al_{0.1}Ga_{0.9}N$ implanted with $1x10^{14}$ cm^{-2} silicon ions to 35 $cm^2/V{\cdot}s$ obtained for the $Al_{0.5}Ga_{0.5}N$ implanted with $1x10^{15}$ cm^{-2} silicon ions. The cathodoluminescence results support the electrical results in determining the optimal annealing conditions.

15. SUBJECT TERMS

Electrical activation efficiency, AlGaN, Hall effect, Ion Implantation, Cathodoluminescence

16. SECURITY CLASSIFICATION OF:			**17. LIMITATION OF ABSTRACT**	**18. NUMBER OF PAGES**	**19a. NAME OF RESPONSIBLE PERSON**
a. REPORT	**b. ABSTRACT**	**c. THIS PAGE**			Dr. Yung Kee Yeo, ENP
U	**U**	**U**	**UU**	312	**19b. TELEPHONE NUMBER** *(Include area code)* (937) 255-3636, ext 5432